Investigation of Losses Prediction Methods in 1D for Axial Gas Turbines

Article · January 2008

Source: OAI

CITATIONS
9

READS
155

1 author:

Adrian Dahlquist
Siemens Industrial Turbomachinery AB
10 PUBLICATIONS **67** CITATIONS

SEE PROFILE

ISRN LUTMDN/TMHP—09/5183—SE
ISSN 0282-1990

Investigation of Losses Prediction Methods in 1D for Axial Gas Turbines

Adrian N Dahlquist

Thesis for the Degree of Master of Science

Division of Thermal Power Engineering
Department of Energy Sciences
Faculty of Engineering LTH
Lund University
P.O. Box 118
SE – 221 00 Lund
Sweden

ISRN LUTMDN/TMHP—09/5183—SE
ISSN 0282-1990

Investigation of Losses Prediction Methods in 1D for Axial Gas Turbines

Thesis for the Degree of Master of Science
Division of Thermal Power Engineering
Department of Energy Sciences
By

Adrian N Dahlquist

LUND
UNIVERSITY

November 2008
Master Thesis
Department of Heat and Power Engineering
Lund Institute of Technology
Lund University, Sweden

Acknowledgements

I would like to thank all the persons working in the group GRCTA at Siemens in Finspång, Sweden for take time to answer my questions and help me find information. Special thanks to, Mats Annerfeldt that give me the opportunity to make this thesis and involved me in his group (GRCTA), Magnus Genrup that both helped me get contact with Siemens initially and has been my supervised from LTH through the project, Sven Gunnar Sundkvist and Anders Hagg for the help with the structure of the report, Lennart Neas help me gather evaluations for Siemens internal tests and Ake Klang that been my supervisor at Siemens for these six months and with a huge interest has guided and supported me. Ake Klang, I appreciate that you have always answered my question and give me good feedback, Thanks.

And last but not least a huge thank to my girlfriend Sandra Engdahl that has supported me through my entire education and decision to take this thesis work at Siemens. She did a big sacrifice when she quit here fulltime work and moved with me to Finspång. Thanks a lot.

Abstract

A brief description of the physical flow phenomena in a blade row that creates losses in an axial gas turbine and correlations to estimate these losses in a mean line calculation are given. Investigation and comparison of the loss correlations for 1D mean line calculation between the in-house program (CTC) used at Siemens and loss correlations present in the open literature were made. The investigation is primarily focused on the problems associated with modeling off-design effects on profile and secondary losses, and the effect of tip leakage losses at all loads. For the off-design condition both positive and negative flow incidence were covered with internal tests and numerical 2D investigations. The increase in blade losses at high outlet Mach number and how it is related to the shape of the suction surface for a blade profile was investigated with numerical 2D simulation.

The results for the loss models are validated against previous done internal gas turbine test runs at Siemens, external cascade tests and numerical 2D simulations.

The overall conclusions are that the in-house program (CTC) shows good prediction ability for the off-design down to the state where the turbine reaches turn-up mode. But some questions about CTC's distribution between profile and secondary losses are discussed.

For the tip leakage loss it was highlighted that CTC shows a somewhat low loss for a constant clearance and also a rather low increase with relative clearance change. A limitation in the prediction ability because the absence of some believed important parameter was also seen and an alternative model was suggested for unshrouded blades.

It is clear that there for most blade designs is seen a sudden increase in the blade losses at an outlet Mach number in the region of 0.9. But no obvious relations to which blade parameters that determine the absolute increase were found.

Nomenclature

Normal

A	Temporary variable	[-]
B	Temporary variable	[-]
b_c	Centerline camber length	[m]
C	Flow number	[-]
	Absolute fluid velocity	[m/s]
	Temporary variable	[-]
C_L	Lift coefficient	[-]
C_D	Drag coefficient	[-]
	Discharge coefficient	[-]
c	Chord	[m]
c_b	Centerline camber length ($c_c = b_c$)	[m]
c_p	Heat capacity at constant pressure	[J/(kg K)]
CR	Contraction ratio between inlet and truth	[-]
e	Mean radius of the curvature between the throat and trailing edge	[m]
	Loss	[-]
F_i	Incidence parameter	[-]
F_T	Tangential force per unit blade length	[-]
g	body force	[m/s^2]
h	Specific enthalpy	[J/kg]
	Span	[m]
h_T	Rotalpy	[J/kg]
hub	Hub for the blade/stator	
i	Incidence	[deg]
	if def from axial direction as MKT $i = \alpha_1 - \alpha_1'\ stator, or\ i = \beta_2 - \beta_2'\ rotor$	
k	Contraction between inlet and outlet	[-]
	Tip clearance	[m]
ΔL	Overlap between blade tip and casing	[m]
M	Torque	[Nm]
	Mach number	[-]
o	Throat	[m]
P_b	Back pressure at trailing edge	[bar]
q	Heat flow	[$J/(m^2 s)$]
r	Radius	[m]
s	Specific entropy	[J/(kg K)]
	Pitch	[m]
t	Blade thickness	[m]

TI	Turbulent intensity	[%]
tip	Tip for the blade/stator	
U	Blade velocity	[m/s]
W	Power	[J/s]
	Relative velocity	[m/s]
w	Power per unit mass flow	[J/s kg]
Y	Loss coefficient based on total pressure	[-]
z	Distance in the direction of a body force	[m]
Z	AM load parameter	[-]

Greek Characters

ω	Angular velocity	[rad/s]
ξ	Loss coefficient for enthalpy	[-]
ζ	Loss coefficient for enthalpy referred to the isentropic velocity	[-]
ϕ^2	Kinetic energy loss coefficient (actual gas exit velocity/ideal gas exit velocity	[-]
η	Efficiency	[-]
α	Absolute flow angle for C	[deg]
α'	Absolute blade angle for C	[deg]
β	Relative flow angle for W	[deg]
β'	Relative blade angle for W	[deg]
λ	Factor defining secondary loss in AM	[-]
	Or	
	Laval number	[-]
χ	Correction factor/multiplier	[-]
ψ_T	Zweifels loading parameter	[-]
δ	Deviation (turning after the throat) if def from axial direction as MKT $\delta = \alpha_2 - \alpha_2'\ stator, or\ \beta_3 - \beta_3'\ rotor$	[deg]
	Or	
	Boundary layer thickness	[m]
δ^*	Boundary layer displacements thickness	[m]
θ	Camber angle (blade turning) if def from axial direction as MKT $\theta = \alpha_1' + \alpha_2'\ stator\ ,\ or\ \theta = \beta_2' + \beta_3'\ rotor$	[deg]
ε	Turning/Deflection angle if def from axial direction as MKT $\varepsilon = \alpha_1 + \alpha_2\ stator, or\ \varepsilon = \beta_2 + \beta_3\ rotor$	[deg]
γ	Kappa, Ratio of specific heat c_p/c_v	[-]

Suffix

0	Total properties, base loss
1	Stator inlet
2	Rotor inlet, stator outlet
3	Rotor outlet
avg	Average
b	Back Or base
basic	Uncorrected condition
BL-edge	Edge of the boundary layer
c	Critical (for example see critical Mach Number M_c)
comp	Compressible flow
des	Design
Fr	Friction
hub	The hub or root of a blade
i	Incidence loss
in	Inlet to a blade row, stator or rotor
incomp	Incompressible flow
j	Jet (See Tip leakage flow)
k	Clearance
L	Leakage
M	Mach number
	Main
m	Mean
max	Maximum
mid	Middle
min	Minimum
opt	Optimal (minimum loss)
out	Outlet from a blade row, stator or rotor
P	Profile
p	Pressure side of a blade
prim	Primary
r	Radial
rel	Relative
R	Rotor
Re	Reynolds number
S	Secondary
s	Isentropic expansion in one row
	Suction side of a blade
	Stalling
shock	Shockwave
ss	Isentropic expansion in a entire stage
stator	Stator

TC	Tip Clearance
TE	Trailing edge
TEc	Trailing edge curvature
tip	Tip of a blade
tot	Total in a blade row
tt	Total to total
x	Axial
α_m	Mean blade angle (perpendicular to the resulting blade force)
θ	Tangential
*	Critical state where Mach number is one
$\perp$	Perpendicular direction

Abbreviations

AA	Arithmetic average
AAD	Average absolute deviation
AM	Ainley & Mathieson
AMDC	Ainley & Mathieson, Dunham & Came
AMDCKO	Ainley & Mathieson, Dunham & Came, Kacker & Okapuu
BSM	Benner, Sjolander and Moustapha 1995
CC	Craig & Cox
CT	Compressor turbine
HPT	High pressure turbine
LPT	Low pressure turbine
MaKl	Mamaev & Klebanov
MKT	Moustapha, Kacker & Tremblay 1989
MuKr	Mukhatarov & Krichakin
NS	Navier Stroke
PT	Power turbine
SD	Standard deviation
ZS	Zuh & Sjolander 2005
1D	One-Dimensional
2D	Two-Dimensions
3D	Three-Dimensional

Blade Terminology

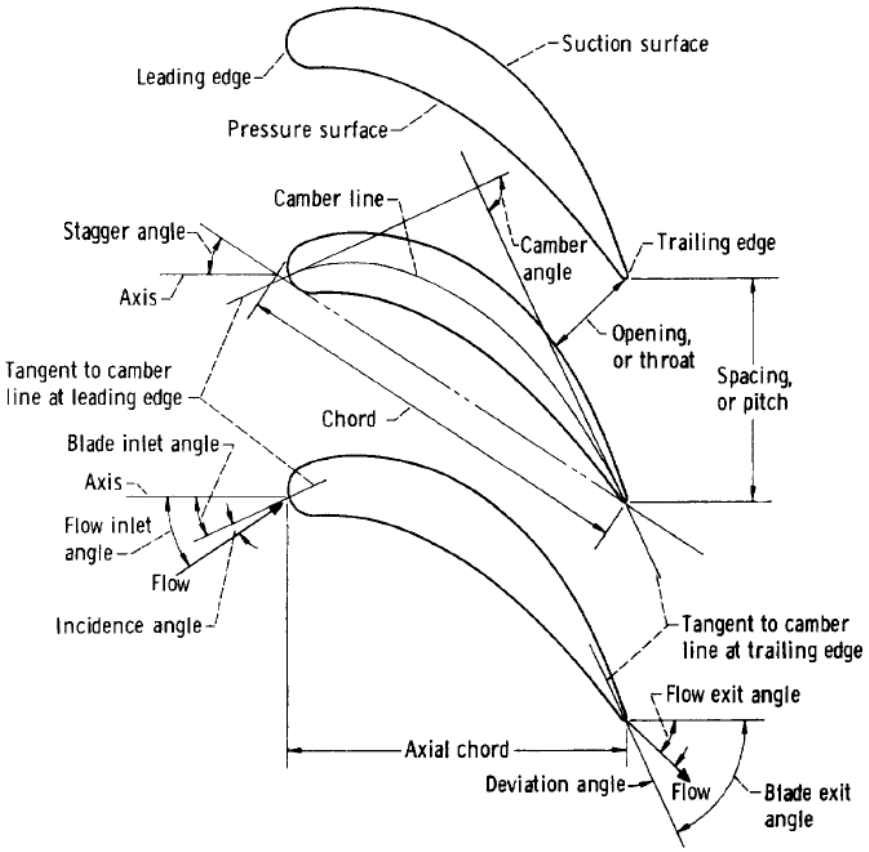

Figure 1.1-1: Blade terminology: Definitions of blade and flow geometry when the angle definition is from the axial direction (NASA-SP-290 J. Glassman fig 2-17).

Angle Definitions for the Different Authors

Ainley & Mathieson (AM)
Dunham & Came (AMDC)

Craig & Cox (CC)
CTC
Mukhatarov & Krichakin (MuKr)
Mamaev & Klebanov (MaKl)

Kacker & Okapuu (AMDCKO)
Moustapha, Kacker & Tremblay (MKT)
Benner, Sjolander & Moustapha (BSM)
Zhu & Sjolander (ZS)
Denton

Table of Contents

1 Introduction

In this first chapter are the objective, limitation, method, disposition, and reading instruction for this thesis described. It should also be mentioned that this Thesis work is done at Siemens Industrial Turbomachinery (SIT) in Finspång, Sweden. SIT is a state of the art high technological company in their business area and their technological acknowledge is interesting for other corporations. Because of this have some materials in this official report been classified as confidential and are therefore excluded or normalized, but this does not affect the general trends or conclusions. I will in the fact of this limitation anyway ask the reader to have forbearing for this.

1.1 Objective

The objective of this work is to investigate and describe the most important physical phenomena of the profile and secondary losses at off-design condition and the loss associated with tip leakage in an axial gas turbine for industrial application. A number of loss models from the open literature should be reviewed and compared to the in-house program CTC, Siemens internal experiments and other external sources of test data. The results of the investigation should be analyzed with the aim to find out if any corrections to the today used correlations could be recommended.

1.2 Limitations

- The investigation is done with correlations for one-dimensional mean line calculations.
- The range of the validation is only done for axial gas turbines in industrial environment and including not any validation against aero engines or steam turbines even if some of the investigated correlations originally were derived for several applications.
- The losses due to blade and disc cooling are not included.
- No own program code for the calculation of mass, energy, momentum and thermodynamic properties is done. Instead is Siemens Industrial Turbomachinery in-house program CTC used as a main program.

1.3 Method

Literature studies in term of articles, reports and in-house descriptions of both the physics behind the fluid flow in a turbine blade row passage, the associated losses and the proposed methodology to model these losses by earlier authors were performed. A summary of the physical phenomena behind the flow is briefly given (see chapter 2). From articles and reports a number of authors with interesting loss models were chosen and their proposed loss models were summarized (see chapter 3 and 5). In this summary the focus was on the modeling of the off-design influence on profile and secondary losses, and the models for losses associated with tip clearance.

The prediction ability for the off-design models was compared to the today used in-house program code CTC and validated against two ranges of turbine tests of SGT-700. In the first test the load was varied from 0-31 MW in steps of 5MW and in the second test the speed was stepped from 50 to 105 percent of the nominal running

condition. In that way the investigation covers both negative and positive blade flow incidence. Influence of incidence on profile loss for a single blade was also made in a two-dimensional numerical investigation based on Navier-Stokes (NS) equations included in the in-house program package Blagen. To see how different parameters affect the loss models a parameter variation was done (see section 4.3.4).

For the investigation of the tip leakage a number of loss models from literature studies were compared against CTC for both an earlier made internal test on the gas turbine GT35P and an external cascade test with measured losses. For the GT35P the tip leakage clearance was actively controlled from 1.7 to 3.3 mm and the generator electric power and some thermodynamic properties was accurately measured.

A critical review of a by AM and CC proposed dependence between the loss and the combination of Mach number and suction sides blade profile after the throat were investigated in a numerical two-dimensional analyze with Navier-Stoke.

A possible error in the conventional way to convert a loss based on pressure to one based on enthalpy was found in the open literature and this has been further investigated.

1.4 Disposition and Reading Instruction

The structure of the report is that first is the objective, limitations, method and disposition of this thesis given (Chapter 1), followed by a chapter with fundamental and important theory (Chapter 2). In the next chapter different loss models and the background of these are summarized and can within some limitations be used as a manual together with the references (Chapter 3). In chapter 4 the off-design investigation is described. Chapter 5 gives complementary theory for tip leakage and the full investigation for this phenomenon is present in chapter 6. In next chapter treat shockwave formation and their relation to Mach number and suction surface curvature compared (Chapter 7), followed by chapter 8 where a comparison of the possible error, highlighted in section 2.3-2.4, that the conversion between a pressure and enthalpy based loss is seen. In each of chapter 4, 6 and 7 is the trends and results discussed under the section named results. The reason for not dividing into two separate sections (results and discussion) is to make it easier for the reader get an overview of what the results show. All of these three chapters (4, 6 and 7) include a separate conclusion, but in chapter 9 the overall conclusions are summed up. Future work is seen in chapter 10 and the reference and appendix is placed in chapter 11 and 12.

2 Theory

2.1 Fundamental Theory for an Axial Gas Turbine

The fundamental idea with a turbine is to extract work from the incoming airflow, and convert it into mechanical work at a rotating axel. The incoming fluid velocity C approaching the stator can be divided into three velocity components axial (C_x), radial (C_r) and tangential (C_θ).

Newton's second law of motion together with these velocity components give that the contribution of torque (M) to the shaft for a fluid element along a streamline at a specific radius r is equal to the change of tangential velocity multiplied by radius and mass flow rate. Integration from the hub to the tip of the blade then give the total contribution of torque in tangential direction (M_θ) at the shaft made by the entire blade, eqn (2-1)

$$M_\theta = \int_{hub}^{tip} \left(\dot{m} \cdot (r_{out} \cdot C_{\theta,out} - r_{in} \cdot C_{\theta,in})\right) dr \qquad (2\text{-}1)$$

The power per unit mass flow $w = \frac{W}{\dot{m}}$ is the product between torque and angular velocity ω over the mass flow and can be written according to eqn (2-2). If the angular velocity is expressed in terms of blade speed the power per unit mass flow (w) may be expressed as eqn (2-3).

$$w = \frac{1}{\dot{m}} \int_{hub}^{tip} \omega \cdot \left(\dot{m} \cdot (r_{out} \cdot C_{\theta,out} - r_{in} \cdot C_{\theta,in})\right) dr \qquad (2\text{-}2)$$

$$\left.\begin{array}{l} eqn\ (2-2) \\ \omega \cdot r = U \end{array}\right\} \Rightarrow$$

$$w = \int_{hub}^{tip} \frac{M \cdot \omega}{\dot{m}} dr = \int_{hub}^{tip} \left((U_{out} \cdot C_{\theta,out} - U_{in} \cdot C_{\theta,in})\right) dr \qquad (2\text{-}3)$$

Where U is the blade speed along a specific streamline, and normally it is approximately constant between inlet and outlet of a blade.

A well known equation is Euler's turbomachine equation that describes the work contribution for a fluid element along a streamline between two points, and is independent of any losses or compression of the fluid between the two points. The equation is simple eqn (2-3) without any integration along the blade, and can be written as eqn (2-4)

Euler's turbomachine equation

$$w = U_{out} \cdot C_{\theta,out} - U_{in} \cdot C_{\theta,in} \qquad (2\text{-}4)$$

When the fluid is passing through the rotor it undergoes a change in total energy. For a turbine with zero degree of reaction this is because of flow turning only. While it for a reaction turbine is due to both the turning and acceleration relative to the rotor that cause a change in tangential velocity for the fluid. With use of the energy equation it can be written as eqn (2-5)

$$dq - dw = d(h + \frac{1}{2}C^2 + g \cdot z) \qquad (2\text{-}5)$$

q = Specific heat transfer to the fluid [J/s Kg]
w = Specific work done by the fluid [J/s Kg]
h = Enthalpy [J/kg K]
C = Velocity [m/s]
g = Body forces, normally gravity [m/s^2]
z = Change in potential height in the direction of the resultant of the acting body forces (g) [m]

If we assume that the turbine is an adiabatic machine, as the heat exchange (q) with the surrounding is small compare to total enthalpy drop and therefore neglected ($q \approx 0$). The same is true for the change of potential height ($z \approx 0$), as also is neglected. These assumptions are normally realistic because the heat transfer and change in potential energy $g \cdot z$ are small compare to the turbine work.
Combined with the use of the total enthalpy (h_0) defined as

For stator

$$h_o = h + \frac{1}{2}C^2$$

For rotor

$$h_{o,rel} = h + \frac{1}{2}W^2$$

Where W is the fluid flow vector velocity in the rotating coordinate system, defined as

$W = C - U$ [m/s]

Eqn (2-5) combined with eqn (2-4) can now be written as

$$\Delta h_0 = U_{out} \cdot C_{\theta,out} - U_{in} \cdot C_{\theta,in} = w \qquad (2\text{-}6)$$

The process when a fluid element is passing through a turbine stage from stator inlet (1) to rotor inlet (2) and out through the rotor to point (3), is drawn in a Mollier diagram as shown in fig (2.1-1) The x-axis is entropy (s), y-axis is enthalpy (h) and the constant pressure line is diverging from each other with the slope locally equal to the local temperature T.

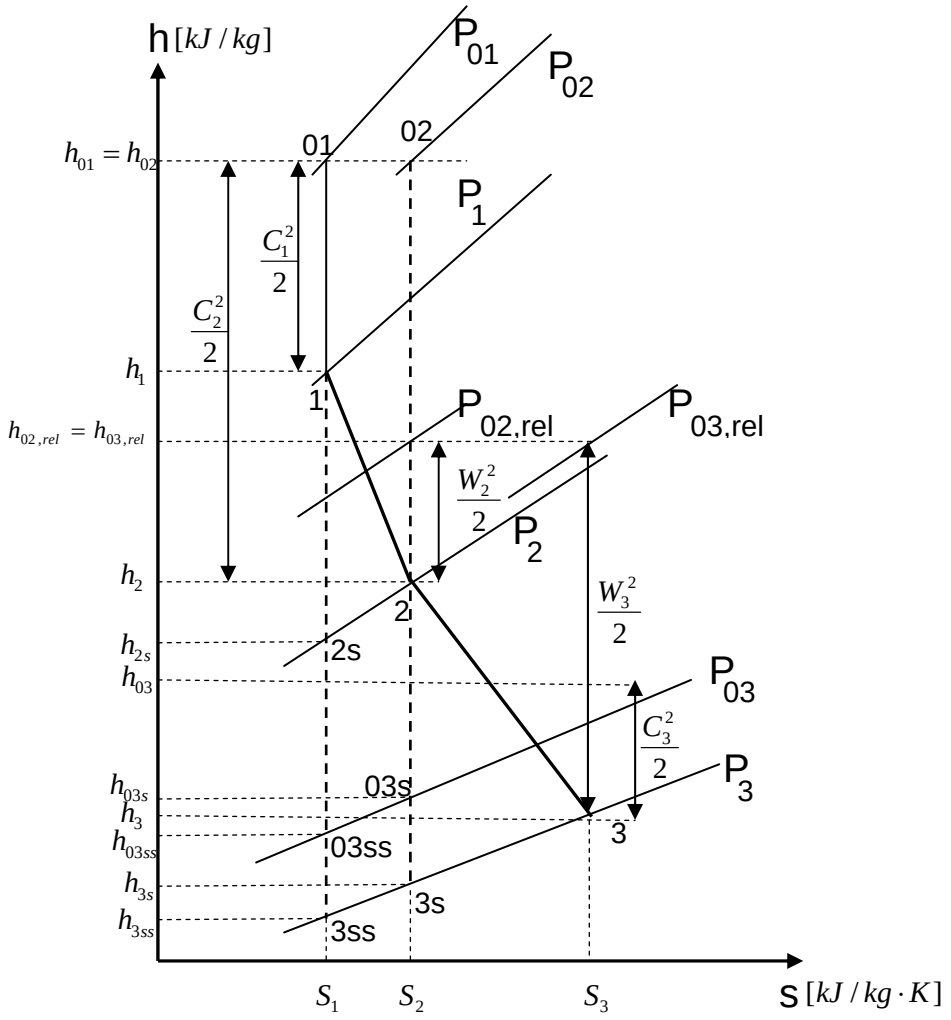

Figure 2.1-1: Enthalpy- entropy diagram showing the expansion through a turbine stage, with both absolute and relative properties. The absolute scale and slope of the expansions is not correct, and should only be used to get a brief understanding.

At the stator inlet the fluid has the static pressure p_1 and a small absolute velocity C_1 that give a total entropy h_{01} as the sum of static enthalpy h_1 and kinetic energy $0.5C_1^2$. In the stator the fluid expands and reach a velocity C_2 much greater then C_1 but with a moderate relative velocity W_2. In the rotor the relative velocity increases to a high level W_3 but with a low absolute velocity C_3 so that the absolute relative enthalpy is constant in the rotor as can be seen in Figure (2.1-1).

No work is extracted in the stator

$$h_{01} = h_{02} \Rightarrow h_1 - h_2 = \frac{1}{2}\left(C_2^2 - C_1^2\right) \qquad (2\text{-}7)$$

In a rotating coordinate system the rothalpy h_T is constant

$$\left.\begin{aligned} h_T &= h_{o,rel} - \frac{1}{2}U^2 \\ h_{0,rel} &= h + \frac{1}{2}W^2 \end{aligned}\right\} \Rightarrow h_T = h + \frac{1}{2}W^2 - \frac{1}{2}U^2 = const \qquad (2\text{-}8)$$

If applied across the rotor between 2 and 3

$$h_2 - h_3 = \frac{1}{2}\left[\left(U_2^2 - U_3^2\right) - \left(W_2^2 - W_3^2\right)\right] \qquad (2\text{-}9)$$

Combined with eqn (2-6) and eqn (2-7)

$$w = h_{02} - h_{03} = \frac{1}{2}\left[\left(U_2^2 - U_3^2\right) - \left(W_2^2 - W_3^2\right) + (C_2^2 - C_3^2)\right] \qquad (2\text{-}10)$$

As argued above the change in blade speed U between inlet and outlet along a streamline is close to zero, and in some cases the term $\left(U_2^2 - U_3^2\right)$ may be neglected form eqn (2-9).

2.2 Efficiency

In all flow field through a turbine there will be some difference between the theoretical ideal isentropic work output and the real work that can be achieved when the expansion is carried out from the same starting point 1 to the same exit pressure p_3. The difference is due to irreversibility in the expansion that creates an increase in specific entropy (s) and in that way moves the expansion line, and the final end point on the constant pressure curve to the right. In that way is the enthalpy drop that can be used for work decreased to a lower value than would be the case for the ideal expansion, where entropy generation is zero ($\Delta s = 0$). The nature of these loss sources are mainly friction in terms of viscous shearing and is given in chapter 2.6.

To express how efficient an expansion through a turbine is, three often used definitions for the efficiency are present below in eqn (2.11-2.13). All the states for these equations are seen in the h-s chart in Figure 2.1-1 where the suffix (ss) describes the final stage for the ideal expansion. The reason to have three definitions of efficiency is that they describe different cases where the exit kinetic energy is assumed to be recovered or not.

Total to total efficiency $$\eta_{tt} = \frac{h_{01} - h_{03}}{h_{01} - h_{03,ss}} \qquad (2\text{-}11)$$

In the total to total efficiency it is assumed that the kinetic energy $\frac{1}{2}C_3^2$ is possible to recover in a later stage. It is primary used for the stages, except the last, in a multistage turbine where the next coming stage will use the kinetic energy and C_3 in a stage n will be C_1 in the following stage.

Total to static efficiency

$$\eta_{ts} = \frac{h_{01} - h_{03}}{h_{01} - h_{3,ss}} \tag{2-12}$$

The total to static efficiency assumes that all the kinetic energy in the exhaust gas flow will be lost. An example is in the last stage of a turbine where the exhaust is blown out into the surrounding environment and all the kinetic energy that the diffuser can not recover to pressure will be lost.

Static to static efficiency

$$\eta_{ss} = \frac{h_1 - h_3}{h_1 - h_{3,ss}} \tag{2-13}$$

In the static to static efficiency the static condition at both inlet and outlet will be used. For the case of a multistage turbine with repeating stage, meaning that both the inlet and outlet velocity (C_1, C_3) is the same to both value and direction there will be no difference from total to total efficiency as can be seen in eqn (2-14) for a stator.

$$\left.\begin{aligned} h_{01} - h_{03} &= (h_1 + \frac{1}{2}\cdot C_1^2) - (h_3 + \frac{1}{2}\cdot C_3^2) \\ C_1 &= C_3 \end{aligned}\right\} \Rightarrow$$

$$h_{01} - h_{03} = (h_1 - h_3) + \frac{1}{2}(C_3^2 - C_1^2) = h_1 - h_3 \tag{2-14}$$

2.3 Loss Coefficients

Another way to describe the ratio between the actual work and an adiabatic expansion is to look at the ratio between the lost work potential compare to the total actually work. That is usually done by relating the loss of enthalpy due to irreversibility to the total useful enthalpy drop. It is also general practice to separate the losses between the stator and rotor into two different loss coefficients as shown below, and in Figure 2.1-1 above.

$$\zeta_S = \frac{h_2 - h_{2s}}{h_{01} - h_2} \tag{2-15}$$

$$\zeta_R = \frac{h_3 - h_{3s}}{h_{02,rel} - h_3} \tag{2-16}$$

$$h_{01} - h_2 = h_2 + \frac{1}{2}\cdot C_2^2 - h_2 = \frac{1}{2}\cdot C_2^2 \tag{2-17}$$

$$h_{03,rel} - h_3 = h_3 + \frac{1}{2}\cdot W_3^2 - h_3 = \frac{1}{2}\cdot W_3^2 \tag{2-18}$$

Combining eqn (2.15) with eqn (2.17) and eqn (2.16) with eqn (2.18) give

$$\zeta_S = \frac{h_2 - h_{2s}}{\frac{1}{2} \cdot C_2^2} \tag{2-19}$$

$$\zeta_R = \frac{h_3 - h_{3s}}{\frac{1}{2} \cdot W_3^2} \tag{2-20}$$

According to the thermodynamic relation, applied along a
$T \cdot ds = dh - v \cdot dp$

As mentioned before and according to the thermodynamic relation applied along a isobar ($dp = 0$) is the slope of the isobar in an h-s chart equal to the locale temperature *T*.

$$\left.\begin{aligned} T \cdot ds &= dh - v \cdot dp \\ dp &= 0 \end{aligned}\right\} \Rightarrow T = \frac{dh}{ds}$$

If the entropy change Δs is small, it can be assumed that the slop is constant and equal to the exit temperature.

$$h_2 - h_{2s} \cong (s_2 - s_1) \cdot T_2 \tag{2-21}$$

$$h_3 - h_{3s} \cong (s_3 - s_2) \cdot T_3 \tag{2-22}$$

Eqn's (2-19) to (2-22) give a new way to express the loss coefficients without any significant error, Denton [3] propose that the error will be on the order of 10^{-3}, and nothing to take care to for ordinary calculations.
The new equations are

$$\zeta_S \cong \frac{(s_2 - s_1) \cdot T_2}{\frac{1}{2} \cdot C_2^2} \tag{2-23}$$

$$\zeta_R \cong \frac{(s_3 - s_2) \cdot T_3}{\frac{1}{2} \cdot W_3^2} \tag{2-24}$$

If the loss coefficients instead are based on the ratio between the lost work potential and the total ideal isentropic work potential two other loss coefficients can be written according to

$$\xi_S = \frac{h_2 - h_{2s}}{h_{01} - h_{2s}} = \frac{h_3 - h_{3s}}{\frac{1}{2} \cdot C_{2s}^2} \tag{2-25}$$

$$\xi_R = \frac{h_3 - h_{3s}}{h_{03,rel} - h_{3s}} = \frac{h_3 - h_{3s}}{\frac{1}{2} \cdot W_{3s}^2} \tag{2-26}$$

The relation between the both loss coefficients are given by (Wei & Svensdotter 1995) and are shown in eqn (2-27) and eqn (2-28).

$$\xi_S = \frac{\zeta_S}{\zeta_S + 1} \tag{2-27}$$

$$\xi_R = \frac{\zeta_R}{\zeta_R + 1} \tag{2-28}$$

In a real turbine or test cascade it is easier to measure the change in total pressure, instead of enthalpy change. Because of this practical benefit with pressure measurements it is common to also define some loss coefficients based on the total pressure. The losses for compressible flow is defined as the loss in total pressure due to irreversibility over the actually expansion pressure as described in eqn (2.29-2.30) and shown in Figure 2.1-1.

$$Y_S = \frac{p_{01} - p_{02}}{p_{02} - p_2} \tag{2-29}$$

$$Y_R = \frac{p_{02,rel} - p_{03,rel}}{p_{03,rel} - p_3} \tag{2-30}$$

The ratio between the actual velocity and that for an isentropic expansion is defined as

$$\phi = \frac{C}{C_s}$$

And then the square expresses the ratio between the kinetic energies, and can be related to the enthalpy losses as in equation (2-31)

$$\left.\begin{aligned} \phi_S^2 &= 1 - \zeta_S \\ \phi_R^2 &= 1 - \zeta_R \end{aligned}\right\} \tag{2-31}$$

To convert the losses between pressure, enthalpy and kinetic energy eqn (2-32) from MKT 1989 [14] and eqn (2-31) can be used.

$$Y = \frac{\left[1 - \frac{\gamma - 1}{2} \cdot M_{out}^2 \cdot \left(\frac{1}{\phi^2} - 1\right)\right]^{-\left(\frac{\gamma}{\gamma - 1}\right)} - 1}{1 - \left[1 + \frac{\gamma - 1}{2} \cdot M_{out}^2\right]^{-\left(\frac{\gamma}{\gamma - 1}\right)}} \tag{2-32}$$

2.4 Alternative Conversion between Pressure and Enthalpy Loss

In eqn (2-31) it is assumed that the density at the outlet will not vary between the real and isentropic states (density at 2s and 2 for an expansion in a stator, Figure 2.1-1). In that sense the second order of density variation is not attracted any attention. Some alternative ways, probated by Lenherr [44], to convert kinetic energy loss into pressure loss are present below. First the compressible effect is not corrected for, but then a correction for the compressible effect is given. It is seen in Figure 2.4-1 that there actually are a significant difference between the two methods. In this section only the final equations are present while the full derive of the equations are present in appendix 12.1

The normal definition of a pressure loss Y between state 1 and 2 is according to eqn (2-29)

$$Y = \frac{p_{01} - p_{02}}{p_{02} - p_2} \tag{2-33}$$

Where the subscript ($_0$) stands for total states and no difference are made between the stator or rotor in term of relative or absolute reference, therefore C should be replaced by W for a rotor.
The loss is defined as

$$\mathrm{e} \equiv 1 - \phi^2 = 1 - \frac{C_2^2}{C_{2s}^2} \tag{2-34}$$

To go from a pressure to enthalpy based loss.

$$\mathrm{e} = \frac{\left(Y \cdot \left[1 - \frac{p_2}{p_{02}}\right] + 1\right)^{\frac{\gamma - 1}{\gamma}} - 1}{\left(Y \cdot \left[1 - \frac{p_2}{p_{02}}\right] + 1\right)^{\frac{\gamma - 1}{\gamma}} \cdot \left(\frac{p_{02}}{p_2}\right)^{\frac{\gamma - 1}{\gamma}} - 1} \tag{2-35}$$

Where the pressure ratio can be expressed in terms of outlet Mach number (M_{out})

$$\frac{p_{02}}{p_2} = \left[1 + \frac{\gamma - 1}{2} \cdot M_{out}^2\right]^{\frac{\gamma}{\gamma - 1}} \tag{2-36}$$

The pressure loss can be expressed explicit in terms of enthalpy loss

$$Y = \frac{\left[\frac{1}{1 - e} \cdot \left(1 - e \cdot \left[1 + \frac{\gamma - 1}{2} \cdot M_{out}^2\right]\right)\right]^{-\left(\frac{\gamma}{\gamma - 1}\right)} - 1}{1 - \left[1 + \frac{\gamma - 1}{2} \cdot M_{out}^2\right]^{-\left(\frac{\gamma}{\gamma - 1}\right)}} \tag{2-37}$$

In these equations it is still assumed that the density does not vary between the isentropic and real expansion paths final state, $\left(\rho_{2s} = \rho_2\right)$.

Definition of the new loss e'' that include the density variation is.

$$e'' = 1 - \phi''^2 = 1 - \frac{\rho_2 \cdot C_2^2}{\rho_{2s} \cdot C_{2s}^2} \tag{2-38}$$

To include this density variation the enthalpy loss e in eqn (2-37) should be replaced by equation (2-39), where eqn (2-36) can be used for a simple Mach number dependence.

$$\left(\frac{p_{02}}{p_2}\right)^{\frac{\gamma - 1}{\gamma}} \cdot e = e'' \tag{2-39}$$

Even if the differences between the two models are not huge there is a clear divergence as the Mach number increases towards or even above one or if the loss component increases as seen for off-design condition at part load. Figure (2.4-1) shows the trend of the both versions with a Mach number of 0.9, ϕ^2 at the x-axis and the pressure loss at y-axis.

A numerical comparison of the influence on the total efficiency for a simulation is present in chapter (8.1).

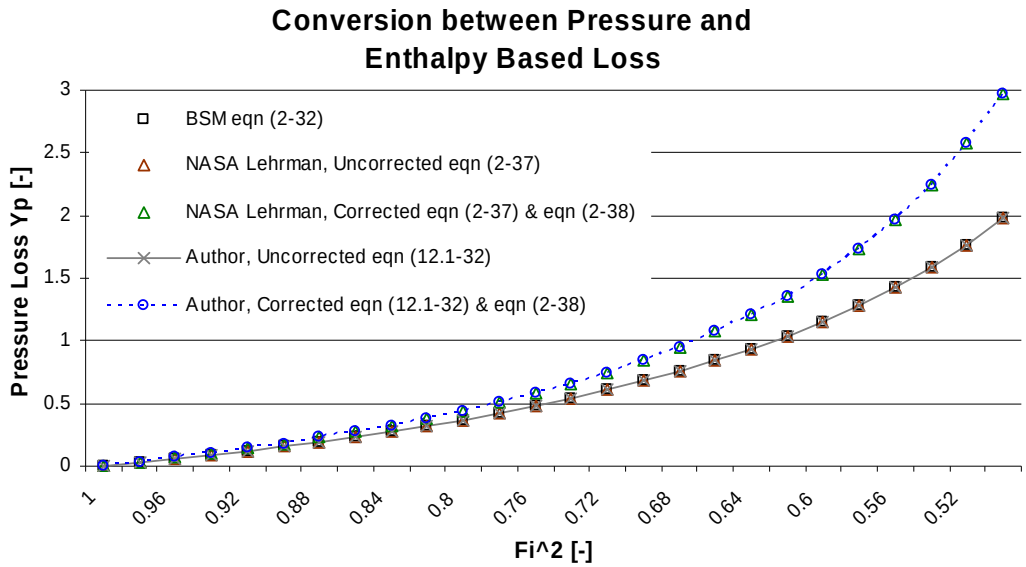

Figure 2.4-1 Compare different models conversions between losses based on kinetic energy and pressure. Both models that pay attention to the second order of density variation and models that do not are seen.

2.5 Way a Need of Loss Correlations in 1D?

When a new or an improvement of an existing blade design should be done some simplified but quite accurate engineering tools are needed to make a fast estimation of the influence on stage and total efficiency that any change of geometric and/or flow field parameter will have. Of course the analyze could be done with a full three dimensional CFD solution using a good turbulence model or DNS solution, but in a early design step the geometrical parameter are not determined yet so a CFD run for all possible geometry would be to expansive in terms of both time and money.
Instead the engineering procedure is an attempt to model the stage efficiency with only a few basic blade parameters that will be determined in an early stage of design and that do not require vast calculation power. This is done by a mean line velocity triangle calculation where it is assumed that the thermodynamic nature of the working fluid can be represented accurate by a midspan gas path and the establishing of loss models that predict the enthalpy or pressure losses over the stage. Even if the loss models has been reviewed and improved for more than a half century the models for primary the secondary, off-design, tip leakage and Mach number effect are still far from complete. The fact that it every year are present a lot of reports and paper at conferences around the world, show that it a

2.6 Flow Field in a Blade Row

The aim of this section is to give a brief physical description and understanding of the different phenomenon that give entropy creation through a turbine stage. The sources of entropy generation are viscous friction (including surface drag, mixing, and shock loss shear work) heat transfer across finite temperature difference and processes that are not in equilibrium.

The flow field in a turbine is a very complicated and a not yet fully understood phenomenon. Just to mention some of its nature it can be said that it is three dimensional, unsteady, both laminar and turbulent at different location at the same time and with high (some time supersonic) velocity in the free stream. There will also be many vortexes, great pressure differences and a multiple length scale, all from the integral length scale at an order of the pitch (s), down to the smallest kolmogorov length scales in the highly turbulent bounder layer where the kinetic energy is dissipated to heat by viscous shearing. Flow could separate from the boundary layer and sometime also reattach in a later section, if the flow is accelerating enough downstream, and in that way it creates separation bubbles and a reverse flow structure.

There is a primary flow field through the blade row, which describe the mean flow path of the flow. Overlapping on this primary flow there will be a secondary flow field as can be seen in Figure 2.6-1. Some of the reasons for this secondary flow are interaction between pressure gradient, centrifugal forces and incidence angle (i), that is the difference between the incoming flow angle and the inlet blade angle. A leakage jet of flow across the tip clearance at a blade will also disturb the primary flow. The path for the tip leakage flow can alternatively be from the pressure to the suction side for unshrouded blades or from upstream to downstream of a blade for shrouded blades, (see chapter 5 for a more complete description).

The wake that creates at the end of the trailing edge will not be entirely mixed out before it reach and interact with the next blade row. Therefore an unsteady condition will be present that can be difficult to consider in cascade tests. If the Mach number locally exceeds unity as for a transonic blade there will also be shockwaves present at the back of the blades suction surface.

All these complex flow structure are difficult to catch in a normal cascade test structure, that are either based on linear cascade with two-dimensional blade structure, a not rotating annular, or on a full circular annular cascade with three-dimensional blades. Even if the later test structure is much more complicated it still does not catch the unsteady interaction between the different rotor and stator blades as in a real turbine.

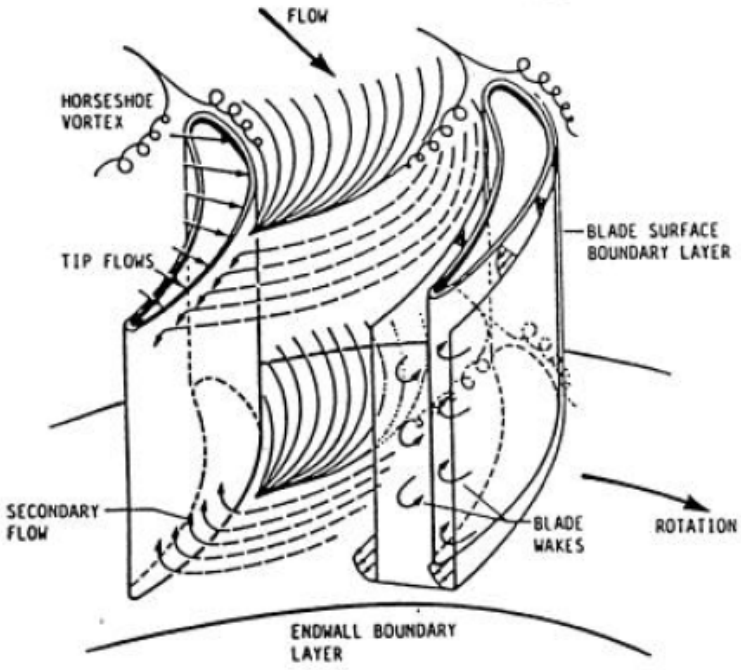

Figure 2.6-1: Flow field in a rotor row from Denton [3].

When the flow in the boundary layer close to the endwall enters a blade row it will feel almost the same great pressure gradient between the pressure and suction surface as the main flow. At the same time will the velocity be lower in the boundary layer. With this knowledge combined with Euler-n equation (2.40), the assumption of inviscid flow and no significant body forces (according to page 2-3 [4]), it is clear that the boundary layer flow will turn around a smaller radius, compare to the main flow (Figure 2.6-2).

Euler-n equation

$$\frac{1}{\rho}\frac{\partial p}{\partial n} = \frac{C^2}{r} \qquad (2\text{-}40)$$

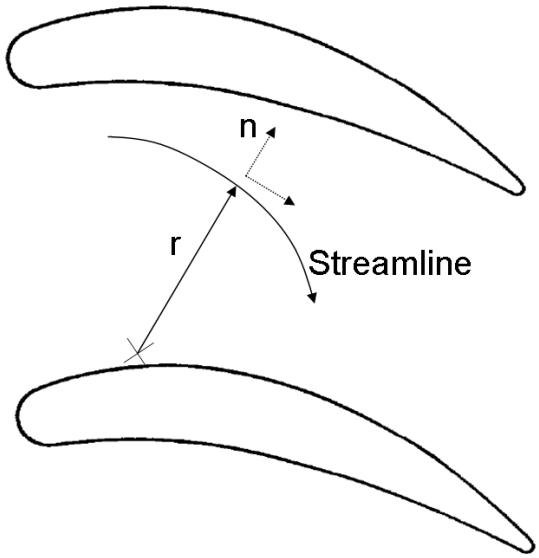

Figure 2.6-2: Secondary turning of the fluid streamline in boundary layer for a blade row, where n is normal to the streamline and r is the locally radius of curvature for the streamline seen at a section of constant blade radius.

It is now clear that keeping the left side constant will provide a smaller radius for decreasing C inside the boundary layer to fulfill the Euler-n equation. There will therefore be a transport of mass from the pressure surface towards the suction side of next blade along the endwall inside the stator and rotor row. To fulfill the continuity equation it creates a recirculation zone closer to the middle and two passage vortexes is created, as is illustrated in Figure 2.6-1 and 2.6-3.

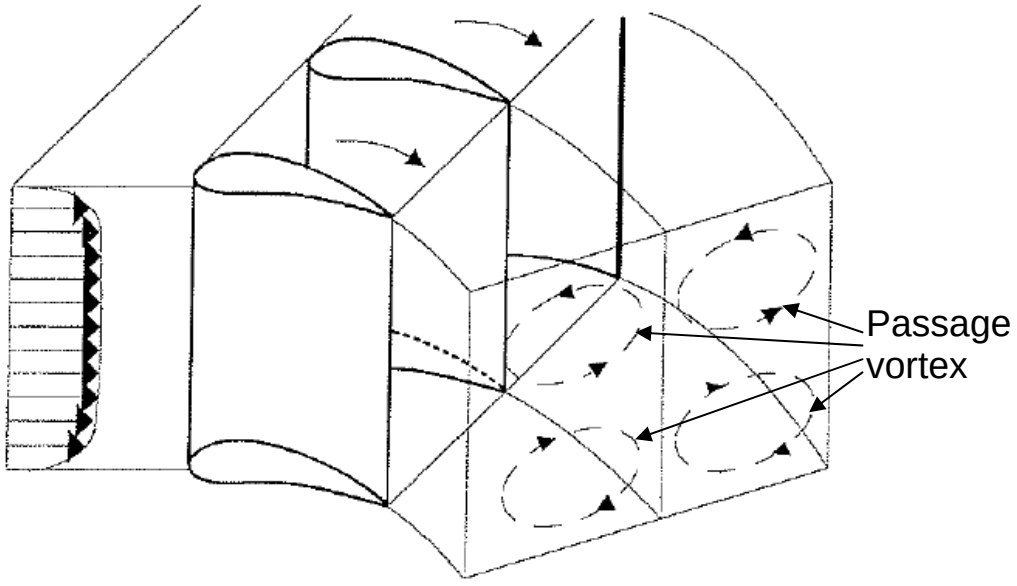

Figure 2.6-3 Passage vortex as a result of lower velocity in boundary layer but nearly the same pressure gradient as in the free flow, see eqn (2-40) , [4] or [46]

Another vortex commonly referred to is the horseshoe or leading edge vortex. The physical explanation to its creation is that the incoming boundary layer when it is approaching the leading edge of the blade is forced to stagnation and some reverse

flow. The exact shape of this phenomenon is not clear, but it will schematically look like Figure 2.6-4 from [34] (originally from Marchal and Sieverding 1977).

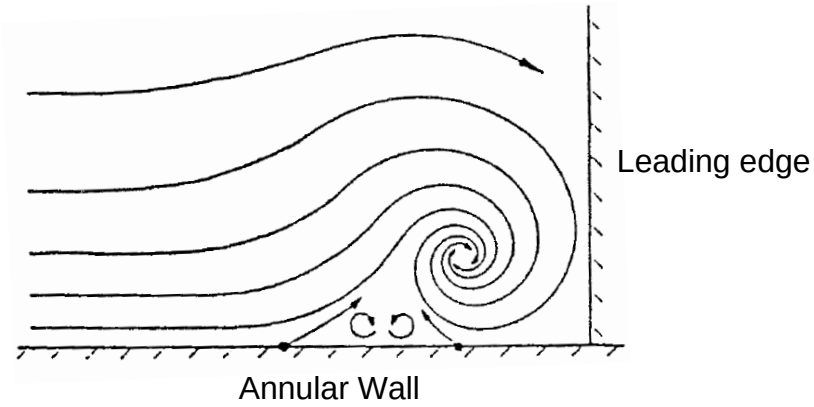

Figure 2.6-4: Formation of leading edge horseshoe vortex [34] (originally from Marchal and Sieverding 1977) or see Sieverding [46]

The flow will role up like a cylinder and then be bend across the leading edge and creating one clockwise rotating and one co-counter rotating vortex at pressure side respective suction side. At the pressure side the horseshoe vortex is rotating clockwise and just strengthens the passage vortex as it is driven by the pressure gradient across the passage and end up at the suction side for next blade. At the suction side the horseshoe vortex and passage vortex is rotating in opposite directions. The interaction between these both can be seen in Figure 2.6-5 originally from Klein and in Figure 2.6-6 originally from Langston. Here it is shown how the leading edge vortex creates a counter rotating vortex at the corner of the suctionside. Note that the flow description given by Klein respectively Langston are roughly the same, but are not exactly equally described, that is because the flow is so complex that it is still not fully understood.

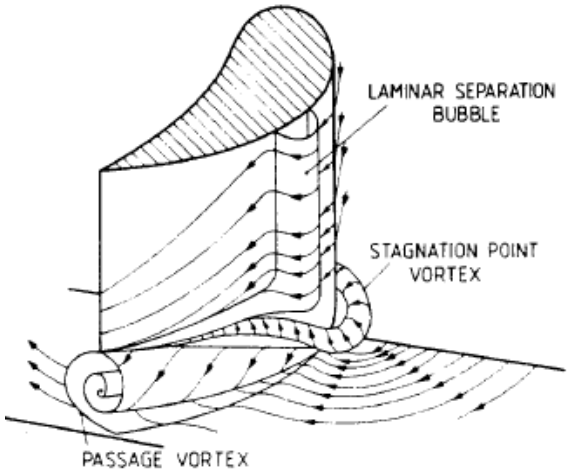

Figure 2.6-5: Interaction between passage vortex and leading edge vortex described by Klein, see [34]

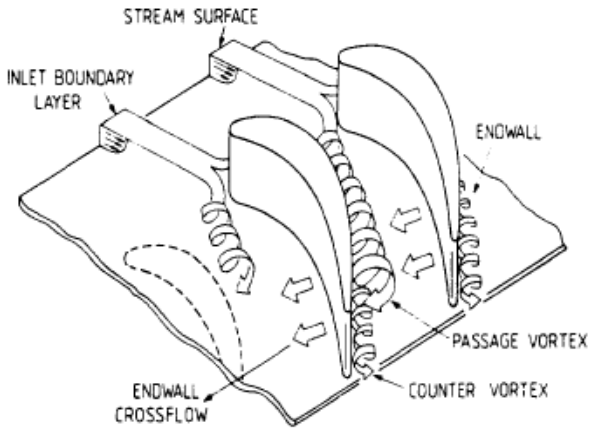

Figure 2.6-6: Illustrate when the leading edge vortex create a counter vortex at the corner of the suctionside described by Langston, see [34]

As the boundary layer flow is driven across the passage from pressure to suction side as Figure 2.6-1 shows, a new very thin and initially laminar boundary layer is created at the backside of the line of separation. Denton [3] proposed that the leading edge vortex would be trapped between two liftoff lines going from the leading edge of one blade towards the trailing edge of the next coming blade. This is discussed more in chapter 3.7.

For the tip leakage flow there will always be a gap between the rotor and the surrounding casing, and between the stator and axel. For the stator this gap is at a much lower radius, and because these blades are not rotating the sealing can be made more advanced and almost make these losses negligible in an aerodynamic sense. The rotor gap leakage will primary consist of air forced by either the pressure difference between up and down stream of the blade or the pressure difference between the pressure and suction side, depending on if the blade tip is shrouded or not. For unshrouded blades this flow across the tip creates a counter rotating vortex on the suction side that will interact with the passage vortex and reinforce it. More of these phenomena can be read in chapter 2.8.2 and 5.1)

2.7 Nature of the Loss Sources

The true nature of all losses may at a microscopic level be referred back to pure viscous shearing that result in an internal energy rise [41]. At a macroscopic level the loss may also be divided into for example four categories as, surface drag, mixing, shock loss and shear work. In this section a simplified description of each of these loss sources will be given, where they are treated as separate losses.

2.7.1 Surface Drag

If the blade is approximated in two-dimensions by a flat plate with the pitch (s) and there is a uniform and incompressible flow condition upstream at state 1. This means that the total pressure, static pressure and velocity at inlet are constant across the whole pitch, denoted with p_{01}, p_1 and C_1. At the trailing edge of the blade (plate) is the velocity not uniform anymore because of the surface drag along the surface of the plate, but still will the static pressure be approximately constant, the properties are denoted as p_{02}, p_2 and C_2. As the flow then continues far downstream it will return to a

uniform condition p_{03}, p_3 and C_3. This is schematically illustrated in Figure 2.7-1 below.

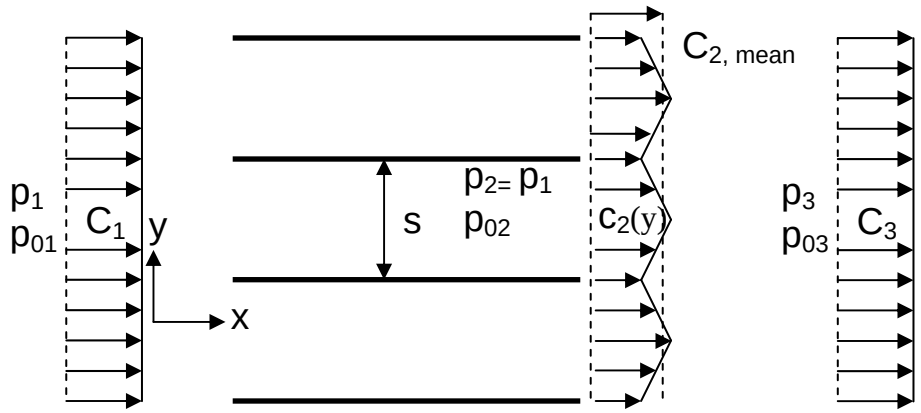

Figure 2.7-1: Surface drag along a flat plate with uniform inlet (1) and downstream (3) condition where the static pressure at station 2 is equal to the inlet condition at station 1.

The assumption of incompressible flow give with the use of continuity equation that the upstream and downstream velocity is equal, C_1=C_3.

If the total displacement thickness in a blade passage is defined as

$$\delta^* = \int_0^s (1 - \frac{c_2(y)}{C_{BL-edge}}) \cdot dy$$

And represent the amount that the thickness of the plate must be increased so that the fictitious uniform inviscid flow has the same mass flow rate as the viscous. Then an equation for the mean velocity C_2 may be derived with the help of continuity equation as.

$$C_1 \cdot s = C_3 \cdot s = \int_0^s c_2 \cdot dy = C_{2,m} \cdot (s - \delta^*)$$

The total force acting on the both sides of one blade because of surface drag is then the difference in static pressure over the span.

$$F = (p_1 - p_3) \cdot s$$

Where the static pressures, because the equal velocity, can be replaced by the total pressure according to

$$F = (p_{01} - p_{03}) \cdot s$$

The uniform distribution also means that the mass average value is equal to the total and therefore the loss can be obtained with only the knowledge of the surface drag.
This derive does not describe the loss mechanism itself but give a way to obtain it from measurements.

2.7.2 Mixing

In a mixing process normally the static pressure will rise at the cost of a decrease in total pressure, as for example is seen in the irreversible mixing process after a sudden increase in a flow area. That is a mixing between two uniform flow conditions, one with high velocity and one with low. Another uniform flow condition that not necessarily causes a large mixing loss is when the high fluid velocity at the back of the blade suction side decelerate from the peak to outlet velocity in a controlled way without any separation. If the flow on the other hand is separated and not reattaches again due to rapid deceleration at the back or a high positive incidence a wake will be present at the trailing edge (TE). For the later case where there is a wake present at TE or as for the tip leakage flow can not the kinetic energy in the leakage flow be recovered to static pressure or work and is instead lost. For the mixing loss the essential condition is the no uniform flow condition, and the ability to separate between these who leads to mixing and these whose not.

2.7.3 Shock Loss

Across a shockwave the flow will undergo a sudden deceleration with a present loss in stagnation press while the static pressure will rise. There will be a higher loss seen for a single and strong shockwave compare to if the total deceleration instead were divided between a series of smaller shocks where only a slightly overall total pressure loss is seen. The single shock is a typical irreversible process while the later is more close to approach a reversible process (even if so is not the case). A controlled shock at a not too high Mach number is actually a quite good and efficient way to decelerate the flow. Therefore is a controlled shock the key to design supersonic blade rows. If the shock on the other hand is not controlled it can lead to separation of the boundary layer and creation of big losses associated with this separation.

2.7.4 Shear Work

As mentioned before is actually shear work the source of all the losses and seen everywhere where there is a velocity difference between two fluids. It is therefore the process associated with energy dissipation in the smallest kolmogorov scale in turbulence. In this section are only steep gradients considered, and is therefore primary in the region of boundary layer, inside wakes and the boundary between a separated flow and the free stream. In a one-dimensional approximation the momentum equation along a streamline is given by

$$\rho \cdot C \cdot \frac{\partial C}{\partial x} = \frac{\partial \tau}{\partial y} - \frac{\partial p}{\partial x}$$

According to Figure 2.7-2

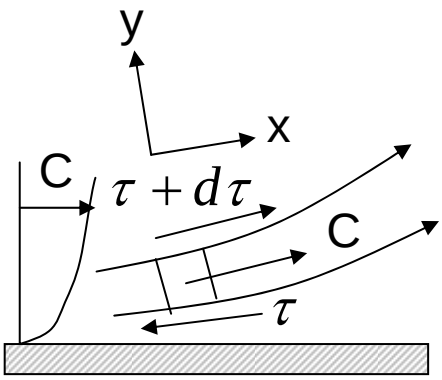

Figure 2.7-2: The shear stresses acting on a fluid element along a streamline

The energy balance of the fluid element including the heat transfer q in y-direction is.

$$\rho \cdot C \cdot \frac{\partial h_0}{\partial x} = -\frac{\partial q}{\partial y} + \frac{\partial (\tau \cdot C)}{\partial y}$$

In combination with the thermodynamic relation $T \cdot ds = dh - \nu \cdot dp$ the result is.

$$T \cdot \frac{\partial s}{\partial x} = -\frac{1}{\rho} \cdot \frac{\partial \tau}{\partial y}$$

And after multiplication with the velocity C the rate of entropy change in the fluid particle can be expressed according to [41] as

$$T \cdot \frac{Ds}{Dt} = -\frac{C \cdot \partial \tau}{\rho \cdot \partial y}$$

Or in a three-dimensional flow as

$$T \cdot \frac{Ds}{Dt} = -\frac{C_i \cdot \partial \tau_{i,j}}{\rho \cdot \partial x_i}$$

2.8 Classification of the Losses

To handle the many different flow phenomena the overall loss in a row will be divided into a number of different regions. These regions are then correlated separately and finally summed up to a total loss for the rotor, stator and total stage. The number of different categories, and which parameters that are included in the correlations both may and will be different in the author's different models, as would be seen in this report.

Sections 2.8-1 to 2.8-5 describe the normal loss categories and give a short explanation of what they are treating. It should be noted that it is only an example and not a recommendation or absolute true classification that is given here.

2.8.1 Profile Loss

This is the loss that occurs on the blade surface due to increasing boundary layer, surface friction and flow blockage as the passage area is decreased because of an increase of the surface boundary layer thickness. It also includes the separation of boundary layer along the blade surface, and in some cases the trailing edge separation and mixing downstream.

Some general trends proposed by Ainley and Mathieson in [5] is that the profile loss in a impulse stage will be higher compare to a reaction stage because the turning will be higher when $\alpha_{in} = \alpha_{out}$ for the stator and then give a bigger wet surface area. Observe that the definition used is according to MKT where both the inlet and outlet angles are positive. The surface area will also increase as the chord increase, but at the same time that gives an ability to reduce the rate of diffusion along the suction surface and risk of separation, so a trade of between diffusion losses and friction loses as function of the pitch to chord ratio is needed. A higher acceleration along the blade passage will prevent separation and give thinner boundary layer, resulting in less surface losses. AM [5] propose that a high outlet Mach number will reduce the profile losses with about 10 percent compare to a lower value, but no exact value for the low Mach number case were given. (An investigation of the Mach number influence on the loss is seen in chapter 7.)

Positive incidence will give a high increase in the profile loss but also negative incidence play an important roll for some blade profiles. At positive incidence it creates a rapid acceleration close to the leading edge suction surface, followed by high diffusion and boundary layer growth. Correction of the profile loss for Reynolds number is often made, and normally the outlet Mach number is taken in consideration as well. According to Denton [3] the enthalpy generation is proportional to the velocity to a power of three, and therefore the greatest part of the profile loss created at the suction surface.

2.8.2 Secondary Loss

Secondary loss is the loss caused by the viscous and turbulent mixing and dissipation of energy when secondary flows and vortices are mixed together with the main flow and wall boundary layer, by some authors called endwall loss. Sometime it is divided into losses inside the blade row (secondary loss) and the loss that occur in the space between the blade rows along the annular wall (annulus loss). The nature of this loss is complicated to understand and describe as mentioned above. Since it stands for an important ratio of the overall losses it is worth a great effort in the attempt to correlate it accurate.

Important parameters are the blade geometry, Mach number and inlet boundary layer. The believed most important blade shape are the turning angle, aspect ratio, pitch to chord ratio, wedge angle and diameter for the leading edge. For a high turning angle the secondary flow will increase, as the blade load and driving pressure gradient increases. The pitch to chord ratio also influence the blade loading, and for a high aspect ratio the endwall flow will have less effect on the overall flow field, as the main part is present at the endwall. The effect of Mach number is that a high acceleration reduces the boundary layer thickness that then reduces the area of secondary losses in the boundary layer. For a transonic blade profile is the Mach number complex dependence upon the blade shape and local Mach number not clearly investigated.

2.8.3 Tip Clearance Loss

Here is only a brief description given, and a more detailed can be seen in chapter 5.1 that consider the tip leakage phenomena and possible treatments.

For a shrouded blade it could be thought of as that the leakage mass flow will not pass through the blade row at all and could therefore not contribute to any useful work. Instead the difference in speed and direction between the leakage and main flow will lead to dissipation of energy and increased entropy creation as it remixes whit the main flow. The inlet flow angle for the next coming blade will also be affected.

For an unshrouded blade the leakage is instead from the pressure to suction surface of the blade. And except the entropy generation and flow turning it also creates an unloading of the tip of the blade and increased secondary flow, so less work can be extracted.

The most important parameters are the relative tip clearance, incoming boundary layer thickness, blade load, and incidence angle.

2.8.4 Trailing Edge Loss

According to AM [5] the finite thickness of the trailing edge at a blade will causes the flow to separate at both the pressure and suction surface close to the trailing edge and create a recirculation zone as can be seen in Figure (2.6-1). In this wake will there be a lower pressure compared to the free stream called back pressure (p_b), and a high velocity gradient is seen between the free stream and the turbulent wake. The dissipation of energy will then be high as the wake is mixing out downstream. The momentum thickness at trailing edge that reduce the effective flow area, and the fact that all mixing would not be completed before it reaches the next blade row also needs to be taken into consideration. At high outlet flow angles a greater ratio of the shaft area will be covered by the wake and then increases the losses.

Substantial parameters are back pressure, outlet flow angle, pitch, trailing edge thickness, Mach number, momentum thickness and if injection of cooling air through a slit in the trailing edge.

2.8.5 Shockwave Loss

Across a shockwave there will be a sudden increase in static pressure, boundary layer thickness and viscous dissipation of energy. To take consideration of this loss a separate shock loss parameter sometimes is introduced and included in the profile loss. The most important parameters are Mach number and Reynolds number [2]. One positive effect of a shock is that if it does not create a massive and instant separation, the energy in the boundary layer increases and therefore withstand a higher rate of diffusion without separation (private conversation with Magnus Genrup). The primary parameters of import are not totally clear, but at least are the suction surface curvature, uncovered turning and local Mach number crucial.

3 Description of Different Loss Models

This chapter aims to give a review of different loss models in axial turbines. The included loss models were originally given by D. G. Ainley & G. C. R. Mathieson (AM), J. Dunham & P. M. Came (DC), S. C. Kacker & U. Okapuu (KO), H. R. M. Craig & H. J. A. Cox (CC), M. Kh. Mukhatarov & V. I. Krichakin (MuKr), M. W. Benner, S. A. Sjolander & S. H. Moustapha (BSM), and I. Mamaev & A. G. Klebanov (MaKl). Most effort will be on the description of secondary flow (S), off-design and Tip leakage losses, but some other groups as profile (P) and trailing edge (TE) losses will also be touch because they are sometime included or used as a datum point for off-design loss correlations. The tip leakage loss from some of the author is described separately in chapter 5. The angle definition used is the authors originally if nothing else is stated.

3.1 Ainley & Mathieson

Ainley and Mathieson (AM) is a well known legends in derive of turbine loss correlation. They have both publish a number of papers relating to the topic of axial gas turbines. This section is, if nothing else is stated, based on reference [7] with improvement from [8]. Note that when these both papers were written 1955 and 1957 they were based on experimental test data from blade design and measurement equipment from that time. Most of the experimental data results are from National Gas Turbine Establishment and collaborating firms, and the turbine blades were of circular-arc, parabolic-arc and that times "conventional" type [7]. Also most of the test data are with low exit Mach number (M_{out}), as was common in the 1950's. That are blade profiles that whit the aerodynamic acknowledge today's would be classified as horrible.

When establishing a new correlation between test results and the supposed important parameters there always need to be a tradeoff between accuracy and the complexities of included parameters. AM aim was to be able to predict the total pressure loss coefficient (Y_{tot}) within ± 15 percent, mean gas exit angle within an error of $\pm 0.02 \cdot \cos^{-1}(o/s)$ and overall efficiency for the stage within ± 2 percent of the true value. This accuracy is supposed to be achieved for comparable blade designs by the authors.

The losses included are profile loss, tip clearance loss, secondary loss and off-design loss due to flow angle incidence (i). The profile loss includes corrections for trailing edge thickness (TE), variation in both Reynolds number (Re) and outlet Mach number (M_{out}), as discussed below. Experimental results for tip leakage were limited so because of that the correlations for shrouded and unshrouded blades are uncertain. The rest of the loss between measured and estimated value was put as a secondary loss term including both secondary and annulus loss with only little physical coupling. For off-design calculation only the profile loss is corrected while the other losses are kept constant.

The correlations should be calculated with the arithmetic mean diameter between inlet and outlet of a blade row and the angles are defined from the axial direction, see the blade terminology.

3.1.1 Profile Loss

When the values of pitch to chord (s/c) ratio and reaction are decided can the profile loss at design condition initially read from chart 12.3-1 and 12.3-2 (impulse and reaction blade). These charts are for a blade geometry with $t_{max}/c = 0.2$, outlet Mach number less then 0.5 and Reynolds number equal to $5 \cdot 10^5$. For intermediate reaction grade a linear interpolation value of these two extremes are used. Corrections for any difference from the bas profiles thickness to chord ratio t_{max}/c and inlet blade angle to outlet flow angle $\alpha_{in}' / \alpha_{out}$ are then done. The valid range for thickness to chord ratio is $0.15 \le t/c \le 0.25$ and outside this range the end values at 0.15 or 0.25 are used, but with the knowledge of its limitation.

The profile loss at design point is then given by eqn (3-1) as

$$Y_{P(i=0)} = \left(Y_{P(\alpha' in=0)} + (\frac{\alpha'_{in}}{\alpha_{out}})^2 \cdot \left[Y_{P(\alpha' in=\alpha out)} - Y_{P(\alpha' in=0)} \right] \right) \left(\frac{t/c}{0.2} \right)^{\frac{-\alpha'_{in}}{\alpha_{out}}} \qquad (3\text{-}1)$$

In ref [7] eqn (3-1) was given without any correction for inlet blade angle to outlet flow angle ratio and the thickness to chord ratio correction as can be seen in the last term of (3-1), but it was added later by themselves in [8].

$$\left(\frac{t/c}{0.2} \right)^{\frac{-\alpha'_{in}}{\alpha_{out}}}$$

When study the influence of incidence they found that for blades with high mean flow acceleration there is a broader incidence range with low profile loss. It is due to the fact that the boundary layer is more likely to be reattached compare to a low reaction blade. They also found that in a small incidence range the profile loss has a significant decreased loss level. The reason for this sudden decrease in loss is expected to be a region with a large level of unseparated laminar boundary layer. In a real turbine with high turbulence level at the inlet this laminar flow is unexpected to be achieve and for that reason it is ignored as a design goal. A chart showing these trends is seen in Figure 12.3-3.

A stalling incidence (i_s) is defined as the incidence where the profile loss equals the double minimum profile loss.

$$Y_{P(i_s)} = 2 \cdot Y_{P(i=0)} \qquad (3\text{-}2)$$

The variation of i_s and α_{out} with s/c and $\alpha'_{in} / \alpha_{out}$ were determined for a wide range of that time's blade profiles, and are shown in Figure 12.3-4, 12.3-5 and 12.3.-6 with a s/c of 0.75 as a datum point. From these three charts the positive stalling incidence i_s

for any s/c ratio is determined with α_{out}, $\alpha'_{in}/\alpha_{out}$ and the actual s/c ratio as input parameters.

The procedure is.

1 With $\alpha_{out\,(s/c=0.75)}$ and s/c the value of α_{out} is read from Figure 12.3-4

2 From Figure 12.3-5 $i_{s(s/c=0.75)}$ is read with the input parameters α_{out} and $\alpha'_{in}/\alpha_{out,(s/c=0.75)}$

3 Finally Figure 12.3-6 give the value of $i_s = \Delta i + i_{s,(s/c=0.75)}$

The accuracy of this correlation was supposed to be within ± 3 percent, at the time of publishing [7], [8].

In [7] AM propose that a single curve can be used to relate the profile loss at no incidence to the actual incidence with only the ratio between incidence and stalling incidence (i/i_s) determined from Figure 12.3-3 down to i/i_s equal to -2.0. But as AM mentions in [7], and stated in [8] the recommendation was instead to use a corrected chart where the negative incidence loss is increasing more rapid, as seen in Figure 12.3-7. The idea behind the correction was to under the assumption of a constant secondary loss, or more exactly a constant value of λ as explained in section 3.1.3, correct the predicted profile loss so it matches the total measured loss in a turbine blade row. The accuracy of the prediction is given to be ± 15 percent of the loss, in a range down to i/i_s of -2.0 [7]. Both the corrected and uncorrected curves are shown in Figure 12.3-7, where the thick line is corrected to data from real turbines, the dotted is uncorrected and based on data from cascade measurements.

A number of corrections to the profile loss should also be made for any difference from the datum point with $s/c = 0.75$, straight back between the throat and trailing edge, $\mathrm{Re} = 2 \cdot 10^5$, and for the fact of a trailing edge thickness and Mach number variation. The recommended procedures are explained below one by one.

Even if the detailed experimental material were few, some approximately trends in the region $5 \cdot 10^4 \le \mathrm{Re} \le 2 \cdot 10^5$ were seen where Re is based on the real chord and outlet condition for density, velocity and viscosity. The experiments were done with T6 and C7 sections profile, for eight different geometry and over variation of Re, (see the text and fig 10 in ref [7] for more details). The relative loss $Y_P / Y_{P(\mathrm{Re}=2\cdot 10^5)}$ for all the profiles is plotted against Re and illustrated in Figure 12.3-11. The general trend is that for decrees in Re the loss are increased, and this appears to become more rapid for Re below$1 \cdot 10^5$. The physical explanation to this is that for a lower Reynolds numbers the boundary layer thickness grows and tend to separate at the back of the suction surface.

The effect of Mach number on the profile loss was only very briefly discussed. The primary reason for this was that the construction material of that time could not handle the high temperature and stresses needed to archive a Mach number exceeding 1.0. Some cascade tests were still done that shows a slightly increase in loss when the peak Mach number at suction surface exceeds unity due to the thickening of boundary layer across the shockwave, and this exit Mach number is defined as the critical Mach number, M_c. For any increase above M_c the increase in losses were believed to be

dependent on the curvature between the throat and trailing edge, def in Figure 12.3-8, and Figure 12a in [7] show these trends. It should be remembered that this conclusion is very approximately and is discussed more in chapter 7.

3.1.2 Outlet Flow Angle

To calculate the outlet flow angle the correlation is divided into different regions depending on M and Re. For outlet Mach number of unity, Re above $2 \cdot 10^5$ and a straight back after the throat can the outlet flow angle be correlated by the area of the throat (A_o) and outlet (A_{out}). This can be approximated by the throat to pitch ratio (o/s) according to eqn (3-3).

$$\alpha_{out} = \cos^{-1}(A_o / A_{out}) \approx \cos^{-1}(o/s) \tag{3-3}$$

For outlet Mach number below 0.5 ($0 \le M_{out} \le 0.5$), high Reynolds number ($\mathrm{Re} \ge 2 \cdot 10^5$) and a curved suction surface after the throat the outlet flow angle increase and can therefore not be correlated by eqn (3-3) anymore. Instead eqn (3-4) should be used, that involves the mean radius of curvature at the back (e).

$$\left.\begin{aligned} &\alpha_{out} = \alpha^* - 4 \cdot (s/e) \\ &\alpha^* = -11.15 + 1.154 \cdot \cos^{-1}(o/s) \\ &e = j^2/(8 \cdot z) \end{aligned}\right\} \Rightarrow$$

$$\alpha_{out} = -11.15 + 1.154 \cdot \cos^{-1}(o/s) - 4 \cdot \left(s / j^2/(8 \cdot z)\right) \tag{3-4}$$

where j and z are illustrated in Figure 12.3-8.

If instead M is high the deviation angle is affected by the curvature (e) because the high losses associated with separate for M_{out} close to 1. The correction to this is shown in Figure 12.3-10.

When the Reynolds number is decreased the boundary layer thickness and area of separated flow at the suction surfaces back will increase and then reduce the effective outlet flow angle. Figure 12.3-11 shows the relation between $\alpha_{out} - \alpha_{out,(\mathrm{Re}=2\cdot10^5)}$ and Re. The tip clearance (that is defined and discussed more in section 3.1.4) also influences the outlet flow angle when its different flow angle mixes with the mainstream. The equation to handle this for Mach number less then 0.5 is shown in eqn (3-5) and for Mach number close to unity eqn (3-3) can be used where the tip clearance is involved in A_t, see eqn (3-6)

$$\alpha_{out,new} = \tan^{-1}\left\{\begin{aligned} &\left[1 - X \cdot (k/h) \cdot \frac{\cos(\alpha'_{in})}{\cos(\alpha_{out})}\right] \cdot \tan(\alpha_{out}) + \\ &+ X \cdot (k/h) \cdot \frac{\cos(\alpha'_{in})}{\cos(\alpha_{out})} \cdot \tan(\alpha'_{in}) \end{aligned}\right\} \tag{3-5}$$

$$for\ M_{out} < 0.5$$

$$X = \begin{cases} 1.35 \text{ for unshrouded} \\ 0.7 \text{ for shrouded} \end{cases}$$

$$k = \text{tip clearance}$$

$$h = \text{blade hight}$$

Equation (3.5) is from ref [8] and is slightly updated compare to the original shown in ref [7].

$$A_{o,new} = A_o\left(1-(k/h)\right) + A_k \text{ for unshrouded}$$
$$A_{o,new} = A_o + A_k \text{ for shrouded} \qquad (3\text{-}6)$$
$$A_k = \text{leakage area}$$

Another method to treat the leakage flow can also be found in [7].
To find the final outlet flow angle for Mach number between 0.5 and 1.0 a linear interpolation can be used.

3.1.3 Secondary Loss

To make correction for the secondary loss that was assumed by AM to mainly be present at the blade ends. AM begin with an assumption of none tip clearance and that the end wall region largely will depend upon the thickness of the boundary layer. From this assumptions can it be seen that the secondary loss will be inverse proportional to the span height ($\text{loss} \propto 1/h$), a trend that agree well with their measurements. The stated a theoretic relation for drag caused by secondary flow that initial was from Carter (1948), see eqn (3) in [7].
The empirical law for secondary loss is

$$C_{D,s} = \lambda \cdot \frac{C_L^{\,2}}{s/c} \qquad (3\text{-}7)$$

C_L is the lift parameter [7] and can be derived from circulation

$$C_L = 2 \cdot \frac{s}{c}\left(\tan(\alpha_{in}) - \tan(\alpha_{out})\right) \cdot \cos(\alpha_m) \qquad (3\text{-}8)$$

Where the constant λ is determine from measurements and is dependent upon the velocity distributions, flow turning, and boundary layer thickness. The trend for λ is to increase with decreasing acceleration through the blade row and as the boundary layer where much of the secondary flow develops increases. From Figure 12.3-14 can a experimental value of λ be read as a function of

$$\frac{\left(A_{in}/A_{out}\right)^2}{1 + r_{hub}/r_{tip}}$$

Where A_{in} and A_{out} is the inlet and outlet flow area from the row normal to the direction of the flow and where r_{hub}, r_{tip} are the inside and outside radius, referred to as hub/tip ratio. With eqn (3-7) and assumption of incompressible flow an equation for the pressure loss can be derived as eqn (3-9), for the complete procedure see [9].

$$\left.\begin{aligned} Y_s &= C_{D,s} \cdot \frac{\cos^2(\alpha_{out})}{\cos^3(\alpha_m)} \cdot \frac{1}{s/c} \\ C_{D,s} &= \lambda \cdot \frac{{C_L}^2}{s/c} \end{aligned}\right\} \Rightarrow$$

$$Y_s = \lambda \cdot \frac{\cos^2(\alpha_{out})}{\cos^3(\alpha_m)} \frac{{C_L}^2}{(s/c)^2} = \lambda \cdot Z \qquad (3\text{-}9)$$

Where Z is Ainley & Mathieson's well known loading parameter.

Eqn (3-9) in eqn (3-8) $\Rightarrow$

$$Y_s = \lambda \cdot \frac{\cos^2(\alpha_{out})}{\cos^3(\alpha_m)} \cdot \left[\frac{2 \cdot \frac{s}{c} \left(\tan(\alpha_{in}) - \tan(\alpha_{out}) \right) \cdot \tan(\alpha_m)}{(s/c)} \right]^2 =$$

$$Y_s = 4 \cdot \lambda \cdot \frac{\cos^2(\alpha_{out})}{\cos(\alpha_m)} \left(\tan(\alpha_{in}) - \tan(\alpha_{out}) \right)^2 \qquad (3\text{-}10)$$

Where the mean angle represent the normal direction to the total force acting on a blade and is defined as

$$\alpha_m = \tan^{-1}\left[\frac{1}{2} \left(\tan(\alpha_{in}) + \tan(\alpha_{out}) \right) \right] \qquad (3\text{-}11)$$

3.1.4 Tip Leakage Loss

Because the lack in accurate test data concerning tip leakage from measurements in open literature as AM argued for in [7], they only give two simple theoretic equation. These equations for the tip leakage loss that they assume would be justifiable until more accurate data had been published. To treat both shrouded and unshrouded blades they simply assumed that the more curved and three-dimensional flow path in a single sealed shrouded blade row would only give half the leakage mass flow compare to an unshrouded. The equation is given as

$$C_{D,TC} = B \cdot \frac{{C_L}^2}{s/c} \cdot (k/h) \qquad (3\text{-}12)$$

$$\text{Where } B = \begin{cases} 0.5 \text{ for unshrouded} \\ 0.25 \text{ for shrouded, or even less for a advanced shroude with multiple seals} \end{cases}$$

k is tip clearance or minimum area in the shroud. With the same procedure as used for the secondary loss eqn (3-14) that expressing the tip leakage can be derived

$$Y_{TC} = C_{D,TC} \cdot \frac{\cos^2(\alpha_{out})}{\cos^3(\alpha_m)} \cdot \frac{1}{s/c} \tag{3-13}$$

Eqn (3-12) and eqn (3-9) in eqn (3-13)

$$Y_{TC} = B \cdot C_L{}^2 \cdot \frac{\cos^2(\alpha_{out})}{\cos^3(\alpha_m)} \cdot \frac{(k/h)}{(s/c)^2}$$

$$= B \cdot \left[2 \cdot \frac{s}{c} \left(\tan(\alpha_{in}) - \tan(\alpha_{out}) \right) \cdot \cos(\alpha_m) \right]^2 \cdot \frac{\cos^2(\alpha_{out})}{\cos^3(\alpha_m)} \cdot \frac{(k/h)}{(s/c)^2} \Rightarrow$$

$$Y_{TC} = 4 \cdot B \cdot (k/h) \frac{\cos^2(\alpha_{out})}{\cos(\alpha_m)} \cdot \left(\tan(\alpha_{in}) - \tan(\alpha_{out}) \right)^2 \tag{3-14}$$

3.1.5 Trailing Edge Loss

The effect of trailing edge thickness on the losses is correlated as a correction factor to the overall losses. In [7] it is shown that the overall losses were increased with about 30 percent when the ratio of trailing edge thickness to pitch (t_{TE}/s) was increased from 0.018 to 0.075. In [8] a new graph based on data from [7] was given to correlate the overall blade loss as function of t_{TE}/s, where $t_{TE}/s = 0.02$ is a datum point. The graph is seen in Figure12.3-13 where the relative total blade loss is plotted against t_{TE}/s.

3.1.6 Summary

To summary the work by Ainley & Mathieson [7],[8], it should not be forgotten that it is over a half of century since the studies were done. So the blade geometry for that times blade differs quite a lot from today's state of the art, even if the basic principals are the same. Today the blades are often working in transonic region, something that was not seen in the 1950. Ainley & Mathieson also more or less stated that the curvature between the throat and trailing edge was just a disadvantage, but to day all blades are more or less curved after the throat. The blade turning and blade thickness is also higher today compare to what were common at the fifties. The data from measurements were limited and made it difficult to establish accurate correlations, particularly for high Mach number, tip clearance and secondary flow. Therefore their correlations should be used careful and with the knowledge of their restriction, especially for the losses at off-design where the models predict higher loss levels than what are seen for modern blade design.

Even if the design has changed a lot upon today, theirs work should not be rejected, because , as seen in the following report, a lot of the engineering achievements seen today is thanks to their work and many improvements have been done with these correlations as the base as will be.

3.2 Dunham & Came

In 1970 J. Dunham and P. M. Came reviewed the correlations from Ainley & Mathieson stated in [7], [8] and their improved correlations are here referred to as AMDC. The review was done with data from original sixteen turbines that were later complemented with further nine turbines to give test data from a total of twenty-five turbines. The primary weakness in Ainley & Mathieson's method was found to be when it was applied to small or unconventional turbines. The modifications were primarily done on the secondary and tip leakage losses but also a new correction for Reynolds number and subsonic outlet Mach number were included, as is shown below. All other cases and corrections for other load cases should still be treated with Ainley & Mathieson's methods from [7],[8].

3.2.1 Profile Loss

The profile loss from Ainley & Mathieson was believed to be quite accurate, so only corrections for Mach number and Reynolds number were introduced.

If $M_{out} > 1$

$$Y_P = Y_{P,AM} \cdot \left[1 + 60 \cdot (M_{out} - 1)^2\right] \tag{3-15}$$

Where $Y_{P,AM}$ is from Ainley and Mathieson in ref [7], [8] and explained under section 3.1.2. The correction should only be done for Mach number exceeding unity. The correction for Reynolds number is made with the assumption that both the secondary and profile losses are proportional to $Re^{-0.2}$.
Then the equation to correct for this is given by

$$(Y_{P,AMDC} + Y_{S,AMDC}) = (Y_P + Y_S) \cdot \left[\frac{\mathrm{Re}}{2 \cdot 10^5}\right]^{-0.2} \tag{3-16}$$

3.2.2 Secondary Loss

From the study of cascade data a new loading parameter was added to AM original secondary flow equation as is shown in eqn (3-8). λ in eqn (3-7) is removed and replaced with a fixed value of 0.0334 and the c/h ratio. This constant is assumed to compensate for the use of a reference radius in the modeling, instead of the actually hub and tip radius where the losses actually take place. The constant was determined from comparing the correlation with overall efficiency data from measurements. There is no parameter included to compensate for variation in inlet endwall boundary layer even if it was known to affect the secondary loss. The reason was their wish to keep the model simple. For the same reason the variation in secondary loss with tip leakage was left out. The result is shown in eqn (3-17)

With the loading parameter (Z) from eqn (3-8), the extra term

$$\frac{\cos(\alpha_{out})}{\cos(\alpha'_{in})}$$

to catch the acceleration in the blade row and with

λ replaced by

$0.0334 \cdot \frac{c}{h}$ in eqn (3-10)

and C_L expressed with use of eqn (3-9) finally give AMDC correlation for secondary loss as

$$Y_S = 0.0334 \cdot \left(\frac{c}{h}\right) \cdot 4 \cdot \frac{\left(\tan(\alpha_{in}) - \tan(\alpha_{out})\right)^2}{\cos(\alpha'_{in})} \frac{\cos^3(\alpha_{out})}{\cos^3(\alpha_m)} \qquad (3\text{-}17)$$

The modification for Re was present above in eqn (3-16)

3.2.3 Tip leakage Loss

The tip loss was still assumed to depend on the blade load (Z) and the effective tip leakage clearance to blade height ratio (k/h). A modification of the linear relation to (k/h) given by Ainley & Mathieson [7] to instead be related as a power law was done on eqn (3-14) that ends up as eqn (3-18). The constant (B) was changed for both shrouded and unshrouded blades.

$$Y_{TC} = 4 \cdot B \cdot (k/h)^{0.78} \frac{\cos^2(\alpha_{out})}{\cos(\alpha_m)} \cdot \left(\tan(\alpha_{in}) - \tan(\alpha_{out})\right)^2 \qquad (3\text{-}18)$$

$$\text{Where } B = \begin{cases} 0.47 \text{ Unshrouded} \\ 0.37 \text{ Shrouded} \end{cases}$$

$$k = \frac{(\text{geometric height, k})}{(\text{number of seals})^{0.42}}$$

The clearance (k) is corrected for the case of multiple seals at the tip that would increase the efficiency of the sealing. The accuracy for this relation and the geometrical design of the sealing was not fully accurate tested and understood at that time.

3.2.4 Summary

The result from their tests of correlations accuracy compared with measurements is seen in [10] and there is an improvement to catch effect of supersonic exit speed shown (Figure 2 in [10]). The model shows also good ability to predict secondary loss for both low aspect ratio and low reaction turbines, something that are not satisfactory done in [7]. Actually their correlation overestimated the secondary loss a little bit for the test turbine afterwards. The author stated that their correlations can predict the flow field within ± 3 percent and the total to total efficiency within ± 2 percent.

3.3 Kacker & Okapuu

A decade after Dunham & Came update the original AM paper, it was time for another review and update to adjust for new improvements in the design and measurements of test data. The two persons to do this were S. C. Kacker and U. Okapuu (KO). They modified the AMDC model in a number of ways, as will be seen below, and then tested it against 33 turbines covering a wide range of sizes and with typical design for that time.

Except from corrections in the correlations for profile, secondary and tip leakage losses to fit the new design improvements, they also give the loss for trailing edge thickness as a separate loss and not as a multiplier to the overall profile and secondary losses as AM and DC used. The Reynolds number correction is now only made on the profile loss. A new way to treat the channel flow acceleration and shockwaves that also handle subsonic speed were included, the full report is seen in [11].

The new structure for the overall losses stated by Kacker & Okapuu in 1981 is

$$Y_{tot} = Y_P \cdot \chi_{\mathrm{Re}} + Y_S + Y_{TC} + Y_{TE} \tag{3-19}$$

The model is here referred to as AMDCKO model.

3.3.1 Profile Loss

The base profile loss is given by the same chart as AM, Figure 12.3-1 and Figure 12.3-2, with a slightly modification to the equation used for interpolation so that it also can handle negative sign in inlet flow angle. The trailing edge loss is, as mentioned above, placed as a separate loss coefficient and therefore the profile loss was modified with a constant value of 0.914 to correct the level down to zero TE thickness according to AM's Figure 12.3-13.

Because the original charts form AM were used while the aerodynamic design improvement from 1950 to 1980 had decreased the profile loss at the design point, a constant factor of 2/3 was applied to the loss coefficient

The profile loss is not independent of Mach number even at subsonic flow. The main reason is that there over the curved surface, primary in the region of the leading edge and TE, will be large deviation from the main flow properties. Close to the blade surface there can be a region of supersonic flow where shock losses will be present. (e.g. see chapter 7 and Figures 7.3-5 to 7.3-9) To fulfill the radial force balance the Mach number at the hub will be higher than the average value at midspan. For a nonfreevortex design the relation between the hub/mid Mach number can be seen in Figure 12.3-15 for a known hub/tip radius ratio.

Eqn (3-20) expresses the shock loss at the hub nondimensionalized by inlet dynamic head.

$$Y_{Shock,in} = 0.75 \cdot (M_{Hub,in} - 0.4)^{1.75} \tag{3-20}$$

The contribution to the total profile loss from the shock loss that primary occurs at the hub and that is assumed to be proportional to hub/tip ratio. To convert the loss from the definition of inlet to outlet dynamic head condition KO also gave eqn (3-21).

$$Y_{shock,out} = Y_{shock,in} \cdot \left(\frac{p_{in}}{p_{out}} \right) \cdot \frac{1 - (1 + \frac{\gamma - 1}{2} \cdot M_{in}^2)^{\frac{\gamma}{\gamma - 1}}}{1 - (1 + \frac{\gamma - 1}{2} \cdot M_{out}^2)^{\frac{\gamma}{\gamma - 1}}} \tag{3-21}$$

Combining eqn (3-20) and (3-21) give a final expression for the contribution of the shock loss to the total profile loss, eqn (3-22).

$$Y_{shock,out} = 0.75 \cdot (M_{in,Hub} - 0.4)^{1.75} \cdot \left(\frac{p_{in}}{p_{out}} \right) \cdot \frac{1 - (1 + \frac{\gamma - 1}{2} \cdot M_{in}^2)^{\frac{\gamma}{\gamma - 1}}}{1 - (1 + \frac{\gamma - 1}{2} \cdot M_{out}^2)^{\frac{\gamma}{\gamma - 1}}} \tag{3-22}$$

In [2] Ning Wie give eqn (3-23), originally form (Hall 1990 at CTH) to calculate the inlet hub Mach number, $M_{hub,in}$ from mean inlet Mach number that can be used instead of Figure 12.3-15.

$$M_{hub,in} = M_{in} \cdot \left(1 + K \left| \frac{r_{hub}}{r_{tip}} - 1 \right|^{2.2} \right) \tag{3-23}$$

Where K is a constant

$$K = \begin{cases} 1.8 \text{ for stator} \\ 5.2 \text{ for rotor} \end{cases}$$

The flow acceleration in a blade row will act suppressing to any local separation, thinning out the boundary layer and therefore decrease the profile loss. This phenomenon is most pronounced when M_{out} is close to one. A constant K_P is introduced to account for this.

$$K_P = 1 - K_2 (1 - K_1) \tag{3-23}$$

where

$$K_1 = \begin{cases} 1 \text{ for } M_{out} < 0.2 \\ 1 - 1.25(M_{out} - 0.2) \text{ for } M_{out} \geq 0.2 \end{cases}$$

$$K_2 = (M_{in} / M_{out})^2$$

To correct for the difference of Re_{out} from the reference value at $2 \cdot 10^5$ eqn (3-24) was suggested. For the region between $2 \cdot 10^5 \leq \mathrm{Re} \leq 10^6$ the correction factor is constant. The reason for this is not the believing of none effect of Re, instead it is the

very complex losses in the region of transition from laminar to turbulent flow that is not fully understood.

$$\chi_{\mathrm{Re}} = \begin{cases} \left(\dfrac{\mathrm{Re}}{2\cdot 10^5}\right)^{-0.4} & \text{for } \mathrm{Re} \le 2\cdot 10^5 \\ 1 & \text{for } 2\cdot 10^5 < \mathrm{Re} < 1\cdot 10^6 \\ \left(\dfrac{\mathrm{Re}}{1\cdot 10^6}\right)^{-0.2} & \text{for } \mathrm{Re} > 1\cdot 10^6 \end{cases} \tag{3-24}$$

3.3.2 Secondary Loss

The original loss model from AMDC was corrected with a multiplier χ_{AR} to give a less steep rise in secondary loss for an aspect ratio (h/c) less than 2, because AMDC model has shown to overestimate the loss for low h/c blade in earlier studies (section 3.2.4). Just as for the profile loss the acceleration in the blade row will affect the boundary layer at the annular wall and then the secondary loss. To include this decrease a parameter (K_S) is introduced as a function of the profile loss constant K_P and proportional to the ratio of axial chord to blade height in square, $\left(\dfrac{c_x}{h}\right)^2$. Because the choice to exclude the trailing edge loss from the secondary loss a factor of 1.2 is added. The equation to describe the total secondary loss is then

$$Y_S = 1.2\cdot\chi_{AR}\cdot 0.0334\cdot 4\cdot\frac{\left(\tan(\alpha_{in})+\tan(\alpha_{out})\right)^2}{\cos(\alpha'_{in})}\cdot \\ \cdot\frac{\cos^3(\alpha_{out})}{\cos(\alpha_m)}\cdot\underbrace{\left[1-\left(\frac{c_x}{h}\right)^2\cdot(1-K_P)\right]}_{K_S} \tag{3-25}$$

where

$$\chi_{AR} = \begin{cases} \dfrac{1-0.25\sqrt{2-h/c}}{h/c} & \text{for } h/c \le 2 \\ \dfrac{c}{h} & \text{for } h/c > 2 \end{cases}$$

Observe the different definition between outlet flow angles between AM and KO models that result in the change form positive to negative sign in eqn (3-25).

3.3.3 Tip Leakage Loss

For the tip leakage loss no change compared to AMDC's eqn (3-18) was done for shrouded blades. When studying unshrouded blades they found that AMDC show a deviation from their measured test data and they then proposed that the loss instead should be correlated with eqn (3-26) that is supposed to be within ± 15 percent. This loss model need that also the efficiency with zero tip clearance to be calculated, and is therefore more time consuming to use.

For unshrouded blades

$$\Delta\eta_{tt} = 0.93 \cdot \frac{\Delta k}{h \cdot \cos(\alpha_{out})} \cdot \frac{r_{tip}}{r_{mean}} \cdot \eta_{0,tt} \qquad (3\text{-}26)$$

$\Delta\eta_{tt}$ = change of efficiency for the stage

$\eta_{0,tt}$ = efficiency at zero tip clearance

k = tip clearance

3.3.4 Trailing Edge Loss

Trailing edge loss is correlated with a function of the trailing edge thickness to throat ratio (t_{TE}/o) and outlet Mach number. The loss is given as kinetic energy loss ($\Delta\phi^2_{TE}$) by two graphs in Figure (11.2-16) that represent one impulse blade and one reaction blade. In an impulse blade the flow is not accelerating and therefore will the boundary layer grow thick and the base pressure at TE be less strong and give lower TE losses compare to a blade with high acceleration of the flow. A another aspect is to say that for blade with low acceleration are the boundary layer thicker and therefore will the influence from TE thickness be less crucial. For blade shape between these to extremes interpolation should be used according to eqn (3-27). To convert the loss to pressure eqn (2-32) can be used.

$$\Delta\phi^2_{TE} = \phi^2_{TE,\alpha in=0}\left(\phi^2_{TE,\alpha' in=0} + \left|\frac{\alpha'_{in}}{\alpha_{out}}\right| \cdot \left(\frac{\alpha'_{in}}{\alpha_{out}}\right) \cdot \left[\phi^2_{TE,\alpha' out=\alpha in} - \phi^2_{TE,\alpha' in=0}\right]\right) \qquad (3\text{-}27)$$

3.3.5 Off Design Loss

Kacker & Okapuu do not give any own correction for off-design loads, instead AM correction should be used. AM correct only the profile loss for off-design with the use of three charts as seen in appendix 12.3-1 Figures 12.3-4, 12.3-5 and 12.3-6, and the method is described in section 3.1.1.

3.3.6 Summary

The correlations were tested by KO against a Smith chart to see how well the profile and to a certain degree the secondary loss were predicted. The turbines used in the test were of old design type with low blade loading and high aspect ratio. The result from the validation can be seen in [11]. A second test with 33 more time typical turbines measured the correlations ability to predict the design efficiency of time typical turbines that most were from Pratt and Whitney. The result and data over the flow coefficient, enthalpy drop, pressure ratio and aspect ratio can be found in ref [11]. The overall conclusion from KO was that the total efficiency was predicted within ± 1.5 percent

3.4 Craig & Cox

H. R. M. Craig and H. J. A. Cox (CC) method for prediction of the losses present in a turbine stage is valid for both gas and steam turbines [12]. This can have a small negative influence of the models prediction accuracy for gas turbine alone compared to if the model had been derived specific for gas turbines. CC claimed that the models

prediction results correlate with an accuracy of ± 1.25 percentage point. The test data used to obtain the correlation for profile and secondary loss were from linear cascade tests, while other losses (such as the tip clearance loss) were derived from specific turbine tests and data from annular air tests [12]. There is a discussion about the probable errors that could be induced in a linear cascade test compare to real turbine. These errors are given in two categories, the first include different working fluid, Reynolds number, scale of blade, surface roughness and Mach number. CC claim that it is possible to fully correct for all these errors [12]. The second category of errors are due to the differences between uniform and disturbed flow, linear to annular flow and stationary to relative movement between blade and wall. These errors are more complicated to correct for [12]. CC based there correlations for secondary loss on basic test data with limited physical coupling and claimed that the theoretical nature of the secondary flow is to complex to describe physically.

The losses in a blade row are divided into the two groups below

1. Profile, secondary and annular loss, in both the stator and rotor.
2. Tip leakage loss in rotor, leakage loss in stator and (balance hole, lacing wire, wetness, disc, partial admission) losses.

Only the first group and the two first losses in the second group are examined below.

The losses in the first group are described by a loss factor, and the losses in the second group are given as a decrease in stage efficiency. The reason for this division is that CC found this to being the easiest way to derive the loss models from test data.

The off-design condition is also treated and included in the loss correlation, as is described in section 3.4.1.

Note that the angles are defined from the tangential plane in CC equations and Figures so that the angles are normally positive at both inlet and outlet.

3.4.1 Profile loss

The overall profile loss is given by a basic base loss coefficient for incompressible flow and then corrected for variation of Reynolds number, trailing edge thickness and incidence by some multipliers to the base loss. For the variation of Mach number and curvature of the suction surface between the throat and tailing edge (e) an added extra loss to the overall profile loss are used.
Structure of the profile loss by CC are seen in eqn (3-28)

$$Y_P = Y_{P0} \cdot \chi_{\mathrm{Re}} \cdot \chi_{TE} \cdot \chi_i + \Delta Y_{P,M} + \Delta Y_{P,TEc} + \Delta Y_{P,TE} \qquad (3\text{-}28)$$

TEc is the trailing edge curvature between throat and TE

The base loss coefficient Y_{P0} was derived with low speed fluid flow and at an incidence corresponding to the minimum profile loss. Y_{P0} is a function of a lift parameter F_L, s/c_c (where c_c is blade center camber line), contraction ratio CR and outlet flow angle α_{out}. F_L is in turn given by a chart, present in Figures 12.2-17 and can be reed with α_{out}, $\alpha_{in-i,\min}$ as parameters.
The contraction ratio (CR) is defined as the inlet to throat area ratio, where inlet area is defined as the maximum arc that can be drawn entirely within the blade passage and

witch is normal to the blade surface. For more details and Figure see Fig.1 in ref [12]. In a new design where all the blade geometry is not still determined, some typical value of blade parameters are given in Figure 12.2-18 for known pitch to chamber line ratio, inlet and outlet flow angle.

Finally Y_{P0} are present in Figure 12.2-19 as a function of $F_{L,}$ CR and s/b_c.
To summarize thus far

$$Y_{P0} = f(CR, F_L, s/c_c) \tag{3-29}$$

$$CR = f\left(c/c_c, 1-\frac{\sin(\alpha_{out})}{\sin(\alpha_{in})}\right) \tag{3-30}$$

$$F_L = f(\alpha_{out}, \alpha_{in} - i_{\min}) \tag{3-31}$$

And can be reed from Figures 12.2-17, 12.2-18 and 12.2-19

Eqn (3-29) is for zero trailing edge thickness. To correct for the loss related to separation for a real thickness at the trailing edge a theoretical derived correlation is present in Figure 12.2-20 as a function of α_{out} and t_{TE}/s. This correlation gives both a multiplier (χ_{TE}) and an extra added loss ($\Delta Y_{P,TE}$) to the base profile loss Y_{P0}.

For the correction of Re another chart is present in Figure 12.2-21 for different surface roughness and Reynolds number inside the range $10^4 \le \mathrm{Re}_o \le 10^6$ where Re_o is based on blade throat opening (o). The trend for this chart is that the multiplier will decrease rapid as Re_o is increased from about 10^4 to 10^5 and then after approximately $5\cdot 10^5$ the loss will be close to constant.

To correct for Mach number in excess of unit, $\Delta Y_{P,M}$ is added as a function of o, t_{Te}, s and Ma_{out}, see Figure 12.2-22. Finally a correction for the mean curvature e between the throat and trailing edge suction surface were present and can be seen in Figure 12.2-23 for the input parameter M_{out}, s/e. Future

The last correction on the profile loss is an off-design multiplier χ_i to the base profile loss because of incidence i. This loss multiplier should be calculated in three different ways depending on if it is a positive or negative stalling and also depending on if the inlet flow angle is less then 90 degree or not. The procedure will be present below and in Figure 12.2-24 the final incidence multiplier can be seen.

The definition of stalling incidence i_{stall} is the same as AM used, namely when the loss is equal to twice the minimum loss at i_{min}. The minimum loss incidence and negative stalling incidence is correlated independently of the positive stalling value.

For $\alpha_{out} \le 90^o$, $i \ge 0$

$$i + stall = (i + stall)_{basic} + (\Delta i + stall)_{s/c_c} + (\Delta i + stall)_{CR} \tag{3-32}$$

Where

$$(i + stall)_{basic} = f(\alpha_{in}, \sin^{-1}(o/s)) \quad (3\text{-}33)$$

Present in 12.2-25

$$(\Delta i + stall)_{s/c_c} = f(s/c_c, \sin^{-1}(o/s)) \quad (3\text{-}34)$$

$$(\Delta i + stall)_{CR} = f(CR, \sin^{-1}(o/s)) \quad (3\text{-}35)$$

Present in Figure 12.2-26

For $\alpha_{out} \le 90^o$, $i < 0$

$$i - stall = (i - stall)_{basic} + (\Delta i - stall)_{s/c_c} \quad (3\text{-}36)$$

$$i - stall = (i - stall)_{basic} + (\Delta i - stall)_{s/c_c} \quad (3\text{-}37)$$

Where

$$(i - stall)_{basic} = f(\alpha_{in}, \sin^{-1}(o/s)) \quad (3\text{-}38)$$

$$(\Delta i + stall)_{s/b_c} = f(s/b_c, \sin^{-1}(o/s)) \quad (3\text{-}39)$$

Present in Figure 12.2-27

For $\alpha_{out} > 90^o$, $i \ge 0$

$$i + stall = \left\{ \begin{array}{l} (i + stall)_{basic} + \left(1 - \dfrac{\alpha_{in} - 90}{90 - \sin^{-1}(o/s)}\right) \cdot \\ \cdot \left[(\Delta i + stall)_{s/c_c} + (\Delta i + stall)_{CR} \right] \end{array} \right\} \quad (3\text{-}40)$$

Where

$$(i + stall)_{basic} = f(\alpha_{in}, \sin^{-1}(o/s)) \quad (3\text{-}41)$$

$$(\Delta i + stall)_{s/bc} = f(s/c_c, \sin^{-1}(o/s)) \quad (3\text{-}42)$$

$$(\Delta i + stall)_{CR} = f(CR, \sin^{-1}(o/s)) \quad (3\text{-}43)$$

Present in Figures 12.2-28 and 12.2-26

For $\alpha_{out} > 90^o$, $i < 0$

$$i - stall = (i + stall)_{basic} + \left(1 - \frac{\alpha_{in} - 90}{90 - \sin^{-1}(o/s)}\right) \cdot (\Delta i + stall)_{s/c_c} \quad (3\text{-}44)$$

Where

$$(i + stall)_{basic} = f(\alpha_{in}, \sin^{-1}(o/s)) \quad (3\text{-}45)$$

$$(\Delta i + stall)_{s/c_c} = f(s/c_c, \sin^{-1}(o/s)) \quad (3\text{-}46)$$

Present in Figures 12.2-28 and 12.2.27

To evaluate the minimum loss incidence finally the equation (3-47) is used together with the incidence parameter F_i from Figure 12.2-29.

$$i_{\min} = \frac{(i + stall) + F_i \cdot (i - stall)}{1 + F_i} \quad (3\text{-}47)$$

When i, $i_{\min}$ and i_{stall} determined as above, the correction multiplier χ_i can be reed in 12.2-27

3.4.2 Secondary Loss

CC involve both true aerodynamic secondary loss and partly also the wall friction in their secondary loss correlation, as is commonly done. They also propose that there is a difference between the losses for shrouded and unshrouded blades even for the secondary loss part even if they finally only present a correlation for shrouded blades, which they claim is approximately valid for unshrouded blades. It is assumed that the secondary loss is close to inverse proportional to aspect ratio for big ratios. When h/c is decreased below a certain value the secondary flow present at the enwalls interacts and the result of these both loss sources will be less than the sum of them individually. Therefore they use a nonlinear relationship to aspect ratio (h/c). CC also proposed a similarly effect on the secondary loss part upon Re_o as for the profile loss but no separate chart were given, maybe the same correction chart as used for the profile loss can be used, present in Figure 12.2-21. When they established the relation between (h/c) and Y_S they use high Reynolds number where the loss coefficient is close to independent on moderate Re variation to ensure that a variation of Y_S due to h/c would not be offset by a simultaneous variation of Re.

The overall secondary loss is given by

$$Y_S = Y_{S0} \cdot \chi_{\mathrm{Re}} \cdot \chi_{h/c} \tag{3-48}$$

Where

$$Y_{S0} = f(F_L \cdot (s/b_c), (C_{in}/C_{out})^2) \tag{3-49}$$

$$\chi_{h/c} = f(C_c/h) \tag{3-50}$$

C represents the relative velocity for a rotor and absolute velocity for a stator, present in Figures 12.2-30 and 12.2-31.

3.4.3 Annular Loss Coefficient

The annular loss Y_{Annular} is separated from the secondary loss by CC and is given as the sum of three separate sources of losses. These sources are annular, cavity and a cavity loss factor due to sudden expansion. These types of losses are more important for to consider when calculation is preformed on steam turbines with bleed of steam to feed water heaters and is therefore not present in this report, for real calculation Figure 19 and 20 in [12] should be used.

3.4.4 Tip Clearance Loss

Tip leakage loss over the blade tip is given by eqn (3-51) that is describing the reduction of overall stage efficiency compare to stage efficiency for zero tip clearance. The area ratio between the tip clearance to throat and an efficiency factor F_k are involved.

$$\Delta\eta_{tt} = F_k \cdot \frac{A_k}{A_o} \cdot \eta_{0,tt} \qquad (3\text{-}51)$$

For an increase in the leakage area (A_k) the efficiency will decrease. The factor F_k takes for a shrouded blade care to the pressure drop across the stage when it relate to the velocity ratio across the stage, $\frac{C_{out}^2 - C_{in}^2}{C_{out}^2}$ and the velocity coefficient $\frac{C}{C_s}$. In Figure 12.2-32 can it be seen that for high velocities, that will create a reduction in the static pressure, F_k increase just as would be expected. Another geometric parameter included is $\Delta L / h$, that describe the decrease in leakage flow if there is an overlap be between the shroud and the annular wall, also shown in Figure 12.2-32. For unshrouded blades the correlation given by AM should be used, see section 3.1.4 above. The effect of $\Delta L / h$ in Figure 12.2-31 were by theme self claimed to need to be modified for turbines with high blade height (h) (especial for steam turbines), but no suggestion was given.

3.4.5 Summary

CC argues that the losses from group 1 should not be calculated at just one mean diameter. Instead they should be calculated for at least three different diameters (root, mean and tip) and then an average value should be calculated with a parabolic loss distribution according to

$$\left(\sum Y\right)_{avg} = (1/6)\cdot\left(\sum Y\right)_{hub} + 1\cdot\left(\sum Y\right)_{tip} + 4\cdot\left(\sum Y\right)_{mid}$$

The prediction accuracy for there model was tested against around fifteen measured turbines efficiency in the range from around 10 to 150 MW. For most of the test the efficiency was prediction within a range of ± 1.25 percent. But there were some prediction differences in the range up to around 3 percent seen mostly for turbines in the range of 10 to 25 MW. CC argued for that no systematic or major discrepancies were found, but consider that it is derived for both gas and steam turbines.

3.5 Mukhatarov & Krichakin

M. Kr. Mukhatarov & V. I. Krichakin (MuKr) have investigated the losses for linear cascades with small cone angles, subsonic outlet Mach number and inlet and outlet flow angle in the span of α_{in}(5-100) and α_{out}(15-50) [13]. The angles are defined from the tangential plane in the whole section below and the relations are based on cascades with optimal solidity (s/c) according to the relation

$$\left(\frac{s}{c}\right)_{opt} = 0.55\left[\frac{180\cdot\sin(\alpha_{in})}{\varepsilon\cdot\sin(\alpha_{out})}\right]^{1/3}\cdot\left(1-\frac{t_{\max}}{s}\right) \qquad (3\text{-}52)$$

3.5.1 Profile loss

The total profile loss is a summation of losses due to friction (Fr), trailing edge (TE), Mach number (M), Reynolds number (Re) and incidence (i) as seen in eqn (3-53).

$$\zeta_P = \zeta_{Fr} + \zeta_{TE} + \Delta\zeta_M + \Delta\zeta_{\mathrm{Re}} + \Delta\zeta_i \tag{3-53}$$

The ζ_{Fr} loss for an optimal outlet velocity, $\mathrm{Re}_{out} > 5 \cdot 10^5$ and with no incidence are given with some unclearness by equation 4 in [13]. The believed way to calculate the friction loss is.

$$\zeta_{Fr} = \left\{ \begin{array}{l} \dfrac{0.0128 \cdot \left(\dfrac{c_c}{c}\right) \cdot \left(\dfrac{c_o}{c}\right)^{2/3}}{\left[1 + (1.1 \cdot k - 1) \cdot \left(\dfrac{c_c}{c}\right)\left(\dfrac{c}{c_o}\right)\right]^{2.53}} \cdot \\ \dfrac{\left(\left[1 + (1.1 \cdot k - 1) \cdot \left(\dfrac{c_c}{c}\right)\left(\dfrac{c}{c_o}\right)\right]^{4.8} - 1\right) \cdot \dfrac{\Delta\zeta_M}{\zeta_{P,0}}}{\sin(\alpha'_{in})^{0.5} \cdot \left(\dfrac{180}{\varepsilon}\right)^{1/3} \cdot \left(1 - \dfrac{t_{\max}}{c}\right) \cdot (1.1 \cdot k - 1)^{2/3}} \end{array} \right\} \tag{3-54}$$

where k is blade contraction between the inlet and outlet

$$k = \frac{\sin(\alpha'_{in})}{\sin(\alpha'_{out})}$$

c_c is the blade centerline length (equal to b_c from some other authors).
c_0 is the length of the middle line of the blade channel up to the throat.

The outlet flow velocity that gives a minimum profile loss is referred to as optimal outlet flow velocity and is a function of k and $\frac{t_{\max}}{c}$, see fig 2 in [13].
Influence from the trailing edge for exit Laval number in the range of 0.7 to 0.9 is given by two simple functions as, eqn (3-55)

$$\left. \begin{array}{l} \zeta_{TE} = 0.2 \cdot \dfrac{d_{out}}{s} \\ \text{Or} \\ \zeta_{TE} = 0.01 + 0.31 \cdot \left(\dfrac{d_{out}}{s}\right)^{3/2} \end{array} \right\} \tag{3-55}$$

The later was proposed to be more accurate and valid for a wider range of trailing edge diameter.

To correct the losses due to Mach number, both a graph and an empirical correction were given with the ratio between Laval number and optimal Laval number as input argument. Only the later will be reviewed here, as eqn (3-56).

$$\frac{\Delta\zeta_M}{\zeta_{P,0}} = 6.05\left(\frac{\lambda_{out}}{\lambda_{out,opt}}\right)^2 - 11.8\left(\frac{\lambda_{out}}{\lambda_{out,opt}}\right)^2 + 6\left(\frac{\lambda_{out}}{\lambda_{out,opt}}\right)^2 - 0.25 \qquad (3\text{-}56)$$

where
$\zeta_{P,0} = \zeta_{Fr} + \zeta_{TE}$ for $\lambda_{out,opt}$

Even if there is some uncertainness it is believed that eqn's (3-54), (3-55) and (3-56) should be solved implicit together.

The correction for Reynolds number different from the ideal value is given by eqn (3-57) and is valid for Re in a range of $1\cdot10^4 < \mathrm{Re} < 1\cdot10^6$, $\lambda_{out,opt} \le 1.0$ and a turbulent intensity (TI) less then 10 percent.

$$\Delta\zeta_{\mathrm{Re}} = \frac{2100}{\mathrm{Re}_{design}} \qquad (3\text{-}57)$$

The effect of incidence is given below in eqn (3-58)

$$\Delta\zeta_i = \left\{ \begin{array}{l} \dfrac{A}{\left(d_{out}/c\right)^{2/3}} \cdot \left[\left(\dfrac{\lambda_{in}}{\lambda_{out}}\right)^2 - \left(\dfrac{\lambda_{in,des}}{\lambda_{out}}\right)^2\right] + \\ + \dfrac{B}{\left(d_{out}/c\right)^{2/3}} \cdot \left(\dfrac{\lambda_{in}}{\lambda_{out}}\right)^2 \cdot \sin(\underbrace{\alpha_{in} - \alpha_{in,des}}_{i,eff}) \end{array} \right\} \qquad (3\text{-}58)$$

where
$\left.\begin{array}{l} A = 0.024 \\ B = 0.144 \end{array}\right\}$ for $\alpha_{in,des} > \alpha_{in}$ Positive incidence
Or
$\left.\begin{array}{l} A = 0.0007 \\ B = 0.206 \end{array}\right\}$ for $\alpha_{in,des} < \alpha_{in}$ Negative incidence

and for a linear flow the Laval number were stated to be related as

$$\frac{\lambda_{in}}{\lambda_{out}} = \frac{\sin(\alpha_{out,des})}{\sin(\alpha_{in,des})}$$

$$\frac{\lambda_{in,des}}{\lambda_{out}} = \frac{\sin(\alpha_{out,des})}{\sin(\alpha_{in})}$$

3.5.2 Secondary loss

For the secondary loss first an ideal secondary loss is calculated as a function of, Reynolds number, inlet and outlet flow angles at design, outlet Laval number, aspect ratio and the profile loss uncorrected for incidence, eqn (3-59). This design secondary loss is then corrected for the incidence, eqn (3-60).
The range of validity is

$\alpha_{in,des}$ =25-90 deg
$\alpha_{out,des}$ =15-40 deg
o/h $\geq$ 1.5
λ_{out} =0.4-0.9
$\mathrm{Re}_{des} = 1\cdot 10^4 - 1\cdot 10^5$.

$$\zeta_{S,0} = f(\mathrm{Re}, \alpha_{in,des}, \alpha_{out,des}, \lambda_{out,des}, (\zeta_p - \Delta\zeta_i), o/h) \quad (3\text{-}59)$$

$$\Delta\zeta_S = \zeta_{S,0}(1 + \Delta\zeta_i) \quad (3\text{-}60)$$

Where

$$\zeta_{S,0} = 0.075 \cdot \mathrm{Re}_{des}^{0.2} \cdot \left(\frac{19}{3} - \frac{(\alpha_{in,des} + \alpha_{out,des})}{30}\right) \cdot \left(\frac{\sin(\alpha_{out,des})}{\sin(\alpha_{in,des})}\right)^{1/2} \cdot \underbrace{(0.825 + 0.25 \cdot \lambda_{out})}_{\text{This part is removed in CTC}} \cdot (\zeta_{pr} - \Delta\zeta_i) \cdot \frac{o}{h} \quad (3\text{-}61)$$

For the calculation of the effect of incidence in eqn (3-60) the relation in eqn (3-62) can be used.

$$\frac{\Delta\zeta_i}{\zeta_{S,0}} = 400x^3 + 76x^2 + 5.6x \quad (3\text{-}62)$$

where

$$x = \underbrace{\frac{\overbrace{\alpha_{in,des} - \alpha_{in}}^{i,eff}}{\alpha_{in,des} + \alpha_{out,des}}}_{\varepsilon} \cdot \left(\frac{\sin(\alpha_{out,des})}{\sin(\alpha_{in,des})}\right)^{2/3}$$

In CTC this polynomial has been modified, but with the same expression for x except from that $\alpha_{out,des}$ has been replaced by α_{out} in the sinus term.

For the secondary loss at design is the first term a correction for Re, then is there a term that take care to the flow turning (increasing loss for high turning), then is care taken to the acceleration of the fluid, and the term including profile loss can in some sense represent the blade load.

So far is it acceptable, but for the last term that scales against the throat to span ratio (o/s) is there some doubt. The fact is that more then half of the secondary loss are

present at the endwall and it is not physical to believe that it will decrease as the pressure gradient from pressure to suction side of two blades increases. More of these trends are seen and discussed in section 2.10 and 4.3.6.

For the off-design condition is a third order polynomial used and its trend can be seen in Figure 4.3-16. The trend of this curve is believed to be good up to at least a positive incidence of around 25-30 deg.

3.6 Moustapha, Kacker & Tremblay

S. H. Moustapha, S. C. Kacker and B. Tremblay (MKT) made 1989 [14] a review of AMDCKO and MuKr correlations for off-design losses and propos to an updated loss model was given. These models have then been further improved by Benner, Sjolander and Moustapha (BSM) 1995 [17], and once more 2005 [26]. They were then completely changed by BSM in 2006 [15] where a totally new method to divide the losses were introduced as can be seen in section 3.7. In MKT's report from 1989 they use the normal and up to that time conventional division between profile and secondary losses. Where the profile loss is measured at midspan of the blade and assumed uniform over the whole span and then is the secondary loss taken as the difference between the total measured loss level and the profile loss with zero tip clearance. The present loss models give only the difference between design and off-design condition and MuKr or AMDCKO original loss model should be used as a datum point.

3.6.1 Profile Loss at Off-Design

MKT compared the profile loss at off-design for both AMDCKO and MuKr and noticed a huge over prediction compare to the measured value. In the development of a new loss correlation the original model by MuKr [13] was retained as a base to do modifications on. One of the believed absolute greatest improvements is the introduction of the models dependence on the leading edge diameter to pitch (d_{in}/s). The correlation gives the change in kinetic energy loss as

$$x' = \left(\frac{d_{in}}{s}\right)^{-1.6} \cdot \underbrace{\left(\frac{\cos(\alpha'_{in})}{\cos(\alpha'_{out})}\right)^{-2}}_{CR^{-2}} \cdot \underbrace{(\alpha_{in} - \alpha_{in,des})}_{\text{effectiv incidence}} \tag{3-63}$$

where

$$\Delta\phi_P^2 = 0.778 \cdot 10^{-5} \cdot x' + 0.56 \cdot 10^{-7} \cdot x'^2 + 0.4 \cdot 10^{-10} \cdot x'^3 + 2.054 \cdot 10^{-19} \cdot x'^6$$
$$for\ 800 > x' > 0$$

and

$$\Delta\phi_P^2 = -5.1734 \cdot 10^{-6} \cdot x' + 7.6902 \cdot 10^{-9} . x'^2$$
$$for\ 0 > x' > -800$$

The trend for this correlation is that a high acceleration (CR), or big inlet diameter (d_{in}) will suppress the effect of incidence.

In the development of this correlation the effect of compressibility, Reynolds number and turbulent intensity were not considered. The reason that these parameters have been omitted is not that BSM believed that they were unimportant. Instead it was the lack of measured data that make the establishing of an accurate correlation impossible and can therefore be of interest to investigate in the future. MKT believe for example that the compressibility will cause shocks at the LE and effecting the acceleration of the fluid inside a row. The leading edge wedge angle (We_{in}) (see section 3.6.2) or if the blade is front or aft loaded will also have influence on the profile loss at off-design.

3.6.2 An Improvement of Off-Design Profile Loss

In [17] an improved correlation for off-design profile losses is introduced by BSM after the study of not only the leading edge diameter but also the discontinuity between the leading edge circular arc and blade surface at both pressure and suction side. To the help in developing their correlation two cascades with approximately identical flow and geometry except from inlet diameter and stagger angle were used. A summary of the parameter for these two cascades referred to as CC2 and CC3 are shown in Table 3-1, [17]. The measurements were done for a wide range of AVR (axial velocity ratio) and then a mean value for the present losses was used. The Reynolds number based on axial chord (c_x) and outlet flow condition was kept constant and the turbulent intensity (TI) of 0.3 %, but higher TI was tested with only a small change in the loss level and was therefore neglected.

Table 3-1: Summary of the parameter for the to cascades referred to as CC2 and CC3

Cascade Parameter	*CC2*	*CC3*
Blade span h [mm]	200	200
Blade spacing, s [mm]	100.7	100.7
True chord, c, [mm]	162.8	162.3
Axial chord, c_x [mm]	150	149.4
Stagger angle, [deg]	23.1	21.6
t_{max}/c	0.182	0.196
Inlet blade angle, [deg]	29.3	25.5
Outlet blade angle, [deg]	57.5	57.5
Leading edge diameter, d_{in} [mm]	9.43	16.7
Leading edge wedge angle, We [deg]	52.4	43
Trailing edge thickness, t_{TE} [mm]	4.2	4.2

BSM show in [17] with positive incidence there is a sudden flow acceleration at the leading edge, followed by a deceleration and risk of separation. Actually this phenomenon, called overshoot will be most substantial for CC3 with the large leading edge diameter and not as might be expected by the CC2. BSM believed that the missing factor to explain this trend is as mentioned above the discontinuity between leading edge and blade surface downstream, and that it could be satisfactory expressed by the inlet wedge angle (We_{in}).

A short summary to the explanation of the effect by discontinuities from [17] is given below. At the blend point where the leading edges circle or ellipse meets the suction

surface blade profile there will be a discontinuity in the curvature. At this point a separation bubble is created that could lead to a transition from a laminar to a turbulent boundary layer, but in most case the overall favorable pressure gradient just after the overshoot will get the flow to reattach again. The seeming for transition is linked to the discontinuity in geometry so that an elliptic leading edge will be more tolerant to higher incidence just as a smaller circular arc would be. When the positive incidence is increased to a certain point the flow would be decelerated over most of the suction surface after the overshoot, and no relaminarization that can prevent the separation is possible. Therefore the separation will start to have a greater influence on the loss. The same trend is seen for negative incidence where a separation bubble is formed at the pressure side, but here the bubble will in most cases reattach. Then the loss will be of less substance and it is now primary the length of the separated bubble that is determined by the value of the negative incidence angle.

Whit this acknowledges as a background a modification to MKT's correlations for profile loss in section 3.6.1 was made. The test data to develop this modification came from eight cascades with measured value of We, CC2, CC3 and three cascades from Perdichizzi & Dossena (1993), to sum up with test data from totally 13 cascades. They were claimed to coverer a wide range of We and d_{in}/s, [17]. In the new correlation the leading edge diameter influence are much smaller compare to the originally given by MKT. Instead includes it the We to a power of -0.2. The suggested equation to replace eqn (3-63) is eqn (3-64)

$$x = \left(\frac{d_{in}}{s}\right)^{-0.05} \cdot We^{-0.2} \cdot \left(\frac{\cos(\alpha'_{in})}{\cos(\alpha'_{out})}\right)^{-1.4} \cdot \underbrace{(\alpha_{in} - \alpha_{in(design)})}_{effectiv\ incidence} \qquad (3\text{-}64)$$

where
For $x \geq 0$

$$\Delta\phi_P^2 = 3.711\cdot10^{-7}\cdot x^8 - 5.318\cdot10^{-6}\cdot x^7 + 1.106\cdot10^{-5}\cdot x^6 + 9.017\cdot10^{-5}\cdot x^5 - 1.542\cdot10^{-4}\cdot x^4 - $$
$$- 2.506\cdot10^{-4}\cdot x^3 + 1.327\cdot10^{-3}\cdot x^2 - 6.149\cdot10^{-5}\cdot x$$

and
For $x < 0$

$$\Delta\phi_P^2 = 1.358\cdot10^{-4}\cdot x - 8.720\cdot10^{-4}.x$$

With this new correlation for profile loss at off-design it is assumed that the loss level would be less sensitive to the leading edge diameter and instead that it is the discontinuity in blade curvature (here related to We) that will be the main important parameter. These two parameter are actually coupled to each other so that a big d_{in} normally also correspond to a big We_{in}.

3.6.3 Secondary Loss at Off-Design

MuKr and AM secondary loss models at off-design were compared by BSM. The comparison shows that MuKr model was better than AM, but still with a great scatter in the prediction as seen in Figure 13 in [14]. The derive procedure for BSM model is analogy to the method used for profile loss. They started from MuKr model and added the influence of d_{in}/s and did some corrections. The final correlation that gives the deviation from the original design loss by MuKr [14] or AMDCKO [11] is

$$x'' = \frac{\alpha_{in} - \alpha'_{in}}{180 - (\alpha'_{in} + \alpha'_{out})} \cdot \left(\frac{\cos(\alpha'_{in})}{\cos(\alpha'_{out})} \right)^{-1.5} \cdot \left(\frac{d_{in}}{c} \right)^{-0.3} \qquad (3\text{-}65)$$

where
for 0.3>x”>0

$$\left(\frac{Y}{Y_{des}} \right)_S = \exp(0.9 \cdot x'') + 13x''^2 + 400x''^4$$

and
for 0>x”>-0.4

$$\left(\frac{Y}{Y_{(des)}} \right)_S = \exp(0.9 \cdot x'')$$

The trend for this correlation is that for low acceleration (CR) or high values of turning (ε), inlet diameter (d_{in}) and incidence will the loss be high.

It is very interesting to note that the dependence on the parameter d_{in} / s in eqn (3-65) predict that the secondary loss should increase more rapid for a small leading edge compare to a bigger. This was later confronted by them self in [15] and [16] where measurements show the opposite trend. Perhaps is the reason for this inconsistency that the secondary loss depends upon even another so far not included parameter. This show that the secondary loss and flow phenomena sill is far from being enough understood and the associated problems in finding a general correlation for 1D program at off-design loads.

3.6.4 Modified Profile Loss at Design

2005 J. Zhu and S. Sjolander once more published a new review of AMDCKO profile loss at design point [26]. For off-design load cases it is recommended to be used together with the correction from BSM 1995 that is described in section 3.6.2 and [17]. The modifications were due to influence of Reynolds number less then $2 \cdot 10^5$, t_{max}/c greater than 0.2 and for the difference between how the stator and rotor blades are treated. Beside these differences the corrections are analogous to AMDCKO profile loss at design point. The profile losses are calculated according to eqn (3-66) and (3-67), with the use of AM eqn (3-1)

$$Y_{P,AM(i=0)} =$$
$$= \left\{ Y_{P(\alpha'_{in}=0)} + \left| \frac{\alpha'_{in}}{\alpha_{out}} \right| \cdot \frac{\alpha'_{in}}{\alpha_{out}} \cdot \left[Y_{P(\alpha'_{in}=\alpha'_{out})} - Y_{P(\alpha'_{in}=0)} \right] \cdot \left(\frac{t/c}{0.2} \right)^{k_m} \cdot \frac{\alpha'_{in}}{\alpha_{out}} \right\} \qquad (3\text{-}66)$$

$$Y_P = 0.914 \cdot (k_{in} \cdot K_P \cdot Y_{P,AM(i=0)} + Y_{shock}) \cdot \chi_{\mathrm{Re}} + Y_{TE} \qquad (3\text{-}67)$$

$$\chi_{\mathrm{Re}} = \left(\frac{\mathrm{Re}}{2 \cdot 10^5} \right)^{-0.575} \quad \text{if } \mathrm{Re} \le 2 \cdot 10^5$$

$$k_m = \begin{cases} 1 \text{ if } t/c \le 0.2 \\ -1 \text{ if } t/c > 0.2 \end{cases}$$

$$k_{in} = \begin{cases} 2/3 \text{ for rotor} \\ 0.825 \text{ for stator} \end{cases}$$

3.6.5 Summary

To sum up it can be seen that MKT correlation from 1989 for profile losses at off-design gives a very low penalty for negative incidence for all inlet diameters and also for positive incidence if the inlet diameter is relatively big. For smaller d_{in} the loss increase rapid with both incidence and decreasing d_{in}. This trends are illustrated in Figures 4.15 and 4.16 where the change in profile loss with both d_{in} and i is plotted.
For BSM's correlation from 1995 the direct dependence on d_{in} is not so pronounced even if there is a clear trend. Instead now the We_{in} play an important roll in the loss calculation for off-design. Both these trends are shown in Figures 4.17 and 4.18. Both models use the same correction for secondary flow at off-design that only include inlet flow angle, inlet and outlet blade angles and ratio of inlet blade diameter to chord. The positive incidence is much more devastating for the efficiency. It agrees well with there own test results that comparing losses at both positive and negative incidence.

It was also shown that for a high convergence the loss level was lower compared tom blade with a less strong acceleration of the flow. A blade with large leading edge radius is less sensitive to incidence according to there model. The test data were from totally 36 linear cascade and can be found in appendix 1 and 2 in [14] where also a graph show the ability to predict off-design losses compare to AM and MuKr for the 36 cascades.

3.7 Benner, Sjolander & Moustapha

From 1989 and up to today (2008) a effort to understand the physical flow phenomena at both design and off-design were made by primary S. A. Sjolander, M.W. Benner and S. H. Moustapha, but also some other persons were involved in some of the investigations. This section will just give a brief overview of the trends and result so far present in ref [16], [17], [18], [20], [21], [22], [23] that lead up to the conclusion present in section 3.7.3. The results and trends are still not fully understood and should only be seen as a suggestion and not an absolute true until more results have been present in the future.

3.7.1 Measurements and Studies of Physical Flow Phenomena

At the design point the flow is normally accelerated smooth up to around 50-80 percent of axial chord, depending on if it is front or aft loaded. An aft loaded blade can have an even later velocity peak. There will then be a deceleration and a risk for a possible separation. Even if the flow fields trend is similar between the endwall and midspan, the endwall shown a higher pressure coefficient at suction surface for the

first 2/3 of c_x probably due to a lower dynamic pressure. There are also signs of a higher resistance against separation at the trailing edge close to the endwall [20] compare to the rest of the span. With increased positive incidence it is shown that the blade load will shift towards more frontload. The pressure difference between the suction and pressure side that driving the secondary flow will also decrease for the last 80 percent of c_x as can be seen in Figure 3 and 4 in [20].

The believed flow field at design incidence from [20],[21] can be summarized with the help of Figure 3.7.1 and 3.7.2 from [21].

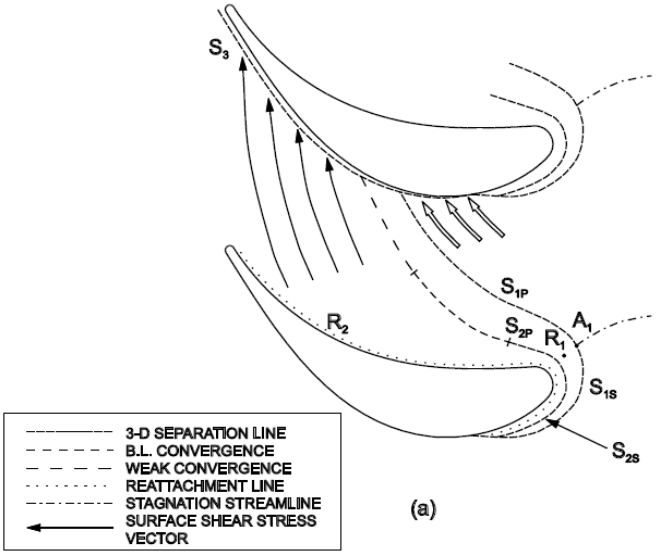

Figure 3.7-1: Schematic sketch of the endwall flow structure at design incidence [21]

In the Figure 3.7-1 the endwall flow structure is schematic represented. The streamline leading to the stagnation point A_1 located at the major endwall boundary layer separation line S_1 is seen and this streamline divides the horseshoe vortex into one suction (s) and one pressure (p) side. The line S_2 represents the liftoff for the horseshoe vortex, describes more in [6]. As S_{1s} and S_{2s} are rounding the leading edge into the suction side they converge and end up at the blades suction surface. At this point a new separation line originates, called S_3. A part of the inlet boundary layer ends up directly at the suction surface without first interact with the separation line S_1 as indicated by the double lined arrows and this fluid is believed to be involved in production of high losses downstream.

At the suction surface sketched in Figure 3.7-2 the separation line S_4 and S_5 are shown, S_4 is associated with the passage vortex and S_5 with the intersection between the entrapped fluid between passage vortex and the suction side of the horseshoe vortex.

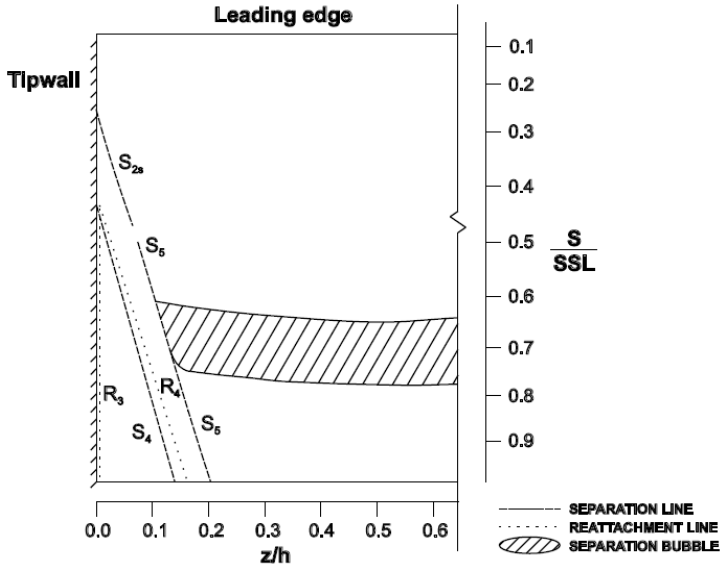

Figure 3.7-2: Schematic sketch of the suction surface flow structure at design incidence [21]

Figure 3.7-3 shows the vortex SS1 and SS2 that are present between S_4 and S_5 and spited by a separation line R_4. It is also shown how the passage vortex is believed to correspond to S_4, a small but strong vortex SS1 and a quite bigger but weaker vortex SS2.

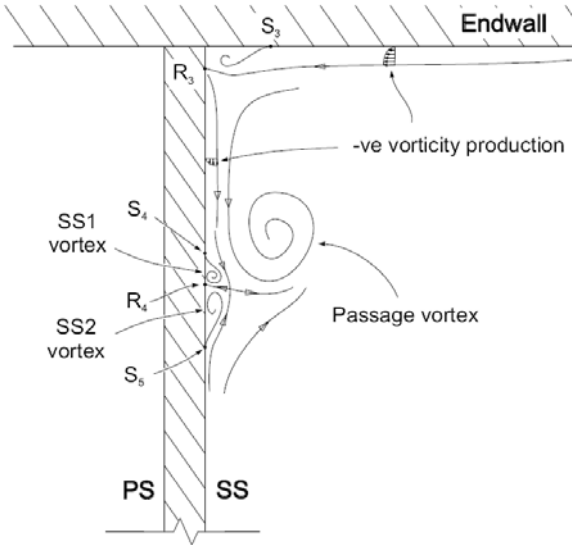

Figure 3.7-3: Schematic sketch of the endwall flow structure [21]

As the positive incidence increases a shift towards a more front loaded blade will be seen as described above. The stagnation streamline is then shifted towards the middle of the pitch and the separation lines S_1 and S_2 are moved upstream. Then the entrapped fluid between S_{1p} and S_{2s} is decreasing when S_{1p} close to intersect $S_{2s,}$ see fig 6b in [20]. Instead the suction side of the horseshoe vortex is growing as more boundary layer fluid is involved. Separation line S_4 moves upstream and will not make a straight line towards the trailing edge anymore.

From measurements of the mixed out losses it was found that the leading edge structure were only of a minor importance and that the blade loading was of much more relevance for the secondary loss. With a frontloaded blade the inlet boundary

layer will feel a stronger pressure gradient between the pressure and suction side, and then a more pronounced passage vortex will be present. Even if there were some uncertainness in the data present in [16] it indicates that a smaller leading edge will suffer from less secondary loss at off-design, a contradiction to the earlier prediction supposed by MKT. The passage vortex is initially increasing in strength with incidence and then it remains close to constant. That is probably due to a longer interaction time between passage vortex and opposite directed vortex as the deceleration of the flow increases with positive incidence [16] page 9.

3.7.2 A New Division between Profile and Secondary Losses

The information to the following section has been collected mainly from [15] and [16]. In section 3.6 it was mention that a new empirical loss model for mean line design was developed with the aim to give a more reasonable relation to the underlying physical phenomena and a more accurate loss prediction. With the conventional loss breakdown they showed in [16] that the secondary loss would decrees and finally be negative as the incidence increases, something that is not physically reasonable. In [16] they make loss measurements for the two low speed linear cascade CC2 and CC3 from Table 3-1 that primary differ in the radius of the leading edge, with the same loading and flow angles.

Figure 3.7-4 show the unrealistic division between secondary and profile losses with the conventional loss division for a small leading edge radius. In Figure 3.7-4 it is seen that the losses increase more rapid after around +10 deg incidence, that is because a separation bubble is present over a large part of the suction surface at the trailing edge.

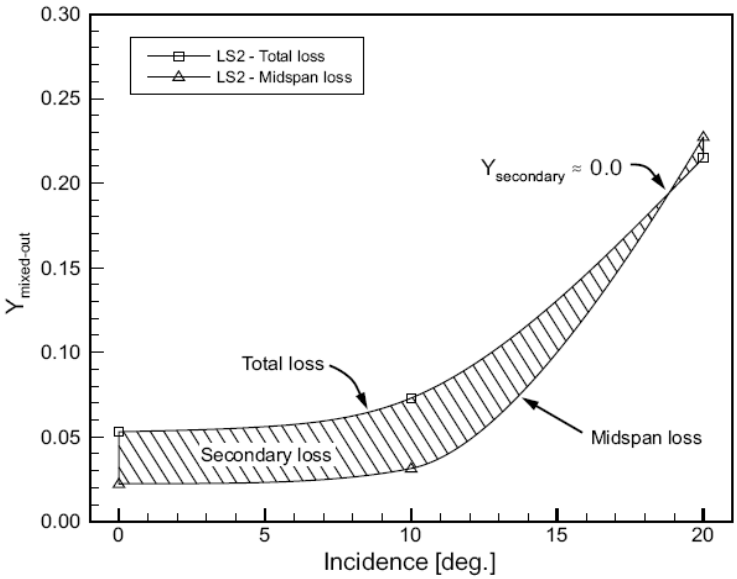

Figure 3.7-4: The unrealistic division between secondary loss and primary loss with the conventional loss division. [16]

The new loss model is based on a new breakdown scheme between the primary and secondary losses that do not use the loss at midspan as a representative loss measurement for the profile loss over the entire blade span (h). Still the conventional loss breakdown of the total loss to a profile, a secondary and a tip leakage loss part are used. The major difference to the conventional method is the division between

secondary and profile losses, which is estimated at zero tip leakage. They believe that the source for the losses at suction surface can be divided into two main regions here referred to as the primary and secondary as shown in Figure 3.7-5 from [15].

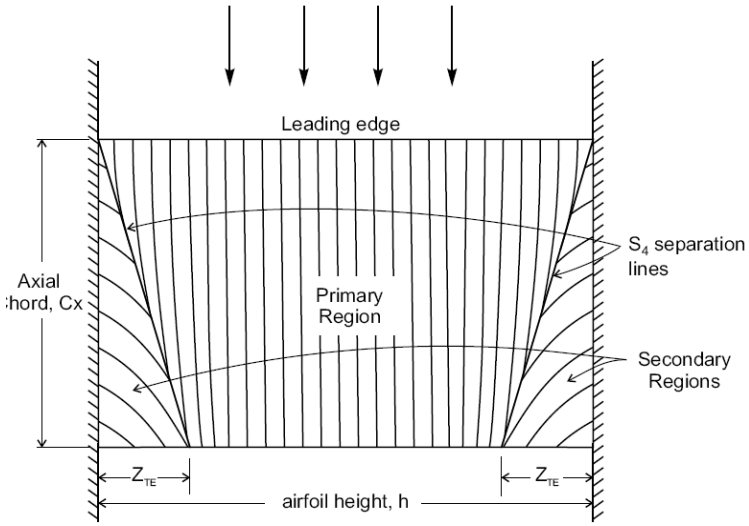

Figure 3.7-5: Division between primary and secondary loss region at suction surface with the new loss breakdown. [15]

The division between these two regions is made by the passage vortex separation line (S_4), as described in [16]. In the primary region the main influencing parameters on the loss are believed to be the pressure distribution, Reynolds number and Mach number. In the secondary region the parameters are believed to depend on the passage vortex strength and to a small amount on the chord wise pressure distribution. For that reason the earlier assumption of a constant loss in both regions seen for the conventional loss division makes no sense.

In the primary region the loss is assumed to be uninfected by the secondary flow and equal to the midspan loss. With the definition of the average loss in the primary region, an assumption that the suction surface area equals axial chord times the span, a expression for the primary loss can be expressed as eqn (3-68), (derived in [15] with equation (2) to (5)). Z_{TE} stands for the distance from the endwall that the passage vortex separation line crosses the trailing edge, see Figure 3.7-5. It is assumed that these distance are equal from both the inner and outer annular wall, and that the separation line starts from the front leading edges upper corner and then follow a linear curve towards the trailing edge. These assumptions are known not to be totally correct, but believed to be enough satisfactory for this proposal. The profile loss is constant to the midspan loss over the entire primary area

$$Y_P = Y_{mid} \cdot \left(\frac{A_{prim}}{A_s} \right)$$

Total blade area taken as the axial chord multiplied by span

$$A_s = c_x \cdot h$$

Primary area according to Figure 3.7-5

$$A_{prim} = c_x \cdot h - 2 \cdot \left(0.5 \cdot Z_{TE} \cdot c_x\right)$$

The new total profile loss

$$Y_P = Y_{mid} \cdot \left(1 - \frac{Z_{TE}}{h}\right) \tag{3-68}$$

The profile loss at midspan should be evaluated as proposed by Kacker and Okapuu under section 3.3.1 for design incidence and as proposed by themselves in [17] for off-design, see eqn (3-64). The parameter Z_{TE} is needed to make use of eqn (3-68). Sharma and Butler (1987) proposed a relation to estimate this but BSM derive a new relation that also include the pitch to chord ratio (s/c), based on test data from 19 linear cascades. The other included parameters that is believed to effect the passage vortex size and then also S_4 are the turning (ε), inlet boundary layer thickness ratio to span (δ_{in}/h), contraction ratio (CR). CR represent the flow acceleration and ε together with s/c the blade load.

The penetration deep Z_{TE} can be estimated by eqn (3.69) that was derived with an optimization method for the believed important parameter and measured test results.

$$Z_{TE} = \left(\frac{0.10 \cdot F_\theta{}^{0.79}}{\sqrt{CR} \cdot \left(\frac{h}{c}\right)^{0.55}} + 32.7 \cdot \frac{\delta^*}{h} \right) \cdot h \tag{3-69}$$

where the boundary layer thickness is defined as

$$\delta^* = \int_0^\delta \left(1 - \frac{V}{V_{BL-edge}}\right) \cdot dz \tag{3-70}$$

This thickness can be difficult to calculate, because it is not a mean line value as wanted in the pre-design stage. From the tested cascades it is seen that the value of δ^*/h use to be between 0.008 and 0.061, so perhaps an estimated value there between can be used instead in the early design stage.

The tangential loading parameter defined as

$$F_\theta = 2 \cdot \frac{s}{c_x} \left(\tan(\alpha_{in}) + \tan(\alpha_{out})\right) \cdot \cos^2(\alpha_m) \tag{3-71}$$

The only difference between Zweifels blade loading and the F_θ is that the later is nondimensionalized by dynamic pressure based on mean vector velocity instead of exit velocity as for Zweifels, thereby the both are simply related as equation (3-72).

$$F_\theta = \psi_T \cdot \frac{\cos^2(\alpha_{out})}{\cos^2(\alpha_m)} \tag{3-72}$$

The choice to use F_θ was because it showed the best curve fitting between the correlation and measured value.

Initially in the optimization process the stagger angle was included to represent the growth of passage vortex for a more frontloaded blade, that the increase in stager angle will give, but no significant relation was found so it was excluded in the final relation.

The relation in eqn (3-69) makes a reasonable physical sense where for high flow acceleration the vortex will be stretched and its radius decrease, at the same time as the bounder layer thickness where the secondary flow originate get thinner as captured with the division of CR $\geq$ 1.0. The driving pressure gradient between the pressure to suction side for the secondary flow is catch with the tangential load parameter F_θ. The relation to h/c could not be direct physically explained, but there was no doubt about its significant relation to the Z_{TE} in the tests [15]. Perhaps h/c catching two different phenomena because the different trends shown if the chord is increased compare to if the span are decreased, as discussed in [15].

Figure 7 in ref [15] show the predicted compare to measured values for Z_{TE}/h with equation (3-72) where most of the points are within $\pm$ 0.025.

When derive the correlation for the secondary loss data from 34 linear cascades were used and is summarized in appendix 2 in ref [15]. The cascade were said to cover a wide range of incidence from -23 to +20, CR of 0.98.3.88 , h/c of 0.79-3.0, blade turning (ε) of 47-110 deg, and endwall boundary layer displacement thickness δ^*/h of 0.6-6 percent. A limitation is that the passage vortexes is not allowed to merge together at the midspan. Thus the range for how low aspect ratio that can be used without any absolute given value is limited, ($Z_{TE}/h \leq 0.5$).

The empirical correlation for the secondary loss was derived as eqn (3-73) after an optimization process similar to that made for Z_{TE} with a number of parameters that were believed to play a significant role. Initial the tangential loading and skin friction factor were also included but after the optimization process both were excluded because no significant relation was found for the measured data point. The excluding of F_θ is not conformably to some of the earlier studies made on turbine losses.

Secondary loss
For $h/c \leq 2.0$

$$Y_S = \frac{0.038 + 0.41 \cdot \tanh(1.20 \cdot \delta^*/h)}{\sqrt{\cos(\gamma)} \cdot CR \cdot \left(\frac{h}{c}\right)^{0.55} \cdot \left(\frac{c \cdot \cos(\alpha_{out})}{c_x}\right)^{0.55}} \tag{3-73a}$$

For $h/c > 2.0$

$$Y_S = \frac{0.052 + 0.56 \cdot \tanh(1.20 \cdot \delta^* / h)}{\sqrt{\cos(\gamma)} \cdot CR \cdot \left(\frac{h}{c}\right) \cdot \left(\frac{c \cdot \cos(\alpha_{out})}{c_x}\right)^{0.55}} \quad \text{(3-73b)}$$

The stager angle should represent the blade loading distribution so that a frontloaded blade will get a higher secondary loss and the displacement thickness to span height ratio represent the mass flow ratio in the end wall boundary layer. The terms,

$$\left(\frac{h \cdot \cos(\alpha_{out})}{c_x}\right)^{0.55} \text{ or } \left(\frac{c \cdot \cos(\alpha_{out})}{c_x}\right)^{0.55} \cdot \left(\frac{h}{c}\right)$$

altered between because of h/c ratio, should capture influence of endwall surface area. The secondary loss varies linear to the inverse of CR, just as were supposed by AM, AMDC and AMDCKO. The annular area is related to the axial chord c_x instead of the conventional true chord c.

The total loss for the primary and secondary loss is then calculated as

$$Y_{P+S} = Y_{mid} \cdot \left(1 - \frac{Z_{TE}}{h}\right) + Y_S \quad \text{(3-74)}$$

Note should be done to the fact that the test data used to derive this correlation is from linear cascades, so to be able to apply it to a real turbine a multiplier factor is needed that was not given in any of their papers, and is a major drawback.

3.8 Mamaev & Klebanov

In 1969 B. I. Mamaev and A. G. Klebanov (MaKl) published a paper [19] where they describe how to decide optimal pitch to chord ratio (s/c). Some of these correlations, with a few small modifications at some points are still used today in Siemens in-house program CTC. MaKr used test results from 58 straight cascade where air where blown through. The flow was always free from shocks ($\lambda_{out} \approx 0.8$), Re in the range of $(0.4-1.2)\cdot 10^6$, TI_{in} of 1-2 percent, α_{in} in the range of 22-101 deg and α_{out} in the range of 14-50 deg defined from the tangential plane.

In the attempt to find a optimal s/c the profile loss was examined and the highest value of s/c that give a value close to the minimum loss was said to be the optimal ($(s/c)_{opt,0}$). In the cascade test the losses due to trailing edge thickness was excluded with a correlation given by G. Flügel (not given in this text). In the derive of the correction they examined the value of $(s/c)_{opt,0}$ as a function of α_{out}, where small variation in the cascade value of α_{in} was put together, the result can be seen in Figure 3.8-1.

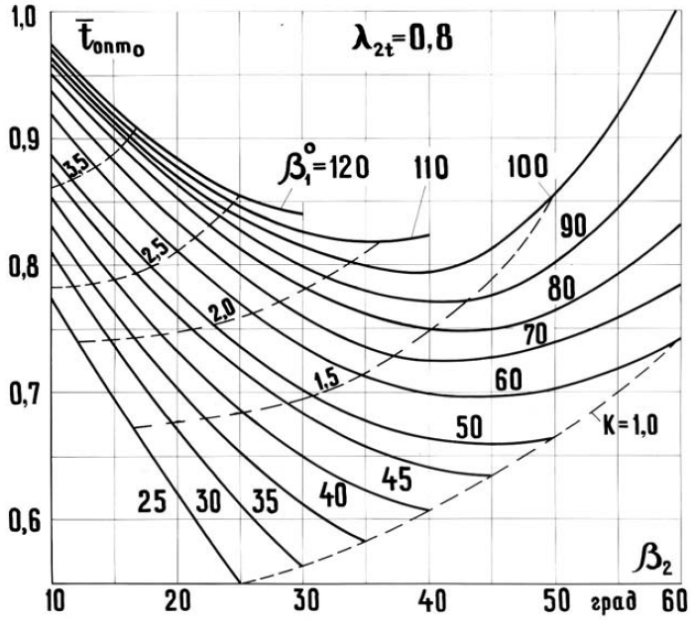

Figure 3.8-1: Value of optimal pitch chord ratio as a function of α_{out}, where the angles are defined from the tangential plane (original from) [19].

From Figure 3.8-1 it is seen that for a constant acceleration (CR = const) that means that the turning in the row decreases will the optimal pitch increase, as illustrated by the dotted line. If instead the acceleration in the row is increased is there first a decrease in the pitch because a higher need of controlling the flow. Then with an outlet flow angle greater then 45-50 deg will the decrease in turning (ε) have a higher influence than the increasing CR and therefore is the optimal pitch increasing again.

The equation to describe $(s/c)_{opt,0}$ as a function of $\alpha_{in}, \alpha_{out}$ in radians from [19] is given for two ranges of contraction between the inlet and outlet area as

For $1 \le k \le 1.5$

$$(s/c)_{opt,0} = (\frac{1.727}{k} - 0.869) \cdot \varepsilon^{-(1/3)} - \frac{1.71}{k} + 1.604 \qquad (3\text{-}75a)$$

For $1.5 \le k$

$$(s/c)_{opt,0} = \frac{0.327}{k^{0.371}} \cdot \varepsilon^{-(1/3)} - \frac{0.994}{k^{0.395}} + 1.314 \qquad (3\text{-}75b)$$

Where ε it the deflection and k stands for the blade contraction and aim to catch the influence of flow acceleration.

$$k = \frac{\sin(\alpha'_{in})}{\sin(\alpha'_{out})}$$

Equation (3-75) give a increase in of $(s/c)_{opt,0}$ for a increase of k, and the opposite is true for ε but with less strength if the convergence is high.

The effect of trailing edge thickness and outlet Laval number were also investigated and two approximately equations were given, eqn's (3-76) and (3-77).

$$\chi_{TE} = 1 + \left(0.0375 \cdot (s/c)_{opt,0} - 0.006\right) \cdot \frac{d_{out}}{c} - 0.0015 \cdot \left(\frac{d_{out}}{c}\right)^2 \quad (3\text{-}76)$$

For $0.5 \le \lambda_{out} \le 1.15$

$$\Delta(s/c)_{opt} = 0.016 + 0.48\lambda_{out} - 0.625\lambda_{out}^2 \quad (3\text{-}77)$$

Equation (3-76) is used in CTC, but in eqn (3-77) the constants has been changed, and is shown below as eqn (3-78). If this modification is done by MaKl themselves, by any other research group or if it is an internal modification on Siemens is not clear.

For $0.5 \le \lambda_{out} \le 1.20$

$$\Delta(s/c)_{opt} = 0.022 + 0.369\lambda_{out} - 0.391\lambda_{out}^2 \quad (3\text{-}78)$$

The final value is then obtained from

$$(s/c)_{opt} = (s/c)_{opt,0} \cdot \chi_{TE} \left(1 + \Delta(s/c)_{opt}\right) \quad (3\text{-}79)$$

In (Profile losses in a turbine cascade) [24] from 1970, MaKl described the procedure to estimate the profile losses for a turbine at design point. This methodology is today partially used in CTC with numerical equations replacing the original graphs given by MaKl. The main steps are given here with some of the graphs replaced by the corresponding equation form CTC, so for the original proposed graphs [24] should be used.

First the loss coefficient for an ideal Laval number and zero trailing edge thickness are used as the datum point. The loss is given by Figure 3 in [24] or by equation (3-80) from CTC [25].

$$\zeta_{Fr} = \frac{0.015}{CR} \cdot \left(1 + \left(\frac{\varepsilon}{1.745}\right)^{1.5}\right) \quad (3\text{-}80)$$

Because different outlet Laval number compared to the optimal the loss is corrected with either a chart originally given in Figure 6 in [24] or the numerical relation from [25] given in eqn (3-81).

$$\Delta\zeta_{Fr,\lambda} = -1584.3 \cdot x^6 + 8255.2 \cdot x^5 - 17687 \cdot x^4 + \\ + 19959 \cdot x^3 - 12520 \cdot x^2 + 4141.5 \cdot x - 564.18 \quad (3\text{-}81)$$

where

$$x = \frac{\lambda_{out}}{\lambda_{opt,out}}$$

To take concern to the deviation from the optimal pitch (s_{opt}) Figure 5 in [24] or from CTC the eqn (3-82) should be applied.

$$\left.\begin{aligned}
&\Delta(s/c) = \frac{(s/c) - (s/c)_{opt}}{(s/c)_{opt}} \\
&\Delta\zeta_{Fr,s} = \left(200 - 451\cdot\Delta(s/c)_{opt} + 264\Delta(s/c)^2{}_{opt}\right)\cdot\Delta(s/c)_1^2 + \frac{\Delta(s/c)_1}{5.6 - 3.75\cdot\Delta(s/c)^2{}_{opt}}
\end{aligned}\right\} \quad \text{(3-82)}$$

where

$$\Delta(s/c)_1 = \begin{cases} \Delta(s/c) & \text{if } \Delta(s/c) \geq 0 \\ \left|\left(0.1666 - 0.6667\cdot(s/c)_{opt}(1-(s/c)_{opt}) + (s/c)\right)\right| & \text{if } \Delta(s/c) \leq 0 \end{cases}$$

Then the effect of the trailing edge thickness is given by eqn (3-83), (this one is not used in CTC).

$$\zeta_{TE} = 0.2\cdot\frac{t_{TE}}{s}\cdot\frac{1}{\sin(\alpha_{out})} \quad \text{(3-83)}$$

If now eqn's (3-81), (3-82) and (3-83) are combined the final profile loss are the sum of both the friction and trailing edge loss corrected for a not optimal value. Its final expression at design point is given by eqn (3-84)

$$\zeta_P = \zeta_{Fr,o}\cdot(1+\Delta\zeta_{Fr,s})\cdot(1+\Delta\zeta_{Fr,\lambda}) + \zeta_{TR} \quad \text{(3-84)}$$

4 Incidence Effect on Profile and Secondary Losses

The aim with this research is to investigate the accuracy of the loss model used in the in-house program CTC at Siemens for primary off-design loads. The investigation is validated against measurements at real gas turbines and numerical experiments with the in-house program code Blagen. The simulation results from CTC are compared with simulations based on a number of the loss models described in chapter 3, see section 4.2.6 below.

4.1 Background

Investigations of different loss models correlations have been done many times before and the results have been present in a lot of reports and engineering paper's all over the globe. The major conclusion that can be drawn is that no universal correlation exist that can be recommended for all kind of gas turbines. One reason for this lack in prediction capacity is the different design philosophy between different designers that will include some geometric variation that can not be caught with a simple 1D analyze. Therefore there is a need for every design center to actual compare and in some case tune the 1D's correlations to test results from there own gas turbines.

The two tests used in this investigation are briefly described in chapter (4.1.2 and 4.1.3), and for Siemens employed the full description can be seen in [27] and [28].

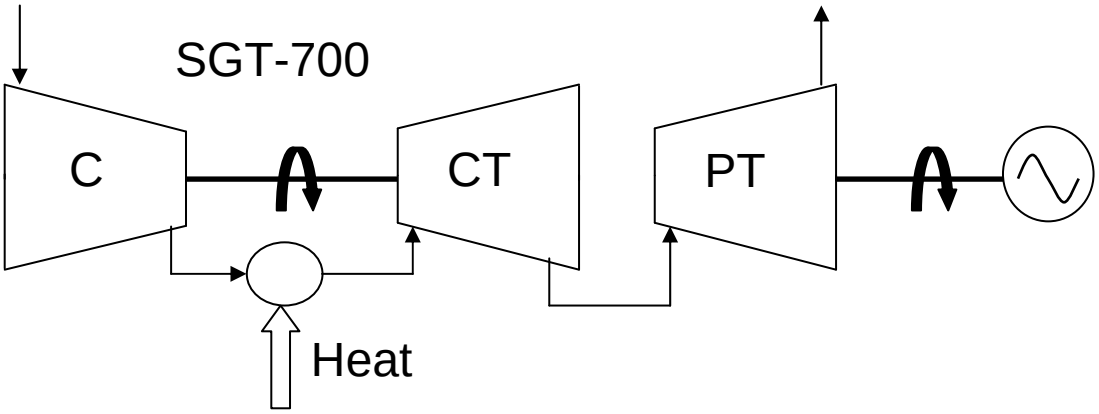

Figure 4.1-1: Structure of SGT-700 (earlier referred to as GT10C). It consist of one compressor (C) that deliver compressed air to both the compressor turbine (CT) driving the compressor and to the power turbine (PT) that deliver the shaft work for external use. Both the CT and PT consist of two turbine stages each.

4.1.2 Experimental Test 1

Test 1 was made on GT10C now referred to as SGT-700, and the test involve seven steps of 5 MW each in the load of the power turbine PT from idle up to full load at 31 MW [27]. At each load step the machine were first running at ten minutes to reach steady state, and then five more minutes at the time the measurements were made. After this the machine was speed up to the next power level for five more minutes, to sum up with a total of 20 minutes between each step. Unfortunately no measurements were made while speeding down, so it can not be totally convinced that the machine were in total thermal equilibrium, something that would effect for example the tip

clearance. Because of a problem in the first test run with the measurements, a second experiment was made. The carbon dioxide (CO) and unburned hydrocarbon (UHC) was now measured for a calculation of the combustion efficiency that was found to differ from the characteristics normally used in the evaluation. For all the loads the total temperature and pressure, mass flows in the turbine sections, the bleed off points from the compressor and overall isentropic efficiency for PT were measured or calculated, so the input data to any future calculations are well provided.

4.1.3 Experimental Test 2

Test 2 was also done at GT10C or today's SGT-700. In this test the consequences of varying the running speed of the PT from 50 to 105 percent of the normal running speed at 6515 rpm were investigated [28]. Test 2 was done on test turbine B860 which is known to have a poor working PT. The main part of these simulations are using input data from an evaluation report of test 2 that later showed to be incorrectly evaluated by Siemens. Later new test evaluations were found where the PT efficiency hade been increased by as much as up to 1.5 percent in some load cases. These results are now used as a reference instead, but still the incorrect input data is used for some of the simulations. The differences are primary in p_{0in}, p_{0out}, T_{0in}, PR and $\dot{m}$. The effect of these differences between evaluation 1 and 2 have been tested by comparing the simulation results from CTC and BSM 1995 limit (described in chapter 3 and 4.2.6) with data from both evaluations. It shows that the changes will only affect the efficiency by around 0.0-0.05 percentage point and are therefore unimportant for the evaluation of the total efficiency for the PT with the other loss models. When comparing the dimensionless numbers (as Flow number C) in section 4.2.6 the changes are more noticeable and the results from the last evaluation (number 2) is used.

As mentioned above the power turbine in version B860 is known to have a low efficiency, so even if the test results are correctly measured the values are not representative for the efficiency of Siemens PT today. The trends are still believed to be representative.

They most important parameters from the tests mentioned above are summarized in Tables 4-1, 4-2 and 4-3. Note that some parameters are confidential and therefore excluded or normalized (norm).

Table 4-1: The main parameter from test 1 where the PT's output was stepped from 0-31MW

Measured Test 1							
	0 MW	*5 MW*	*10 MW*	*15 MW*	*20 MW*	*25 MW*	*31 MW*
Power [MW]	0.72	5.75	10.76	15.8	20.85	25.88	31.76
N [rpm]	6516	6511	6514	6516	6515	6518	6519
PR* [-]	1.34	1.89	2.38	2.78	3.17	3.52	3.86
T_{in}* [C]	**Confidential**						
P_{in}* [Bar]	**Confidential**						
m [kg/s]	36.5	52.8	65.4	73.0	80.0	86.2	92.9
Flow Number C [-]	**Confidential**						
Eta*s (norm) [%]	34.12	84.17	92.90	97.18	98.81	99.92	100.00

Table 4-2 and 4-3: The main parameter from test 2 where the PT's output speed was stepped from 50 to 105 % of normal running speed, for version 2 (evaluation 1 at top and evaluation 2 below)

Table 4-2:*(Evaluation 1)*

Measured Test 2 (Evaluation 1)					
	50%	*70%*	*80%*	*90%*	*105%*
Power [MW]	6.10	12.42	18.44	22.73	23.30
N [rpm]	3258	4561	8952	5864	6842
PR* [-]	1.96	2.59	3.06	3.33	3.34
T_{in}* [C]	**Confidential**				
P_{in}* [Bar]	**Confidential**				
m [kg/s]	50.8	67.6	78.6	84.6	86.2
Flow Number C [-]	**Confidential**				
Eta*s (norm) [%]	93.17	98.50	99.13	99.94	100.00

Table 4-3 *(Evaluation 2)*

Measured Test 2 (Evaluation 2)					
	50%	*70%*	*80%*	*90%*	*105%*
Power [MW]	6.13	12.50	18.56	22.87	23.45
N [rpm]	3258	4561	8952	5864	6842
PR* [-]	1.94	2.56	3.03	3.30	3.33
T_{in}* [C]	**Confidential**				
P_{in}* [Bar]	**Confidential**				
m [kg/s]	50.8	67.2	78.0	83.9	85.4
Flow Number C [-]	**Confidential**				
Eta*s (norm) [%]	94.07	98.88	99.44	100.17	100.00

4.2 Method

4.2.1 Simulating the Efficiency with CTC and Other Loss Correlations

The simulations where done on the PT of today's SGT-700 for all the measured loads in the two tests that were described above. To be able to make the simulation some assumptions and modifications were needed to be done on the original CTC input file for the two stages of the PT.

4.2.2 Cooling Air Temperature

The temperature of the cooling air has to be estimated and this was done with the use of the program "flowbalance". The main steeps for these calculations can be seen in appendix 12.4.

4.2.3 Correction of Mass Flow

The second modification done was to modifying the throat area for stator one (S1) until the measured mass flow at full load (31MW) from test 1 and the result from the CTC simulations match each other (they should both have the same flow number (C)).

4.2.4 Input Data from Measurements to CTC

For the simulation in CTC an input file is needed that contains the blade geometries, thermodynamic properties at the inlet and pressure ratios across the PT. The chosen section from the tests to represent this are inlet at section 61, outlet at section 70 and bleed off's from stage 6 and 11 at the compressor. A number of the loss model need blade geometries that was not represented in CTC, and for these cases the original blade geometry file for SGT-700 were used to decide the value of these. Examples of these parameters are stager angle (γ), maximum profile thickness (t) and the throat (o).

4.2.5 Modeling in CTC

If the in-house program CTC is regarded as a black box it consists of a main program, one input file (runctc.dat) and one account file (account.dat) that link together the main program with the input and output file and include the pressure ratio for the entire turbine. When the main program is running it read in the input file "account.dat" and returns four files containing a user friendly input file, a file containing all the losses, a file containing the calculated results and one real (not user friendly) output file containing all output data without any comments.

In the first step of the investigation when only the test results were compared with the CTC model one separate input file for each specific measured load in both test 1 and 2 were written, under the assumptions mentioned above. The result from these simulations are seen in Figure 4.3-3 to 4.3-6 and discussed in sections 4.3-1 and 4.4.

In the next step test results were compared against some of the other loss models that were described in chapter 3. These loss models need both blade geometries, flow angles and thermodynamic properties to calculate the losses. Those are parameters that CTC use as input or output parameters. Depending on the values of the losses, the

flow and thermodynamic properties will vary through the turbine. That means that an iterative calculation methodology is needed to find a converging solution with other loss models than standard CTC. To do this in a somewhat time efficient way Matlab and CTC were integrated together.

The way to do this coupling is five separate Matlab programs, where some of them consist of many subprograms, as for example the program for the losses calculations, linked together by a main program.
The Matlab programs are

- **Read input data**
  Open and read in the information stored in runctc.dat and runctc_point.txt. It then split the information into separate matrix that contains specific parts of the turbine geometry and input data. Still are the data in the matrix only stored in Matlabs workspace.
- **Input parameters**
  This file chose the separate parameters that are needed for the loss calculations from the matrix created by "Read input data" and store them in smaller matrices or vectors for easy access.
- **Losses**
  Calculate the losses for the different loss models, with the latest parameter from "In parameter". The difference between the standard losses from CTC and the calculated are stored as an extra loss source in CTC.
- **Write CTC input**
  Write a new input data file, which includes the new losses as an extra loss source, which can be either an increase or decrease.
- **Run CTC**
  Run the main CTC program with the new losses and a new runctc_point.txt file is created.
- **Main**
  The main program couple and loop the calculation steps until the PT isentropic efficiency has converged and a final value are reached.

The principal structure and implementation of the Matlab programs are seen in Figure 4.2-1

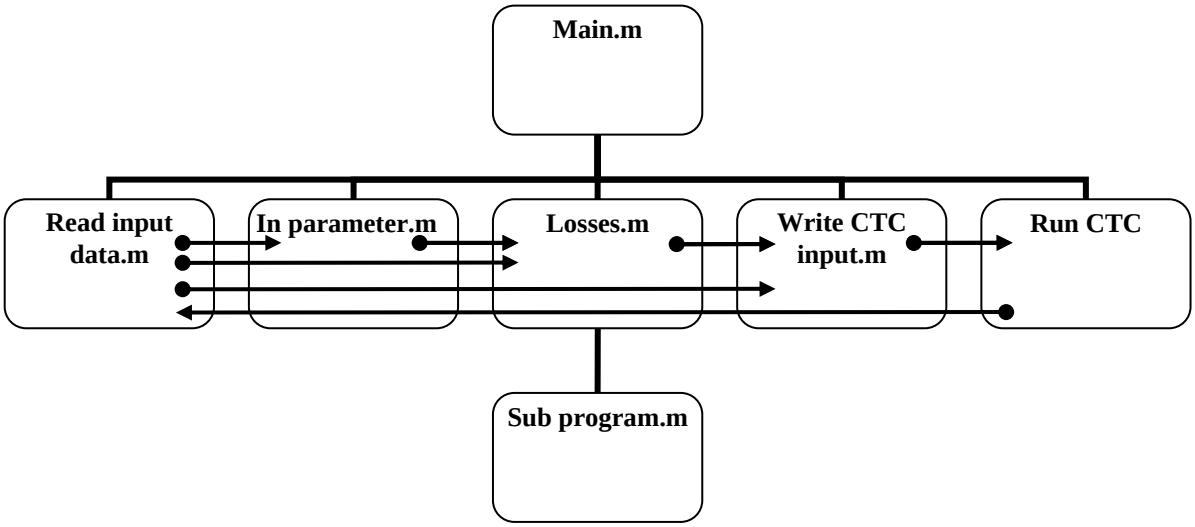

Figure 4.2-1: The principal structure for the implementation of losses in CTC with the use of Matlab.

4.2.6 Investigated Off-Design Loss Models

The investigated loss models are except from CTC standard loss model also, MKT 1989, BSM 1995, ZS 2005. Each one of these models is divided into sub models. The division depends on what losses they use as a datum point when correct for incidence and if there is any limit in how big the loss corrections can be. The specification of each loss model and its result are seen below.

MKT 1989 limit
Here the combined loss model from Ainley & Mathieson, Dunham & Came, Kacker & Okapuu (AMDKCO) from 1980 is used to calculate the profile and secondary losses at the design point. The losses are corrected for off-design incidence with MKT 1989 where the endpoint value is used for the case that the correction in x' and x'' for eqn 3-63 and 3-65 reaches there outer limit.

MKT 1989 no limit
As "*MKT 1989 limit*" where the only difference that now is the losses from eqn 3-63 and eqn 3-65 extrapolated even outside there proposed limits.

BSM 1995 limit
Still AMDCKO is used as the datum point and MKT 1989 to correct for the secondary loss. For the profile loss Benner, Sjolander and Moustapha's loss correlation from 1995 [17] (BSM 1995) is used, see eqn 3-63 and 3-64. Both corrections are limited to their endpoint values.

BSM 1995 no limit
As "*BSM 1995 limit*" but with no limits in the loss correction.

ZS 2005 Version 1 limit
Still AMDCKO loss model is used to find the secondary loss at design. The secondary loss is then being corrected by MKT 1989. When calculation the profile loss the

proposed model from Zhu and Sjolander (ZS) [26] is used and then corrected with BSM 1995 for off-design incidence.

ZS 2005 Version 1 no limit
As "*ZS 2005 Version 1 limit*" but with no limit.

ZS 2005 Version 2 limit
This model is identical to "*ZS 2005 Version 1 limit*" except from that the correction for both profile and secondary losses are done with MKT 1989 and limited endpoint values.

ZS 2005 Version 2 no limit
As "*ZS 2005 Version 2 limit*" but with no limit.

CTC No Loss at all
To see how much of the decrease in efficiency that originated from the profile and secondary loss models and how much that are due to the velocity triangles CTC has been running with no profile or secondary losses at all. Still there will be some decrease in efficiency because the leakage mass flow that do not passes the blade row and therefore do not contribute to any shaft work output.

4.2.7 Numerical 2D Experiment

A numerical investigation of what affect a variation of the incidence has on the profile loss where done in Blagen with NS-2D solver, that use a two-equation turbulent model, namely Coakley's q-ω model [42]. The reason was to see how the loss models predict the losses when the incidence reach a great positive value, something that was not catch in test 1 and 2 as can be seen from the incidence graphs in Figures 4.3-1 and 4.3-2. These tests were made with a representative blade profile for Siemens, and in Blagen the real midsection where used. For the CTC simulations only entire stages can be simulated, so therefore both the stator and rotor was included in the simulation. The thermodynamic properties at the inlet, speed and so on were chosen equal to the full load case from test 1. The cooling air was removed and PR chosen from the full load simulation with the CTC model, and the blade geometries for stator 1 in CTC were modified to match the geometry in Blagen.

The proceeding was that for each value of incidence first run CTC to get a result file. From this result file then the value of kappa (γ) and outlet Laval number from stator 1 were used as input data to setup the numerical calculations in Blagen. The results from Blagen are only 2D and were therefore compared to the profile loss from CTC. The profile loss from CTC is here assumed to include the losses because of friction, roughness, trailing edge, turbulence, Reynolds number and shock losses.

The variation of profile loss for the other loss models was also investigated. First by varying the incidence whiles all other parameters were hold constant to the full load run (31 MW) with no incidence. To future increase the accuracy of the test also the change in the other parameters as Ma, γ, Re etc with incidence (i) were included. To achieve this Matlab has to be integrated and coupled together with CTC. In the section below the numerical results for the profile loss from Blagen in the range of incidence from -50 to +45 deg are compared to the profile loss for "CTC", "MKT 1989 no

limit", "BSM 1995 no limit", "ZS 2005 version 1 no limit" and "ZS2005 version 2 no limit" for incidence -50 to +50 deg. The trends of how both MKT 1989 and BSM 1995 off-design losses change with variation in i, d_{in} and We_{in} are illustrated.

The stator and stage characteristics are summarized in Table 4-4 below. It is seen that the stage loads and flow coefficients are low, (around 1.5 and 0.55). No big variation is seen with incidence, except from at high positive incidence where the stator work more and more as a diffuser, witch is actually the case for more then 40 deg of positive incidence, as seen by the fact that PR_{stator} <1.

Table 4-4: Stage and stator characteristics for the numerical investigation in Blagen of profile loss variation with incidence. The results from CTC are used as input data to Blagen to get a correct comparison between Blagen and the other loss models.

SGT-700 PT						
Incidence	*Incidence, 0 [deg]*		*Incidence, -40 [deg]*		*Incidence, 40 [deg]*	
Parameter	*Stage*	*Vane*	*Stage*	*Vane*	*Stage*	*Vane*
T* [K]	1084	1084	1084	1084	1084	1084
P* [bar]	4.11	4.11	4.11	4.11	4.11	4.11
Pi [-]	2.15	1.31	2.14	1.31	2.12	1.08
Pi* [-]	2.03		2.03		2.03	
u/c* [-]			**Confidential**			
H/u^2 [-]			**Confidential**			
Eta* [%]			**Confidential**			
P [MW]			**Confidential**			
Reaction Mid [-]	0.57		0.56		0.51	
Mach Stator [-]		0.75				0.79

4.2.8 Analysis of the Off-Design Loss Models

A analysis of the behavior of the different models for parameter variation could be found section 4.3.3. The parameters varied are except from incidence (i) the inlet wedge angle (We_{in}) and leading edge diameter (d_{in}). All other parameters are constant to stator 1 on the PT for SGT-700.

4.3 Results

4.3.1 Results from the CTC Simulations

One of the main intentions with this report is to investigate the off-design trends for different loss models that primarily are controlled by the flow incidence angle (i). The incidence angle for each blade row and load case is shown in Table 4-5 and Figure 4.3-1. The incidence are from calculations with CTC's standard loss model, but comparisons with simulation results from the other loss models showed that the accuracy are within ± 1.5 deg which are enough to get a feeling for the off-design flow condition.

Table 4-5: The variation of incidence from calculations with CTC's standard loss model for test 1

Incidence from CTC [deg]				
Power [MW]	*S1*	*R1*	*S2*	*R2*
31	-8.9	-13.6	-0.9	-6.6
25	-8.9	-17.2	-5.1	-13.0
20	-8.9	-20.5	-9.7	-21.0
15	-8.9	-25.7	-17.0	-32.1
10	-8.9	-33.7	-28.2	-44.7
5	-8.9	-42.7	-43.1	-57.7
0	-8.9	-65.3	-68.6	-73.1

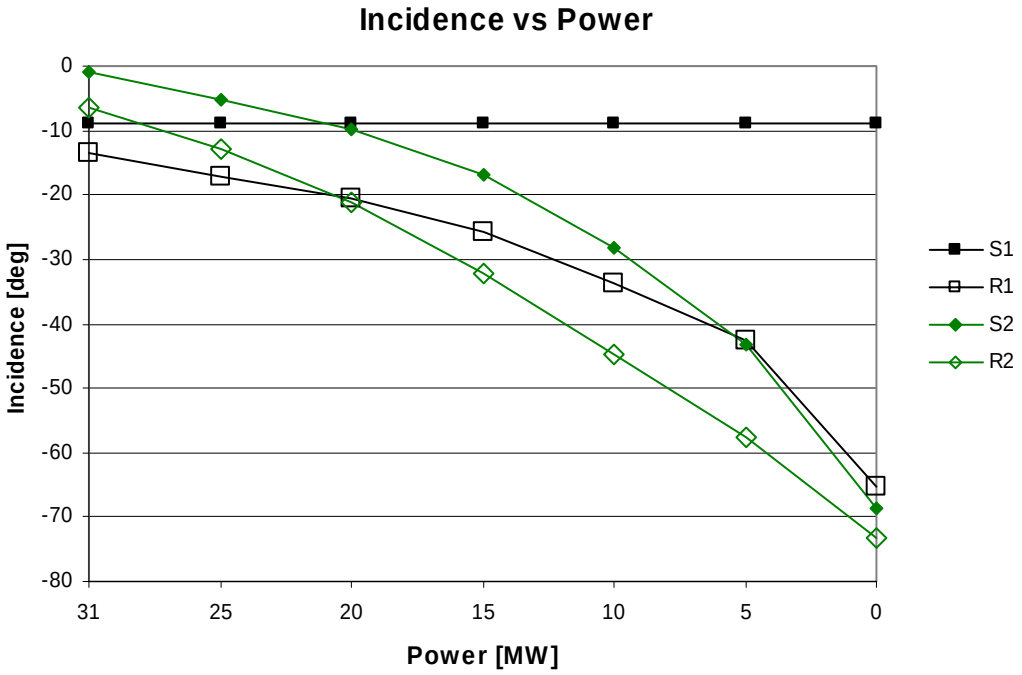

Figure 4.3-1: The variation of incidence from the CTC simulation for test 1 represented as a chart. It is seen that the incidence always is negative and vary from 0 to -73 deg, and that all rows follow the same trends, except from stator 1.

Table 4-6: The variation of incidence from the CTC simulation for test 2.

Incidence from CTC [deg]				
Speed [%]	*S1*	*R1*	*S2*	*R2*
50	-8.9	12.6	15.9	6.8
70	-8.9	3.6	9.1	-2.5
80	-8.9	-0.7	8.1	-0.4
90	-8.9	-7.5	3.4	-5.0
105	-8.9	-24.1	-11.7	-21.3

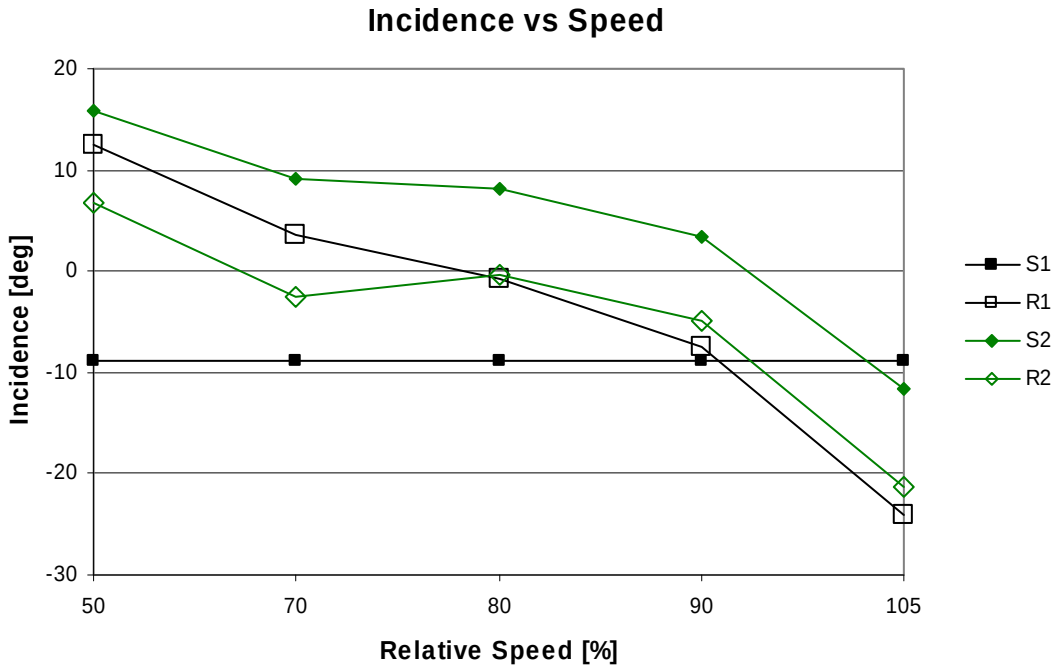

Figure 4.3-2: The variation of incidence from the CTC simulation for test 2 represented as a chart. Here the incidence is both positive and negative and vary from plus 16 to minus 24 deg. The same trends are seen for the three last rows, R1, S2 and R3.

Simulations were also done with the new breakdown scheme from BSM 2006 as is described in section 3.7. As mentions in [23] are the correlations based on cascade experiments and should therefore be modified with a correction or more advanced parameters to better predict a real turbines 3-D flow field. To do this improve accurate a lot of test data are needed, and there is no point that from just one or two tests tune in a correlation, as would be the alternative. That is why no results from BSM 2006 are presented in this section.

4.3.2 Results Related to Test 1

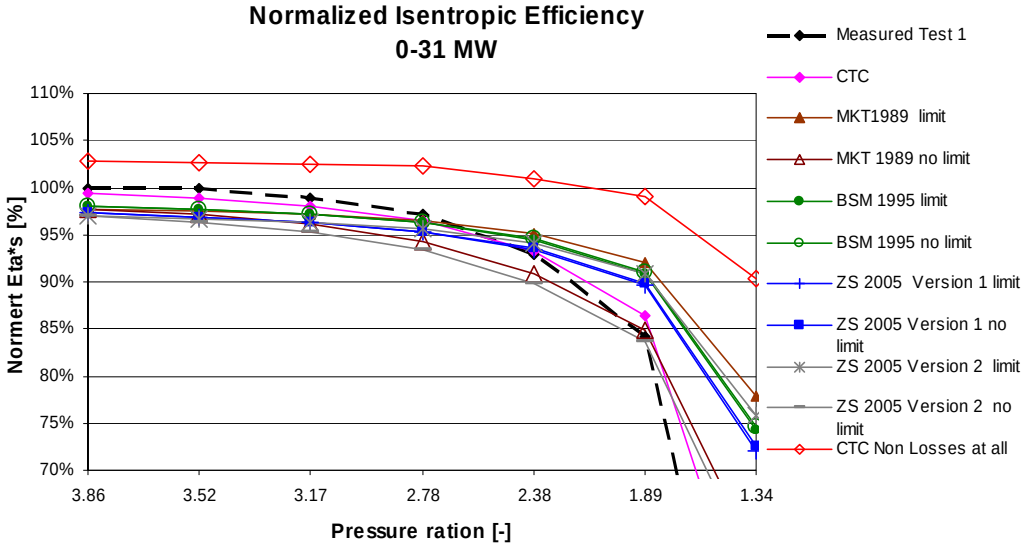

Figure 4.3-3: Comparison of the normalized efficiency from measurement, CTC and other loss models.

The isentropic efficiency for the simulation with different loss models for the PT in test 1 is present in Figure 4.3.3. It is seen that the measured efficiency is higher than the predicted for high loads, but as the load (represented by PR) decrease no of the models catch the decreasing trend satisfying. As the turbine reach the low load of 5 MW rotor 2 will not contribute to shaft work any longer. It is seen by the fact that the enthalpy over the last blade do not decreases anymore, here referred to as the last stage is running in a (Turn-up Mode) or is (Ventilating). At this condition it is difficult to calculate any accurate efficiency (private communication with Ake Klang). The y-label in Figure 4.3-3 has been cutoff at 70 percent even if some curves are beyond that value for the lowest PR. The reason for this is to make it possible to separate the curves from each other at the higher PR. For Siemens employees these low values or any other more precise value are seen in Table 4-7.

Included in Figure 4.3.3, 4.3.5, Table 4-7 and Table 4-9 is the efficiency of the PT with no loss at all except from leakage flow (see section 4.2-6). The intention with this is to illustrate the effect on efficiency that the velocity vectors themselves have and how much of the efficiency decrease that actually originate from the loss model.

Table 4-7: The Table shows the simulated isentropic efficiency for test 1 with different loss models. These results are also present in Figure 4.3-4.

Simulated Isentropic Stagnation Efficiency (norm) [%]								
Model	*PR [-]*	*3.86*	*3.52*	*3.17*	*2.78*	*2.38*	*1.89*	*1.34*
Measured Test 1		100.0	99.9	98.8	97.2	92.9	84.2	34.1
CTC		99.4	98.9	98.0	96.4	93.2	86.4	50.5
MKT1989 limit		97.8	97.5	97.1	96.5	95.1	92.0	77.9
MKT 1989 no limit		97.8	97.2	96.2	94.3	90.9	84.9	61.0
BSM 1995 limit		98.0	97.7	97.2	96.3	94.5	90.8	74.2
BSM 1995 no limit		98.0	97.7	97.2	96.3	94.6	91.0	74.7
ZS 2005 Version 1 limit		97.3	96.9	96.3	95.4	93.5	89.6	72.1
ZS 2005 Version 1 no limit		97.3	96.9	96.3	95.4	93.6	89.8	72.6
ZS 2005 Version 2 limit		97.0	96.7	96.3	95.6	94.1	90.8	75.8
ZS 2005 Version 2 no limit		97.0	96.4	95.3	93.4	89.9	83.7	59.0
CTC No Loss at all		102.9	102.7	102.4	102.3	100.9	99.0	90.3

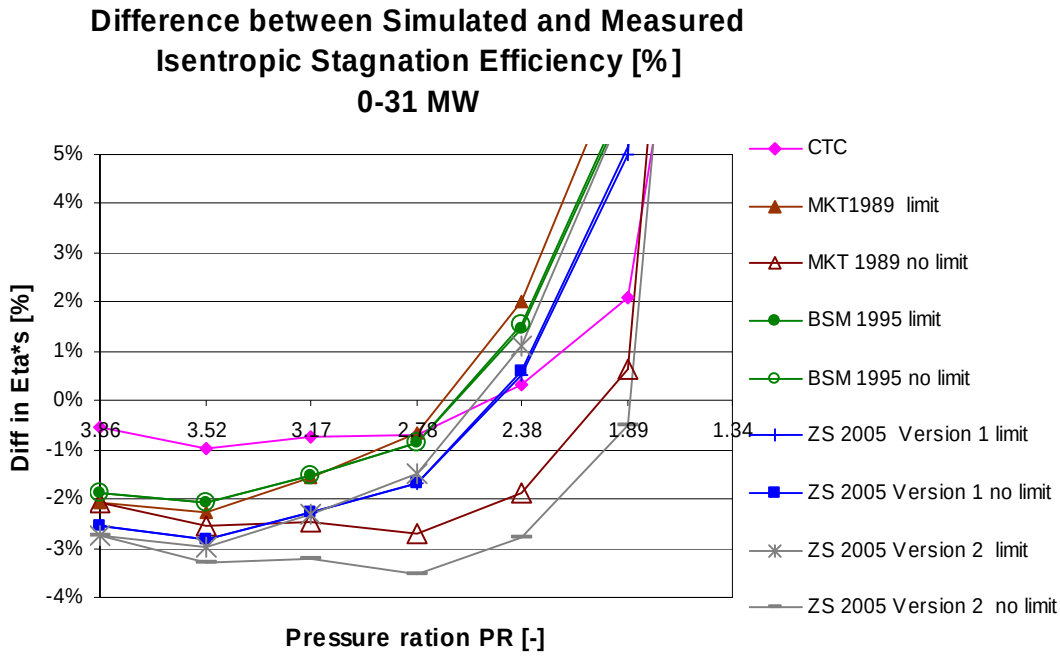

Figure 4.3-4: The difference between simulated and measured isentropic stagnation efficiency for test 1. To catch the trend the difference should be as close to a horizontal line as possible, and to be accurate in absolute value it should be close to zero.

Table 4-8: The Table shows the difference between simulated and measured isentropic efficiency for test 1 with different loss models. These results are also present in Figure 4.3-5.

Difference Between Simulated and Measured Isentropic Stagnation Efficiency [%]								
Model	*PR [-]*	3.86	3.52	3.17	2.78	2.38	1.89	1.34
CTC		-0.54	-0.97	-0.72	-0.70	0.31	2.09	15.15
MKT1989 limit		-2.07	-2.29	-1.58	-0.67	2.02	7.25	40.45
MKT 1989 no limit		-2.07	-2.56	-2.45	-2.69	-1.86	0.62	24.88
BSM 1995 limit		-1.87	-2.09	-1.52	-0.85	1.47	6.16	37.06
BSM 1995 no limit		-1.87	-2.09	-1.52	-0.85	1.54	6.31	37.51
ZS 2005 Version 1 limit		-2.53	-2.81	-2.29	-1.69	0.52	5.01	35.11
ZS 2005 Version 1 no limit		-2.53	-2.81	-2.29	-1.69	0.60	5.17	35.54
ZS 2005 Version 2 limit		-2.75	-2.99	-2.33	-1.49	1.09	6.12	38.52
ZS 2005 Version 2 no limit		-2.75	-3.29	-3.23	-3.54	-2.80	-0.49	23.03

4.3.3 Results Related to Test 2

In this section is the chart and table for the loss models simulations seen for test 2. The trends are well re-produced for most of the models. The results from test 2 are discussed in the conclusions of chapter 4.

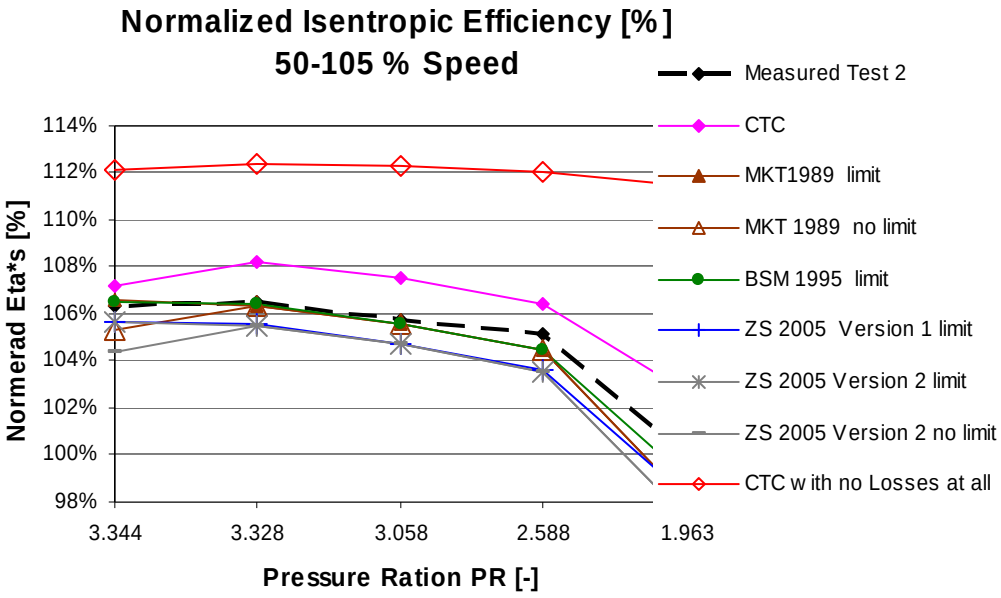

Figure 4.3-5: The different loss models normalized isentropic efficiency for the PT in test 2. The efficiency for the flow case with no row losses is also included.

Table 4-9: The Table shows different loss models simulated isentropic efficiency for test 2. These results are also present in Figure 4.3-5.

Simulated Isentropic Stagnation Efficiency (norm) [%]						
Model	*PR [-]*	*1.96*	*2.59*	*3.06*	*3.33*	*3.34*
Measured Test 2		94.1	98.9	99.4	100.2	100.0
CTC		96.6	100.1	101.1	101.8	100.9
MKT1989 limit		92.3	98.2	99.3	100.0	100.2
MKT 1989 no limit		92.3	98.2	99.3	100.0	99.0
BSM 1995 limit		93.1	98.3	99.3	100.1	100.2
ZS 2005 Version 1 limit		92.4	97.4	98.5	99.3	99.4
ZS 2005 Version 2 limit		91.6	97.4	98.5	99.2	99.4
ZS 2005 Version 2 no limit		91.6	97.4	98.5	99.2	98.2
CTC with no Loss at all		104.8	105.4	105.7	105.8	105.5

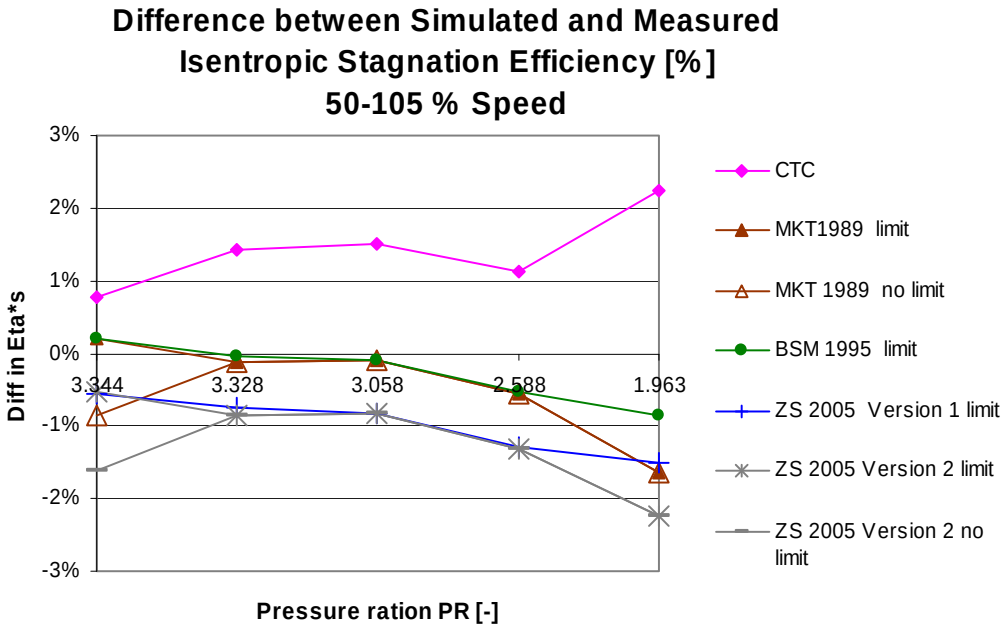

Figure 4.3-6: The difference between simulated and measured isentropic stagnation efficiency for test 2. To catch the trend the difference should be as close to a horizontal line as possible, and to be accurate in absolute value it should be close to zero.

Table 4-10: The Table shows the difference between simulated and measured isentropic efficiency for test 2. These results are also seen in Figure 4.3-6.

Difference Between Simulated and Measured Isentropic Stagnation Efficiency [%]						
Model	*PR [-]*	*1.963*	*2.588*	*3.058*	*3.328*	*3.344*
CTC		2.25	1.13	1.52	1.43	0.78
MKT1989 limit		-1.63	-0.57	-0.10	-0.12	0.21
MKT 1989 no limit		-1.63	-0.57	-0.10	-0.12	-0.86
BSM 1995 limit		-0.85	-0.53	-0.10	-0.03	0.20
ZS 2005 Version 1 limit		-1.51	-1.29	-0.82	-0.74	-0.55
ZS 2005 Version 2 limit		-2.23	-1.32	-0.82	-0.85	-0.52
ZS 2005 Version 2 no limit		-2.23	-1.32	-0.82	-0.85	-1.61

4.3.4 Statistic Results for both Loads

In this section are the results from all the loads for both tests summarized. First in Figure 4.3-7 where the predicted results are compared with the measured efficiency for both test 1 and 2. The standard deviation (SD), arithmetic average (AA) and average absolute deviation (AAD) for the loads are represented in Table 4-11. The definition can be seen in appendix 12.3.

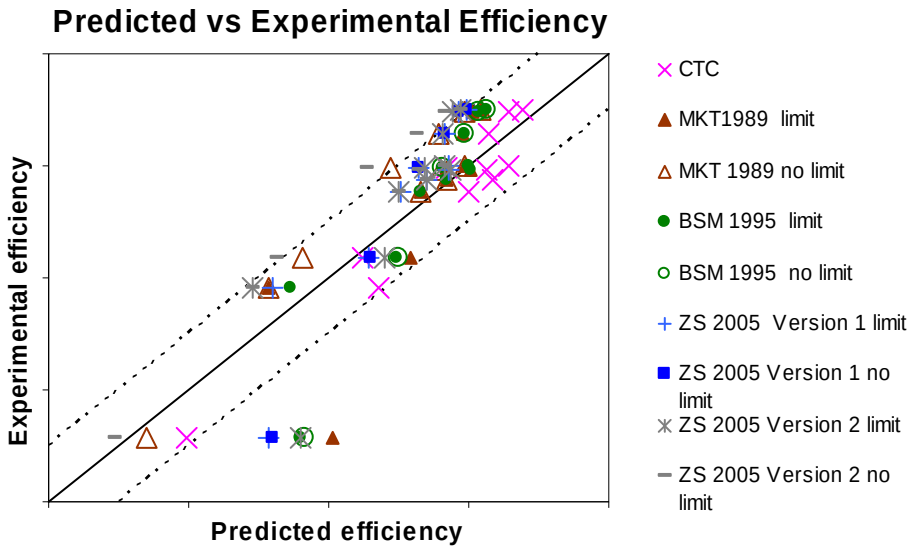

Figure 4.3-7: Evaluation of the loss models predicted efficiency compare to the experimental from both the load variation (test 1) and speed variation (test 2). The dotted lines represent an offset of ± 2.5 percentage point from the measured value.

Table 4-11: Statistic results for both tests.

Statistic Results for both Tests			
Model	*AA*	*AAD*	*SD*
CTC	0.60	1.13	1.19
MKT1989 limit	0.04	1.68	2.69
MKT 1989 no limit	-1.30	1.41	1.14
BSM 1995 limit	0.00	1.42	2.28
BSM 1995 no limit	0.25	2.36	3.25
ZS 2005 Version 1 limit	-0.79	1.80	2.15
ZS 2005 Version 1 no limit	-0.59	2.51	3.08
ZS 2005 Version 2 limit	-0.73	2.05	2.55
ZS 2005 Version 2 no limit	-2.08	2.08	1.11

From Table 4-11 can it be seen that the value of the average absolute deviation (AAD) for “CTC”, “MKT 1989 no limit” and “BSM 1995 limit” is low. This means that these models in an average predict an offset of around 1.1 to 1.4 percentage point from the measured. The standard deviation is also seen to be low for “CTC”, “MKT 1989 no limit” and “ZS 2005 Version 2 no limit”. It shows that these models have a low scatter in there prediction error, and therefore at least catch the trends well.

4.3.5 Division of the Losses

To get a better understanding of how the loss models correct for off-design condition have the losses for the simulation in test 1 and test 2 been divided into profile loss at design, profile loss due to incidence and secondary loss. The split has been done for the loads of 31MW, 10 MW, 5MW, 105% speed and 50% speed. In that way are the normal running condition and both positive and negative incidences covered. The compared models are CTC, both models of MKT 1989, BSM 1995 and ZS 2005. Only some graphs are present here, in Figure 4.3-8 to 4.3-11, but all of them can be seen in the appendix 11.4 for Siemens employees. (In the public report are the absolute values excluded).

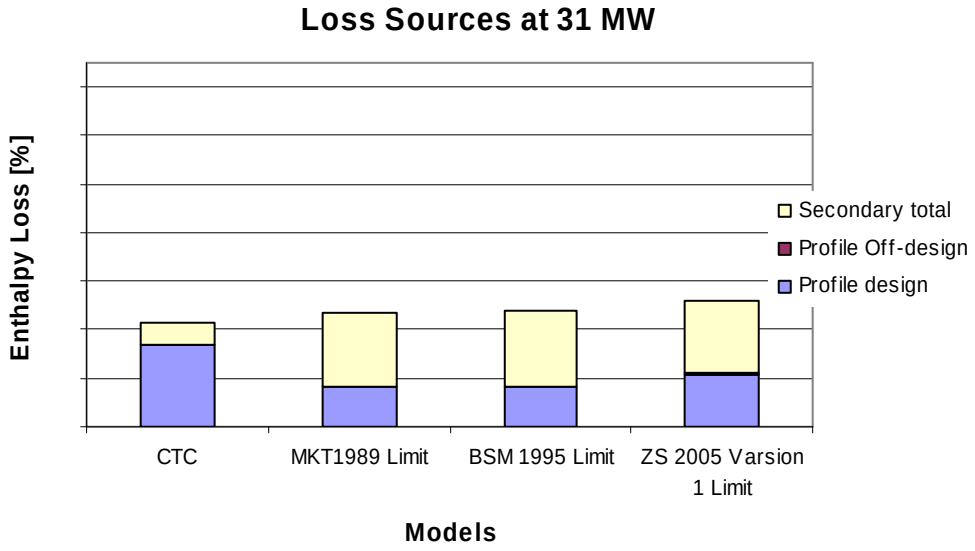

Figure 4.3-8: At full load stator 2 work with nearly no incidence at all. The total loss level for all models is within 1 percent. CTC have a profile loss twice that of the other and a secondary loss that is only a third of the others.

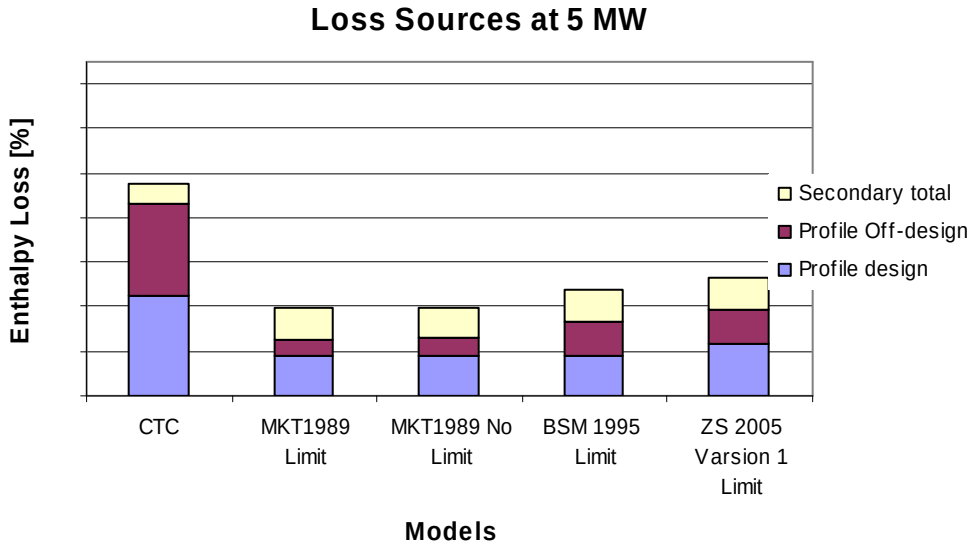

Figure 4.3-9: At 5 MW is the negative incidence for stator 2 around -45 deg. All models except from CTC show a compare to CTC constant loss trend, while CTC has more than doubled there loss due to the increases in profile loss.

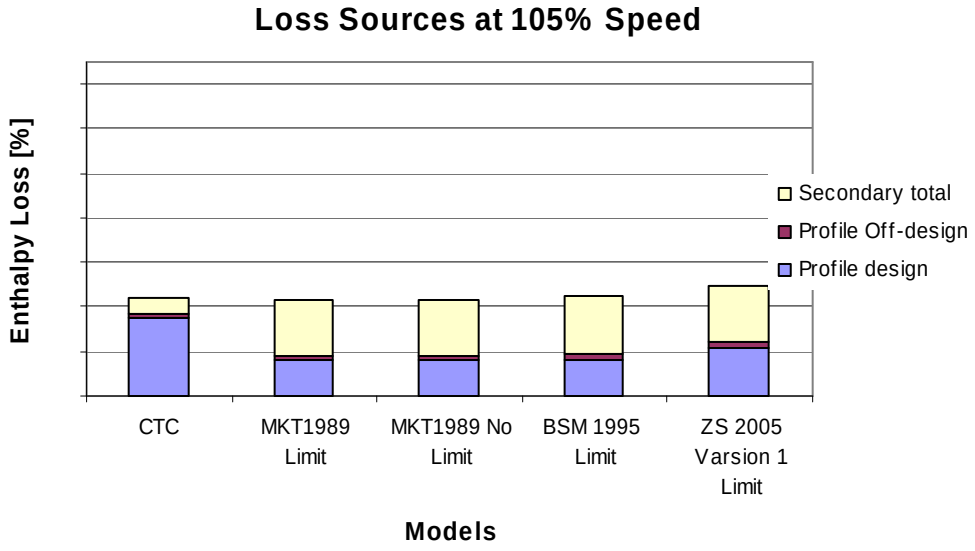

Figure 4.3-10: At 105 percent speed is the incidence around -11 deg and the sum of the losses is nearly constant within 1 percent. precisely to the 31 MW load has CTC a division between the loss sources with a large profile loss and only a tiny secondary loss part while the other loss models has a more equal division between the profile and secondary losses.

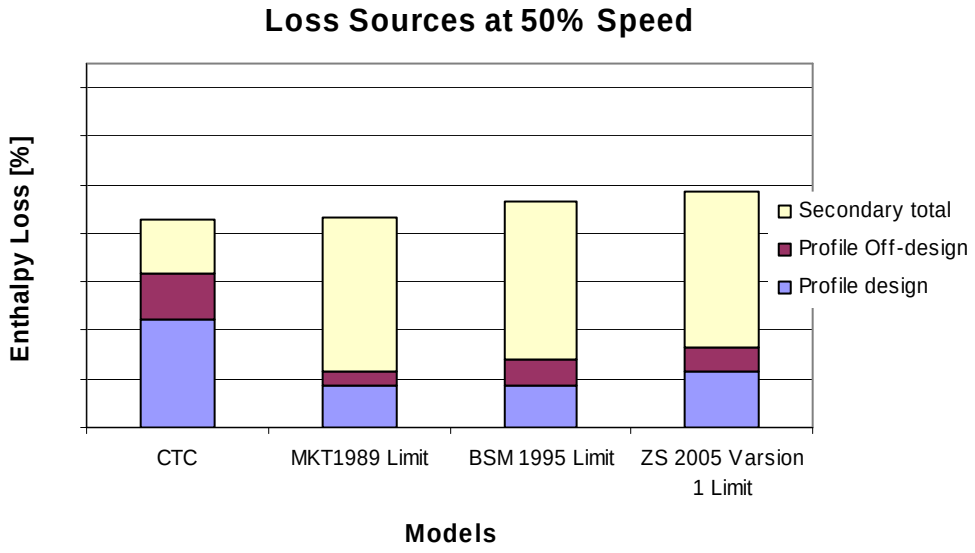

Figure 4.3-11: At 50 percent speed is the incidence around + 16 deg and the profile loss show only a slightly increase for all models except from CTC. The secondary loss in CTC increases with less then 40 percent compared with the other models secondary loss increase.

The trends that can be seen are that CTC have a small secondary loss at full load. Even if the secondary loss increase at positive incidence with the same relative rate as the other models is the absolute increase in percentage point less compared to the other loss models. Instead CTC compensate for this behavior with a high profile loss at full load so that the overall loss level is comparable equal between the different models. CTC's profile loss show a fast increasing rate at negative incidence (part loads 10 to 5 MW), compare to the limited loss models.

When deriving a complete loss model the profile loss is first determined in a cascade test and then the secondary loss is taken as the rest of the measured loss to match the total loss. If there then is an overestimation of the profile loss the secondary loss will automatically be underestimated by the same amount in the loss model. This can possible explain the low secondary loss seen for the CTC model.

MKT 1989 no limit were also compared because the original limitation for the secondary loss will reach the limit already at a negative incidence of around 20-25 deg. The exact point depends on the blade angles and ratio of inlet diameter to pitch (eqn (3-63)), and then is the increment depending on a second order polynomial. This limitation at a negative incidence of about 20-25 deg in BSM 1989 is far too early for industrial application and should maybe be corrected for with a change of range and modified polynomial.

4.3.6 Dimensionless Parameter

To compare the two tests to each other over the different test loads two dimensionless numbers were plotted against PR. The dimensionless numbers are mass flow and speed number defined as.

$$\text{Mass flow number} : C \equiv \frac{\dot{m} \cdot \sqrt{T_{0,in}}}{P_{0,in}}$$

$$\text{Speed number} \equiv \frac{n}{\sqrt{T_{0,in}}}$$

The results from the measurements and simulations with, CTC and ZS 2005 version 1 limited for test 1 and BSM 1995 for test 2 are compared. Note that for the Speed number all included parameters are specified in the input file and will therefore not change with the loss models in use.

The results are seen in Figure 4.3-12-13. For low speed number as for test 2 at a PR around two, the effect of positive incidence on efficiency are both being covered and catch with these tests. The reason for the difference in flow number is that the losses affect the static pressure and temperature in both the throat and outlet of stator 1 and therefore also the mass flow. The differences should actually be even a little more in reality because a limitation in the program code that do not make it possible to correct the losses in the throat.

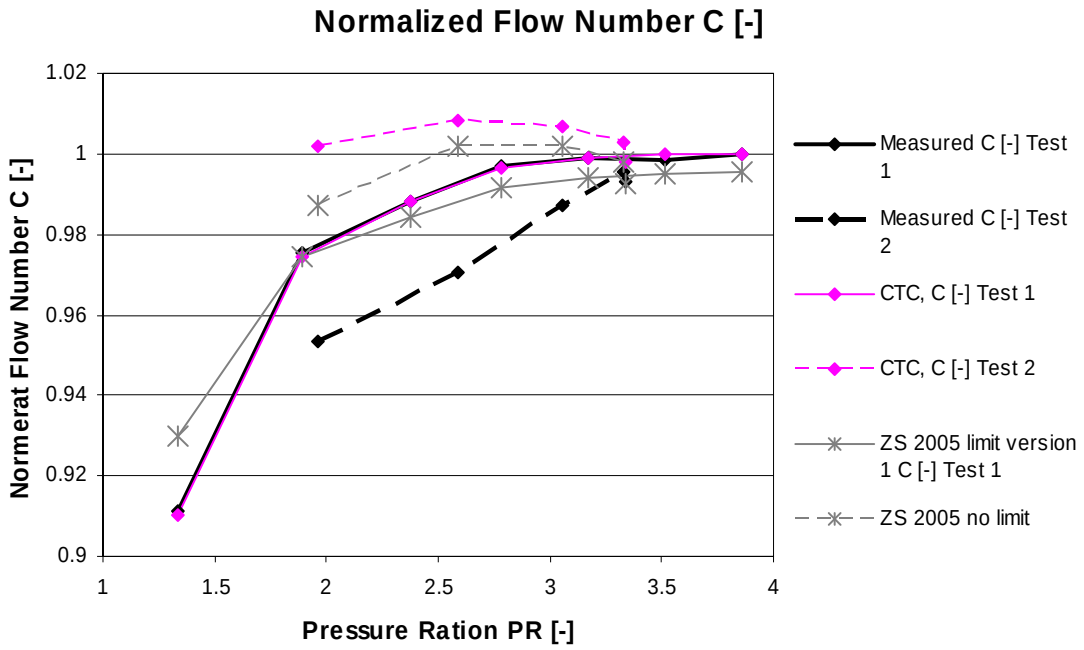

Figure 4.3-12: Flow number (C) for the measurements and simulations of test 1 and 2.

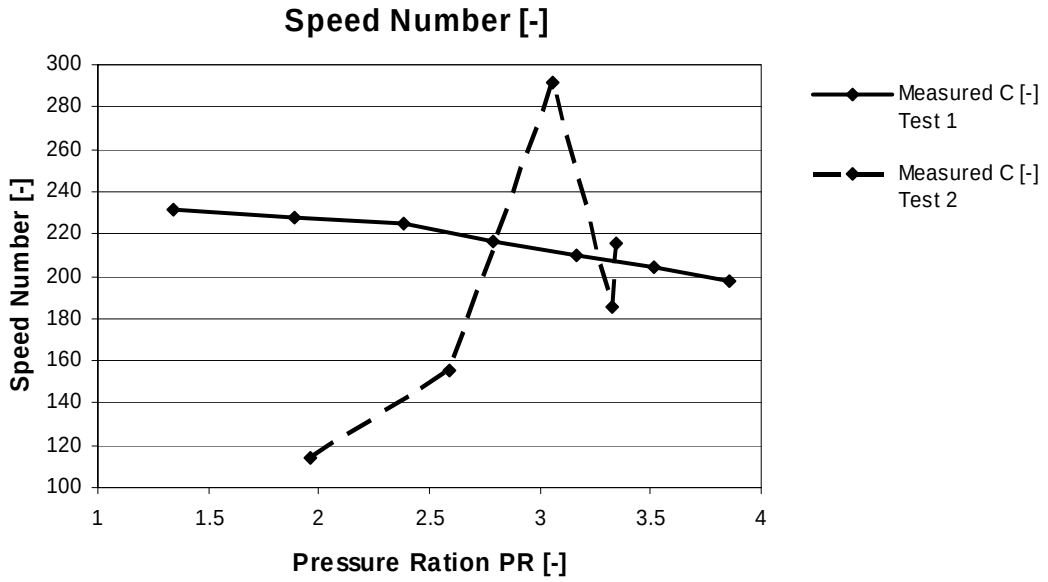

Figure 4.3-13: Speed number for the measurements and simulations of test 1 and 2.

4.3.7 Results Related to Numerical 2D Experiment

A comparison between the profile losses from the CTC and Blagen shows that the losses from CTC are overestimated over the whole range even if the trends at positive incidence are quite good. For the range of negative incidence the trends differ a lot between the two curves where Blagen only show a low loss increase in opposite to CTC significant higher rate. Actual the losses in Blagen are close to constant from -10 to -30 deg incidence as seen in Figure 4.3-10. The from Blagen close to constant low profile loss at negative incidence can be supported by experimental results at off-

design from a annular test turbine that Ning Wei show in Figure 4.1.3 page 69 [2]. One believed reason for this insensitiveness to the high negative incidence is that in modern blade design the acceleration of the fluid is high and will suppress the separation at the pressure side of the blade. The absolute value from Blagen is maybe little low and should possible be shifted upwards with 1-2 percentage points.

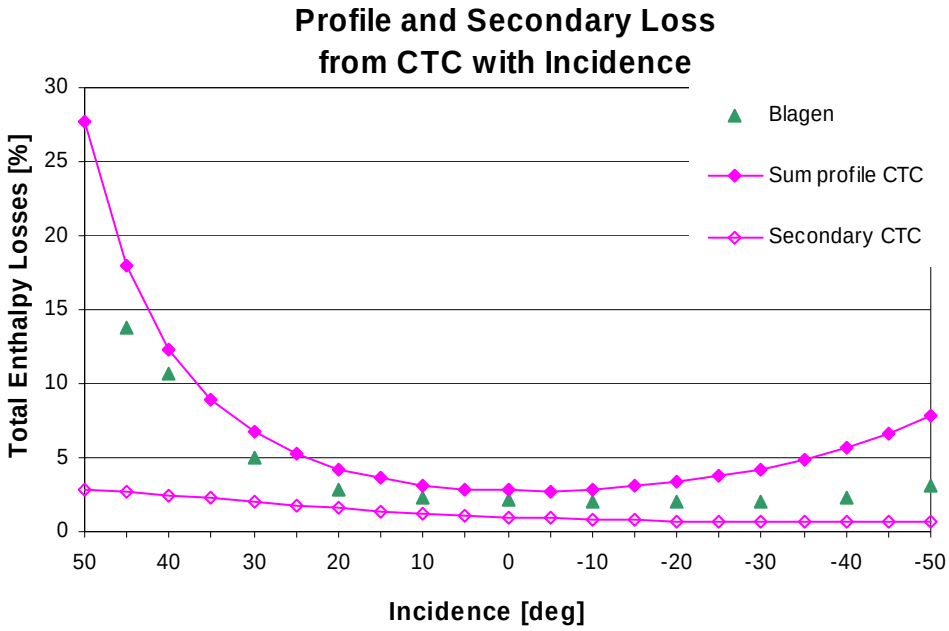

Figure 4.3-14: Comparison between the profile loss from both standard CTC and Blagen. Also the secondary loss from CTC is seen.

The secondary loss has also been included in Figure 4.3-14 even if there are no calculated values to compare with. The reason is that it gives a view of how the secondary loss is modeled with varied incidence. It is interesting to note that CTC give a strange secondary loss prediction with only a slightly increase at high positive incidence. The reason for this slightly increase in CTC is as mention in 4.3.5 for the first that CTC give a low secondary loss at the design point compared to the other models. CTC give only around one percent where MKT 1989 give around 4 percent at the design point. The second source is that CTC use a much weaker incidence influence on the secondary loss. CTC give one correlation in the CTC manual while another is used in the program code. To illustrate this trends the secondary loss correlation for incidence from the CTC code, CTC manual, Mukhatarov & Krichakin (that are the underlying material for the developing of CTC) and MKT 1989 (also originally based on Mukhatarov & Krichakin) are plotted in Figure (4.3-16) below. It is there seen that the code used in CTC have the absolute weakest influence increase at positive incidence above around 20-25 deg, and at the negative incidence it decreases most. The combined effect of the low secondary loss at design and the weak effect of incidence are the underlying reasons for the strange secondary loss that were seen in Figure 4.3-14.

The secondary loss in CTC is most probable not modeled in a fully satisfied way. It was mentioned in section 2.8.2 that the important parameters were inlet boundary layer thickness, pressure between the suction and pressure surface, acceleration of the flow in the row, pitch and the endwall area that is affected by the secondary flow. In

CTC the three first parameters are represented by a constant for the boundary layer thickness, blade load with the profile loss parameter and the acceleration with the ratio of $\sin(\alpha_{out})/\sin(\alpha'_{in})$. So far it is acceptable, but the effected area is in CTC direct proportional to the ratio of the throat width to span height (o/h). This has the consequence that for small throat (as the row is being closed) the predicted loss will decrease. It makes more physical sense that for a constant blade load will a smaller throat increase the pressure gradient between the suction and pressure surface. This pressure gradient increase will probably then lead to a stronger secondary flow in term of for example the passage vortex and a intensified loss generation and probably not the overall decreasing trend as CTC predict even if the effected area decrease. The greatest part of the secondary loss occurs in the endwall region, and therefore would a more realistic parameter to scale against be the aspect ratio, (c/h). The fundamental idea to scale against o/h is that the largest secondary vortices in the endwall will be at the order of the throat (o), but a drawback is that no care is then taken to the fact that the vortices intensity is increased.

The parameter variation in Figure 4.3-11 was made on stator 1 in the PT of SGT-700 analogously as for the numerical test in Blagen.

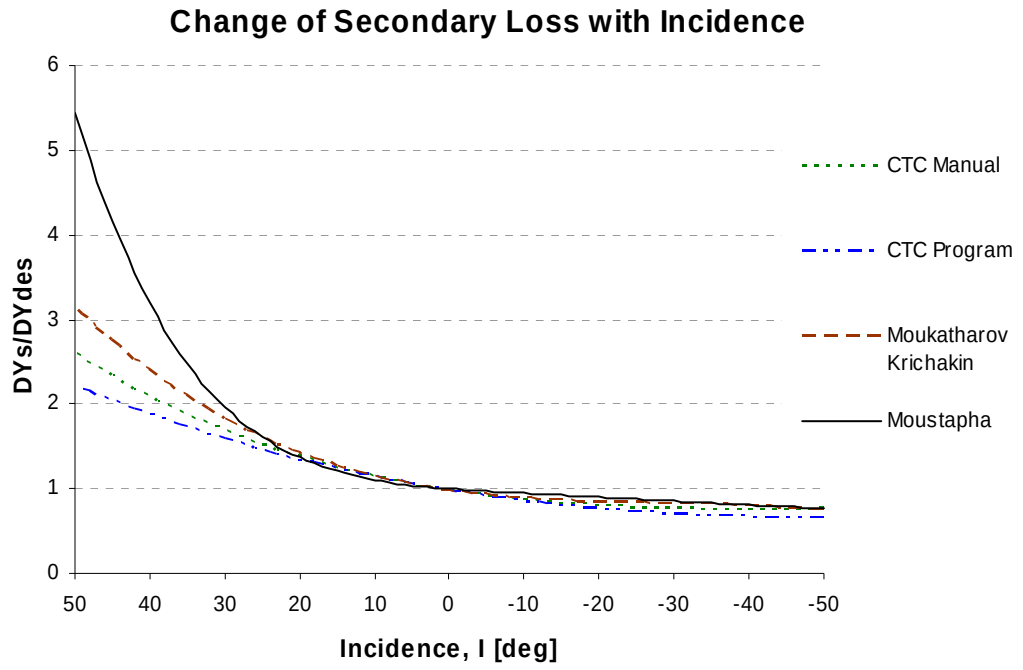

Figure 4.3-15: Influence of secondary loss with incidence for CTC code, CTC manual, MuKr and MKT.

Figure 4.3-16 show the variations in the profile and secondary loss for "MKT 1989 no limit "with incidence. The profile loss is instead seen to be under predicted at positive incidence with about the same absolute value as CTC over predicted with. At negative incidence "MKT 1989 no limit" show the same trend as the numerical experiment and predict only a slow increasing trend.

A small change in the blade geometry concerning the inlet diameter (d_{in}) was done in the loss model from 4 to 3 mm. The reason for this change is that d_{in} is one of the most important parameters controlling the variation of the profile loss with incidence

(see eqn 3-63). After this change the predicted profile loss agree well with Blagen concerning both the trend and absolute value at positive incidence, as seen in Figure 4.3-16. Possible should this change be done to MKT's loss model.

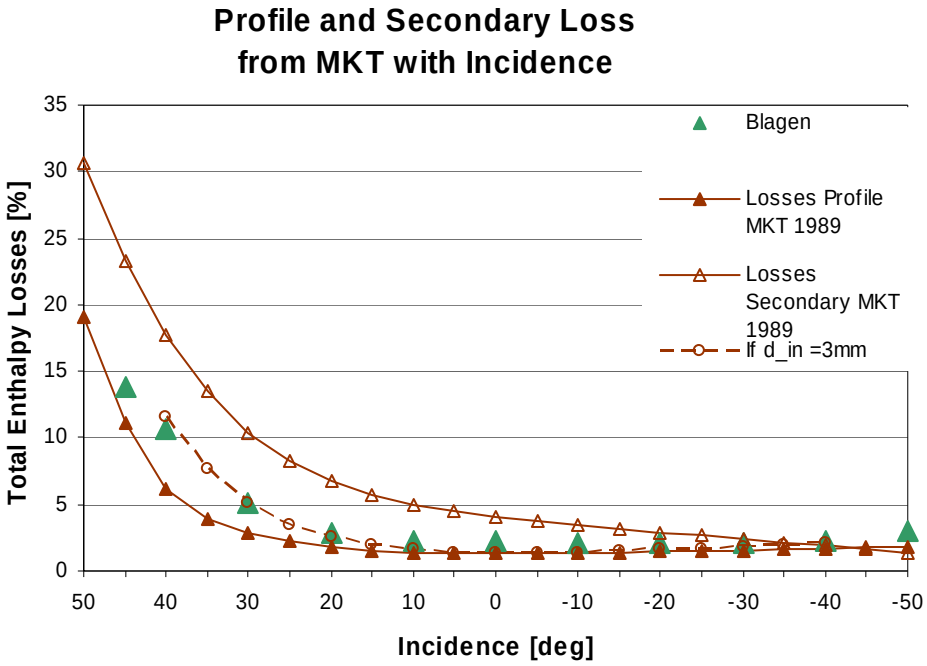

Figure 4.3-16: Comparison between profile loss for MKT 1989 no limit and Blagen. A modification of din from 4 to 3 mm to the blade geometry in MKT are also seen and the secondary loss from MKT.

Figure 4.3-17 show the variation of the profile and secondary losses from "BSM 1995 no limit" and the profile loss calculated with Blagen. Both the trend and absolute value of the profile loss are caught sufficient well.

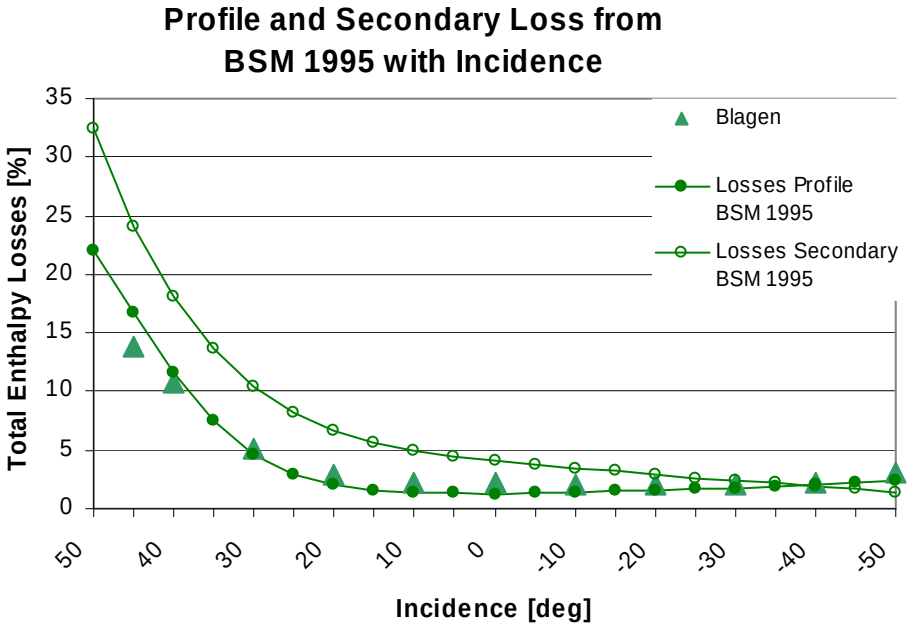

Figure 4.3-17: Comparison between profile and secondary losses for MKT 1995 no limit and the profile loss from Blagen.

Figure 4.3-18 show the variation of profile and secondary losses for ZS 2005 Version 1 and Version 2 compare to the profile losses from Blagen. Both versions are “no limit”, and perhaps is the absolute best agreement between the simulations and the numerical calculation for all investigated loss models over the whole range of incidence seen for the simulations with “ZS 2005 Version 1 no limit”.

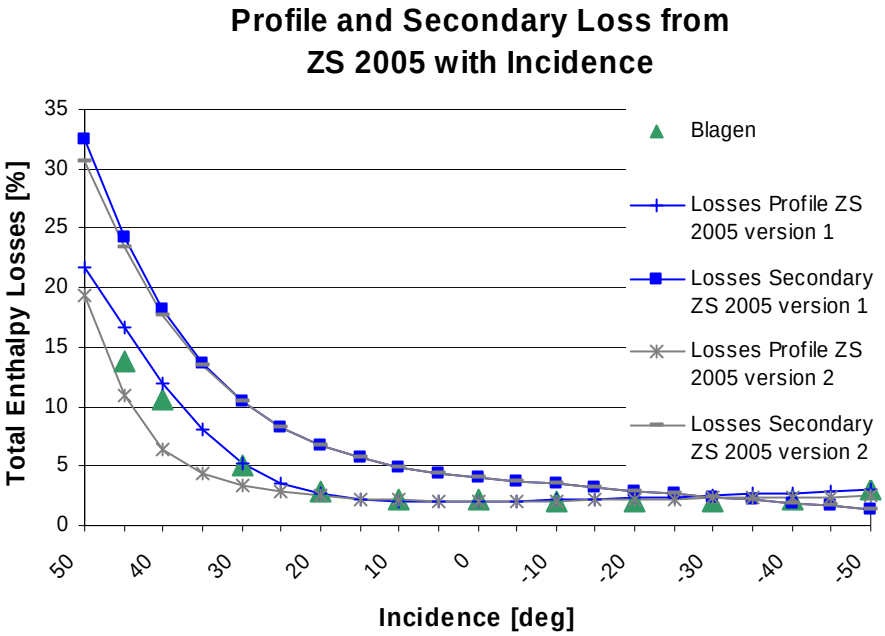

Figure 4.3-18: Comparison between ZS 2005 Version 1 and Version 2 profile and secondary losses with the profile losses from Blagen. Both versions are “no limit”.

In Figure 4.3-19 all the different loss models result for the profile loss is summarized. It is clear that all the simulated loss models, except from CTC, follow the same trend for negative incidence as was predicted with Blagen even if the absolute value will differ some between them. CTC predicted not this trend at all. When looking at positive incidence, the trend is best followed by “BSM 1995” and “ZS 2005 version 1”. For incidence above 30 deg both models follows close to each other, but in the range from 0 to 30 deg of incidence the prediction from “ZS 2005 version 1” is more accurate. That difference between the both models is that ZS use a slightly different profile loss at the design point compare to AMDCKO.

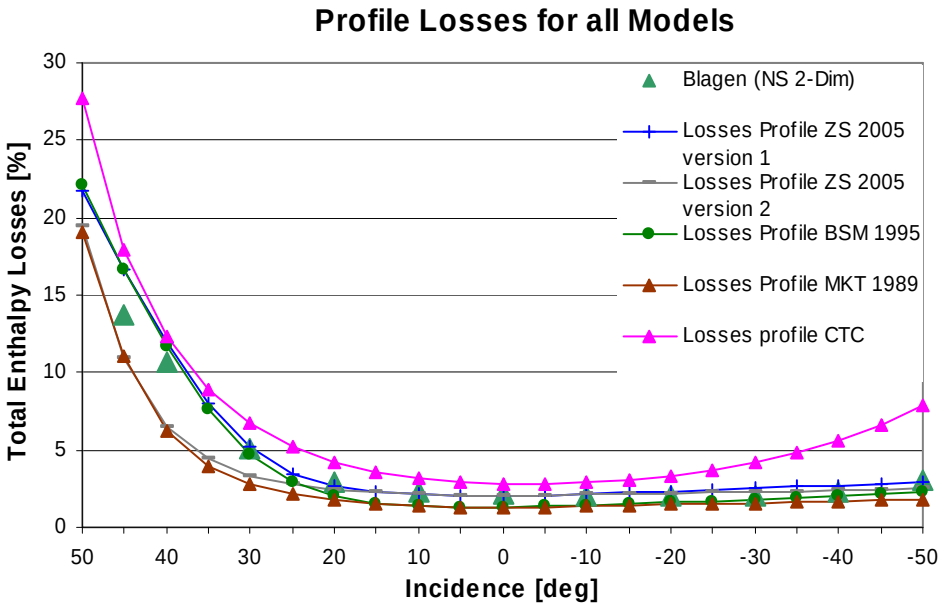

Figure 4.3-19: Finally all the results for the profile loss are summarized in one graph to illustrate the difference between them. "ZS 2005 version 1" is the model that predicts the profile loss most accurate over the full range of incidence compare to the calculated value with NS -2D in Blagen.

Table 4-12: Summarize of the profile losses from different loss models compare to Blagen over the incidence range -50 to +50.

Profile Loss for Variation in Incidence											
Model Incidence	*50*	*45*	*40*	*35*	*30*	*25*	*20*	*15*	*10*	*5*	*0*
Blagen NS 2D		13.8	10.7		5.1		2.9		2.2		2.2
ZS 2005 ver 1	21.8	16.7	11.9	8.0	5.2	3.5	2.6	2.2	2.1	2.0	2.0
ZS 2005 ver 2	19.4	11.0	6.5	4.4	3.4	2.8	2.5	2.2	2.1	2.0	2.0
BSM 1995	22.1	16.7	11.7	7.6	4.7	2.9	2.0	1.6	1.4	1.3	1.3
MKT 1989	19.1	11.1	6.2	4.0	2.8	2.2	1.8	1.6	1.4	1.3	1.3
CTC	27.7	18.0	12.4	8.9	6.7	5.2	4.3	3.6	3.2	2.9	2.8
Model Incidence	*0*	*-5*	*-10*	*-15*	*-20*	*-25*	*-30*	*-35*	*-40*	*-45*	*-50*
Blagen NS 2D	2.2		2.1		2.1		2.0		2.3		3.1
ZS 2005 ver 1	2.0	2.1	2.2	2.2	2.3	2.4	2.5	2.6	2.7	2.8	3.0
ZS 2005 ver 2	2.0	2.1	2.1	2.1	2.2	2.2	2.3	2.3	2.4	2.4	2.5
BSM 1995	1.3	1.3	1.4	1.5	1.6	1.7	1.8	1.9	2.0	2.1	2.3
MKT 1989	1.3	1.3	1.4	1.4	1.5	1.5	1.6	1.6	1.7	1.7	1.8
CTC	2.8	2.8	2.9	3.1	3.4	3.7	4.2	4.9	5.6	6.6	7.9

4.3.8 Trends for the Loss Models

The variation of profile loss for both MKT 1989 and MKT 1995 with i, d_{in} and We_{in} are shown in this section. No absolute value of the loss is given because that is irrelevant without something to compare against. An alternative would be to do a numerical study of the loss changes with Blagen. To achieve that new blade profile needs to be designed for all geometrical parameters change in We_{in} and d_{in}. Such a new blade design is difficult and time consuming to do if the final result should be satisfactory and the results of the comparison any useful, end were therefore not done.

For the done parameter variation is first the change for "MKT 1989 limit" shown for different d_{in} in Figure 4.3-20 then the variation for "MKT 1995 no limit" with changes in d_{in} and We_{in} in seen in Figures 4.3-21. The profile or secondary losses in CTC are not influenced at all by any of the two believed important parameters (d_{in} or We_{in}).

The trend is that for a small value of d_{in} "MKT 1989 limit" will be much more sensitive to incidence compared to bigger d_{in}, see Figure 4.3-21. For "BSM 1995 No Limit" d_{in} will play a minor matter and the trend is close to that for "MKT 1989 Limit" with a d_{in} of 3mm, see Figure 4.3-22. Instead We_{in} is a more important parameter and the profile loss increases steeper for a small We_{in} compare to a bigger, see Figure (4.3-23). The dependences on We_{in} and d_{in} are rather insensitive as long as the geometric values do not get to small (d_{in} > 4mm and We_{in} > 20 deg).

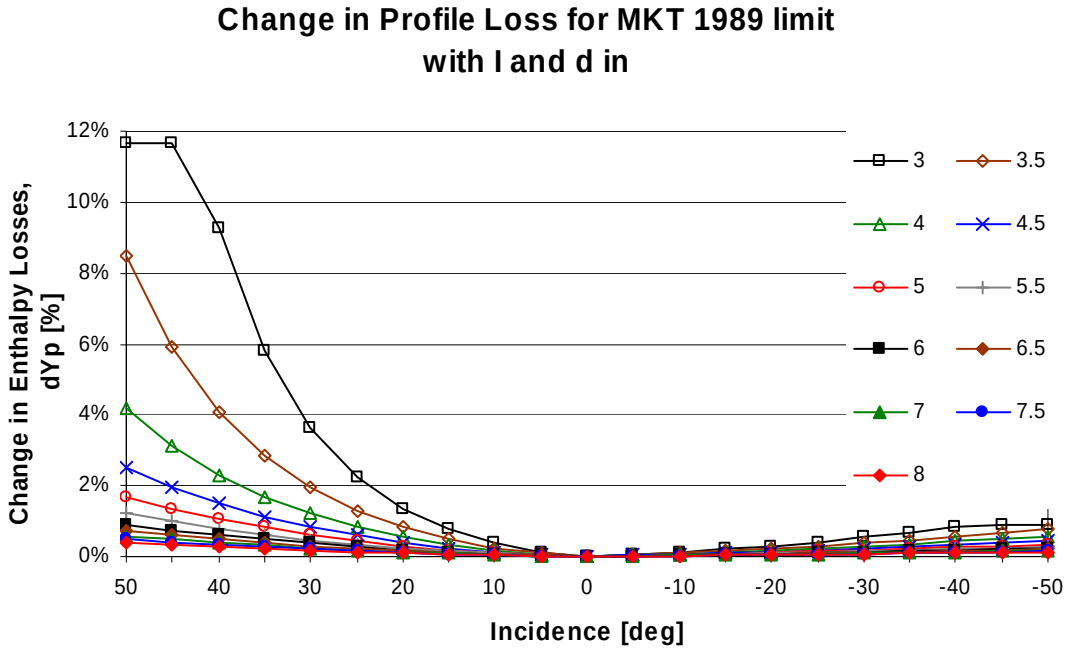

Figure 4.3-20: Extra add to the profile loss with incidence for different leading edge diameter in the range of 3-8 [mm] for MKT 1989 limit.

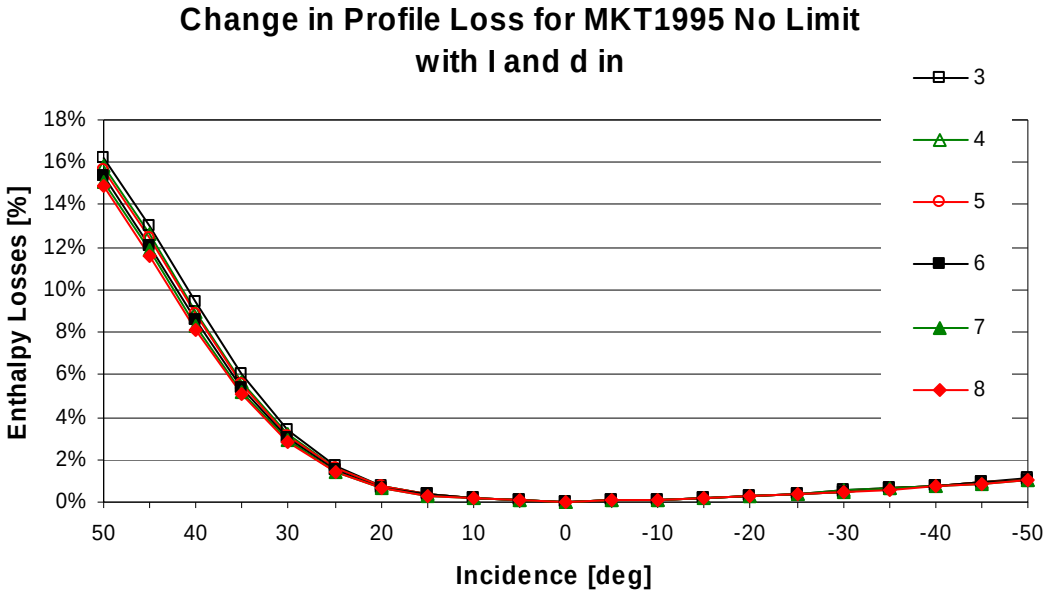

Figure 4.3-21: Change in profile loss with incidence for different leading edge diameter in the range of 3-8 [mm] for BSM 1995 no limit.

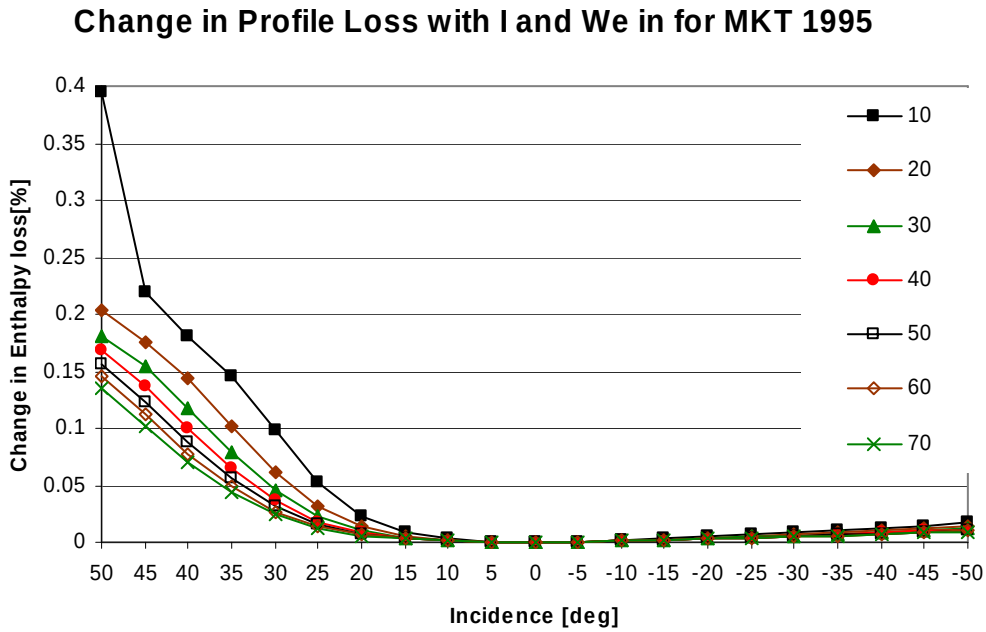

Figure 4.3-22: Change in profile loss with incidence and Wedge angle in for BSM 1995 no limit.

4.4 Conclusions

Test 1

The simulations show that for high loads all models underestimate the efficiency for a PR up to about 2.5 and then above this PR the efficiency are underestimated. No one of the loss models is fully capable to catch the trend of a fast decreasing efficiency when the PR decreases. It is also worth to note that for test 1 the incidence for all blades are always negative and increase with the decreasing load , see Figure 4-2. Negative incidence is a condition that does not give any high extra loss due to incidence because the risks for separation that do not reattach rapidly are small up to a high level of negative incidence. If one model should be chosen from these results it is the original CTC model that differ less over the entire load range.

Test 2

In test 2 the blades are working with positive incidence at the lower speed numbers and PR while it goes over to negative incidence as the speed approach towards full load. All the loss models show a good ability to catch the trend of the efficiency quite good. Absolute closest to the measured results is the loss model "BSM 1995 limit". The span of efficiency difference for this loss model is from -0.41 to +0.20 percentage point, so the difference between maximum and minimum offset in efficiency prediction is only 0.61 percentage point. These conclusions are only valid under the assumption that the measured efficiencies are correct and representative for Siemens gas turbines today. Under the assumption that the trend is correct but the absolute measured value incorrect a shift of the measured efficiency curve could do it possible to find a good agreement between the measured and almost all loss models prediction.

In section 4.1.2 it was mentioned that the PT efficiency is known to be to low, and to represent the PT efficiency of Siemens gas turbines today the measured efficiency should be increased. After such increase CTC could be a good represent for the efficiency of the PT even for test 2.

If only the trend for CTC is studied can actually a drop in the predicted efficiency at over speed be seen, something that almost is not seen from the measurement in test 2. At the lowest speeds where positive incidence is present it is also seen that CTC do not catch the fast efficiency drop as well as some of the other loss models do. Therefore would it be very interesting to future investigate CTC's efficiency prediction at even higher positive incidence to see if this only is a temporary offset or a general trend. The two models to predict the trends best are "BSM 1995 limit" and "ZS 2005 version 1 limit".

In Figure 4.3-7 the predicted and measured efficiency for both test 1 and test 2 are compared. All the models efficiency predict are almost within 2.5 percentage point and perhaps "MKT 1989 no limit" is the model, except from CTC, with the overall lowest divergence.

In the study of how the models divide the total loss (see section 4.3.5) between the different loss sources CTC show up a most probably unrealistic division between the profile and secondary losses. It where seen that the profile loss stand for about 75-95

percent of the total sum of profile and secondary loss and not at all in the region of 50 percent as normally is purported. CTC also show a fast increase of the profile loss at negative incidence, something that was not seen for any of the other models, the numerical simulations in NS-2D or recently done external experiment.

This division can actually be the reason that CTC show a better loss prediction at low loads (negative incidence). While the profile loss is increasing at negative incidence the secondary loss models is decreasing. Therefore CTC will give a higher loss level at negative incidence compared to the other models. If a high profile loss is to prefer or not is not clear, but it show at least a better prediction of overall loss level.

A possible but not obvious drawback in the loss included in CTC model for the correlation of secondary loss in CTC has been highlighted. It is the method to scale against the throat (o), instead as for example the chord (c) or pitch (s). Which of these three parameters that is best to use is not totally clear and had been investigated before. Dunham [43] found 1970 that there was no direct evidence to decide between these alternatives.

A possible risk with CTC's loss division is that in the attempt to decrease the losses for a blade wrong parameter will be tuned in believe that the profile loss is huge, whilst it actually maybe is the secondary loss that has the biggest potential to be improved. For example would this program be favorable for short blades with large pitch, small leading edge and large trailing edge. To avoid making this possible error in the creation of a new design the loss division in CTC needs to be future investigated. That is an investigation that is beyond the range of this thesis that not originally should include the losses at the design point.

A drawback in the test is that a parameter that as well effect the secondary loss is the influence of tip leakage that will vary with both speed and temperature over the load steps because the thermal expansion and centrifugal forces at rotor blades with the tests. These effects were not included in the simulations here, where CTC's tip leakage model was used with a constant tip clearance independent of load case.

5 Tip Leakage

5.1 Theory

There is always a clearance between the stator and turbine shaft or rotor and turbine casing to satisfy safe running conditions with none scratching of the tips. This clearance will vary in both a short and long time aspect. In a short aspect it is due to different loads, rotation speeds, thermal heating, different expansion rates in the disc, blade and casing and so on. In a long time aspects it is primary due to abrasion of the seal because the abrasive environment in a gas turbine. Because of this variation in clearance over time, not only the loss at design clearance is of interest, but also the variation of efficiency with increasing clearance ($d\eta / d(k/h)$). For the stator the clearance will be at smaller radius and therefore give less leakage area, and here the seals may also be done more advanced because of the absence of centrifugal stress. The pressure ratio across the clearance will drive a leakage mass flow from the high to the low pressure side.

The blades can be categorized into the two main groups shrouded and unshrouded blades. In between is it possible to make future divisions into other subgroups with partial shrouded blades and so on.

Unshrouded blades: For unshrouded blades the flow is driven by the static pressure difference between the blades pressure and suction side. As the flow passes the edge at the pressure side it usually separates, create a recirculation bubble that reduces the effective area for the leakage flow. If the blade thickness is large enough the bubble will reattach, the flow diffuse, get turbulent and its entropy increase [6]. The size of the separation bubble depends partially on the corner radius between the pressure surface and the tip of the blade. For a larger radius the bubble will decrease and possible disappear totally (not the case in real machines). A normal rule of tumble is that the critical blade thickness for a reattachment is 2.5 times the clearance, but also the Reynolds number in the tip based on tip clearance and the tip geometry are crucial [30].

When the flow enters the suction side a vortex is build up that interacts with the secondary passage vortex. The leakage flow will also affect the work potential by causing an unloading of the upper part of the blade.

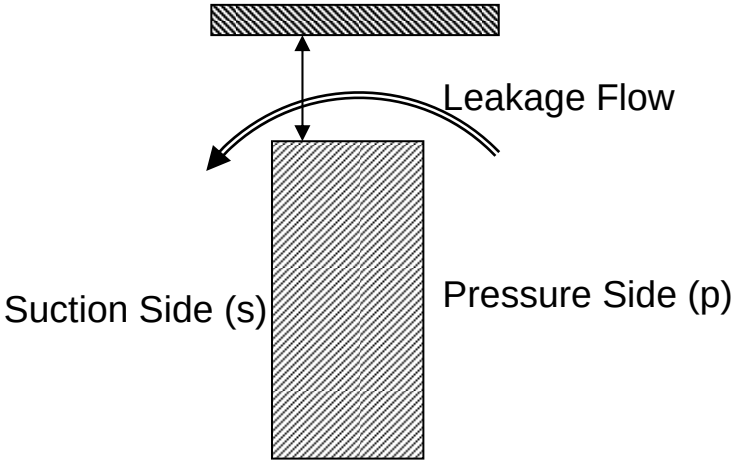

Figure 5.1-1: The leakage path from pressure to suction side across the tip clearance of an unshrouded blade.

Shrouded blades: For a shrouded blade is it not pressure drop from the pressure to suction side that drives the leakage flow. Instead it is the total pressure drop across the entire blade row that is the driving force. For most blade design these both pressure differences are at the same order, except for impulse blade where there is no pressure drop across the rotor blades row. The shroud will get the leakage flow to be skewed due to a great shear in the clearance gap, and affect the main flow angle after it is remixed downstream [4].

As mentioned above the pressure ratio under normal running condition is comparable for the shrouded and unshrouded configuration, but clear benefits for the shrouded blade row is the possibility of using multiple seals and maybe also extract some work from the leakage flow as discusses later. The possibility to place sealing's along the whole chord will decrease the slope rate of loss to relative clearance compared to the unshrouded. Already with two seals the loss will be only about half that of unshrouded and then decrease further with additional sealing's, see [6] and Figure 4.1 in [30].

Except from the small amount of skewing across the top the leakage flow will approximately have the same tangential flow direction after it has passed the shroud as at the inlet, while the main flow has been turned several degrees. This difference lead to a pure loss in terms of entropy generation as the leakage flow mixes out behind the blade row. In a attempt to reduce this loss and actually extract some benefit from the leakage flow, fences can be placed at the blade top after the sealing's [30]. Example of the use of fences is seen for Rolls-Royce where the fences simply are flat plates. The extremely low aspect ratio, high relative tip clearance, and low Re for the fence will give a highly complex structure that differs a lot from the normal unshrouded blade, and the actually benefit of this structure is not clear. Beside the work extraction will the fences also turn the leakage flow direction so it better match the main flow downstream and in that way reduce some of the mixing losses associated with the remixing.

Another effect of the shroud that is not completely certain but were proposed by Ruston (2003) [30] is that with a shroud at the blade tip the main flow is separated from the original boundary layer at the casing upstream as it enters the passage. This

means that it is only the new and much thinner boundary layer that starts to build up in the passage that is affected by the crosswise pressure gradient between the pressure and suction side that creates the passage vortex. This gives a lower secondary loss as can be seen in Figure 4.24 in [30].

One of the main problems with shrouded blades compared to unshrouded is that they will increase the centrifugal blade stress, and make it more difficult and expensive to cool the shroud. This is why they usually are not seen in the first stage of the turbine where the highest temperature is seen.

The geometry around the shroud can be varied in numberless ways, and in an attempt to understand the trends U.S. Air Force (USAF) investigated twelve geometries with a relative clearance of 1.5 and 3.0 percent, that is summarized in [31]. The geometries are seen in Figure 5 in [31], where the blade tip was in line as well as overlapping the casing. Different configurations of steps before and after the blade were tested as well (all without any seals). The results were that the simple straight tip with no overlap and no step were the most efficient. But for a high tip clearance ratio the overlapped tip shows less sensitiveness and can be to prefer for high clearance level, or variation of relative clearance.

The leakage flow through a multiple seal will undergo a pressure loss for each seal that gets the density to reduce and in that way to keep the mass flow constant the Mach number will increase, (if the sealing clearance is equal). This increase in Mach number lead to a grater pressure loss across the sealing's downstream. For an incompressible assumption the pressure loss is divided equally between the seals and the leakage mass flow is proportional to (number of seals)$^{-0.5}$.

To make the sealing more efficient the clearance gap of the following seal should be shifted in radial position to prevent the jet leaving one seal from going through the next one without first diffuse sufficiently, see VKI 2004 chapter 4.5 [30]. Still inline seals are often used because they are easier to fabricate and less sensitive for axial variation between the turbine axis and the surrounding casing.

The effect of variation in Reynolds number in the seal are not totally clear, where neither (Zimmermann and Wolff) (1998), or Takayuki Matsunuma [32] could find any evidence of any Re dependence. Something that Rhode (1993) refuse to agree with as he argue for a reduction in the leakage resistance at increasing Re [30].

5.2 Loss Models not Earlier Described

5.2.1 Denton

Denton has in contrast to many of the other loss models in the literature tried to estimate the leakage mass flow and the losses associated with it in a more physically sense. In the derive of these equation several simplifications are done so the absolute value should maybe not be fully trusted before any correction compared to real turbine experiments are made, but the trends should be more trusty. A comparison between the predicted value and the measured value by Takayuki Matsunuma in [32] shows actually quite god accuracy.

The equation to calculate tip leakage losses for both shrouded and unshrouded blades are seen below. For the shrouded blade two variations of the equation are given, one for a linear cascade and one for an annular, after corrections for obvious disadvantages in the original derive. The full derive of these are present in appendix 12.4-1.

5.2.2 Shrouded Blades

Under the assumption of a single sealed blade, incompressible flow, that the leakage flow up to the throat is approximately isentropic and the same total temperature in the leakage flow and mainstream when they mixes together after the blade row, are the losses in term of enthalpy determined by the relative sealing clearance (k/h), contraction coefficient (C_c) and the inlet and outlet flow angles (α_{in}), (α_{out}).

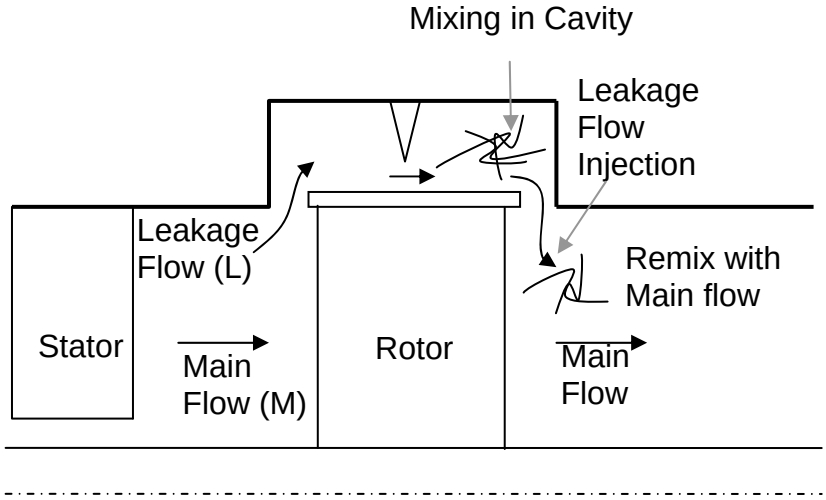

Figure 5.2-1: The flow path over a shrouded blade with a single seal and the remix of the fluid downstream, [3] fig 29.

The enthalpy generation in a mixing between one small and one big stream can be calculated as eqn (5-1) (see appendix 12.4), where m_L and m_M stands for the mass flow of the leakage and main flow.

$$\frac{T \cdot \Delta s}{0.5 \cdot V_{out}^2} = 2 \cdot \frac{m_L}{m_M}\left[1 - \sin^2(\alpha_{out}) \cdot \frac{\tan(\alpha_{in})}{\tan(\alpha_{out})}\right] \qquad (5\text{-}1)$$

Where the relative leakage flow $\frac{m_L}{m_M}$ for either a linear cascade or annular turbine can be determined by eqn (5-2a) or eqn (5-2b).

Linear cascade

$$\frac{m_L}{m_M} = \frac{k}{h} \cdot C_C \cdot \sqrt{\frac{1}{\cos^2(\alpha_{out})} - \tan^2(\alpha_{in})} \qquad (5\text{-}2a)$$

Annular turbine

$$\frac{m'_L}{m'_M} = \frac{k}{h} \cdot C_C \cdot \sqrt{\frac{1}{\cos^2(\alpha_{out})} - \tan^2(\alpha_{in})} \qquad (5\text{-}2b)$$

5.2.3 Unshrouded Blades

For an unshrouded blade the leakage flow goes from the pressure to the suction side of the blade, across the blade tip. The velocity at the pressure respective suctionside in the direction of the chord are C_p and C_s, and if it is assumed that the velocity component along the chord for the leakage jet are constant and equal to the pressure sides, $C_{j,chord} = C_{p,chord} = C_p$ and that the mixing occur immediately as the leakage flow enters the suction side. Then the losses can be estimated in term of enthalpy loss as

Linear cascade

$$\zeta = 2 \cdot \frac{k}{h} \cdot C_C \cdot \frac{1}{s \cdot \cos(\alpha_{out})} \cdot \int_0^c \frac{C_s^3}{C_{out}^3} \cdot \left(1 - \frac{C_p}{C_s}\right) \cdot \sqrt{(1 - \frac{C_p^2}{C_s^2})} \cdot dr \qquad (5\text{-}3a)$$

Annular turbine

$$\zeta' = 2 \cdot C_C \cdot \frac{k \cdot (z-1)}{\pi \cdot \left(r_{tip}^2 - r_{rot}^2\right) \cdot \cos(\alpha_{out})} \cdot \int_0^c \frac{C_s^3}{C_{out}^3} \cdot \left(1 - \frac{C_p}{C_s}\right) \cdot \sqrt{(1 - \frac{C_p^2}{C_s^2})} \cdot dr \qquad (5\text{-}3b)$$

In eqn's (5-3a and 5-3b) the ratio between the velocities at the pressure and suction side is needed and they can be estimated as

$$\frac{C_s}{C_{out}} = \frac{\cos(\alpha_{out})}{\cos(\alpha')} + \frac{1}{2} \cdot \frac{s}{c} \cdot \left[\tan(\alpha_{out}) - \tan(\alpha_{in})\right] \cdot \cos(\alpha_{out}) \qquad (5\text{-}4)$$

$$\frac{C_p}{C_{out}} = \frac{\cos(\alpha_{out})}{\cos(\alpha')} - \frac{1}{2}\cdot\frac{s}{c}\cdot\left[\tan(\alpha_{out}) - \tan(\alpha_{in})\right]\cdot\cos(\alpha_{out}) \quad (5\text{-}5)$$

Where α' is the local blade angle and were supposed by Denton to vary linear between the inlet and outlet. For more precise calculations a more sophisticated polynomial could be used.

Denton also proposed a more simple correlation that gives the change in efficiency compared to the zero tip clearance efficiency.
The equation is

$$\frac{\Delta\eta}{\eta_{TC=0}} = 0.60\cdot\left(\frac{k}{h}\right)\cdot\left(\frac{c}{s}\right)\cdot\cos^{-1}(\alpha_{out}) \quad (5\text{-}6)$$

here refereed to as Denton 2 in this report.

5.2.4 Cambridge

The Cambridge Turbomachinery Course from 2004 [33] and Turbomachinery Aerodynamics [34] are also an attempt to give a physical description of the losses due to tip clearance. It is to a high degree based on Dentons theory [3], but not exactly the same physical assumptions are made as will be seen. Only the results are present here and the full derive are past to the appendix 12.4.2.

5.3 Unshrouded Blades

equation for unshrouded blades is

$$Y = \frac{\Delta p_0}{\frac{1}{2}\cdot\rho\cdot C_2^2} = \left\{\begin{array}{l} 2\cdot C_C\cdot\dfrac{k}{h}\cdot\dfrac{c}{s}\cdot\left[1-\dfrac{C_p}{C_s}\right]\cdot \\ \cdot\left[\dfrac{2\cdot s\cdot\left[\tan(\alpha_{out})-\tan(\alpha_{in})\right]}{c_x}\right]^{3/2}\cdot\cos^2(\alpha_{out}) \end{array}\right\} \quad (5\text{-}7)$$

Where the velocities C_p and C_s are estimated in a similar way as before with eqn (5-4) and eqn (5-5).

5.3.1 Shrouded Blades

The driving force is the pressure gradient across the whole blade row, and if the skewing as the flow crosses the tip are neglected the tangential velocity of the leakage flow will be kept constant across the clearance, ($\Delta C_{j,\theta} = 0$). Under the assumption that the leakage flow is isentropic up to the mixing point and that the axial velocity of the main stream is constant, the relative leakage mass flow can be estimated, see appendix 12.4.2.

When the leakage jet mixes out after the seals, all of its axial kinetic energy will be lost with a negligible increase in total pressure. The loss will then be approximately equal to the axial velocity of the leakage jet and can be expressed as

$$Y = \frac{2 \cdot r_t \cdot k \cdot C_C}{(r_t^{\,2} - r_r^{\,2})} \cdot \left[\tan^2(\alpha_{out}) - \tan^2(\alpha_{in}) + 1\right]^{3/2} \cdot \cos(\alpha_{out}) \qquad (5\text{-}8)$$

There will also be a difference between the leakage jet and main flow in tangential direction because the turning of the main flow. The loss associated with the remix of these velocity are represented by eqn (5-9)

$$Y = \left\{ \begin{array}{c} \dfrac{2 \cdot r_t \cdot k \cdot C_C \cdot \sqrt{\tan^2(\alpha_{out}) - \tan^2(\alpha_{in}) + 1}}{(r_t^{\,2} - r_r^{\,2})} \cdot \\ \cdot \left[\tan(\alpha_{in}) - \tan(\alpha_{out})\right]^2 \cdot \cos^2(\alpha_{out}) \end{array} \right\} \qquad (5\text{-}9)$$

To get the total loss the summation of eqn (5-8) and eqn (5-9) should be used.

5.3.2 CTC

5.3.3 Unshrouded Blades

The tip leakage loss for unshrouded blades in CTC is very simple and originates from Abiant. The included parameters are the ratio between tip clearance and total flow area, chord to pitch ratio, density variation between middle and tip radius, outlet flow angle, and two constants that take into consideration if the tip is overlapped into the casing or if the blade has winglet/minishroud. These two constants have only two values so there is none change with the degree that the casing overlaps the tip or any other geometry variation.

$$\Delta\eta = A \cdot \chi_{Area} \cdot \frac{\rho_{tip}}{\rho_{mid}} \cdot \left[1 + B \cdot 0.3 \cdot \left(\frac{c}{s}\right) \cdot \frac{1}{\sin(\alpha_{out})}\right] \qquad (5\text{-}10)$$

Where A is one constant that depends on the tip is overlapped by the casing or not

$$\mathrm{A} = \begin{cases} 1 \text{ if there are non overlapping} \\ 0.58 \text{ if there are a overlapping or if casing and tip is at the same radius} \end{cases}$$

And B is one coefficient allowing for the effect of winglet/minishroud

$$B = \begin{cases} 1 \text{if no mini shroud} \\ 0.5 \text{if mini shrouded} \end{cases}$$

$\frac{\rho_{tip}}{\rho_{mid}}$ = density variation between the tip and middle radius at the blade, normally in the range of 1.01-1.03.

χ_{Area} = ratio between the clearance area and the area of the flow path in the annular direction.

5.3.4 Sjolander and Yaras

Sjolander and Yaras [37] reviewed loss models for calculating the tip leakage loss originally from for example AM, AMDC, Lakshminarayana and Horlock (1965). At the same time they made experimental measurements of a cascade with advanced measurement points both inside the clearance and downstream. They once more pointed out that the secondary and tip leakage flow interacts and together creates a total loss that is difficult to separate from each other. They also show that the kinetic energy of the tip leakage initial to a partial degree is recovered into static pressure as it rolls up into a vortex. They also found that the loss created inside the clearance together with the magnitude of the kinetic energy that first were seen to be recovered into static pressure, well represented the overall losses seen in the final mixed out loss one chord downstream. Therefore the kinetic energy perpendicular to the main flow is believed to be representative for the overall mixed out tip leakage loss. It should be noted that this loss is first seen at around the length of one chord downstream, thus the next row will not initially experience this overall loss, if the blades are closely spaced.

Therefore, the most important parameters are to estimate the mass flow and velocity of the leakage. They proposed that even if it is well known that the blade get unloaded towards the tip due to the leakage, is this not the case inside the boundary layer. Therefore the assumed load for no clearance can be used in the calculation of both the mass flow and velocity of the leakage flow. A correction for the reduced flow area inside the gap due to presents of a separation bubble gives a measured discharge coefficient C_D in the span of 0.9-0.7 depending on clearance, see fig 4 in [37].

The kinetic energy of the leakage will then be an integral of the pressure difference along the chord as

$$\Delta E = \sqrt{\frac{2}{\rho}} \cdot C_D \cdot k \cdot \int_0^c (p_p - p_s)^{1.5} \cdot dx$$

For an early stage of design calculation, a simplified model for the tip clearance loss coefficient after nondimensionalized with the overall energy in the main passage was given as

$$Y_{TC} = 2 \cdot K_E \cdot \frac{c}{s} \cdot \frac{k}{h} \cdot C_D \cdot \frac{\cos^2(\alpha_{out})}{\cos^3(\alpha_m)} \cdot C_L^{1.5} \qquad (5\text{-}11)$$

Where K_E is a quite insensitive constant that take care to the load distribution of the blade and is

$$K_E = \begin{cases} 0.5 \text{ If mid - loaded blade} \\ 0.566 \text{ If front - or aft - loaded blade} \end{cases}$$

And C_D should be taken as a value between 0.7-0.8.

They then summed up the total loss due to both secondary and tip leakage as the sum of the secondary loss at the hub plus the tip leakage loss and a reduction of the secondary loss at the tip, summarized as

$$Y_S + Y_{TC} = Y_{S,Hub} + Y_{TC} + Y_{S,Tip} \cdot \chi_{Red}$$

Where χ_{Red} is a constant less than one and believed dependent on the boundary layer thickness, but not specified in their paper [37]. Therefore has it not been included in this investigation. A small contribution for the loss creation inside the gap itself was also supposed originally but it is as well neglected here.

This model makes physical sense with the including parameter in the kinetic energy approximation at the same time as it is simple to implement in early design state for one-dimensional calculations. One question is of course the uncertain reductions of the secondary loss at the tip that was not given.

6 Investigation of Tip Leakage and its Affect on Efficiency

6.1 Background

Siemens gas turbine GT35P is a twin-shafted gas turbine that consists of a LPC (low pressure compressor) driven by a LPT (low pressure turbine) and a HPC (high pressure compressor) driven by a HPT (high pressure turbine) that also deliver the shaft work. The HPT consist of four stages that all are unshrouded, and with a linear slope at the outer casing. In this turbine it is possible to control the tip clearance while it is running. To achieve this control the HPT axis is pushed in the axial direction by hydraulics, the maximum movement is 6 mm in the axial direction, corresponding to a change of clearance of 1.6 mm.

In a test from 1992 [35] the shaft power from the HPT was measured with two different clearances, 3.3 and 1.7 mm. The clearance was only measured at one stage so the absolute value can be uncertain. As mentioned above casing and the unshrouded blades tips are along a linear line, so the clearance change will be the same for all stages (1.6 mm). As the active clearance control was switched on and off the shaft power at part load change from 13.0 to 13.8 MW. The total power from the HPT is in the range of 30 MW, but the HPC use the rest. Today GT35P are not produced any more and no follower has replaced it.

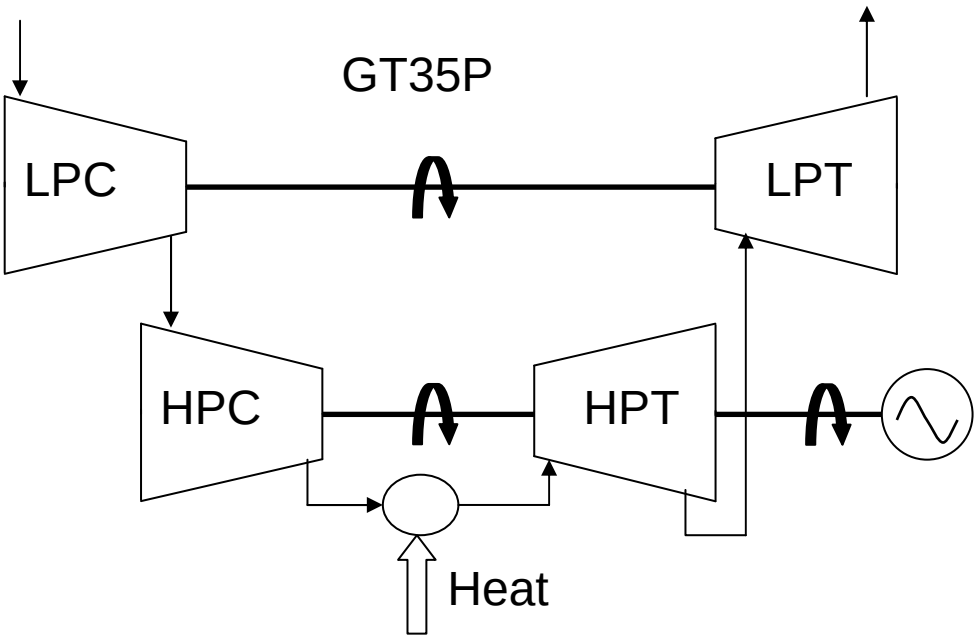

Figure 6.1-1: Structure of the GT35P. Note that the HPT both drive the HPC and give the shaft power.

6.2 Method

To compare different loss models abilities to predict the decrees in efficiency with increasing relative clearance a number of loss models were used. The simulations were done with CTC as a base structure where extra losses were added with Matlab scripts in the same way as described in section 4.2.5. The main input parameters to the first comparison of the models came from a simulation in Ipse pro (a commercial program for thermodynamic power cycle calculations) and is summarized in Table 6-1.

Table 6-1: Input data from Ipse Pro simulation.

Input data from Ipse Pro		
Parameter	*Var 1*	*Var 2*
Clearance rotor [mm]	1.7	3.3
P^*_{in} [bar]	10.9	10.9
P^*_{out} [bar]	2.72	2.72
T^*_{in} [K]	1108	1108
PR [-]	4.00	4.00
m [kg/s]	90.4	---

6.2.1 The Simulated Models

The models used are CTC eqn (5-10), Ainley Mathieson eqn (3-14), Dunham & Came eqn (3-18), Kacker & Okapuu eqn (3-26), Denton (linear, annular and a simple correlation for change of efficiency) eqn's (5-3a), (5-3b) and (5-6), Cambridge eqn (5-7) and Sjolander eqn (5-11). The changes in efficiency are seen in Figure 6.3-1 to 6.3-4 both for the whole PT and for each stage separately. For the loss models where the loss is given as a pressure loss (Y) the converting to an enthalpy loss (ζ) is, to be consistent in the report, done by eqn (2-32). In the loss model from Denton and Kacker & Okapuu that give a change in efficiency related to no clearance at all, the CTC model has been run with no clearance at all to get a datum point.

The models are reviewed below for an overview and feeling of the controlling parameter for the unshrouded loss models. Note the different definitions in angle between the models.

Ainley & Mathieson

$$Y_{TC} = 2 \cdot (k/h) \frac{\cos^2(\alpha_{out})}{\cos(\alpha_m)} \cdot \left(\tan(\alpha_{in}) - \tan(\alpha_{out})\right)^2 \cdot \left[\frac{\mathrm{Re}_{out}}{2 \cdot 10^5}\right]^{-0.2} \qquad (3\text{-}14)$$

Dunham & Came

$$Y_{TC} = 1.88 \cdot (c/h) \cdot \left(\frac{k}{c}\right)^{0.78} \cdot \frac{\cos^2(\alpha_{out})}{\cos(\alpha_m)} \cdot \left(\tan(\alpha_{in}) - \tan(\alpha_{out})\right)^2 \qquad (3\text{-}18)$$

Kacker & Okapuu

$$\Delta\eta_{tt} = 0.93 \cdot \frac{\Delta k}{h \cdot \cos(\alpha_{out})} \cdot \frac{r_{tip}}{r_{mean}} \cdot \eta_{0,tt} \tag{3-26}$$

Denton Linear

$$\zeta = 2 \cdot \frac{k}{h} \cdot C_C \cdot \frac{1}{s \cdot \cos(\alpha_{out})} \cdot \int_0^c \frac{C_s^3}{C_{out}^3} \cdot \left(1 - \frac{C_p}{C_s}\right) \cdot \sqrt{(1 - \frac{C_p^2}{C_s^2})} \cdot dr \tag{5-3a}$$

Denton Annular

$$\zeta' = 2 \cdot C_C \cdot \frac{k \cdot (z-1)}{\pi \cdot \left(r_{tip}^2 - r_{rot}^2\right) \cdot \cos(\alpha_{out})} \cdot \int_0^c \frac{C_s^3}{C_{out}^3} \cdot \left(1 - \frac{C_p}{C_s}\right) \cdot \sqrt{(1 - \frac{C_p^2}{C_s^2})} \cdot dr \tag{5-3b}$$

Denton 2

$$\frac{\Delta\eta}{\eta_{TC=0}} = 0.60 \cdot \left(\frac{k}{h}\right) \cdot \left(\frac{c}{s}\right) \cdot \cos(\alpha_{out})^{-1} \tag{5-6}$$

Cambridge

$$Y = \left\{ \begin{array}{l} \dfrac{\Delta p_0}{\frac{1}{2} \cdot \rho \cdot C_2^2} = 2 \cdot C_C \cdot \dfrac{k}{h} \cdot \dfrac{c}{s} \cdot \left[1 - \dfrac{C_p}{C_s}\right] \cdot \\ \cdot \left[\dfrac{2 \cdot s \cdot \left[\tan(\alpha_{out}) - \tan(\alpha_{in})\right]}{c_x}\right]^{3/2} \cdot \cos^2(\alpha_{out}) \end{array} \right\} \tag{5-7}$$

CTC

$$\Delta\eta = A \cdot \chi_{Area} \cdot \frac{\rho_{tip}}{\rho_{mid}} \cdot \left[1 + B \cdot 0.3 \cdot \left(\frac{c}{s}\right) \cdot \frac{1}{\sin(\alpha_{out})}\right] \tag{5-10}$$

Sjolander

$$Y = 2 \cdot K_E \cdot \left(\frac{c}{s}\right) \cdot \left(\frac{k}{h}\right) \cdot C_D \cdot \frac{\cos^2(\alpha_{out})}{\cos^3(\alpha_m)} \cdot C_L^{1.5} \tag{5-11}$$

where

$$K_E = \begin{cases} 0.500 \text{ if mid - loaded} \\ 0.566 \text{ if front - or aft - loaded} \end{cases}$$

$$Cd = 0.8$$

6.2.2 Turbine Characteristics

The output data concerning the most important turbine characteristics for GT35P from a simulation in CTC are summarized in the Table 6.2 It is seen that both the stage loads and flow coefficient are low, so a high efficiency is expected. At part load where the measurements were done is the mean Mach number at the throat low and subsonic.

Table 6-2: The turbine characteristics for the four stages in GT35P's HP turbine.

GT35P								
Clearance, k [mm]	*Stage 1*		*Stage 2*		*Stage 3*		*Stage 4*	
Parameter	*1.7*	*3.3*	*1.7*	*3.3*	*1.7*	*3.3*	*1.7*	*3.3*
Pi* [-]	1.65	1.59	1.41	1.37	1.42	1.38	1.39	1.33
u/c* [-]	0.54	0.52	0.71	0.68	0.76	0.72	0.86	0.8
H/u^2 [-]	1.54	1.47	0.82	0.9	0.81	0.8	0.61	0.61
Eta* [%]	87	84	91	88	90	89	86	87
P [MW]	11.01	10.65	7.09	6.92	6.75	6.66	5.53	5.54
Reaction Tip [-]	0.31	0.29	0.62	0.61	0.65	0.65	0.65	0.65
Reaction Mid [-]	0.29	0.27	0.55	0.54	0.56	0.57	0.56	0.56
Reaction Rot [-]	0.25	0.22	0.44	0.43	0.45	0.44	0.41	0.4
Mach Stator [-]	0.75	0.76	0.49	0.5	0.48	0.51	0.46	0.49
Mach Rotor [-]	0.59	0.58	0.57	0.61	0.61	0.64	0.6	0.63
Relative Clearance k/h [%]	2.2%	4.2%	1.9%	3.8%	1.6%	3.0%	1.4%	2.7%

6.2.3 Cascade Measurements

The different loss models predictions are compared with an external cascade test on an annular wind tunnel made by Takayuki Matsunuma [32], where the geometry, flow condition and tipleakage loss was well documented. The blade geometry is seen in Table 6-3, and the results from these simulations in Matlab can be found in section 6.3.2.

Table 6-3: Blade parameter used as base parameters in the analyze, originally from [32]

Parameter	*Value*
Number of Blades, z	28
Chord, c [mm]	67.6
Axial Chord, cx [mm]	42.8
Span, h [mm]	75
Pitch, s [mm]	47.7
Inlet Blade/Flow angle [deg]	0
Outlet Blade/Flow angle [deg]	67.4
Tip Radius, R_{tip} [mm]	175
Rot Radius, R_{rot} [mm]	250
Tip Clearance [mm]	0.5

6.2.4 Analysis of the Loss Models Behavior

Analyses of the different loss models behavior are present in section 6.3.3. The parameters varied are clearance and outlet flow angle. All other parameters are constant and equal to the ones in the cascade measurements from Takayuki Matsunuma [32], seen in Table 6-3.

6.3 Results

6.3.1 GT35P

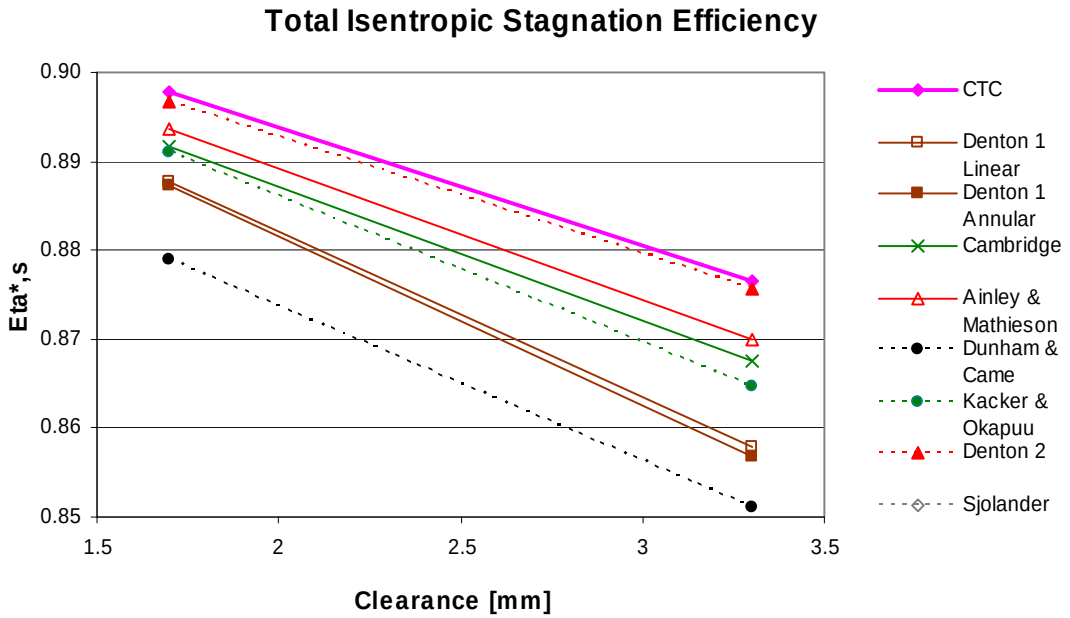

Figure 6.3-1: The total isentropic stagnation efficiency for the whole turbine for different loss models with the two tip clearances of 1.7 and 3.3 mm.

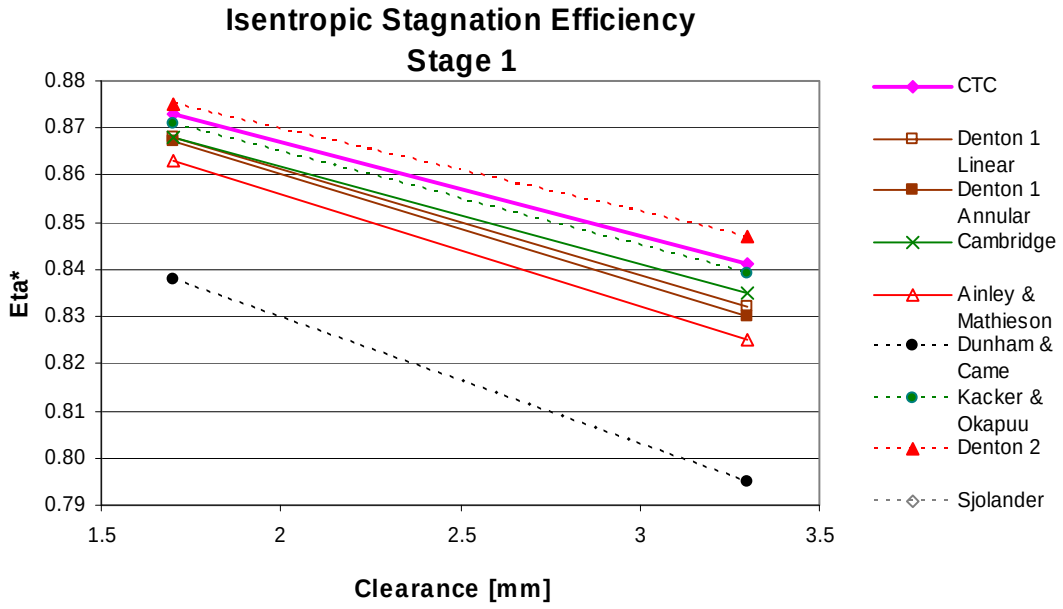

Figure 6.3-2: The total efficiency for stage 1 in the HP turbine for different loss models.

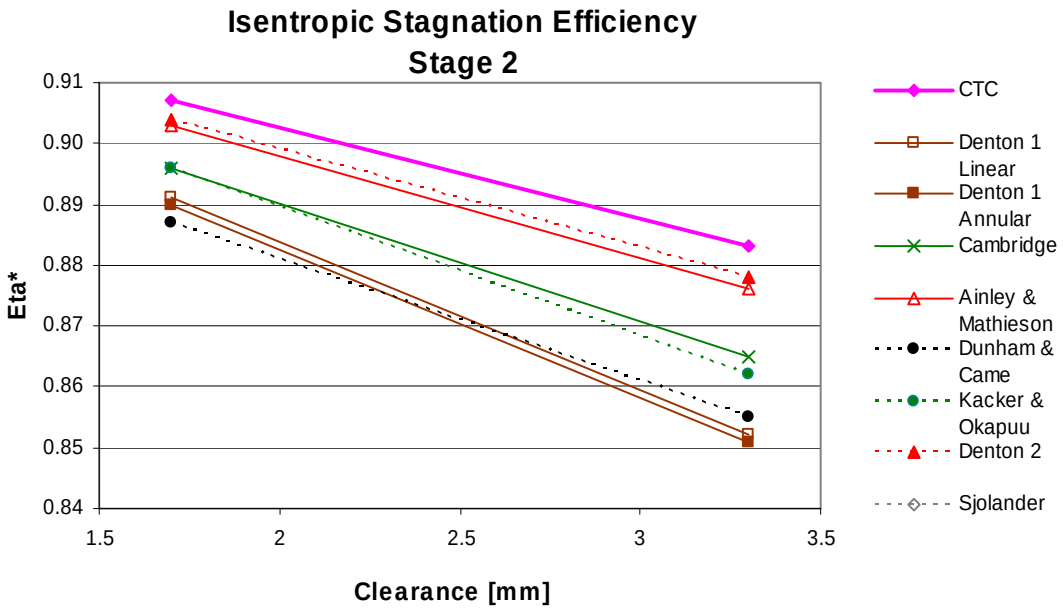

Figure 6.3-3: The total efficiency for stage 2 in the HP turbine for different loss models.

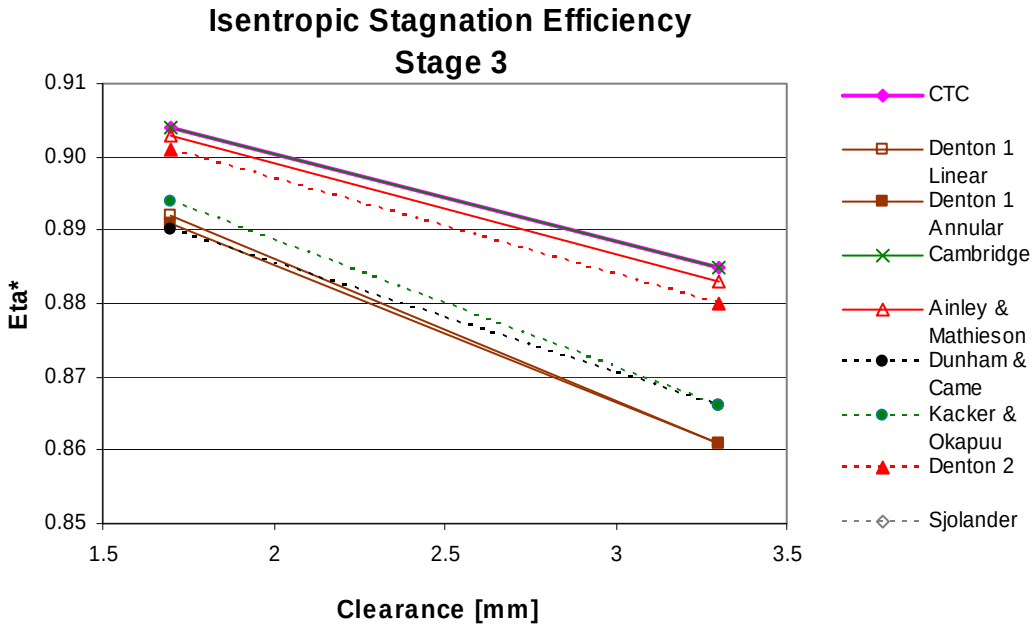

Figure 6.3-4: The total efficiency for stage 3 in the HP turbine for different loss models.

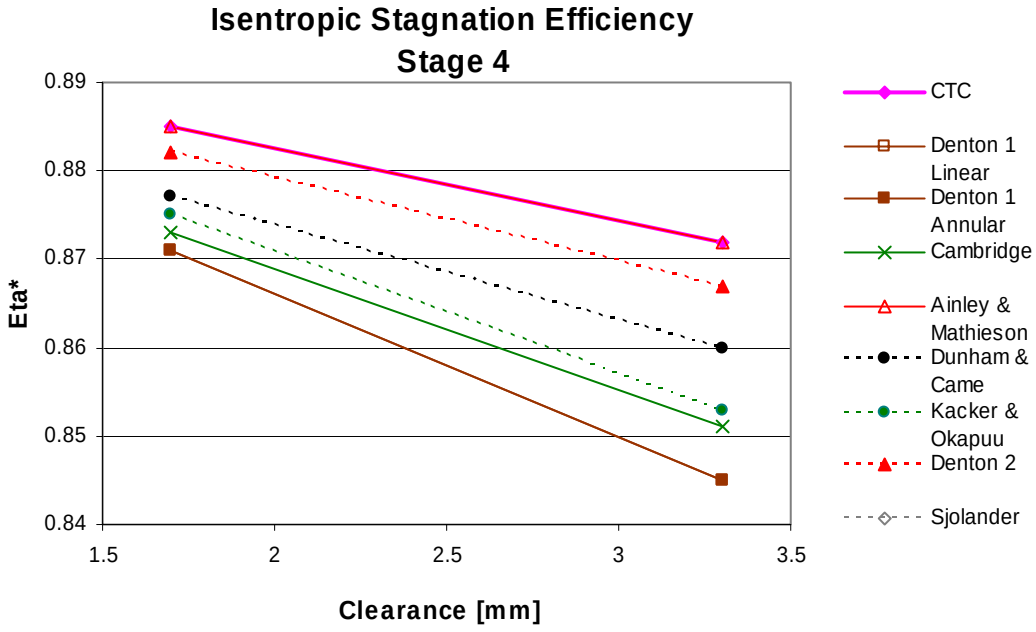

Figure 6.3-5: The total efficiency for stage 4 in the HP turbine for different loss models.

Studying Figure 6.3-1 to 6.3-5 it is seen that the slope of the loss models are changed from one stage to another. In the same Figures it is also seen that one loss model not always give a higher loss level compared to other loss models. That is seen from the fact that the order of the by the models predicted efficiency are changed from on stage to another. For example AM model give the lowest efficiency for stage 1 with a efficiency decrease of about 4 percent while its predicted efficiency level are highest for stage 4 with a decrease of only about 2.5 percent. This shows that the loss level from the different models is strongly dependent on the blade and flow parameter and

which of these parameters that a specific model involves. Note also that CTC is in the top regions of η with one of the smallest decreasing rates for all four stages.

The change in HPT power and the change in shaft work for the simulation of the HPT of GT35P with varying clearance are seen in Figure 6.3-6 and 6.3-7. Figure 6.3-6 shows how much the power decrease when the clearance is increased with 1.6 mm. The absolute value of the power can not be compared because the HPT also produce the power to the HPC and could not be measured separately. Instead the simulated decrease in efficiency with clearance is compared.

In Figure 6.3-7 the predicted power is seen, but no reference value can be included as explained above. Figure 6.3-7 illustrate that the loss level change with different relative clearance will differ a lot between the models. CTC and Denton 2 gives the lowest loss level and loss increase with clearance. Dunham and Came give both a high loss level for a specific clearance and a high loss increase with clearance change. There between are the results from the other loss models spread.

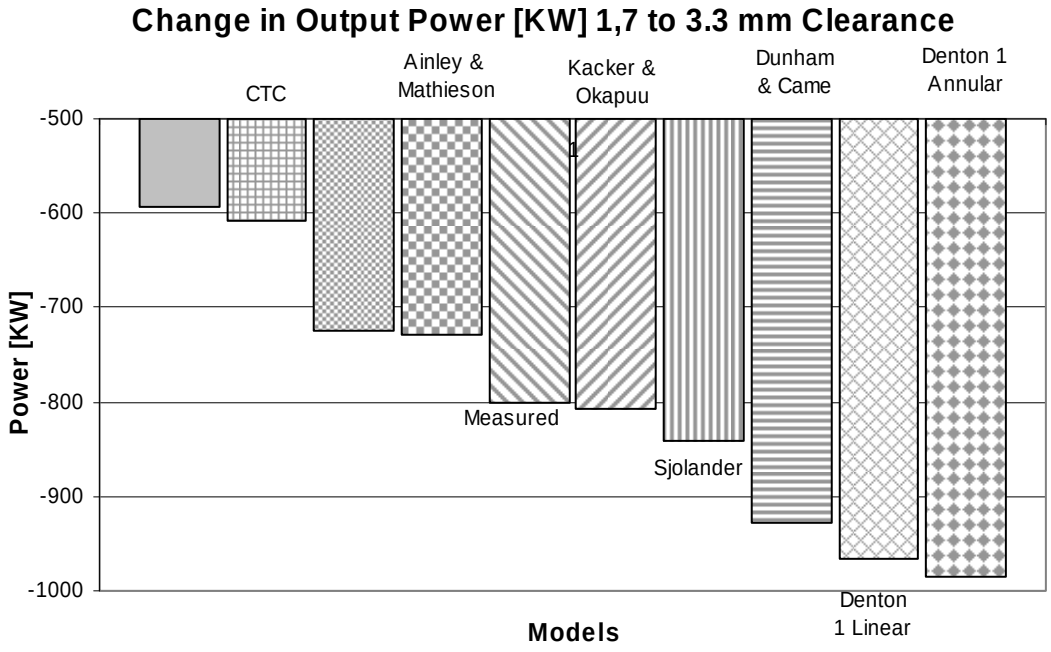

Figure 6.3-6: Change in HPT output shaft power with 1.7 and 3.3 mm clearance at each stage.

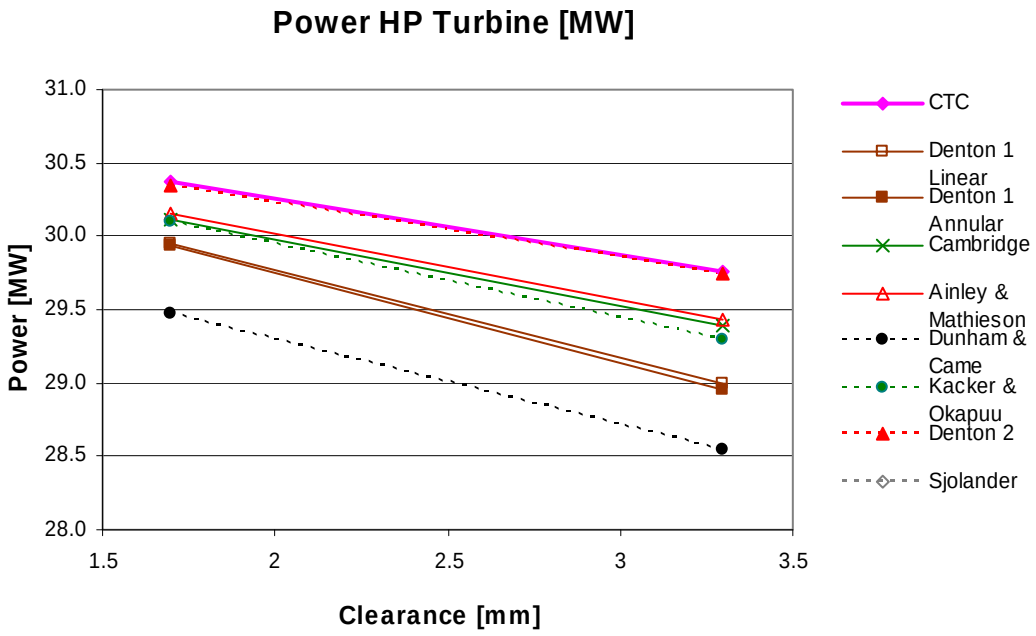

Figure 6.3-7: Change in HPT total power with 1.7 and 3.3 mm clearance at each stage

6.3.2 Validation against Cascade Measurement

In [32] an experimental test for an annular cascade, with the geometry seen in Table 6-3, was made in a wind tunnel. This measurement is compared to other loss models in Figure 6.3-8.

Even if this cascade geometry is forgiving to such models as CTC that do not include inlet angle, the result is that CTC underestimate the loss with a relative value of around -30 percent or absolute value of 0.47 percentage point of total loss. Closer are KO, the three models from Denton and the model from Sjolander.

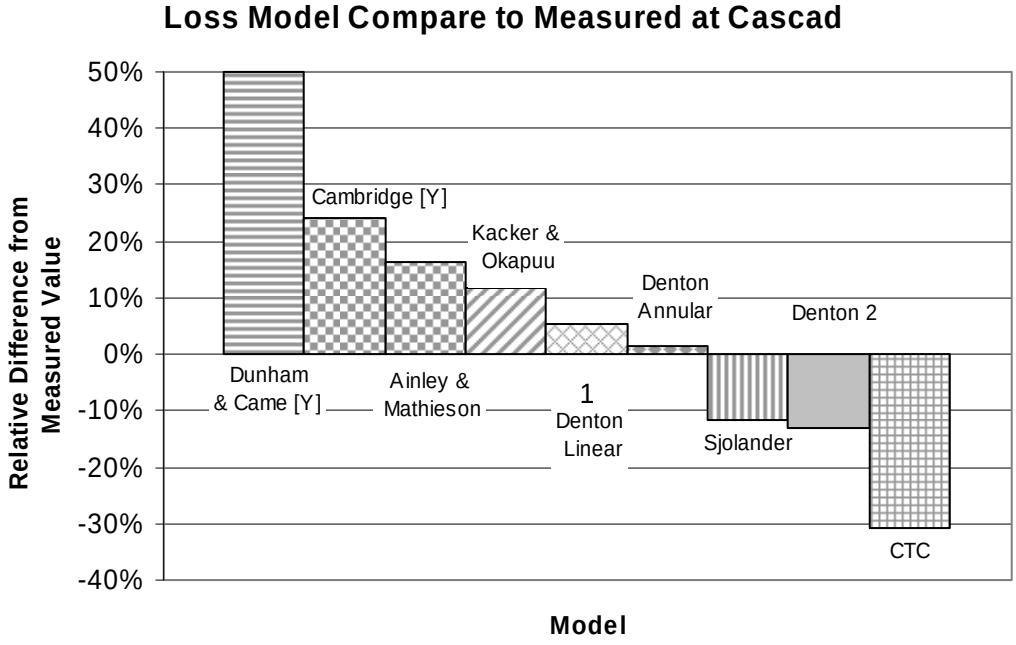

Figure 6.3-8: Relative difference in predicted and measured value of the tip leakage loss for the profile from [32], (DC model overestimate the loss with 221 percent).

6.3.3 Trends for the Loss Models

The losses are plotted against outlet flow angle in the range of 0 to 75 deg and for a tip clearance of 0.5 to 3 mm in steps of 0.5 mm. The loss variation with outlet flow angle for the clearance of 3.0 mm are seen in Figure 6.3-9, and the results for the each of the individual loss models with the variation in both clearance and outlet flow angle are seen in the appendix for chapter 6 (Appendix 12.5). The variation of outlet flow angle represents the flow turning and blade load and the losses should therefore increase with it.

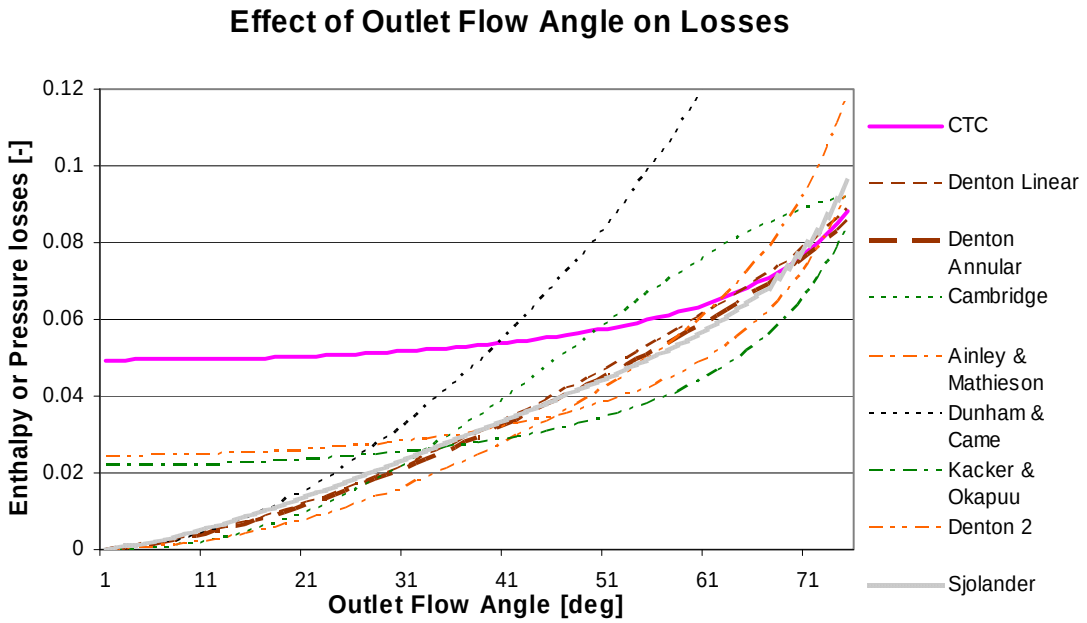

Figure 6.3-9: Variation in loss for a clearance of 3.0 mm with outlet flow angle.

It should be noted that the loss in some of these models seen above are based on pressure (Y) and some are on enthalpy (ζ). In a simple parameter variation as this where no outlet Mach number are known can the losses therefore not be related to each other exactly. For low Mach number the value of both a pressure and enthalpy based loss is close to each other, (see chapter 8).

From Figure 6.3-9 some trends that can be seen are

- Dunham & Came predict a loss that fast groves to twice the value of the other for a reasonable flow turning.

- Denton 2 and Kacker & Okapuu's models are both based on a change in efficiency compared to zero tip clearance, see eqn (3-26) and eqn (5-6). A drawback here is that the term $\cos^{-1}(\alpha_{out})$ that compensate for the flow turning only include the outlet angle and can therefore be misleading if non-zero inlet flow angle. For example can these models not predict low loss levels as $\cos^{-1}(\alpha_{out})$ can not be less then 1. A third problem is more of a programming problem and it is the need of an iterative solution for both the real clearance and zero clearance at the same time, which is time consuming.

- Denton's equations for both the linear and the annular cascade shows linear variation with the flow turning, compared to the other models that shows an accelerating or decelerating behavior with flow turning.

- Cambridge's model is s-shaped where first an acceleration and then a deceleration of the loss levels increasing rate are seen. Note that this is not the original model from Cambridge, instead it has been modified by the author of this report because of an assumed error in the original text, see appendix 12.4.2.1

- The high loss level at low Reynolds number in AM loss model is trend that has not been confirmed by measurements and was highlighted as a drawback in
  [32].

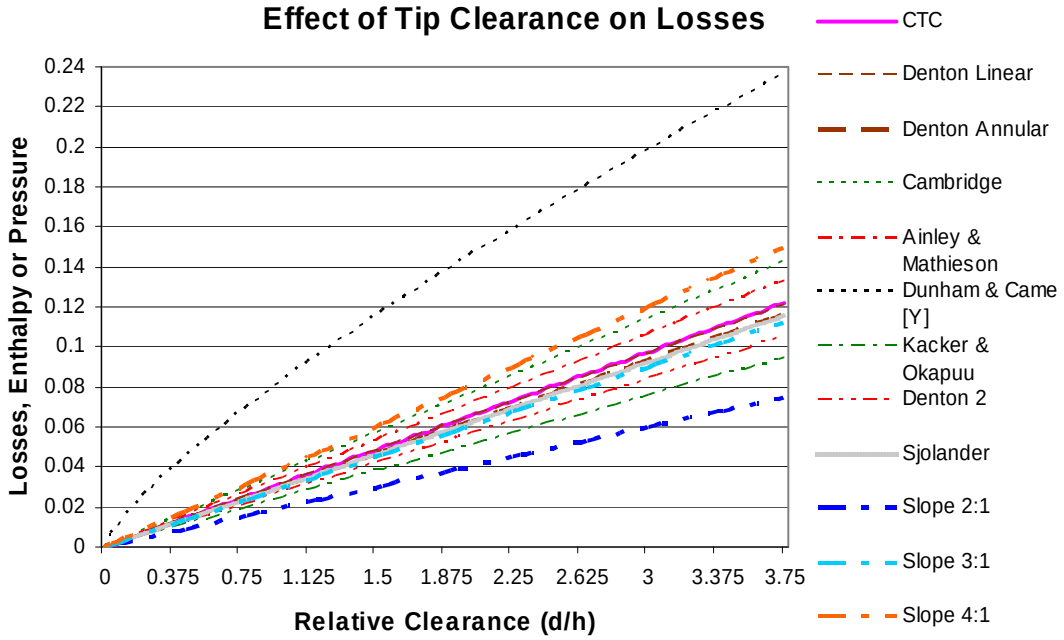

Figure 6.3-10: The effect of the relative tip clearance on the loss.

In Figure 6.3-10 a parameter variation of the relative clearance (k/h) are seen. It is once more seen that all models are varying linear with the tip clearance except from Dunham & Came, where the other blade and flow parameter decides the slope. The three lines with the slope 2:1, 3:1 and 4:1 are plotted and it is seen that all models (except from Dunham & Came) predict an increase within this range. Cambridge, Ainley & Mathieson and Denton show highest increase most (slope between 1:3 -1:4) and some lower increasing rate are seen for Denton 2 and Kacker and Okapuu that both are models based on efficiency change compare to at none clearance at all.

The high prediction of decreasing efficiency with relative clearance is a little surprising because earlier measurements summarized and present by Sjolander in [36] shows a slope close to the region of 2:1, see Figure 12.5-11 in appendix.

6.4 Conclusions

- In the simulation for the GT35P CTC underestimated the loss by nearly 200 kW or 0.7 percentage point in efficiency compared with experiment. Closer were the simulations with KO and Sjolander's loss model that only overestimated the with 7 and 60 kW power, an offset of less then 0.2 percentage point. CTC and Denton 2 were less accurate, two models that are based on change in total efficiency and do not include the inlet flow angle α_{in} (See Figure 6.3-6 for the comparison). CTC shows the same trend for the cascade test in Figure 6.3-8 where it underestimates the loss. A drawback for KO model is that just like CTC it neither include the inlet flow angle or blade load, and is therefore not recommended. So even KO shows good accuracy in these tests it may have problem with other loads or blade profiles.

- CTC's does not show any trend of underestimation in Figure 6.3-9 and 6.3-10 where the effect of outlet flow angle and relative tip clearance were compared for the blade geometry in Table 6-3 [32]. In Figure 6.3-9 shows CTC the highest loss level of all the models investigated for low flow turning. For a more generally level of flow turning, in the range around 60-70 deg, the predicted loss level is comparable to the other models. The loss change with relative clearance for CTC is comparable to the other loss models with a slope close to 3:1. Note that earlier external tests have showed that the slope normally would be around 2:1, see Figure 2.11 in [30] (originally from Hourmouziadis & Albrecht 1987).

- As mention above is a major drawback with CTC's loss model that it does not include the inlet flow angle. Therefore it is not possible to include the blade load variation for non-zero inlet flow angle. This limitation was not captured in section 6.3.2 and 6.3.3 because the inlet flow angle was axial there.

- A good loss model should both predict the absolute value of tip leakage loss and at the same time have an accurate efficiency change for variation in clearance. The absolute value is important for new design cases and is compared in Figure 6.3-8. While the efficiency change is important for understanding and predict the effect of a parameter change as compared in Figure 6.3-6. With these requirements to fulfill and at the same time the knowledge that CTC is not able to catch the influence of inlet flow angle, it is recommended to either replace it with Sjolanders model or at least modify it to a more satisfying loss level and involve more parameters. For with the possible underestimation of the tip leakage loss in CTC today there is a risk that the consequence of reducing the tip clearance is underestimated.

- Sjolander model involve the inlet flow angles, pitch to chord ratio, contraction coefficient over the tip and the blade load distribution. It is still a simple model compare to the other interesting models from Denton and Cambridge. It should be noted that Sjolanders model has not the ability to take care to the effects of winglet or overlap between casing and rotor, something that need feature research.

7 Mach number Influence on Profile Loss

7.1 Background

Already Ainley and Mathieson present in their report 1955 [7] two graphs and a short description about how the profile loss is effected by Mach number (M) and mean turning radius after the throat (e). Their graph for the Mach number effect on profile loss for varying s/e ratio is seen in Figure 7.1-1, originally fig 12.a in [7].

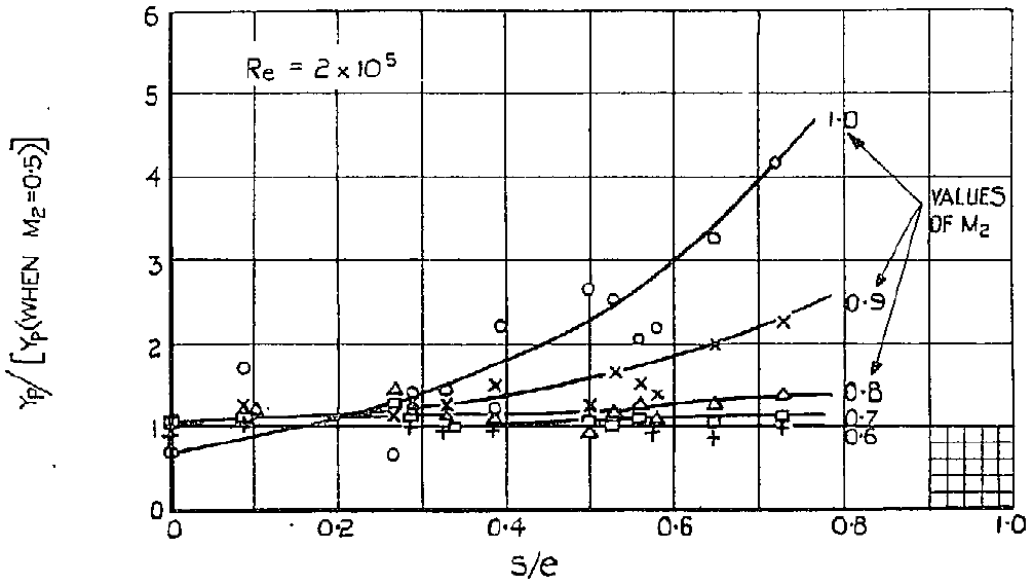

Figure 7.1-1: The Mach number effect of profile losses for varying s/e supposed by Ainley & Mathieson 1955 [7], fig 12a in [7].

Figure 7.1-1 shows that the Mach number has practically no influence at all as long as it below 0.8, but for values above 0.8 the influence increases quite rapidly. It is also seen that for a ratio of the pitch to mean turning radius (s/e) less than 0.3 there is no dependence but above this ratio the profile losses increases fast for high Mach numbers.

1970 Craig & Cox publish a graph in there paper, [12] for prediction of the increase in profile loss with s/e. In their graph, seen in Figure 7.1-2 and 12.3-23, they cover the wide range of outlet Mach numbers from 0.8 and up to 2.0. Even if the charts from both AM and CC are pretty similar, a difference is that AM give it as a multiplier to the base profile loss while CC give an extra increase independent of the base loss.

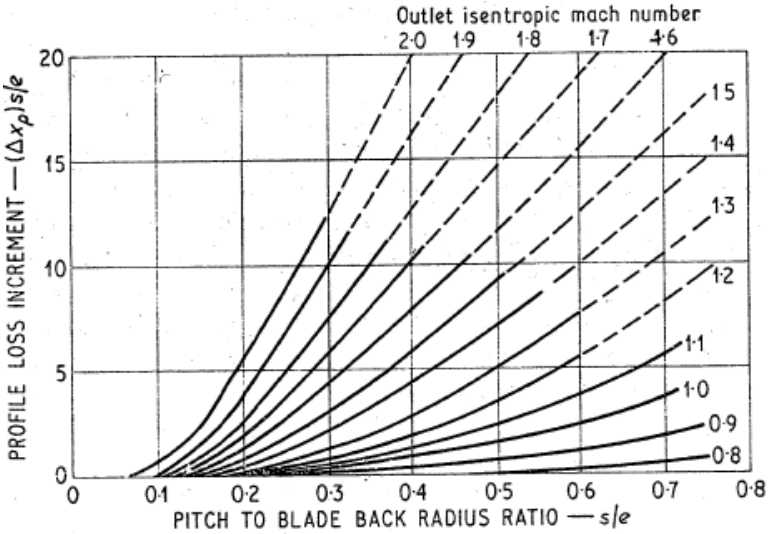

Figure 7.1-2: The Mach number effect on profile losses for varying s/e proposed by Craig & Cox 1970 in [12] Figure 9.

CTC takes no care to these suggested trends at all today, so in an attempt to improve the prediction ability in CTC, a numerical experiment in NS 2D program included in Blagen was done to investigate if these trends also were seen here.

The Mach number influence on the total loss is compared with the loss correlations for Mach number in CTC and measurements made by Teik Lin Chu [39].

7.2 Method

The procedure for the numerical investigation was to use Navier Strokes (NS) 2D solver involved in the program package Blagen, (as also was used when the effect of incidence on profile loss was examined in section 4).

Blade sections were created at the middle radius for a number of real blade geometries from Siemens. These blade sections were then tested for a range of Laval number from 0.5 up to 1.15, (corresponding to a range of Mach number from 0.47 to 1.18). The profile loss from NS 2D and the corresponding ratio of s/e were then plotted in an analog way to Figure 7.1-1 and 7.1-2 to see if the trends from AM and CC could be confirmed. Figure 12.2-8 illustrates the definition of mean radius of curvature (e). e is the radius that a smooth circle arc would have to create the same uncovered turning between the throat and trailing edge with a smooth circle arc.

The used blade sections for this test were all at midsection and representative for Siemens blade profiles. In all the tests the incidence was zero and all other parameters except from λ were kept constant to a normal load simulation in CTC, see the value in Table 7-1.

Table 7-1: Blade parameters for representative blade profiles

	Representative Blade Profiles									
Parameter	*B*	C	D	E	F	G	H	I	J	K
Number blades					**Confidential**					
P* [bar]					**Confidential**					
T* [K]					**Confidential**					
T_w* [K]					**Confidential**					
Alfa in [deg]					**Confidential**					
Alfa out [deg]					**Confidential**					
Chord c [mm]					**Confidential**					
Pitch s [mm]					**Confidential**					
e/s	0.701	0.367	0.469	0.448	0.536	0.566	0.605	0.491	0.307	0.404
R_{mean} [mm]					**Confidential**					
e					**Confidential**					
s/c	0.701	0.812	0.680	0.783	0.865	0.876	0.807	0.815	0.834	0.777
Turning					**Confidential**					
Uncovered Turning/e					**Confidential**					
Deviation					**Confidential**					

In NS 2D solver the input parameter is Laval number instead of Mach number as Ainley & Mathieson and Craig & Cox were using. Laval number is defined as the local velocity nondimensionalized by a reference speed of sound (normally at the throat or outlet). In that way it gives a better comparison of the actual flow speed in the whole section. To go between Laval and Mach number [38] give eqn (7-1), that has been used for the conversion from Laval to Mach number. Derivation of the relationship in eqn (7-1) is shown in appendix (12.7.1).

$$Ma = \sqrt{\frac{2 \cdot \lambda^2}{(\gamma+1) - (\gamma-1) \cdot \lambda^2}} \qquad (7\text{-}1)$$

For the modeling of CTC's loss correlations Matlab was used to show the trends of these losses with outlet Mach number. The used input data for the modeling are summed up in Table 7-2.

Table 7-2: Parameters used in Matlab modeling of the Mach number influence on losses, where the angle are defined from tangential direction as in CTC.

Alfa in	80
Alfa out	20
Blade Angle in	83
Blade Angle out	15
Deviation	5
Kappa	1.33
M out	0.80-1.20

The equations for CTC's loss increase due to Mach number originate from MuKr with some modifications. These modifications are classified as confidential and therefore excluded.

7.3 Results

The simulation results from NS 2D have been processed and are shown in a couple of graphs. The first two charts attempt to recreate the original results from Ainley & Mathieson seen in Figure 7.1-1. In Figure 7.3-1 the change is relative to the loss at Mach number 0.5. The losses often show a minimum some later at Mach number around 0.8 and therefore a second chart is visualized in Figure 7.3-2 related to the losses at M 0.8.

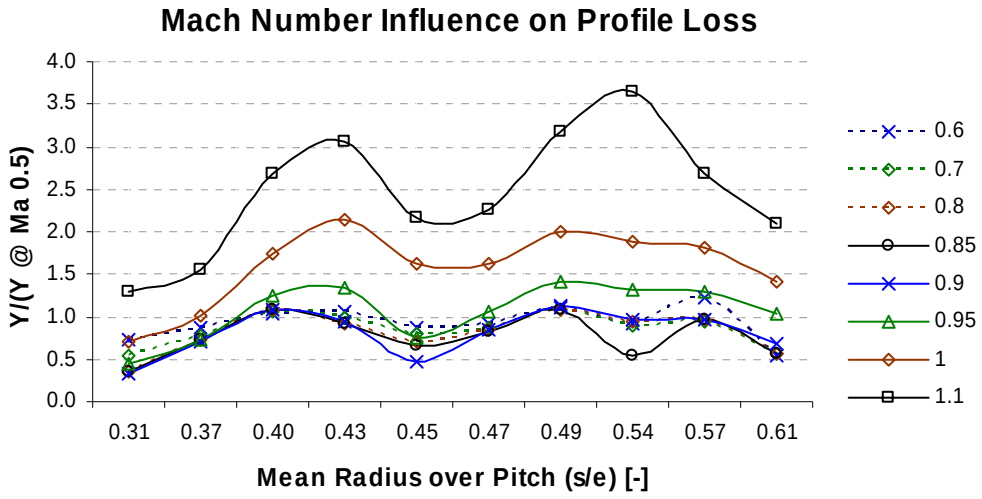

Figure 7.3-1: The change in profile loss with Mach number and (s/e) relative to the loss at M =0.5

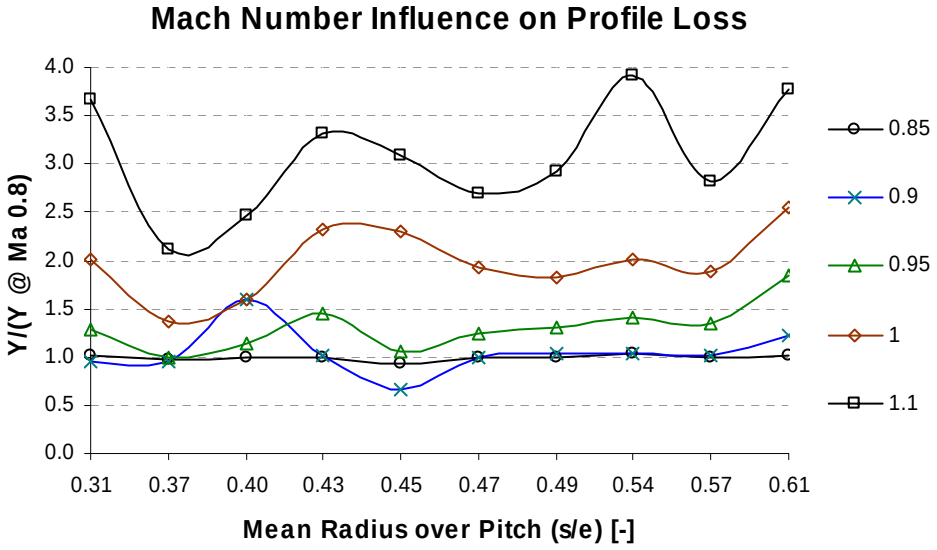

Figure 7.3-2: The change in profile loss with Mach number and (s/e) relative to the loss at M =0.8

Eventually a weak increasing trend can be seen, but not enough significant to draw any certain conclusions. For the investigated blades the range of s/e lays within 0.30-0.61 which can be a drawback. If the measured points above 0.6 are excluded, in Ainley & Mathieson's chart, the scatter of the points also is so big that no certain trends can be seen. To investigate if perhaps the methodology from Craig & Cox was more accurate, the simulated results are visualized in an analogy way to CC in Figure 7.3-3. The chart does not show any sign that confirm Craig & Cox original chart.

Neither any simple trend was found for the losses related to other parameter combinations of deviation, pitch to chord or overall turning.

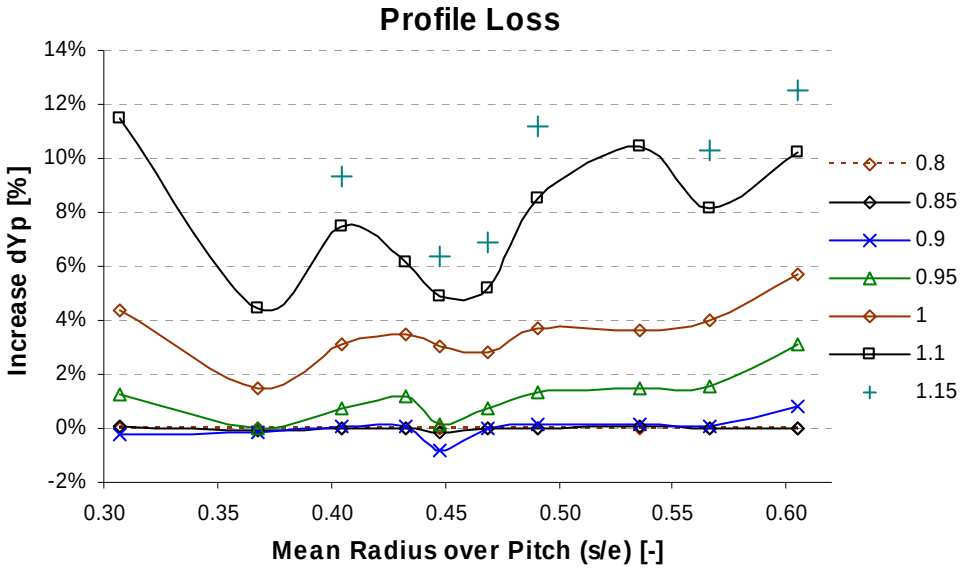

Figure 7.3-3: The increase dYp for different s/e and outlet Mach number in a attempt to recreate a chart equal to Craig & Cox Figure (7.1-2).

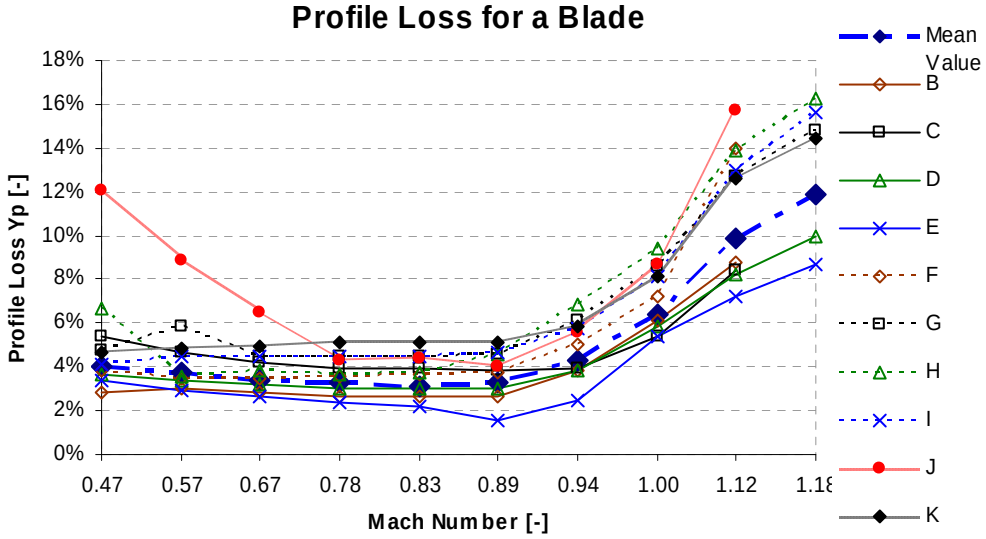

Figure 7.3-4: The total profile loss for the different blade profiles for a range of outlet Mach number of 0.47-1.18. A mean value to all the profiles is also included.

From Figure 7.3-4 it is seen that the profile loss (including shock loss) is rather constant up to a Mach number of around 0.85-0.90. Then it shows a steep increasing trend up to at least a Mach number of 1.18. The parameter that determines the precise point when the increasing in loss starts has not been found. It is assumed that the parameter is influenced by a multiple of other parameters and some indications are that it is related to the s/e ratio.

With consideration to the trends of the loss increase seen in Figure 7.3-4, where the first six curves increases with a stepper slope than the last four, the blades can be divided into two groups. The first group has an s/e ratio within the range 0.49-0.61 plus two blades with s/e value of 0.31 and 0.40. The later group has the s/e ratio from 0.33 to 0.47, (see Table 7-1).

The believed reason for this sudden loss increase and division between the both groups is that for a relatively low uncovered turning radius (e) (large value of s/e) the diverging of the streamline near the suction surface gets large. Thus also a risk that the sonic fluid velocity at the suction surface is future accelerated. The acceleration may lead to a shockwave and a risk for separation of the boundary layer which creates losses. This can be confirmed from the NS 2D simulation where it can be seen that the shock and region of supersonic Mach number increases with the s/e ratio, except for the two blades with a s/e ratio of 0.31 and 0.40 from that even if they have a low s/e ratio show an early and large supersonic area and steep loss increase. The trend with the presence of a supersonic bubble at the suction surface for subsonic outlet Laval number is illustrated in Figure 7.3-5 to 7.3-7. Figure 7.3-5 shows the presence of a supersonic bubble at blade "H" with λ_{out} 0.85 and the ratio s/e 0.61. Figure 7.3-6 shows that for the same value of λ_{out} 0.85 for blade "B", no supersonic region is seen at all.

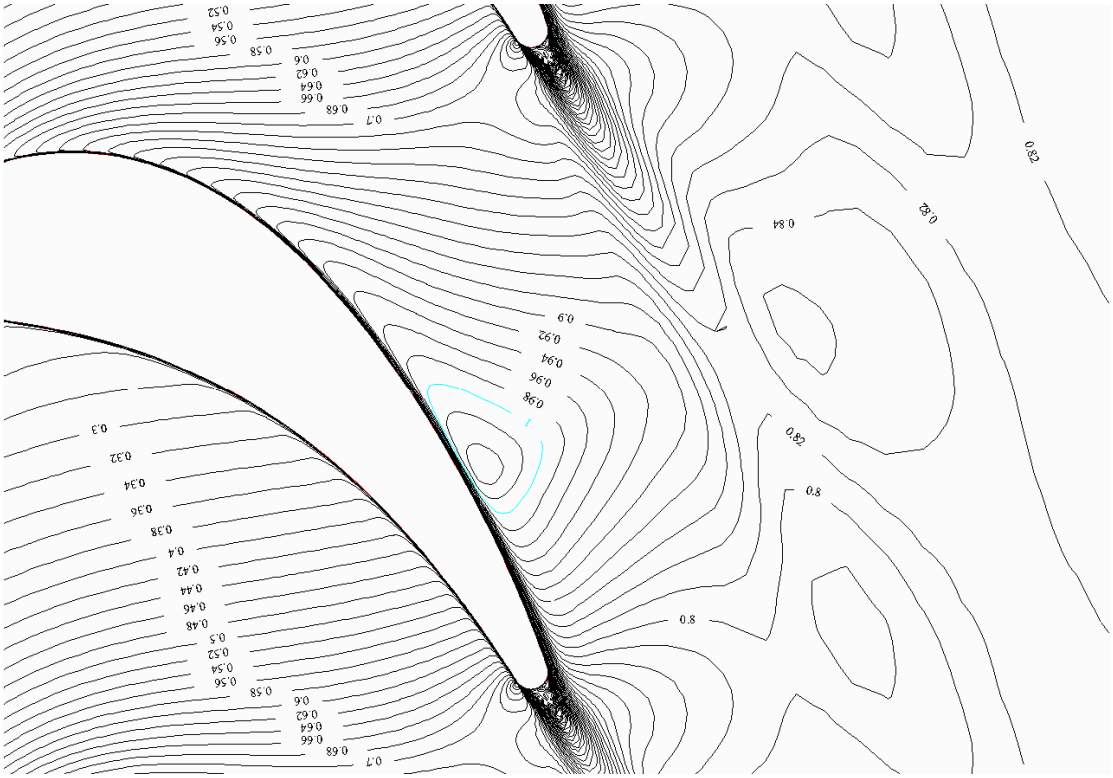

Figure 7.3-5: The presence of a supersonic bubble at the suction surface of blade "H" with a subsonic outlet Laval number of 0.85 and an s/e ratio of 0.61.

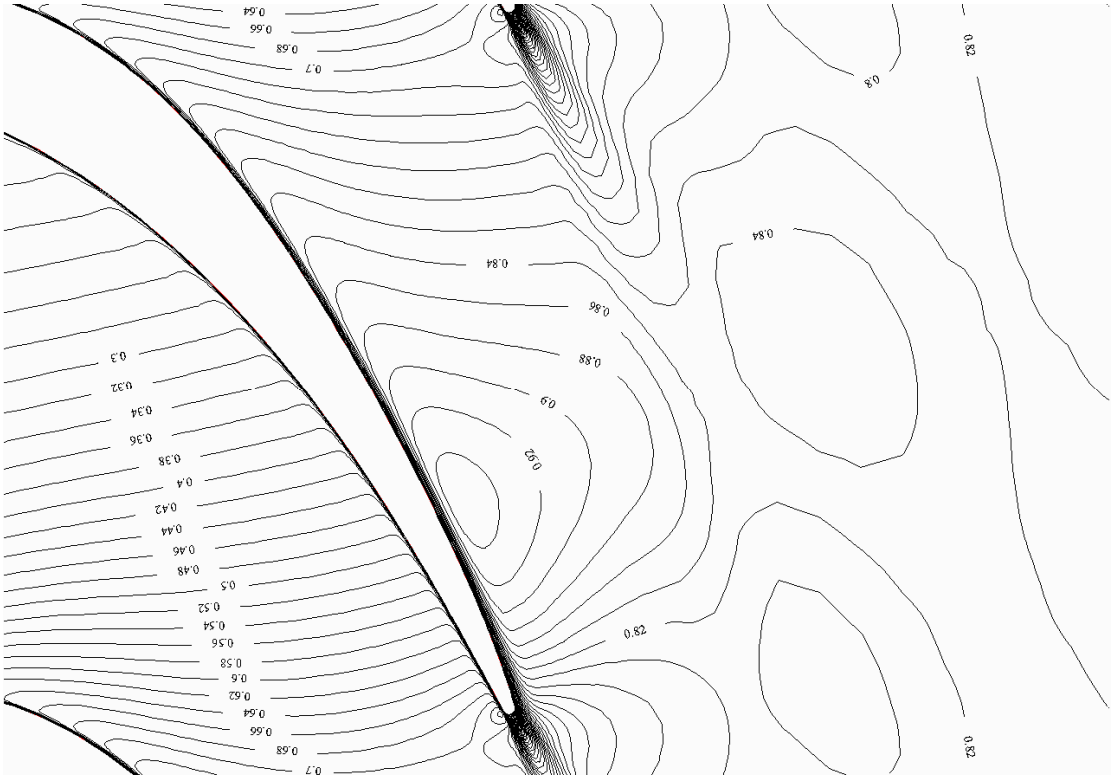

Figure 7.3-6: The absence of a supersonic bubble at the suction surface of blade "B", with subsonic Laval number of 0.85 and the low turning value s/e of 0.33

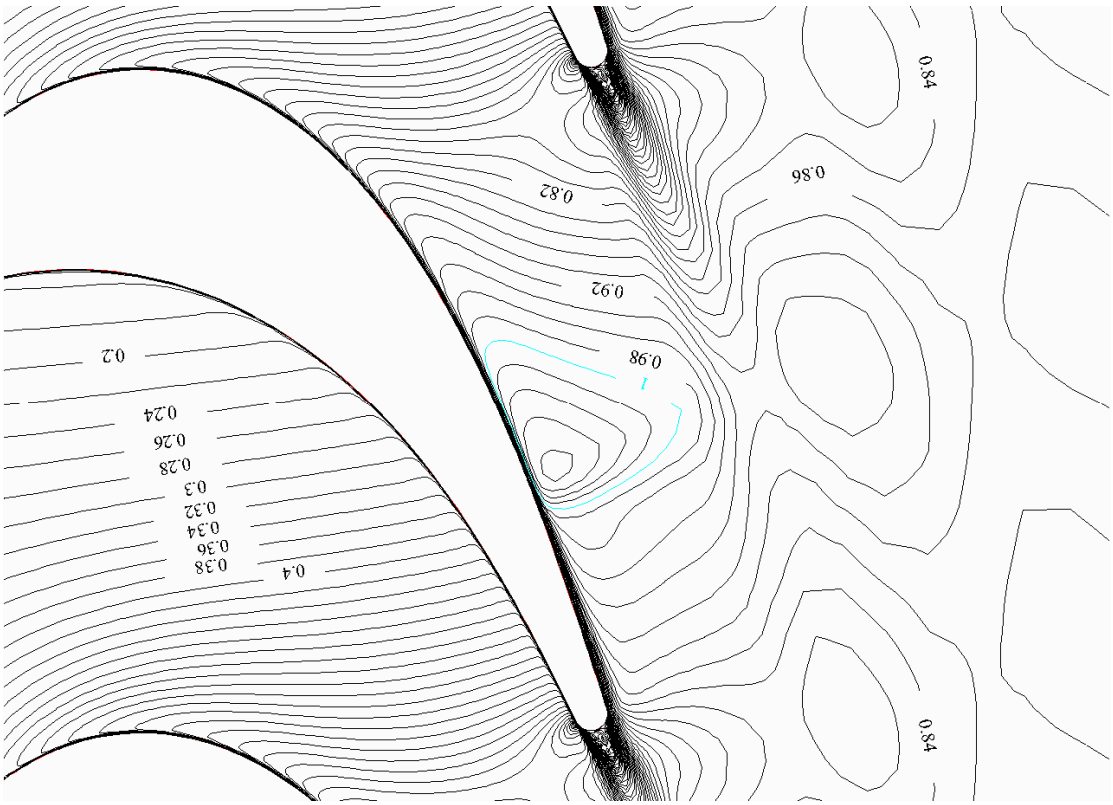

Figure 7.3-7: Illustration of the presence of a supersonic bubble at the uncovered part of the suction surface of blade "K" at a outlet Laval number of 0.90.

The presence of this supersonic bubble in Figure 7.3-7 is linked to the sudden increase in loss for the Mach number variation. This blade shows up a large supersonic bubble even if the s/e ratio is as small as 0.41, indicating that the loss can not simple be correlated to only the s/e ratio.

In ref [39] Teik Lin Chu has studied the Mach number effect on two linear cascades, and the results from this report confirm the same trends as seen in Figure 7.3-4, with an initial constant loss that sudden increases for M around 0.95. There were also signs seen in [39] that the loss would reach a maximum for M around 1.10, when the shockwave tends to bend backwards with increasing Mach number, and therefore will be weaker. This trend with a maximum loss can not be confirmed from the NS 2D simulation, where only a decrease in the increasing loss rate is seen for M above 1.10. The trend of the backward bending shockwave for the outlet Laval numbers of 0.95 and 1.10 for blade "H" is confirmed and illustrated in Figure 7.3-8 and 7.3-9. The red line indicates M equal to one in the Figures 7.3-5 to 7.3-9.

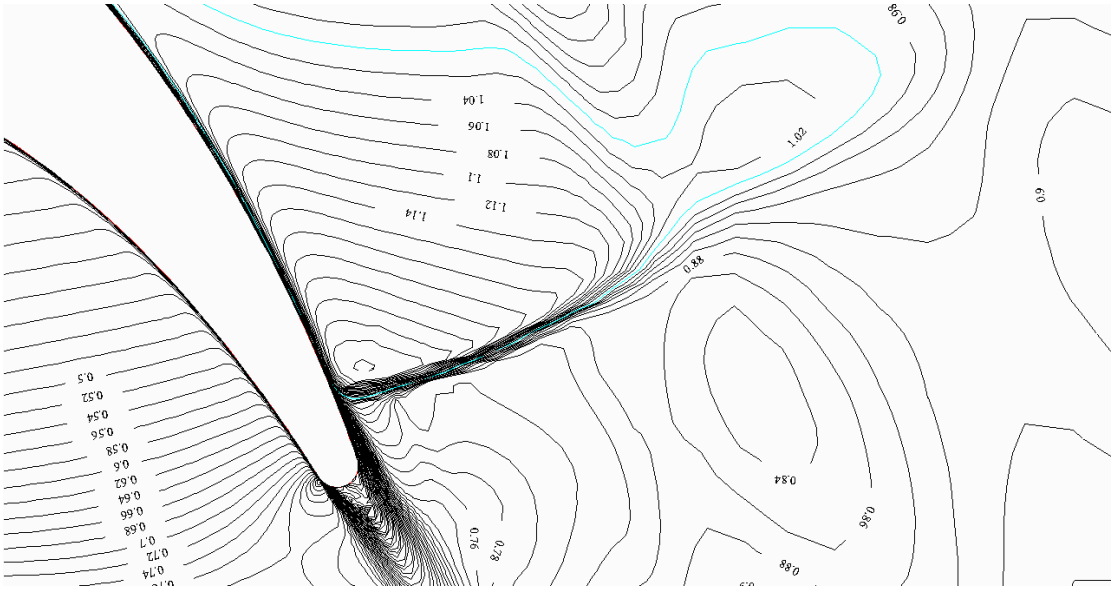

Figure 7.3-8: The Mach number and close to perpendicular shock at the suction surface near the trailing edge for blade "H" at outlet Laval number of 0.95.

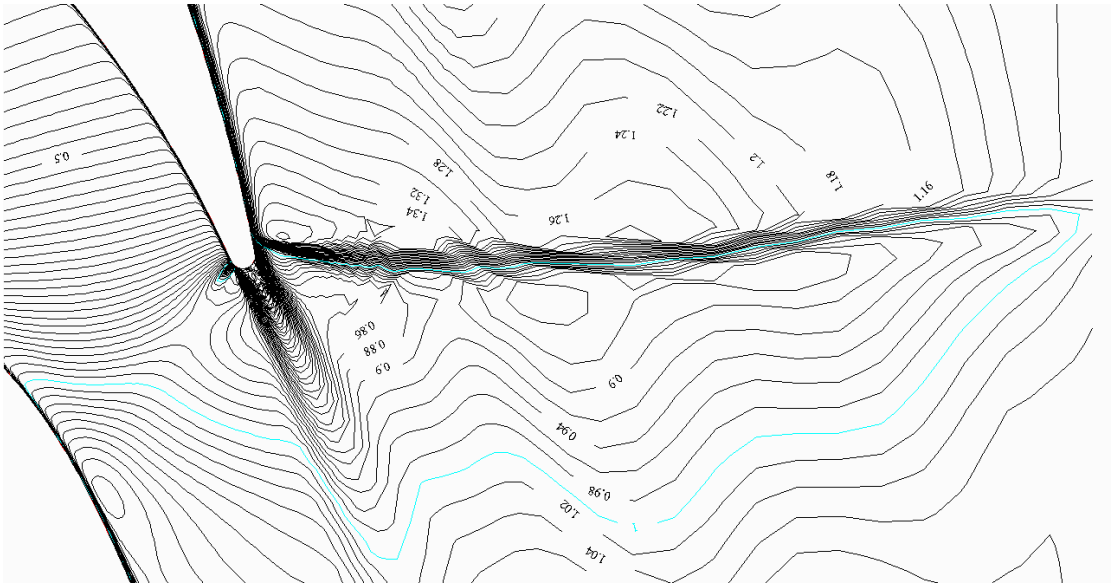

Figure 7.3-9: The Mach number and shock at the suction surface near the trailing edge for blade "H" at a outlet Laval number of 1.10. It is here seen that the shock tends to bend backwards and is placed closer to the trailing edge. This is assumed to be the reason for the decreases in loss for Laval numbers above 1.10 in [39]. However the NS-2D simulations do not confirm it.

The fact that both these numerical simulations and the experimental study in [39] confirm the sudden increase in loss, already at subsonic outlet Mach number, shows that there is a need to investigate how well CTC predicts these losses. The correction factors to the loss due to outlet Mach number from CTC are compared with the mean value of all the simulations, a polynomial fit to this curve, Dunham & Came correction, eqn (3-15), Craig & Cox loss correction in Figure 7.1-2, and a proposed correction factor from Teik Lin Chu [39].

For Craig & Cox a range of different s/e values were tested. Even if the values were seen to affect the increase rate they were not even near to reach the value from the simulation for any s/e ratio. Therefore only the s/e ratio of 0.5 is shown here. The mean value of the profile loss from the simulations in NS 2D at an outlet Laval number of 0.8 was 3.5 percent is used as a datum point to get the relative percentage increase when the loss increase was in absolute value as for CC. The results are shown in Figure 7.3-10, where it is seen that not any of the models will predict the trend.

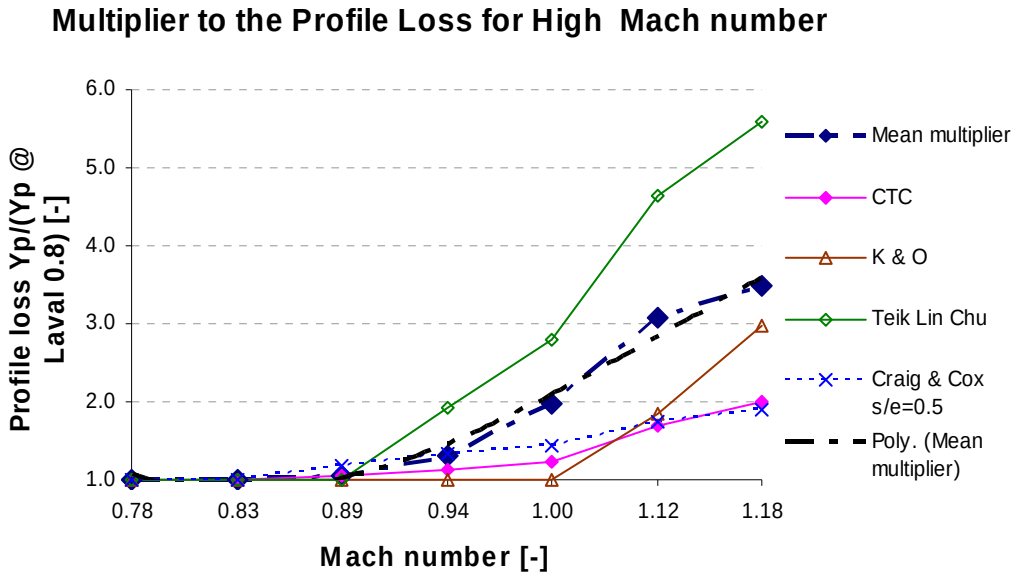

Figure 7.3-10: A comparison of the prediction accuracy for CTC, Kacker & Okapuu, Teik Lin Chu and Craig & Cox to the mean of the measured value in NS 2D.

In Figure 7.3-10 it is shown that even if CTC starts to increase the loss already at M_{out} around 0.85 the rate is far to low. At Mach numbers around one CTC has only increased the loss with 25 percent while the NS-2D simulations show a 100 percent increase. It should also be noted that this extra penalty in CTC is to the optimal profile loss $\zeta_{P,opt}$ and not the actual which takes care to the pitch and might be even higher. Therefore the increase shown for CTC will be even less than that illustrated in Figure 7.3-10.

The model from Craig & Cox and CTC shows compared with measurements, for a s/e ratio of 0.5, a close to equal trend with a small loss increase already at low Mach numbers. Then the increasing rate is to low in as M increases. The variation with s/e ratio used in CC is not negligible in the loss estimation, but it is far from enough to reach the simulated value. KO loss correction does not start before M reaches one, and therefore it lacks in accuracy, even if the increasing rate is closer to the calculated. For the Teik Lin Chu correlation the increasing rate is too fast and it therefore means that it over predicts the loss, even if the loss level increase is rather close to the simulated value for blade "H" with s/e of 0.61 (shown in Figure 7.3-4).

The steep increase is seen at the same time as a supersonic flow region is present at the suction surface of a blade, as illustrated in Figure (7.3-5)

7.4 Conclusions

The conclusion of the Mach number influence on the loss is that it is believed to be a function of multiple parameters and not just the pitch to uncovered turning radius ratio (s/e). Therefore the chart from Ainley & Mathieson, see Figure (7.1-1), and Craig & Cox, see Figure (7.1-2), can not be confirmed after comparison with the simulated results seen in Figure 7.3-1 to 7.3-3. This unclear loss trend is confirmed by Venedictov and Rudenko in [40], where they show the loss as a function of Laval number and uncovered turning. The Figure can be seen in appendix 12.6.2

When studying the trends of how the mean value of the loss increases with outlet Mach numbers, as seen in Figure 7.3-4, it is visualized that a sudden increase is seen for a M_{out} of around 0.90. This loss increase is not in a satisfactory way taken into consideration in CTC's loss model. Therefore a replacement of the now used loss correlation for the extra loss due to Laval number above the optimal ($\lambda_{out} > \lambda_{out}^{opt}$) with a new polynomial is suggested. A suggestion is also that, in a further work try to find out more about which parameters that influences the exact initial point where the loss starts to increase and from this knowledge refine and divide CTC's loss models polynomial into subgroups.

8 Numerical Comparison of the Converting between a Enthalpy and Pressure Based Loss

8.1 Results

In the section below the terms compressible and incompressible are used and refer then to the second order of compressibility as is described in chapter 2.4, and not the first order of compressibility that always is taken into account with both methods. The effect of transfer the losses from kinetic energy (ϕ^2) to pressure losses (Y) with a incompressible equation as proposed by MKT in eqn (2-32) and the compressible proposed by Lehrman [44] with eqn (2-37) and (2-39) are studied. This will only influence the loss models that give any losses in the term of pressure or ϕ^2, and in that way not CTC. The compressible loss Y_{comp} will be larger than the incompressible Y_{incomp} for any given value of ϕ^2, ξ or ζ. That means that for a given value of Y as is the case in all AMDCKO loss models the enthalpy loss will decrease with the Y_{comp} relation. Whit this decreasing enthalpy loss the efficiency will increase, and that is shown in Figure 8.1-1 and Table 8.1 where the simulation with (BSM 1995 limit) for both test 1 and 2 are compared for both methods. The values of the increase in efficiency are around 0.5 percentage point for these tests and the difference is therefore important to consider when calculating the efficiency.

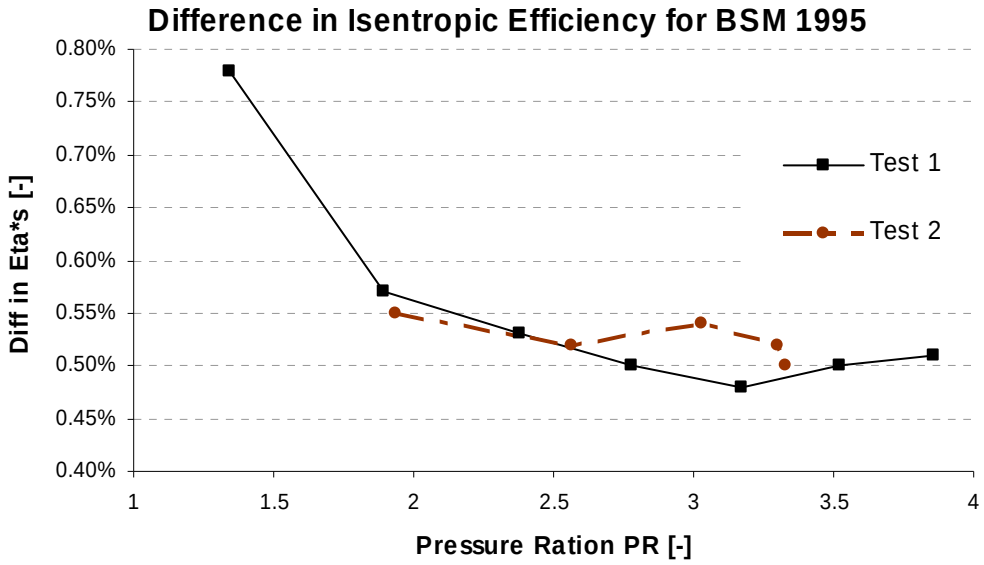

Figure 8.1-1: Change in isentropic stagnation efficiency if the second order of compressibility is included or not in the converting between a pressure and enthalpy based loss, as described in section 2.4. It is seen that the increase in efficiency for these two tests is around 0.5 percentage point.

Table 8-1: Show the difference in efficiency for BSM 1995 if include the secondary influence of density variation when convert between a pressure and enthalpy based loss.

Difference in Isentropic Efficiency							
Pressure ratio PR [-]	*3.86*	*3.52*	*3.17*	*2.78*	*2.38*	*1.89*	*1.34*
Test 1	0.51	0.50	0.48	0.50	0.53	0.57	0.78
Pressure ratio PR [-]	*1.94*	*2.56*	*3.03*	*3.30*	*3.33*		
Test 2	0.55	0.52	0.54	0.52	0.50		

9 Overall Conclusions

Primary the secondary but also the profile loss and the associated flow phenomena are sill far from being fully understood. Therefore is there a risk that not all the most important parameters will be included in the today used loss models. This can explain why experiments and correlations not always show the same trends, and that it is difficult to find any general correlation for 1D program at off-design loads. The fact that all Siemens gas turbines in the range of 15-50 MW have been developed with different design philosophy make it even more difficult to draw any general recommendations for the loss correlations in CTC from this limited investigation. Some conclusions and recommendations that whoever can be given are

- For the off-design calculations CTC show the best overall predictions ability, and it was possible to predict the loss level down to a high degree of off-design (in the region of where the turbine reaches turn-up mode). When examine the division between the different losses was a question that arise if there is a realistic division between secondary and profile loss in CTC. If the loss division aren't correct there is a risk that the improvements effort is put at wrong blade section.

- The secondary loss in CTC that scale against the throat should be future investigated in an attempt to perhaps better match the secondary loss level. If then the profile loss was decreased with the same amount a more physical division between profile and secondary losses would be possible to find.

- The interaction between secondary and tip leakage flow that both are present in the same region of the blade tips make it difficult to draw any accuracy results from the limited test data. Still it looks like CTC give both to low loss for a specific clearance and also one to weak increase with increasing relative clearance. There is neither any involved coupling to the believed important inlet flow angle or blade load in CTC. Therefore would a future exam of this be interesting where perhaps the correlation from Sjolander (eqn (5-11)) that show up a good prediction accuracy, is physically interesting without being advanced, be interesting.

- No of the simple relations between the loss and e/s ratio as Ainly & Mathieson or Craig & Cox suggested can be confirmed. At the same time was a strong increase seen for Mach number above 0.90, that was many times stronger then the correlation used in CTC today. Therefore could an adjustment to the today used correlation for loss increase at high outlet flow speed be interesting.

- It has been shown that there is a small but clear error in the converting between the pressure and enthalpy loss in MKT eqn (2-32). Even if correction of this can result in a efficiency change of around 0.5 percentage point for the total turbine is this more of a academic interest.

10 Future Work

It should be interesting to investigate the off-design performance on SGT-800 that have a different design philosophy with only a small uncovered turning compare to SGT-700 high uncovered turning value that has primary been investigated in this report.

An investigation of the effect of tip clearance with shrouded blades would also be of huge interest to investigate. If an accurate estimation of the tip clearance can be performed on SGT-800 can this machine be a good and interesting alternative. An internal test made at Siemens for GT35C where the tip clearance was alternated analog to GT35P has also in a late stage be found and can possible be used for future exam of unshrouded loss models.

A wish to examine and give some suggestions on possible parameter in the different loss correlations that could be used to tune in the models against the measured values was desiderated. This can not in an easy way be done in a general scheme due to the different design philosophies between the turbines. But in a future and more intensively work could maybe some proposal be drawn with the new acknowledge about the loss division and limitations gain from this report.

Try to find out which parameter that more exactly control the creation of a supersonic bubble at blade suction surface that is coupled with the sudden loss increase at high outlet Mach number.

11 Reference

1 **O. Söderberg** (1989)
Termiska Strömningsmaskiner
KTH

2 **Ning WEI** (2000)
Significance of Loss Models in Aerothermodynamics Simulation for Axial Turbines
KTH ISBN 91-7170-540-6

3 **J. D. Denton** (1993)
LOSS MACHANISMS IN TURBOMACHINES
CAMBRIDGE 93-GT-435

4 **Introduction to Turbomachinery**
David Japikse & Nicholas C. Baines

5 **Axial and Radial Turbines** (2003)
Hany Moustapha, Mark F. Zelesky, Nicholas C. Baines, David Japikse
ISBN 0-933283-12-0

6 **Cambridge Turbomachinery Aerodynamics course**
2004

7 **D.G. Ainley and G.C.R. Mathieson** (1955)
An examination of the Flow and Pressure Losses in Blade Rows of Axial - Flow Turbines. R. & M. No. 2891

8 **D.G. Ainley and G.C.R. Mathieson** (1957)
An examination of the Flow and Pressure Losses in Blade Rows of Axial - Flow Turbines R. & M. No. 2974

9 **S.L. Dixon, B.Eng., PH.D.** (1998)
Fluid Mechanics, Thermodynamics of Turbomachinery
Senior Fellow at the University of Liverpool
Fourth Edition ISBN 0 7506 7059 2

10 **J. Dunham & P. M Came** (1970)
Improvements to the Ainley-Mathieson Method of Turbine Performance Prediction.
ASME

11 **S. C. Kacker & U Okapuu** (1980)
A Mean Line Prediction Method for Axial Flow Turbine Efficiency.
ASME 81-GT-58

12 **H. R. M Craig & H. J. A. Cox**. (1970)
Performance Estimation Of Axial Flow Turbines.
Instn Mech Engres, Vol 185 32/71, Page 407-424

13 **M. Kh. Mukhatarov & V. I. Krichakin** (1969)
Procedure for estimating flow section losses in axial-flow turbines when calculating their characteristics.
Teploenergetika 1969 vol.16 No7 page 76-79

14 **S. H. Moustapha, S. C Kacker, B. Tremblay** (1990)
An Improved Incidence Losses Prediction Method For Turbine Airfoils.
ASME 89-Gt-284

15 **S. H. Moustapha, S.A Sjolander, M W Benner** (2006)
An Empirical Prediction Method For Secondary Losses In Turbines, Part I and Part II. Journal of Turbomachinery April 2006 vil. 128 p 273-288

16 **S. H. Moustapha, S.A Sjolander, M W Benner** (2004)
MEASUREMENTS OF SECONDARY FLOWS DOWNSTREAM OF A TURBINE CASCADE AT OFF-DESIGN INCIDENCE
ASME Turbo Expo 2004. GT-2004-53786

17 **S. H. Moustapha, S.A Sjolander, M W Benner** (1995)
Influence of leading-edge geometry on profile losses in turbines at off-design incidence: Experimental results and an improved correlation
ASME 95-GT-289

18 **B.Tremblay, A.S.Sjölander & S.H.Moustapha** (1990)
Off-Design Performance of a Linear Cascade of Turbine Blades
90-GT-314

19 **B.I. Mamaev & A. G. Klebanov** (1969)
Optimal pitch for a turbine blade cascade.
Kuibyshev Motor Works, UDC 621.165.533.6

20 **M.W.Benner, A.S.Sjolander & S.H.Moustapha** (1997)
Measurements of secondary flows in a turbine cascade at off-design incidence
97-GT-382

21 **M.W.Benner, A.S.Sjolander & S.H.Moustapha** (2003)
The influence of leading-edge geometry on secondary losses in a turbine cascade at the design incidence
GT2003-38107

22 **T.Zoric, I.Popovic, A.S.Sjolander,T.Praisner & E.Grover** (2007)
Comparative investigation of three highly loaded lp turbine airfoils:
Part 1-Measured profile and secondary losses at design incidence
GT2007-27537

23 **T.Zoric, I.Popovic, A.S.Sjolander,T.Praisner & E.Grover** (2007)
Comparative investigation of three highly loaded lp turbine airfoils:
Part 2-Measured profile and secondary losses at off-design incidence
GT2007-27538

24 **B.I. Mamaev & A. G. Klebanov** (1970)
Profile losses in a turbine cascade
Kuibyshev Motor Works, UDC 621.165.001.5
Teploenergetika 1970 17 (6) 38-42

25 Program **CTC Version 2.0**
ALSTORM Power Uniturbo Moscow 2003
B.Mamaev and E. Ryabov 1102004/TR001

26 **Junqiang Zuh & Steen A Sjolander** (2005)
Improved profile loss and deviation correlations for axial turbine blade rows
ASME GT2005-69077

27 **GT10C, EVALUATED PT EFFICIENCY AND COMBUSTION EFFICIENCY FROM RIGG TEST**
RT GRP 78/04

28 **AERODYNAMIC EVALUATION TEST 6, PT VARIABLE SPEED TESTS GT10C**
RT T10 012/02 2002-08-06
Ver 1.0 (Evaluation 1)
Ver 1.2 (Evaluation 2)

29 **A. F. Carter, M. Platt and F.K. Lenherr**
Analysis of geometry and design point performance of axial flow turbines
NASA CR-1181

30 **Aerothermal Implications of Shroudless and Shrouded Blades** (2004)
Turbine Blade Tip Design and Tip Clearance Treatment
VKI 19-23 January 2004 Lecture Series 2004-02.

31 **An Experimental Investigation of Turbine Case Treatments** (1987)
L.S. Offenberg, J.D. Fischer, T.J. Vander Hoel
Garrett Turbine Engine Company Phoenix Arizona AIAA-87-1919

32 **Takayuki Matsunuma** (2006)
Effect Of Reynolds Number And Freestream Turbulence On Turbine Tip Clearance Flow
Journal Of Turbomachinery Vol.128, January 2006, page 166-177

33 **R. J. Miller** (2004)
Cambridge Turbomachinery Course
21 June 2004

34 **Turbomachinery Aerodynamics** (1996)
Cambridge 17-21 June 1996 Volume One

35 **GT35P Driftsättning av Aktiv Spelkontroll**
05-20-1992

36 **Secondary and Tip-Clearance Flow in Axial Turbines** (1997)
VIK February 10-13 1997
S.A.Sjolander Charlton University, Canada.

37 **S. A. Sjolander and M. I Yaras** (1992)
Prediction of Tip-Leakage Losses in Axial Turbines.
ASME, Journal Of Turbomachinery Vol.114 January 1992, page 204-210

38 **Stephan Conway** (2004)
Implementation and Validation of an Engine Nacelle Boundary Condition in Edge 3.2, chapter 2,
FOI-R 1320 SE September 2004, 1650-1942

39 **Teik Lin Chu** (1999)
Effect of Mach Number and Flow Incidence on Aerodynamic Losses of Steam Turbine Blades
Virginia Polytechnic Institute and Stated University

40 **V.D. Venedictov and S. V. Rudenko** (1998)
A New Highly-Efficient Model for the Profile Losses in the Transonic Cascades of Turbine Blades
Central Institute of Aircraft Engine Building (TsIAM).
Aviamotornaya ul. 2, Moscow, 111250 Russia.
Thermal Engineering Vol 45, No. 2. 1998 pp 145-152.

41 **Compressor Aerodynamics**
N A Cumpsty
ISBN 0-582-01364-X

42 **Development of Postprocessor and Graphic Interface for the 2D NS Program set Within the Framework of Turbine Designing**
ALSTORM Power Uniturbo Moscow WI 01/003

43 **J. Dunham** (1970)
A REVIEW OF CASCADE DATA ON SECONDARY LOSSES IN TURBINES
Journal Mechanical Engineering Science Vol 12 No 1 1970

44 **A.F.Carter, M. Platt and F.K. Lenherr** (1967)
ANALYSIS OF GEOMETRY AND DESIGN POINT PERFORMANCE OF AXIAL FLOW TURBINES
Development of the Analysis Method and the Loss Coefficient Correlation
NASA CR-1181, 1967

45 **Ascher H Shapiro** (1953)
THE DYNAMICS AND THERMODYNAMICS OF COMPRESSIBLE FLUID FLOW
MIT 1953 Card Number 53-8869

46 **C. H. Sieverding** (1985)
Recent Progress in the Understanding of Basic Aspects of Secondary Flows in Turbine Blade Passage
Von Karma Institute for Fluid Dynamics
ASME Vol.107 April 1985 page (248-257)

12 Appendix

12.1 Appendix Chapter 2

Derive of the relationship for convert a loss between one based on pressure and one based on enthalpy. Start with the normal definition of pressure losses, where the subscript ($_0$) stands for total or stagnation states.

$$Y = \frac{p_{01} - p_{02}}{p_{02} - p_2} \tag{12.1-1}$$

And the relation between pressure and temperature for an isentropic expansion is

$$\frac{p_{01}}{p_{02}} = \left(\frac{T_{01}}{T_{02}} \right)^{\frac{\gamma}{\gamma - 1}} \tag{12.1.1}$$

Divide eqn (12-1) with p_{02}

$$Y = \frac{\frac{p_{01}}{p_{02}} - 1}{1 - \frac{p_2}{p_{02}}} \tag{12.1-3}$$

Use the relation between static and total temperatures under the assumption of constant c_p

$$T_{02} = T_2 + \frac{C_2^2}{2 \cdot c_p} \tag{12.1-4}$$

$$T_{01} = T_2 + \frac{C_{2s}^2}{2 \cdot c_p} \tag{12.1-5}$$

The loss (e) is defined as

$$\mathrm{e} \equiv 1 - \phi^2 = 1 - \frac{C_2^2}{C_{2s}^2} \tag{12.1-6}$$

Combining eqn (12.1-4), eqn (12.1-5) and eqn (12.1-6)

$$e = 1 - \frac{2 \cdot c_p \cdot (T_{02} - T_2)}{2 \cdot c_p \cdot (T_{01} - T_2)} = 1 - \frac{(1 - \frac{T_2}{T_{02}})}{(1 - \frac{T_2}{T_{01}})} \cdot \frac{T_{02}}{T_{02s}} \qquad (12.1\text{-}7)$$

Where the use of that $T_{02} = T_{01}$ and eqn (12.1-2) give

$$e = 1 - \frac{1 - \left(\frac{p_2}{p_{02}}\right)^{\frac{\gamma-1}{\gamma}}}{1 - \left(\frac{p_2}{p_{01}}\right)^{\frac{\gamma-1}{\gamma}}} = \frac{1 - \left(\frac{p_2}{p_{01}}\right)^{\frac{\gamma-1}{\gamma}} - 1 + \left(\frac{p_2}{p_{02}}\right)^{\frac{\gamma-1}{\gamma}}}{1 - \left(\frac{p_2}{p_{01}}\right)^{\frac{\gamma-1}{\gamma}}} \qquad (12.1\text{-}8)$$

Expand with

$$\left(\frac{p_{01}}{p_2}\right)^{\frac{\gamma-1}{\gamma}} \Rightarrow$$

$$e = \frac{\left(\frac{p_2}{p_{02}}\right)^{\frac{\gamma-1}{\gamma}} \cdot \left(\frac{p_{02s}}{p_2}\right)^{\frac{\gamma-1}{\gamma}} - \left(\frac{p_2}{p_{01}}\right)^{\frac{\gamma-1}{\gamma}} \cdot \left(\frac{p_{01}}{p_2}\right)^{\frac{\gamma-1}{\gamma}}}{\left(\frac{p_{01}}{p_2}\right)^{\frac{\gamma-1}{\gamma}} - \left(\frac{p_2}{p_{01}}\right)^{\frac{\gamma-1}{\gamma}} \cdot \left(\frac{p_{01}}{p_2}\right)^{\frac{\gamma-1}{\gamma}}} = \frac{\left(\frac{p_{01}}{p_{02}}\right)^{\frac{\gamma-1}{\gamma}} - 1}{\left(\frac{p_{01}}{p_2}\right)^{\frac{\gamma-1}{\gamma}} - 1} =$$

$$= \frac{\left(\frac{p_{01}}{p_{02}}\right)^{\frac{\gamma-1}{\gamma}} - 1}{\left(\frac{p_{01}}{p_{02}}\right)^{\frac{\gamma-1}{\gamma}} \cdot \left(\frac{p_{02}}{p_2}\right)^{\frac{\gamma-1}{\gamma}} - 1} \qquad (12.1\text{-}9)$$

From eqn (12.1-3)

$$\frac{p_{01}}{p_{02}} = Y \cdot \left[1 - \frac{p_2}{p_{02}}\right] + 1 \qquad (12.1\text{-}10)$$

Insert eqn (12.1-10) in eqn (12.1-9)

$$e = \frac{\left(Y \cdot \left[1 - \frac{p_2}{p_{02}}\right] + 1\right)^{\frac{\gamma-1}{\gamma}} - 1}{\left(Y \cdot \left[1 - \frac{p_2}{p_{02}}\right] + 1\right)^{\frac{\gamma-1}{\gamma}} \cdot \left(\frac{p_{02}}{p_2}\right)^{\frac{\gamma-1}{\gamma}} - 1} \qquad \text{(12.1-11)= (2-35)}$$

To derive a expression that express the pressure loss (Y) in an explicit form introduce the temporary variable A and B and insert they into eqn (12.1-11).

$$A = 1 - \frac{p_2}{p_{02}} \qquad \text{(12.1-12)}$$

$$B = \left(\frac{p_{02}}{p_2}\right)^{\frac{\gamma-1}{\gamma}} \qquad \text{(12.1-13)}$$

$$e = \frac{\left(1 + Y \cdot A\right)^{\frac{\gamma-1}{\gamma}} - 1}{\left(B \cdot \left(1 + Y \cdot A\right)^{\frac{\gamma-1}{\gamma}} - 1\right)} \Rightarrow \qquad \text{(12.1-14)}$$

$$e \cdot B \cdot \left(1 + Y \cdot A\right)^{\frac{\gamma-1}{\gamma}} - e = \left(1 + Y \cdot A\right)^{\frac{\gamma-1}{\gamma}} - 1 \Rightarrow$$

$$\left(1 + Y \cdot A\right)^{\frac{\gamma-1}{\gamma}} - e \cdot B \cdot \left(1 + Y \cdot A\right)^{\frac{\gamma-1}{\gamma}} = 1 - e \Rightarrow$$

$$\left(1 + Y \cdot A\right)^{\frac{\gamma-1}{\gamma}} \cdot (1 - e \cdot B) = 1 - e \Rightarrow$$

$$\left(1 + Y \cdot A\right)^{\frac{\gamma-1}{\gamma}} = \frac{1-e}{1-e \cdot B} \Rightarrow \cdot$$

$$Y = \frac{\left(\frac{1-e}{1-e \cdot B}\right)^{\frac{\gamma}{\gamma-1}} - 1}{A} = \frac{\left(\frac{1-e \cdot B}{1-e}\right)^{-\left(\frac{\gamma}{\gamma-1}\right)} - 1}{A} = \frac{\left(\frac{1}{1-e} - \frac{e \cdot B}{1-e}\right)^{-\left(\frac{\gamma}{\gamma-1}\right)} - 1}{A} \Rightarrow$$

$$Y = \frac{\left(\frac{1}{1-e} - \frac{e}{1-e} \cdot \left(\frac{p_{02}}{p_2} \right)^{\frac{\gamma-1}{\gamma}} \right)^{-\left(\frac{\gamma}{\gamma-1}\right)} - 1}{1 - \frac{p_2}{p_{02}}} \qquad (12.1\text{-}15)$$

Or

$$Y = \frac{\left[\frac{1}{1-e} \cdot \left(1 - e \cdot \left(\frac{p_{02}}{p_2} \right)^{\frac{\gamma-1}{\gamma}} \right) \right]^{-\left(\frac{\gamma}{\gamma-1}\right)} - 1}{1 - \frac{p_2}{p_{02}}} \qquad (12.1\text{-}16)$$

Where the pressure ratio can be expressed as

$$\frac{p_{02}}{p_2} = \left[1 + \frac{\gamma-1}{2} \cdot M_{out}^2 \right]^{\frac{\gamma}{\gamma-1}} \qquad (12.1\text{-}17) = (2\text{-}36)$$

This give the pressure loss term explicate expressed in enthalpy loss as

$$Y = \frac{\left[\frac{1}{1-e} \cdot \left(1 - e \cdot \left[1 + \frac{\gamma-1}{2} \cdot M_{out}^2 \right] \right) \right]^{-\left(\frac{\gamma}{\gamma-1}\right)} - 1}{1 - \left[1 + \frac{\gamma-1}{2} \cdot M_{out}^2 \right]^{-\left(\frac{\gamma}{\gamma-1}\right)}} \qquad (12.1\text{-}18)=(2\text{-}37)$$

In this derivation it is still assumed that the density does not vary between the isentropic and real expansion paths final state ($\rho_{2s} = \rho_2$) If take care to this variation the following equations are valid.

Start to define the new loss (e'') as

$$e'' = 1 - \phi''^2 = 1 - \frac{\rho_2 \cdot C_2^2}{\rho_{2s} \cdot C_{2s}^2} = 1 - \frac{C_2^2}{C_{2s}^2} \cdot \left(\frac{p_{02}}{p_{01}} \right)^{\frac{\gamma-1}{\gamma}} \qquad (12.1\text{-}19)$$

Where the ratio between the density can be expressed as

$$\rho = \frac{\mathrm{p}}{\mathrm{RT}} \Rightarrow \frac{\rho_2}{\rho_{2s}} = \frac{\frac{\mathrm{p}_2}{\mathrm{RT}_2}}{\frac{\mathrm{p}_{2s}}{\mathrm{RT}_{2s}}} = \frac{\mathrm{T}_{2s}}{\mathrm{T}_2} = \left(\frac{p_{02}}{p_{01}}\right)^{\frac{\gamma-1}{\gamma}} \tag{12.1-20}$$

$$\mathrm{e''} = 1 - (1-e)\cdot\left(\frac{p_{02}}{p_{01}}\right)^{\frac{\gamma-1}{\gamma}} \tag{12.1-21}$$

Insert eqn (12.1-10) and the temporary variable A, B and C

$$\frac{p_{01}}{p_{02}} = A$$

$$\frac{\gamma-1}{\gamma} = B$$

$$\frac{p_{02}}{p_2} = C$$

Eqn (12.1-9) is then

$$e = \frac{A^B - 1}{A^B \cdot C^B - 1} \Rightarrow A^B \cdot C^B \cdot e - e = A^B - 1 \Rightarrow$$

$$A^B = \frac{e-1}{C^B \cdot e - 1} \Rightarrow$$

Replace the constants A, B and C

$$\frac{p_{02}}{p_{01}} = \left[\frac{\left(\frac{p_{02}}{p_2}\right)^{\frac{\gamma-1}{\gamma}} \cdot e - 1}{e-1}\right]^{\frac{\gamma}{\gamma-1}} \tag{12.1-22}$$

Eqn (12.1-22) in eqn (12.1-21) give

$$e'' = 1-(1-e)\cdot\left(\left[\frac{\left(\frac{p_{02}}{p_2}\right)^{\frac{\gamma-1}{\gamma}}\cdot e-1}{e-1}\right]^{\frac{\gamma}{\gamma-1}}\right)^{\frac{\gamma-1}{\gamma}} = 1-(1-e)\cdot\left[\frac{\left(\frac{p_{02}}{p_2}\right)^{\frac{\gamma-1}{\gamma}}\cdot e-1}{e-1}\right] = 1+\frac{(e-1)}{(e-1)}\cdot\left(\left(\frac{p_{02}}{p_2}\right)^{\frac{\gamma-1}{\gamma}}\cdot e-1\right) =$$

$$= \left(\frac{p_{02}}{p_2}\right)^{\frac{\gamma-1}{\gamma}}\cdot e = e'' \qquad (12.1\text{-}23)$$

$$= (2\text{-}39)$$

Where $\left(\frac{p_{02}}{p_2}\right)^{\frac{\gamma-1}{\gamma}}$ can be replaced by an expression in outlet Mach number (M_{out}) with eqn (12.1-17) or eqn (2-36) as

$$\left(\frac{p_{02}}{p_2}\right)^{\frac{\gamma-1}{\gamma}} = \left[1+\frac{\gamma-1}{2}\cdot M_{out}^2\right]$$

Eqn (12.1-23) or (2-39) give the compressible convention term that should be used to take care to the compressible effects when it replace the loss term (e) term in eqn (12.1-18) or (2-37).

An alternative way to derive the relation is seen below, but the final expression is the same as MKT and Lehman's uncorrected model. This alternative equation can also be corrected for the second order of compressibility with eqn (12.1-23) or (2-39).

Start with the same expression for a pressure loss (Y) eqn (12.1-1)

$$Y = \frac{p_{01} - p_{02}}{p_{02} - p_2}$$

Divide now instead with p_2

$$Y = \frac{\frac{p_{01}}{p_2} - \frac{p_{02}}{p_2}}{\frac{p_{02}}{p_2} - 1}$$

With the relation from eqn (12.1-17) or eqn (2-36) applied between the different states

$$Y = \frac{\left[1+\frac{\gamma-1}{2}\cdot M_{out,s}^2\right]^{\frac{\gamma}{\gamma-1}} - \left[1+\frac{\gamma-1}{2}\cdot M_{out}^2\right]^{\frac{\gamma}{\gamma-1}}}{\left[1+\frac{\gamma-1}{2}\cdot M_{out}^2\right]^{\frac{\gamma}{\gamma-1}} - 1} \tag{12.1-24}$$

Some thermodynamic relations, eqn (12.1-4) and eqn (12.1-5) combined together give

$$\left.\begin{array}{l} c_p - c_v = R \\ \gamma = \dfrac{c_p}{c_v} \end{array}\right\} \Rightarrow c_p = \frac{\gamma\cdot R}{\gamma-1} \tag{12.1-25}$$

$$C_2^2 = 2\cdot c_p\cdot(T_{02}-T_2) = \frac{2\cdot\gamma\cdot R}{\gamma-1}\cdot(T_{02}-T_2) = \frac{2\cdot\gamma\cdot R}{\gamma-1}\cdot T_2\cdot(\frac{T_{02}}{T_2}-1) \tag{12.1-26}$$

$$C_{2s}^2 = 2\cdot c_p\cdot(T_{02}-T_{2s}) = \frac{2\cdot\gamma\cdot R}{\gamma-1}\cdot(T_{02}-T_{2s}) = \frac{2\cdot\gamma\cdot R}{\gamma-1}\cdot T_{2s}\cdot(\frac{T_{02}}{T_{2s}}-1) \tag{12.1-27}$$

Now can ϕ^2 be expressed as

$$\phi^2 = \frac{C_2^2}{C_{2s}^2} = \frac{T_2}{T_{2s}}\cdot\frac{(\frac{T_{02}}{T_2}-1)}{(\frac{T_{02}}{T_{2s}}-1)} = \frac{T_2}{T_{2s}}\cdot\frac{(\left[1+\frac{\gamma-1}{2}\cdot M_{out}^2\right]-1)}{(\left[1+\frac{\gamma-1}{2}\cdot M_{out,s}^2\right]-1)} \tag{12.1-28}$$

Because the expansion between T_2 and T_{2s} is not isentropic the isentropic relations can not be used. Instead a relation is derived with the normal isentropic relations according to

$$p_{2s} = p_2$$
$$T_{01} = T_{02}$$

$$\frac{T_{02}}{T_{2s}} = \left(\frac{p_{01}}{p_{2s}}\right)^{\frac{\gamma-1}{\gamma}} = \left(\frac{p_{01}}{p_2}\right)^{\frac{\gamma-1}{\gamma}} \tag{12.1-29}$$

$$\frac{T_{02}}{T_2} = \left(\frac{p_{02}}{p_2}\right)^{\frac{\gamma-1}{\gamma}} \Rightarrow T_{02} = T_2\cdot\left(\frac{p_{02}}{p_2}\right)^{\frac{\gamma-1}{\gamma}} \tag{12.1-30}$$

Insert eqn (12.1-30) in eqn (12.1-29)

$$\frac{T_2}{T_{2s}}\cdot\left(\frac{p_{02}}{p_2}\right)^{\frac{\gamma-1}{\gamma}}=\left(\frac{p_{01}}{p_2}\right)^{\frac{\gamma-1}{\gamma}}\Rightarrow\frac{T_2}{T_{2s}}=\left(\frac{p_{01}}{p_2}\right)^{\frac{\gamma-1}{\gamma}}\cdot\left(\frac{p_{02}}{p_2}\right)^{-\left(\frac{\gamma-1}{\gamma}\right)}=\left(\frac{p_{01}}{p_2}\right)^{\frac{\gamma-1}{\gamma}}\cdot\left(\frac{p_2}{p_{02}}\right)^{\frac{\gamma-1}{\gamma}}=\left(\frac{p_{02}}{p_{01}}\right)^{-\left(\frac{\gamma-1}{\gamma}\right)}$$

$$\frac{T_2}{T_{2s}}=\left(\frac{p_{02}}{p_{01}}\right)^{-\left(\frac{\gamma-1}{\gamma}\right)} \qquad (12.1\text{-}31)$$

With eqn (12.1-31) inserted into eqn (12.1-28) the isentropic Mach number can be expressed that then is inserted into eqn (12.1-24)

$$M_{out,s}^2=\frac{M_{out}^2}{\phi^2}\cdot\left(\frac{p_{02}}{p_{01}}\right)^{-\left(\frac{\gamma-1}{\gamma}\right)}$$

$$Y=\frac{\left[1+\frac{\gamma-1}{2}\cdot\frac{M_{out}^2}{\phi^2}\cdot\left(\frac{p_{02}}{p_{01}}\right)^{-\left(\frac{\gamma-1}{\gamma}\right)}\right]^{\frac{\gamma}{\gamma-1}}-\left[1+\frac{\gamma-1}{2}\cdot M_{out}^2\right]^{\frac{\gamma}{\gamma-1}}}{\left[1+\frac{\gamma-1}{2}\cdot M_{out}^2\right]^{\frac{\gamma}{\gamma-1}}-1} \qquad (12.1\text{-}32)$$

Where $\frac{p_{02}}{p_{01}}$ are expressed with eqn (12.1-22) and eqn (12.1-17) or (2-36)

12.2 Appendix Chapter 3

12.2.1 D.G. Ainley & G. C. R. Mathieson

In the Figure in this chapter 12.2.1 of appendix the notations in the chart are
β = blade angle, and equal to α' in the report.
$\alpha_1 = \alpha_1$ or β_2 and written as α_{in} in the report
$\alpha_2 = \alpha_2$ or β_3 and written as α_{out} in the report

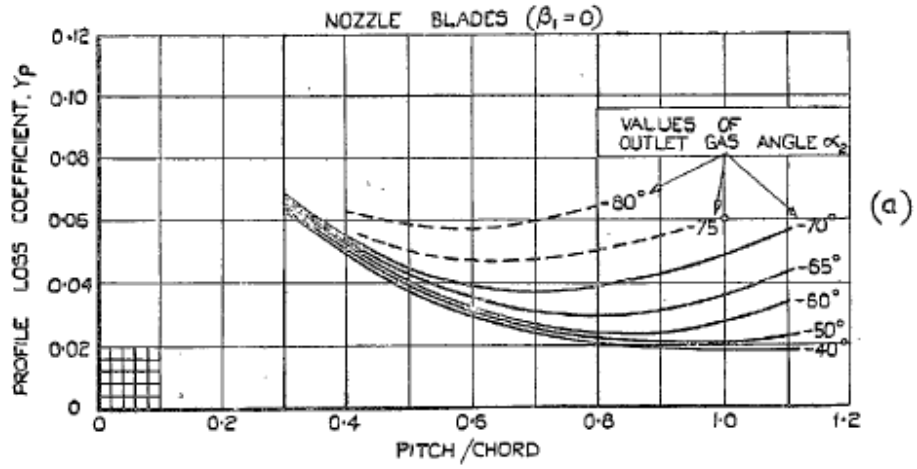

Figure 12.2-1: Profile loss (Yp) for a reaction blade. i=0, t/c=0.2, Re= $2 \cdot 10^5$ **$M_{out} \leq$ 0.6. [7]**

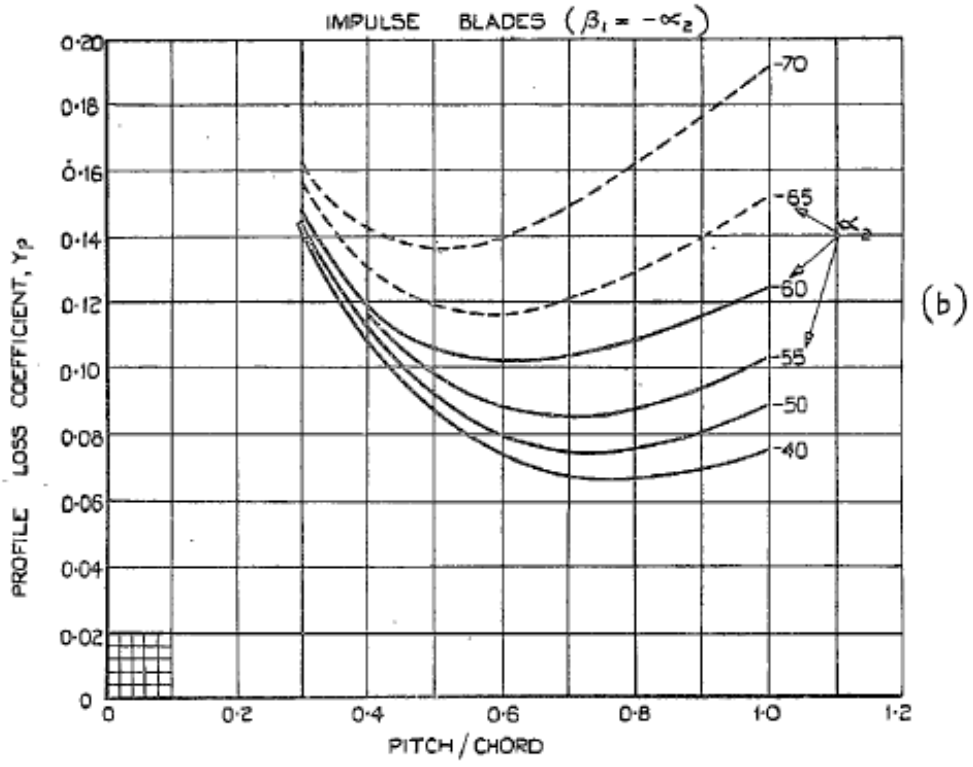

Figure 12.2-2: Profile loss (Yp) for impulse blade. i=0, t/c=0.2, Re= $2 \cdot 10^5$ **, $M_{out} \leq$ 0.6. [7]**

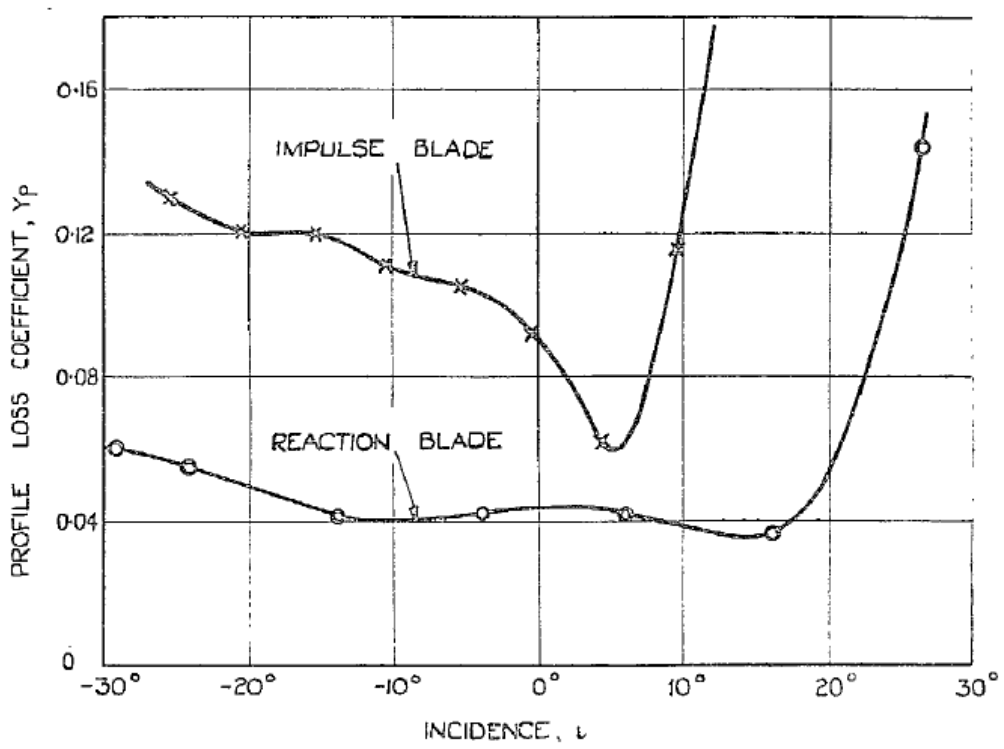

Figure 12.2-3: Variation in profile loss coefficient (Y_p) with incidence for an impulse or reaction blade. It shows a narrow range of low loss for the impulse blade for i around +5 deg, and a not so strong effect of negative incidence for reaction blade, [7].

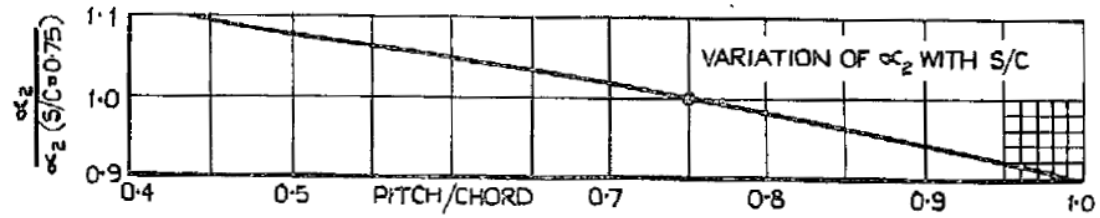

Figure 12.2-4: The ratio between the actually outlet flow angle and outlet flow angle at s/c=0.75 as a function of pitch/chord (s/c), [7].

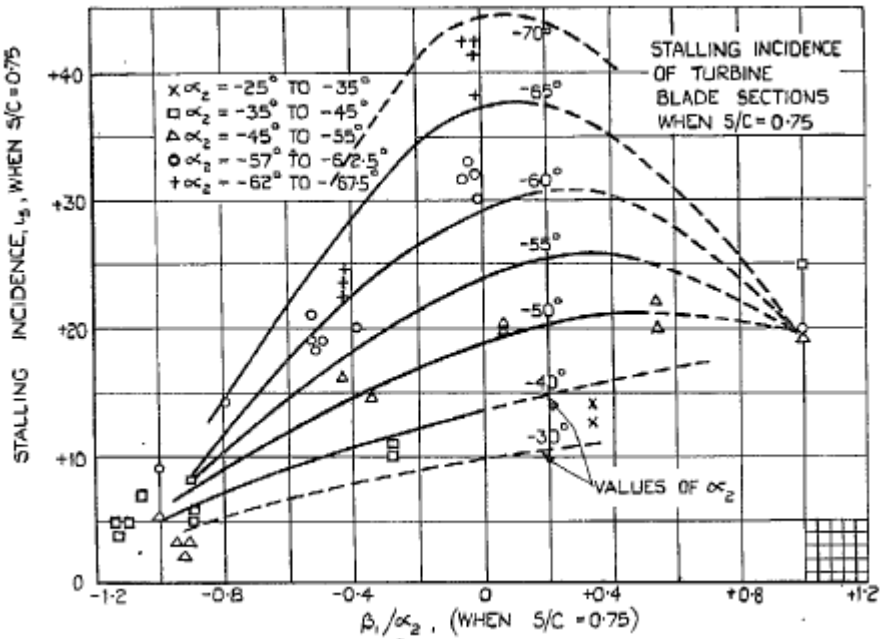

Figure 12.2-5: Variation of stalling incidence $i_{s(s/c=0.75)}$ with the ratio between blade inlet angle to outlet flow angle $\alpha'_{in} / \alpha_{out,(s/c=0.75)}$ and actually outlet flow angle α_{out}, [7].

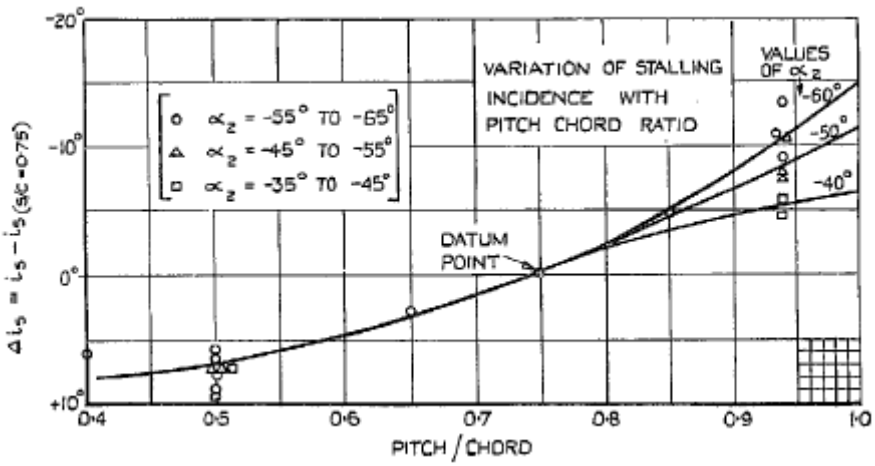

Figure 12.2-6: variation of Δi_s with s/c and outlet flow angle α_{out}, [7].

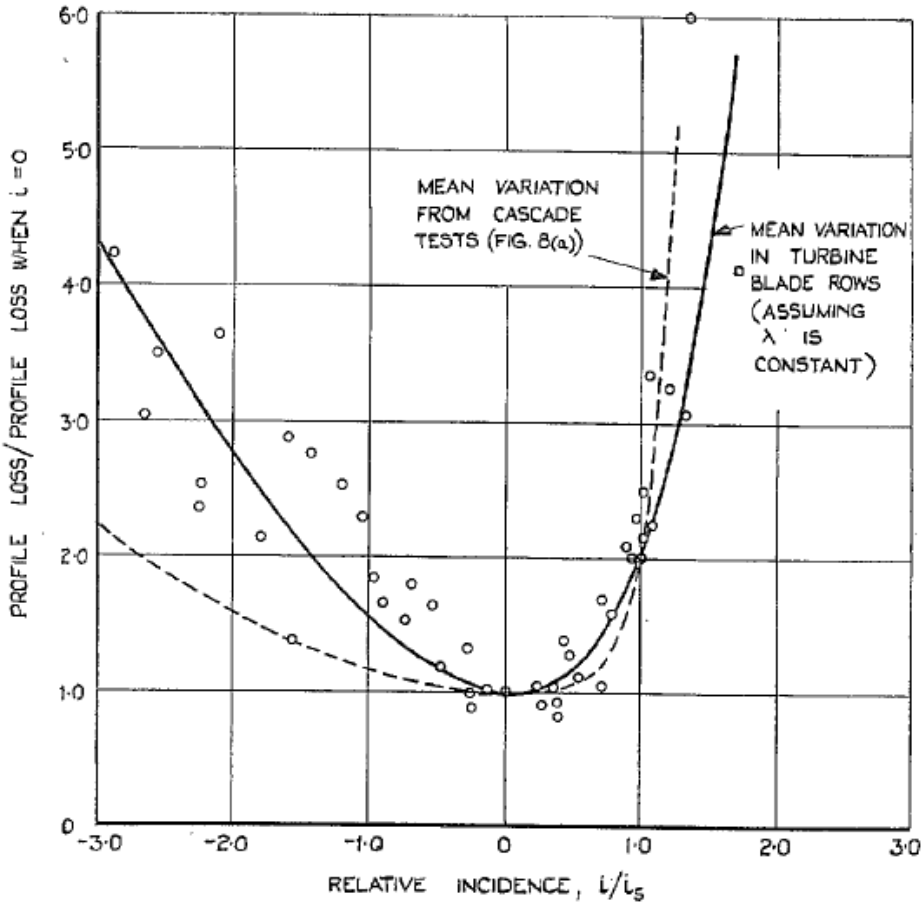

Figure 12.2-7: The correction to the profile loss (Y_p) because of incidence for both corrected turbine row measurements (thick line), and uncorrected measurement of cascade (dotted line). The recommendation is to use the corrected line that is valid down to i/i_s of -2.0, [7].

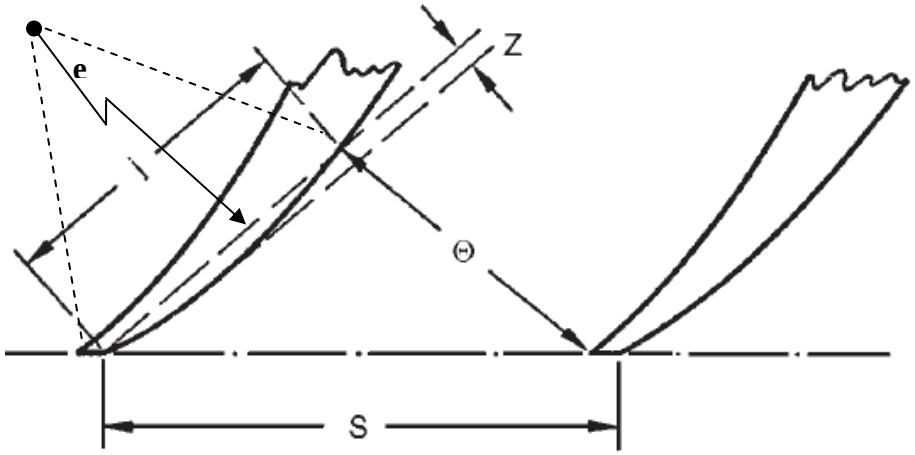

Figure 12.2-8: Illustrate the mean radius of curvature (e) between the throat and trailing edge, [8].

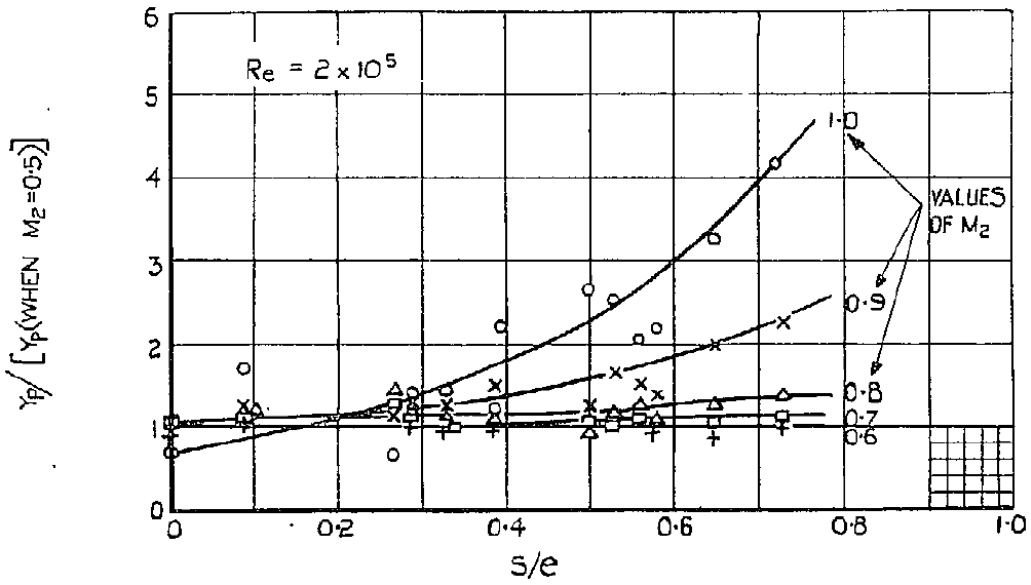

Figure 12.2-9: The outlet Mach number (M_{out}) effect on the profile losses for varying s/e supposed by AM fig 12a in [7].

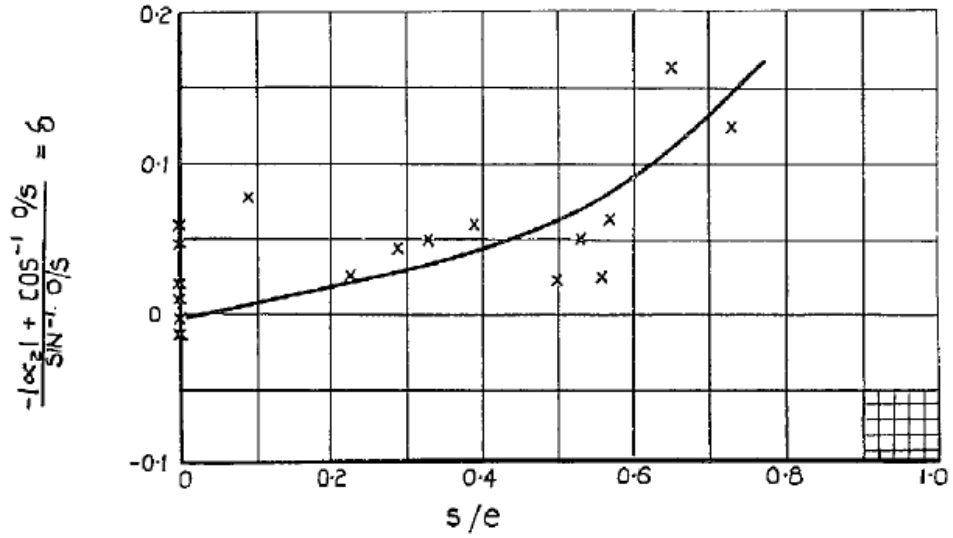

Figure 12.2-10: Correction of the outlet flow angle for the high losses that occurs at Mach number close to unit as a function of s/e. [7]

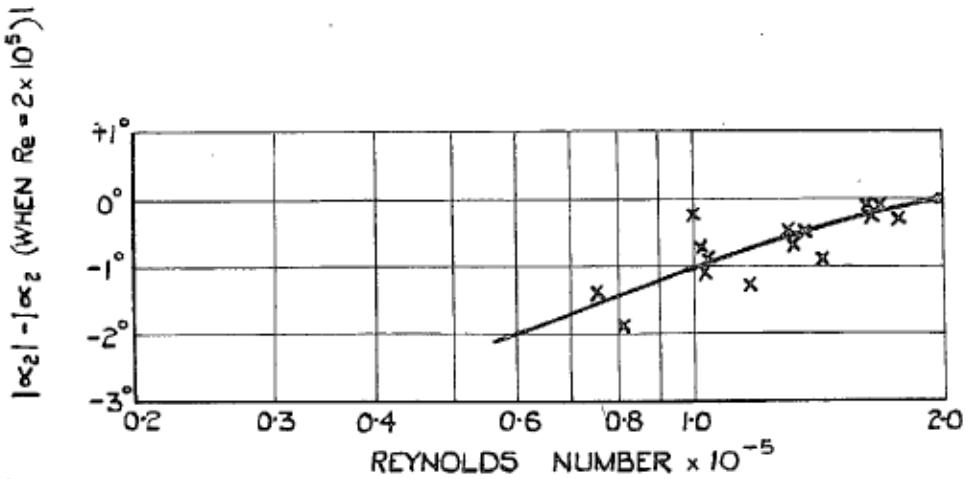

Figure 12.2-11: Shows the correction of the outlet flow angle ($\alpha_{out} - \alpha_{out,(\mathrm{Re}=2\cdot 10^5)}$) because of Re relation between, [7].

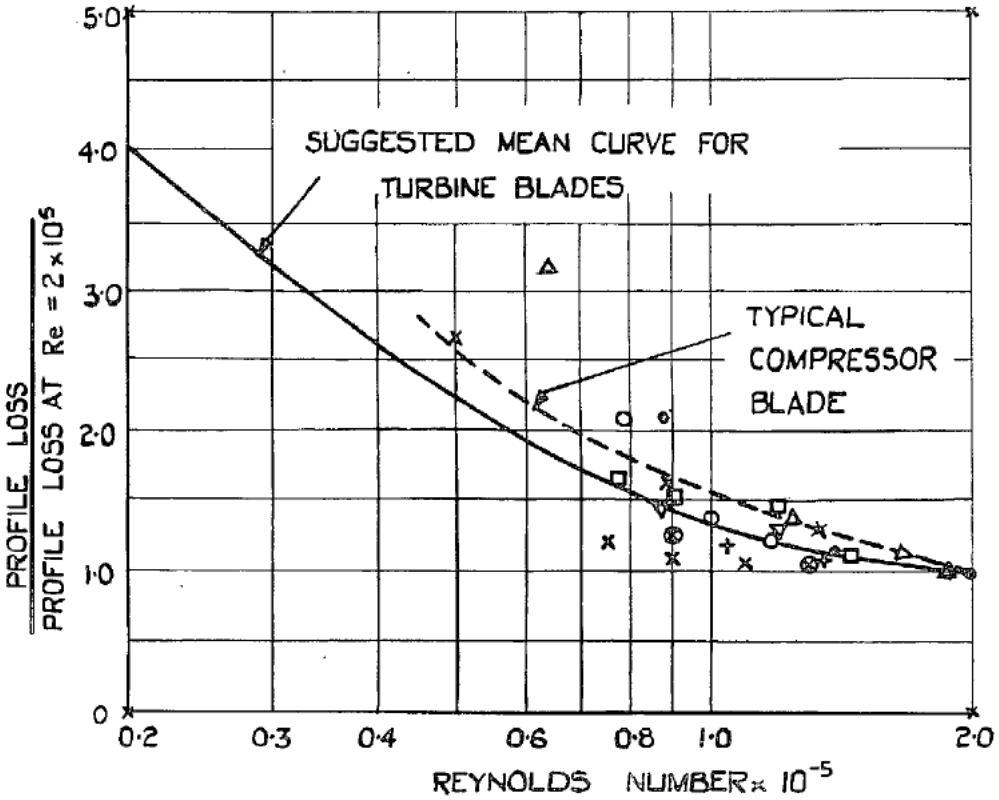

Figure 12.2-12: The relative profile loss as a function of Re in the range $5\cdot 10^4 \le \mathrm{Re} \le 2\cdot 10^5$**.**

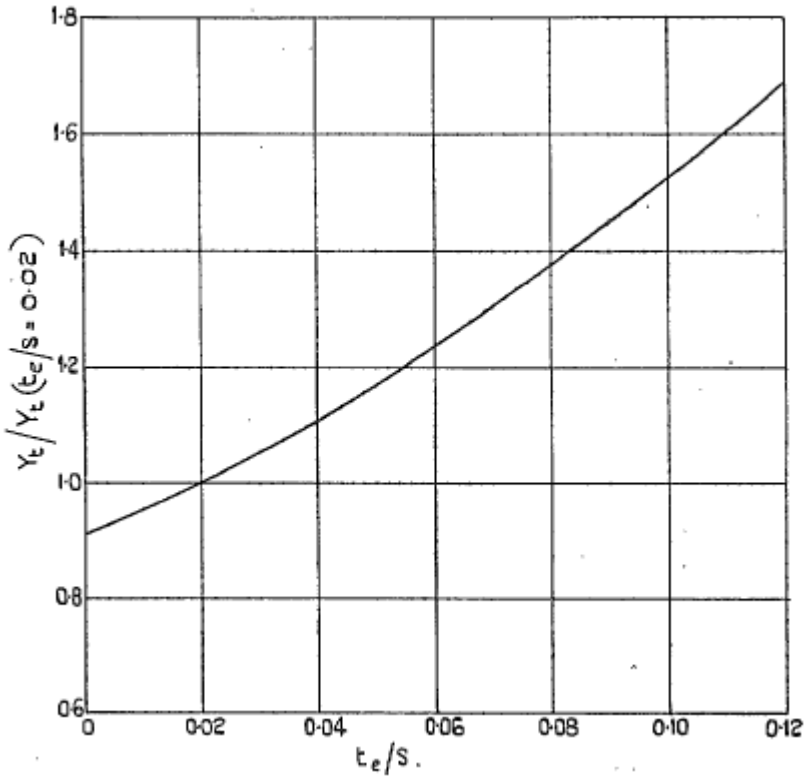

Figure 12.2-13: The relative change in total blade loss because of trailing edge thickness as a function of t_{TE}/s. The datum point is as t_{TE}/s=0.02, [8].

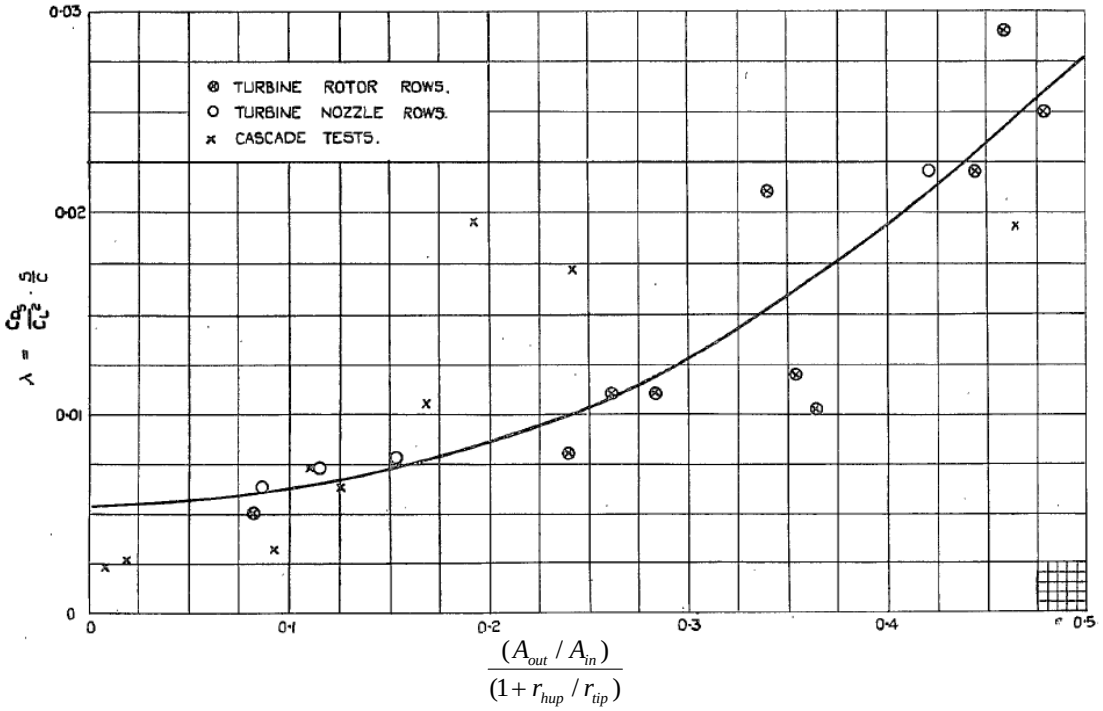

Figure 12.2-14: Secondary loss for stator and rotor as function of the blade area ratio between the outlet and inlet. It is valid for an annular wall boundary layer thickness of 10-15 percent of the total blade height.

12.2.2 S. C. Kacker & U. Okapuu

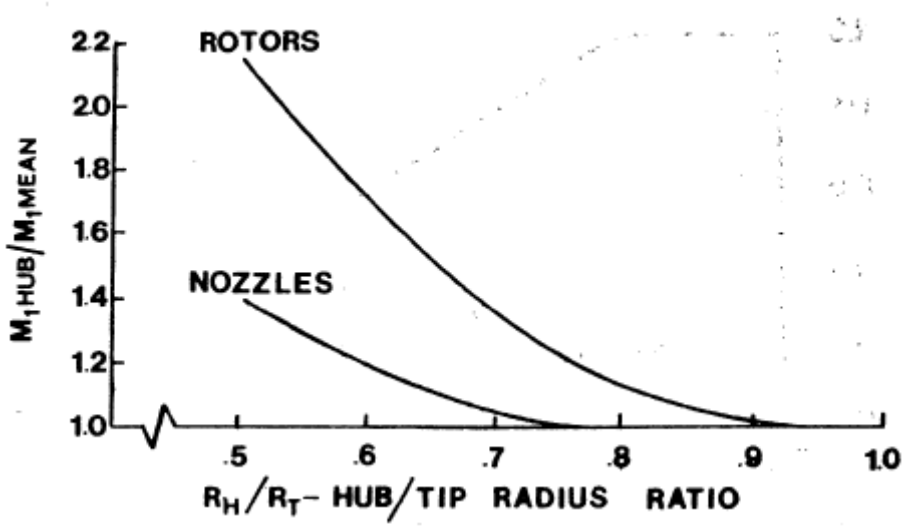

Figure 12.2-15: The ratio between the hub Mach number and that present at the mean radius. The difference is a result of the need to fulfill the radial equilibrium force balance. This chart is originally from KO in [11] and a difference between a nozzle and rotor is seen.

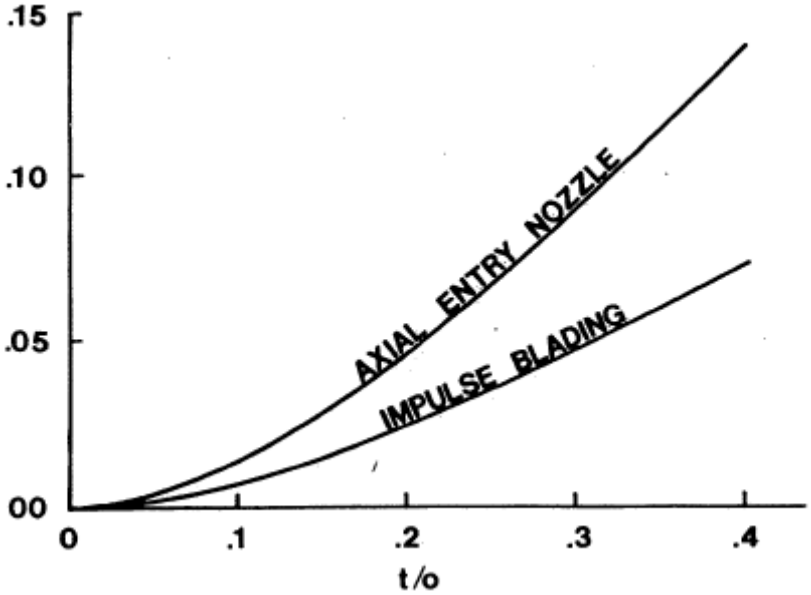

Figure 12.2-16: The loss due to the trailing edge in terms of kinetic energy loss for an impulse blade and reaction (axial entry) blade. For blade shape between these to extremes interpolation should be used according to eqn (3-27). At the x-axis is the ratio of trailing edge thickness to throat, and at the y-axis is change in the kinetic energy loss, $\Delta\phi_{TE}$, [11].

12.2.3 H. R. M Craig & H. J. A. Cox

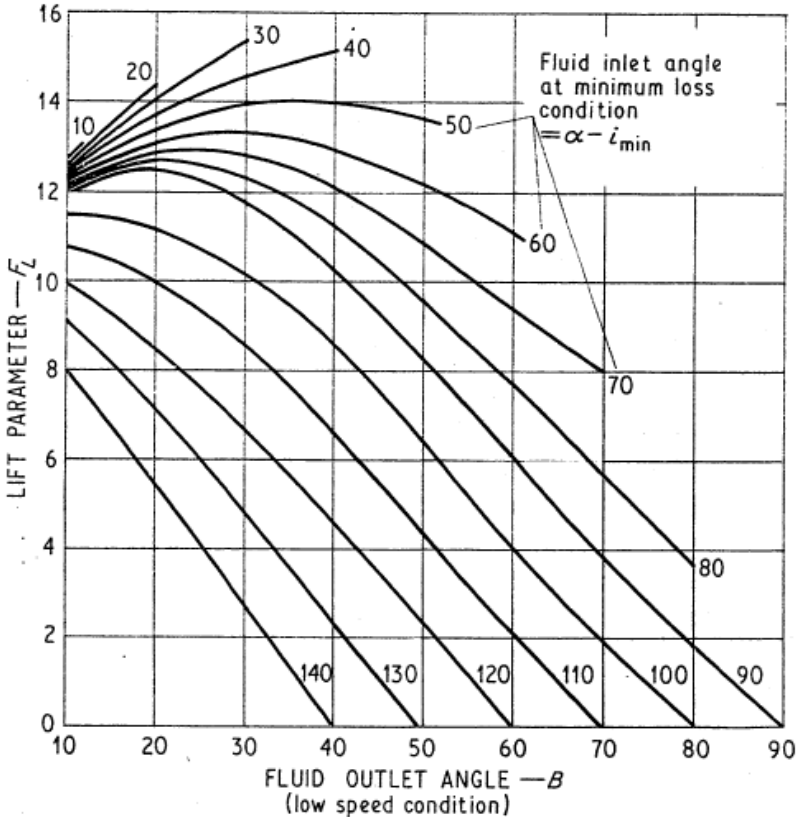

Figure 12.2-17: Craig & Cox lift parameter, F_L as a function of that inlet flow angle corresponding to the minimum profile loss and the real outlet flow angle, [12].

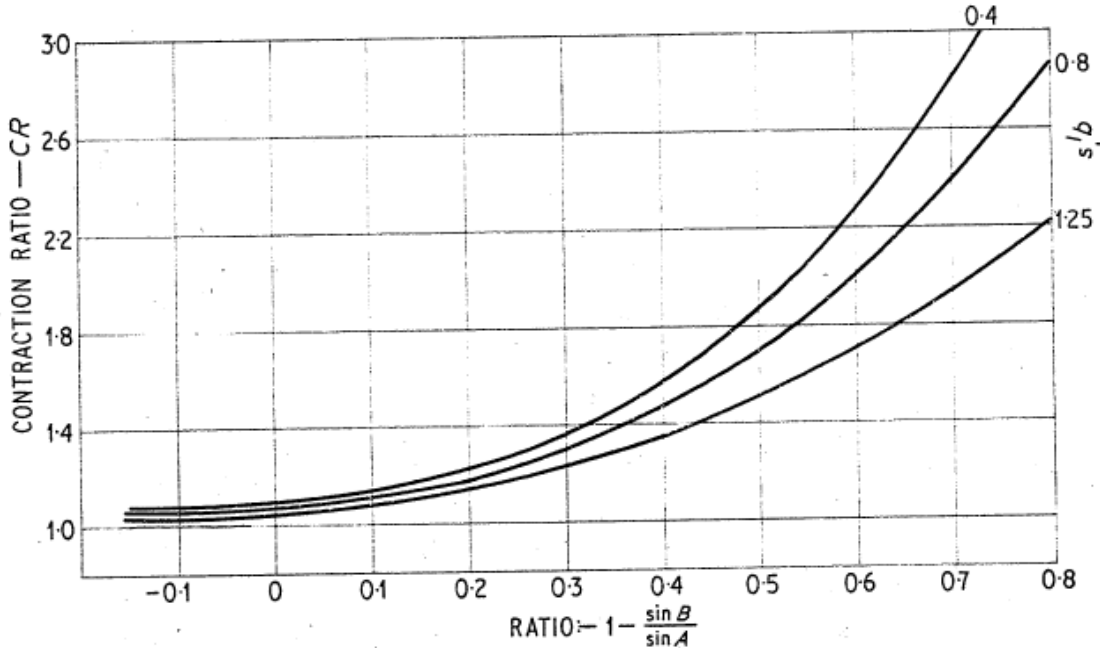

Figure 12.2-18: Contraction ratio (CR) as a function of s/b_c, inlet and outlet flow angles. This char should be used in early design step of a turbine row when the blade geometry is not fully decided, [12].

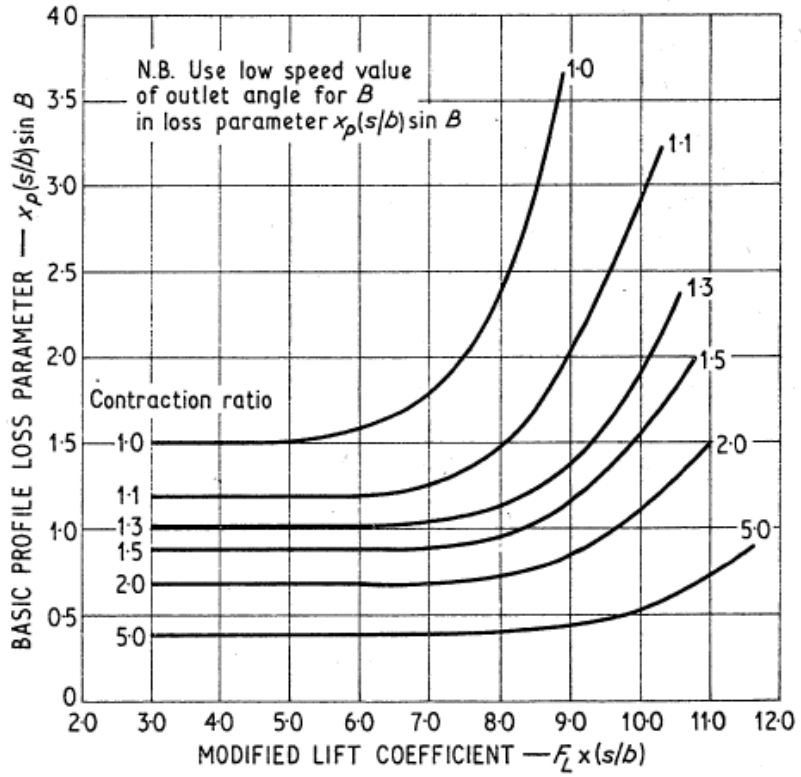

Figure 12.2-19: Base profile loss Y_{P0} for the lift coefficient (F_L) and pitch to centerline camber length ratio (s/b_c) where b_c is represented by b in the Figure, [12].

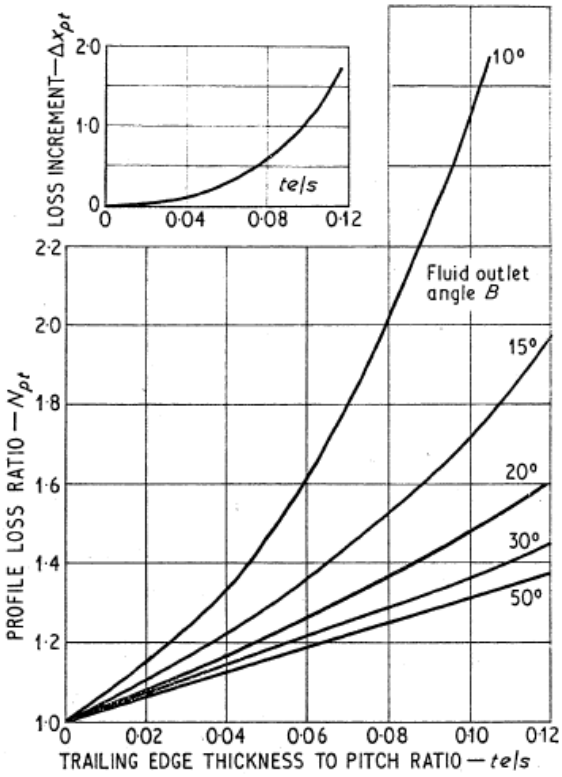

Figure 12.2-20: Both an extra profile loss add and a bas profile loss multiplier due to the trailing edge thickness, [12].

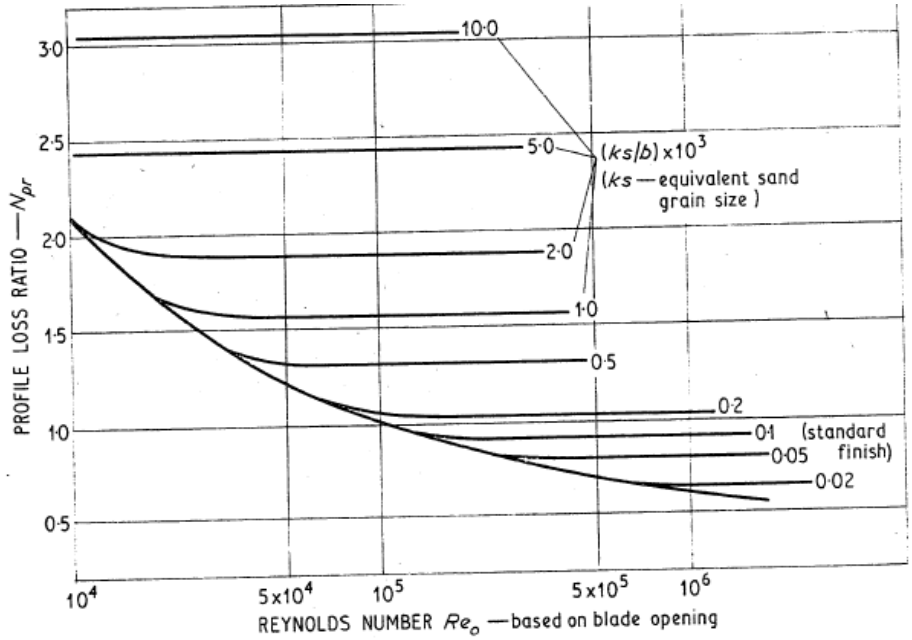

Figure 12.2-21: Multiplier to the profile loss due to Reynolds number, [12].

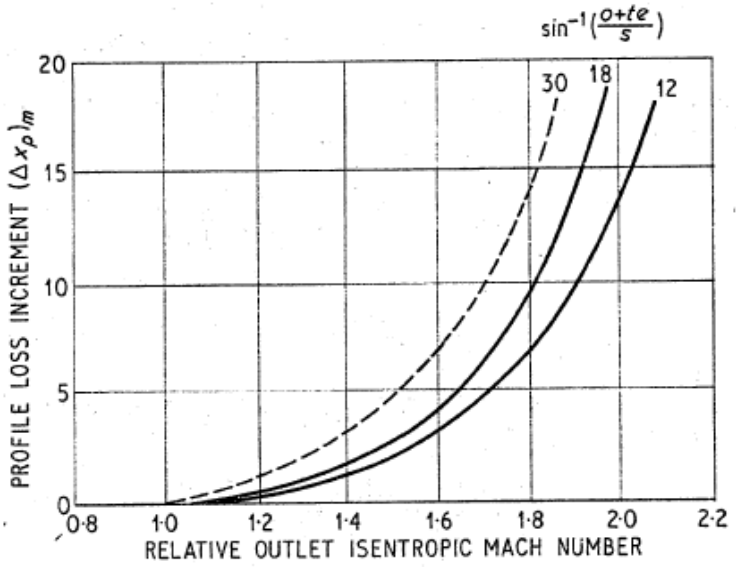

Figure 12.2-22: Extra profile loss if the outlet Mach number exceed unit. [12]

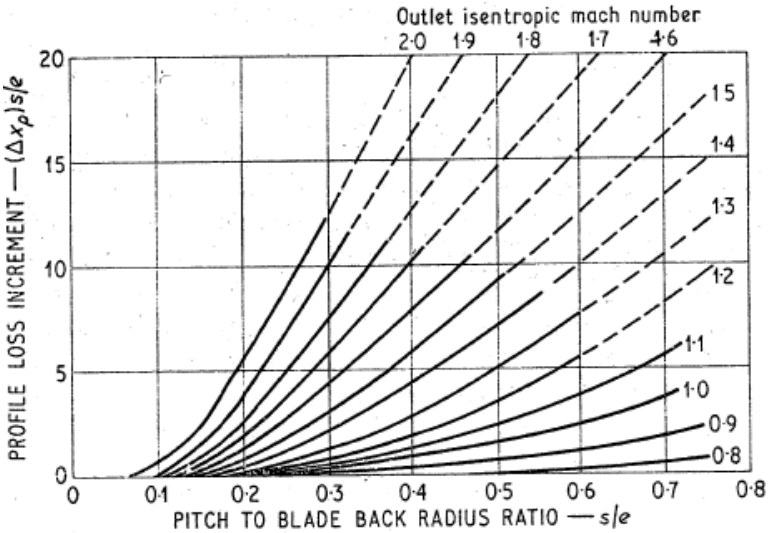

Figure 12.2-23: Add to overall profile loss due to the mean curvature (e) after the throat, [12].

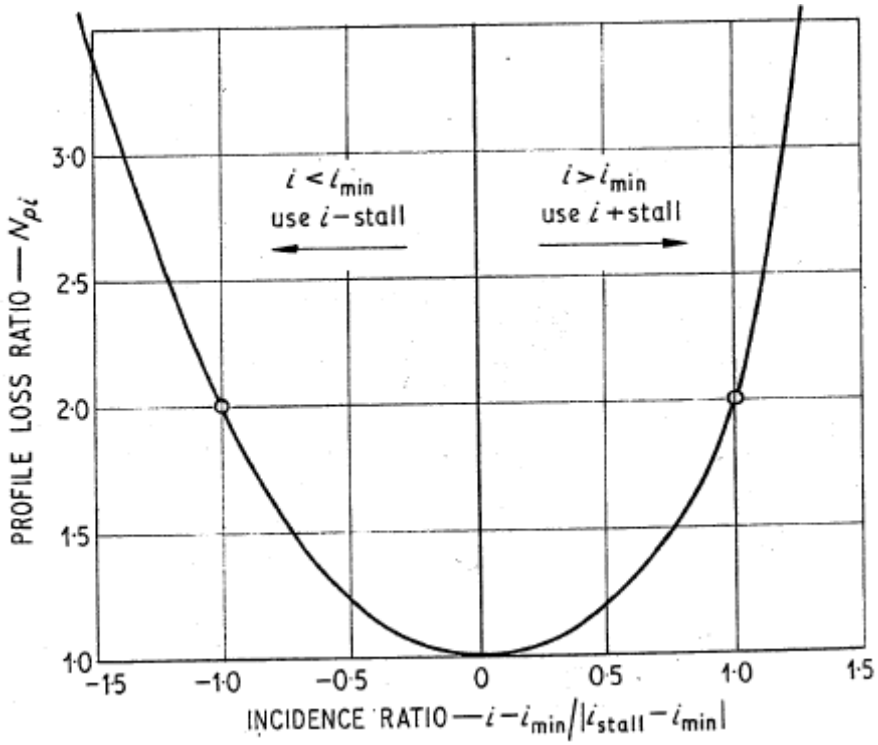

Figure 12.2-24: Profile loss multiplier due to incidence, [12].

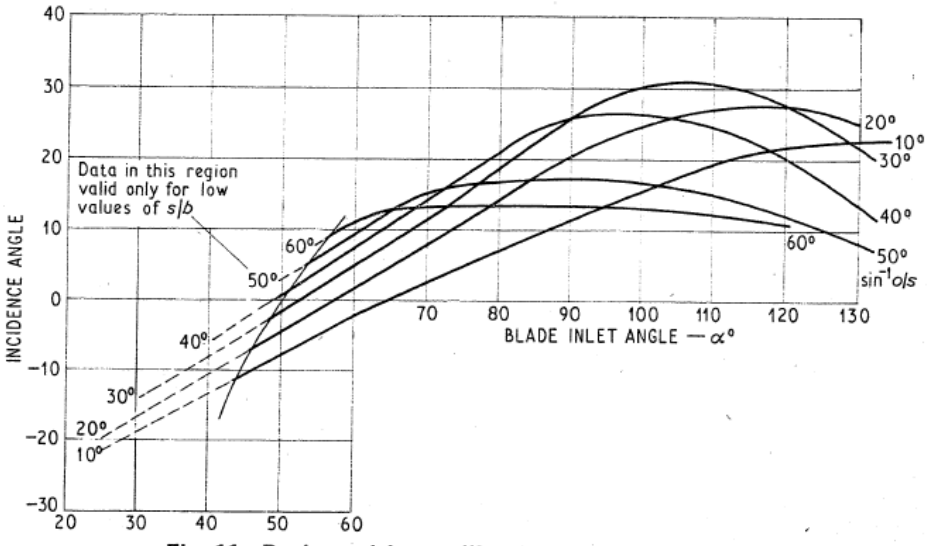

Figure 12.2-25: Basic positive stalling incidence ($(i + stall)_{basic}$), [12].

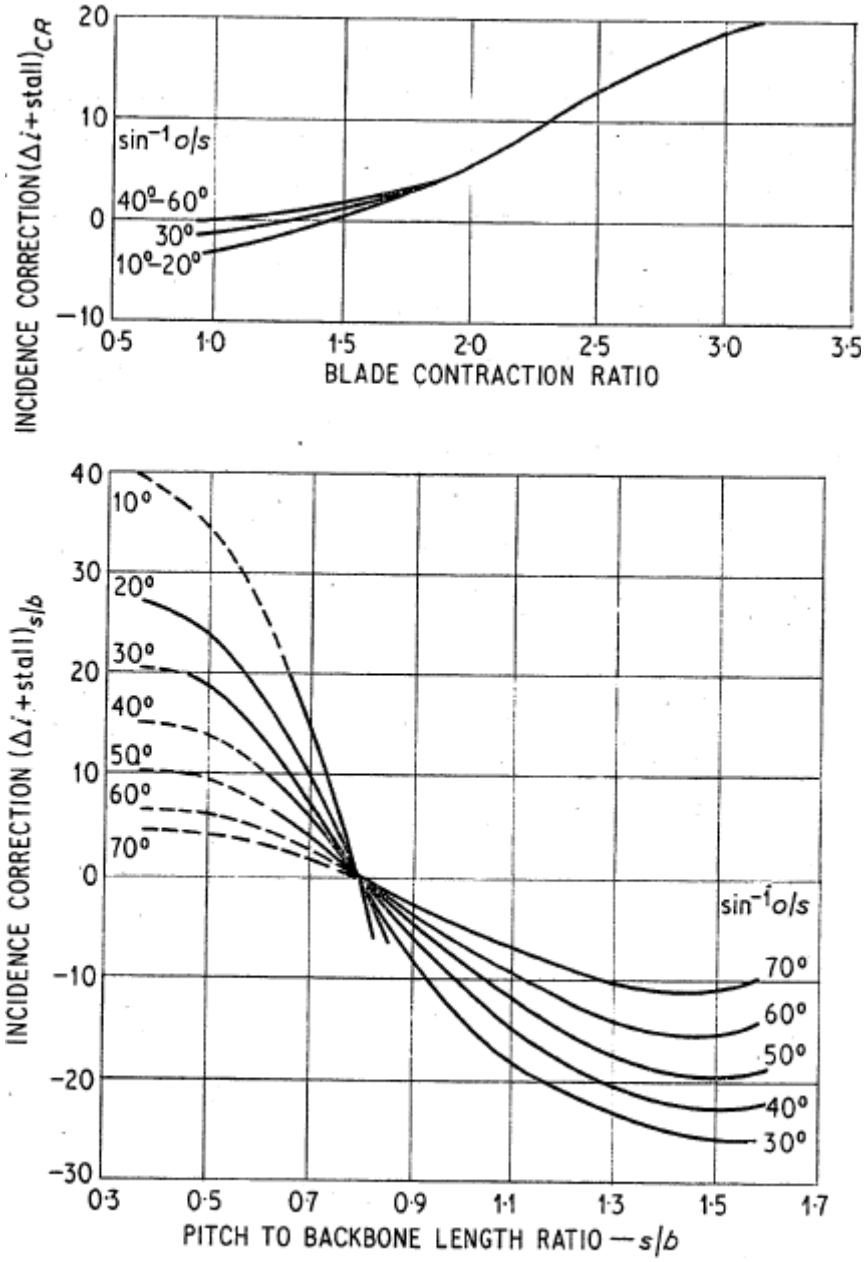

Figure 12.2-26: Correction of stalling angle because of contraction ratio and centerline camber length b_c. b_c is represented by b in the Figure, [12].

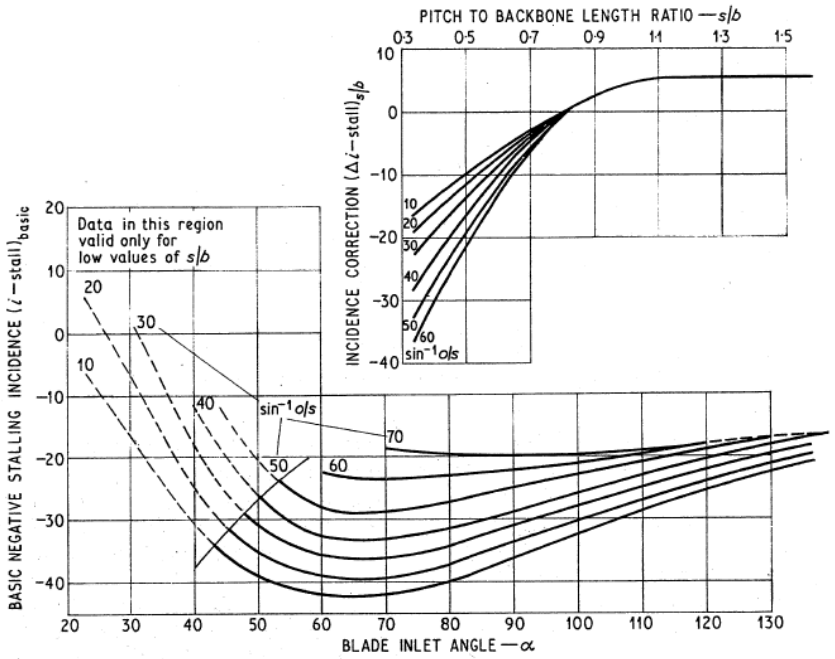

Fig. 13. Negative stalling incidence

Figure 12.2-27: Negative stalling incidence, [12].

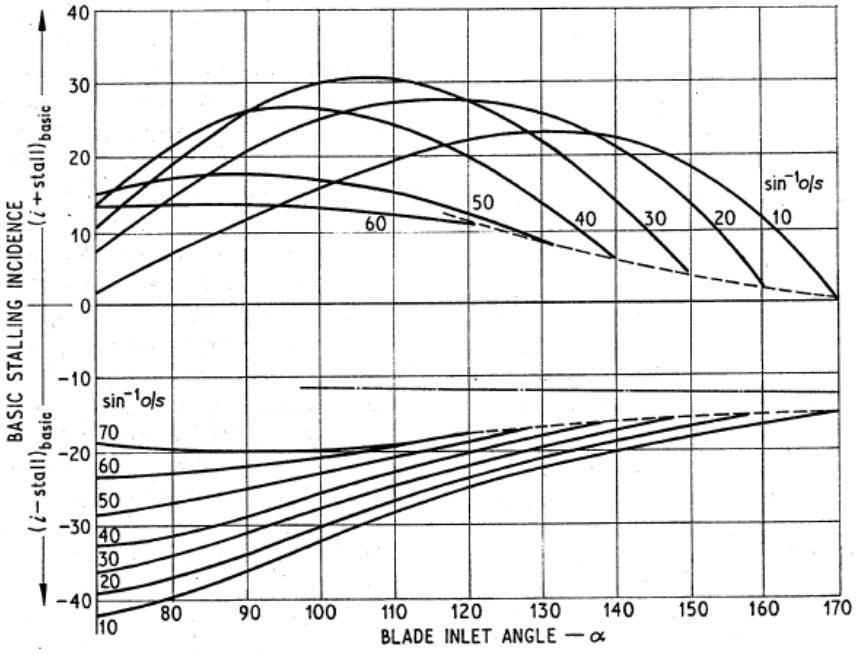

Figure 12.2-28: Basic stalling incidence for a value of inlet blade angle greater than 90 deg, [12].

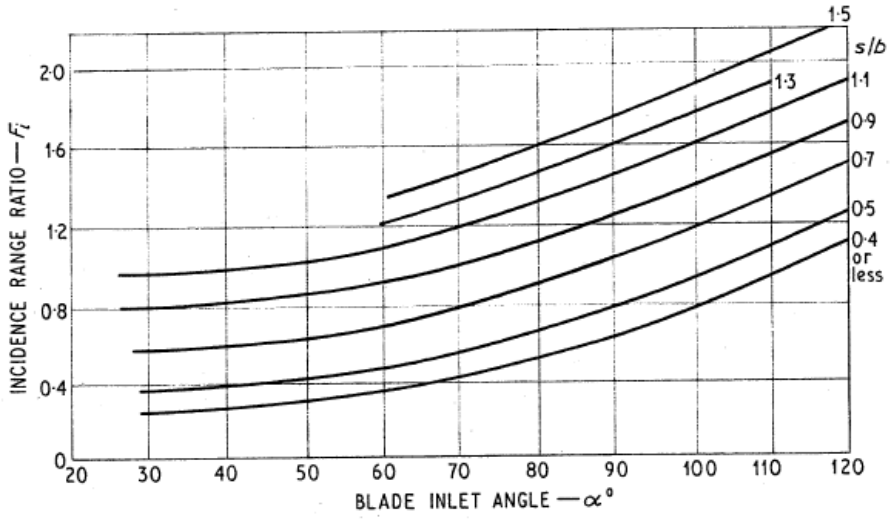

Figure 12.2-29: Minimum loss incidence for inlet blade angle and pitch to centerline camber length (s/b_c), [12].

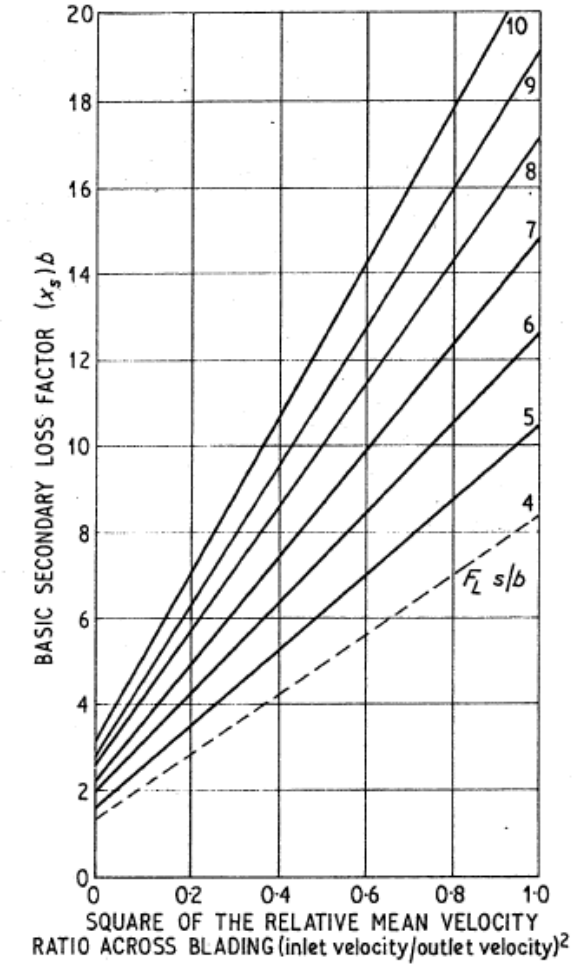

Figure 12.2-30: Basic secondary loss factor Y_{S0} as a function of the square of the inlet to outlet velocity $(C_{in}/ C_{out})^2$ and pitch to centerline camber length (s/b_c), [12].

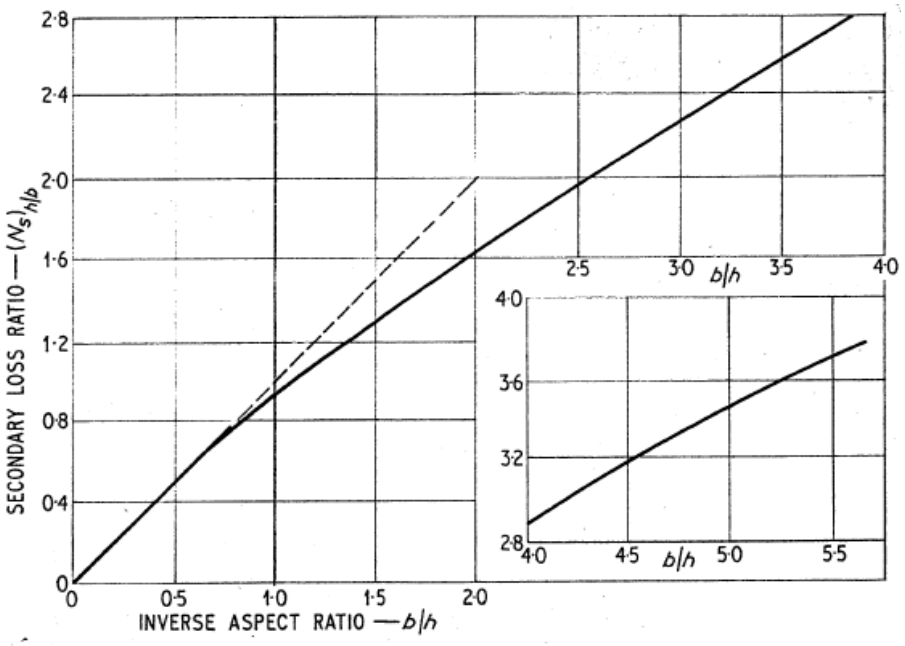

Figure 12.2-31: Multiplier to the secondary loss due to aspect ratio (h/c), [12].

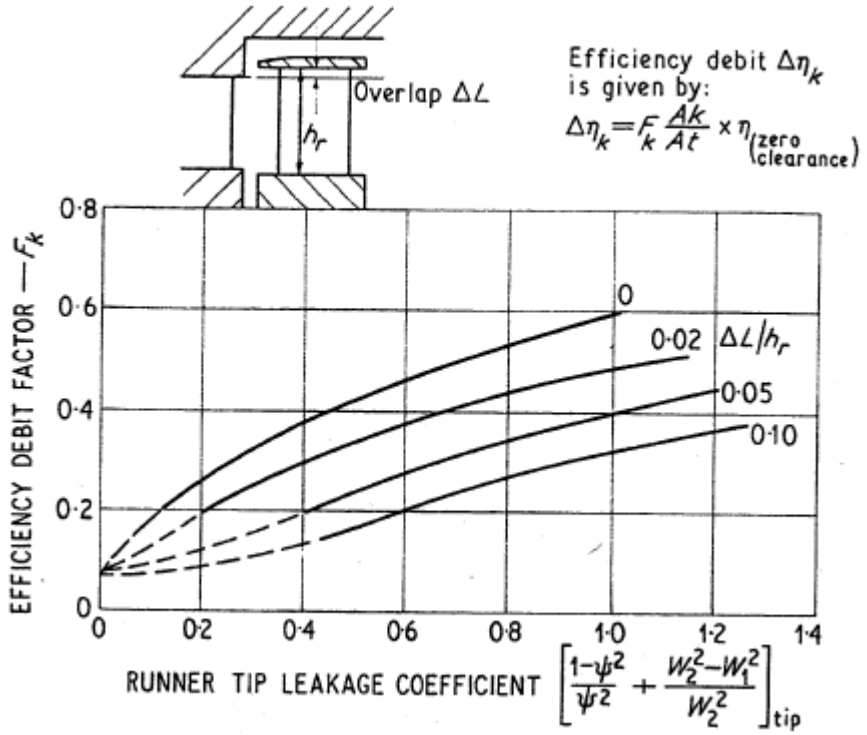

Figure 12.2-32: Efficiency factor to correlate the loss in efficiency due to tip leakage over a shrouded blade, [12].

12.3 Appendix Chapter 4

12.3.1 Cooling Air Temperature

The temperature of the cooling air is estimated with the help of the in-house program flowbalance. The main steeps for these calculations are, with the reference to flowbalance subscript, as follows.

The cooling air for the PT consists of two types, denoted 1 and 2. Type 1 is a mix between two mass flows, one that is cold external (in point 100) to a specific temperature and one bleed off of air from stage 11 in the compressor (point 9). These two streams are then mixed in (point 10) a chamber. Here it is effected by external heating as it flow into the cavity just before Stator 1 in the PT (point 16) on its way to point 76 before it is injected as a cooling flow at the hub.

Type 2 is pure bleed off air from stage 6 in the compressor that has been heated external at its way towards the blade (to point 69).

Under the assumption that the change in temperatures and mass ratio between the external cooled air and bleed off air are independent of the load point of the gas turbine it is possible to calculate the cooling air temperature. With data from flowbalance the following assumed constants were calculated.

$$T_{air\ coold} \cdot \dot{m}_{air\ coold} + T_{bleed,11} \cdot \dot{m}_{bleed} = (\dot{m}_{air\ coold} + \dot{m}_{bleed,11}) \cdot T_{10} \Rightarrow$$
$$\Rightarrow \frac{\dot{m}_{bleed,11}}{\dot{m}_{air\ coold}} = \frac{(T_{air\ coold} - T_{10})}{T_{10} - T_{bleed,11}} \qquad (12.3\text{-}1)$$

$$T_{10} = \frac{(T_{air\ coold} + \frac{\dot{m}_{bleed,11}}{\dot{m}_{air\ coold}} \cdot T_{bleed,11})}{(1 + \frac{\dot{m}_{bleed,11}}{\dot{m}_{air\ coold}})} \qquad (12.3\text{-}2)$$

$$\Delta T_{bleed,6-69} = T_{69} - T_{bleed,6} \qquad (12.3\text{-}3)$$

Where the used temperature are

$T_{air\ coold} = 393.15\,[K]$

$T_{bleed,6} = 531.15\,[K]$

$T_{bleed,11} = 637.15\,[K]$

$T_{10} = 623.15\,[K]$

$T_{69} = 533.15\,[K]$

$T_{76} = 642.15\,[K]$

With the use of eqn's (12.3-1), (12.3-2), (12.3-3) and flowbalance the mass ratio and temperature change will be

$$\frac{\dot{m}_{bleed}}{\dot{m}_{air\ coold}} = 16.44$$

$$T_{bleed} = 46$$

These values are assumed to be constant for all loads, even if it is not fully true the error in the final calculation will be negligible.

12.3.2 Statistic Definition

The statistic definitions for standard deviation (SD), arithmetic average (AA) and average absolute deviation (AAD) are described below, and explained by a simple example of a series of number consisted of 2, -1 and 4.
The parameter used are x_i that represent the difference from measured value as is represented in Table 4-8 and Table 4-10. $\bar{x}$ is the mean of these differences.

Arithmetic Average (AA)
For a series of number it is the sum of all of the numbers divided by the number of numbers in the series.

$$\bar{x} = \frac{1}{n} \cdot \sum_{i=1}^{n} x_i$$

Example $\bar{x} = \frac{1}{3} \cdot (2 + (-1) + 4) = \frac{5}{3} \approx 1.667$

Average Absolute Deviation (AAD)
The average absolute deviation is the average of the absolute value for each of the deviations.

$$AAD = \frac{1}{n} \cdot \sum_{i=1}^{n} |x_i|$$

Example $AAD = \frac{1}{3} \cdot (2 + 1 + 4) = \frac{7}{3} \approx 2.333$

Standard Deviation (SD)
The standard deviation is a measure of the dispersion of a series of numbers.

$$SD = \sqrt{\frac{1}{n-1} \cdot \sum_{i=1}^{n} (x_i - \bar{x})^2}$$

Example

$$SD = \sqrt{\frac{1}{3-1} \cdot \left[\left(2 - \frac{5}{3}\right)^2 + \left((-1) - \frac{5}{3}\right)^2 + \left(4 - \frac{5}{3}\right)^2 \right]} = \sqrt{\frac{1}{2} \cdot \frac{38}{3}} = \sqrt{\frac{19}{3}} \approx 2.517$$

12.3.3 Loss Division

This section is confidential and therefore excluded.

12.4 Appendix Chapter 5

12.4.1 Denton

12.4.1.1 Shrouded Blades

Under the assumption of a single sealed blade, incompressible flow and that the flow up to the throat can be approximated as isentropic, the mass flow is determined by the sealing clearance (k), contraction coefficient (C_c), static pressure in the leakage jet (P_j) and the upstream stagnation pressure (P_{01}). If k is small compare to the height between the shroud and casing it is a good assumption that all the axial velocity (C_j) of the leakage will be lost in the mixing before it is injected to the mean flow, see Figure 5.2-1. If instead concerning the tangential velocity component $C_{j\theta}$. This component undergoes a small but here neglected change due to skewing. With this assumption the tangential velocity for the jet is approximately equal to the inlet condition $C_{\theta,in}$. Apply Bernoulli's equation between the throat, upstream and downstream of the blade with no losses.

$$p_{0in} = p_j + \frac{\rho \cdot C_j^2}{2} + \frac{\rho \cdot C_{j\theta}^2}{2} = p_{out} + \frac{\rho \cdot C_{out}^2}{2} \tag{12.4-1}$$

If now assuming that the flow restrictions between and after the seals are small the static pressure in the jet is equal to the static pressure downstream of the row.

$$p_j = p_{out} \tag{12.4-2}$$

Eqn (12.4-2) in eqn (12.4-1) $\Rightarrow$

$$\mathrm{C_j} = \sqrt{\mathrm{C_{out}^2} - \mathrm{C_{j\theta}^2}} \tag{12.4-3}$$

The leakage mass flow will then be

$$\mathrm{m_L} = \rho \cdot k \cdot C_C \cdot \mathrm{C_j} \tag{12.4-4a}$$

Or more accurate for a annular turbine

$$\mathrm{m'_L} = \rho \cdot \pi \cdot \left[(r_{tip} + k)^2 - r_{tip}^{\ 2} \right] \cdot C_c \tag{12.4-4b}$$

The mean mass flow is

$$\mathrm{m_M} = \rho \cdot h \cdot C_{out,x} = \rho \cdot h \cdot C_{out} \cdot \cos(\alpha_{out}) \tag{12.4-5a}$$

Or

$$\mathrm{m'_M} = \rho \cdot \pi \cdot \left[r_{tip}^{\ 2} - r_{rot}^{\ 2} \right] \cdot C_{out} \cdot \cos(\alpha_{out}) \tag{12.4-5b}$$

The leakage fraction is then

$$\frac{\mathrm{m_L}}{\mathrm{m_M}} = \frac{\rho \cdot k \cdot C_C \cdot \mathrm{C_j}}{\rho \cdot h \cdot C_{out} \cdot Cos(\alpha_{out})} = \frac{k \cdot C_C \cdot \sqrt{\mathrm{C_{out}^2} - \mathrm{C_{j\theta}^2}}}{h \cdot C_{out} \cdot Cos(\alpha_{out})} \qquad (12.4\text{-}6a)$$

Or

$$\frac{\mathrm{m'_L}}{\mathrm{m'_M}} = \left\{ \begin{array}{l} \dfrac{\rho \cdot \pi \cdot \left[(r_{tip} + k)^2 - r_{tip}{}^2 \right] \cdot C_c}{\rho \cdot \pi \cdot \left[r_{tip}{}^2 - r_{rot}{}^2 \right] \cdot C_{out} \cdot Cos(\alpha_{out})} = \\ = \dfrac{\left[2 \cdot r_{tip} \cdot k + k^2 \right] \cdot C_c}{\left[r_{tip}{}^2 - r_{rot}{}^2 \right] \cdot C_{out} \cdot Cos(\alpha_{out})} \approx \\ \approx \dfrac{\left[2 \cdot r_{tip} \cdot k \right] \cdot C_c}{\left[r_{tip}{}^2 - r_{rot}{}^2 \right] \cdot C_{out} \cdot Cos(\alpha_{out})} \end{array} \right\} \qquad (12.4\text{-}6b)$$

If $\mathrm{C_x}$ is constant, $\mathrm{C_{j\theta}^2} = \mathrm{C_{\theta,in}^2}$ and $C_{\theta,in} = C_{in} \cdot \sin(\alpha_{in}) \Rightarrow$

$$\sqrt{\mathrm{C_{out}^2} - \mathrm{C_{\theta,in}^2}} = \sqrt{\mathrm{C_{out}^2} - C_{in}{}^2 \cdot \sin^2(\alpha_{in})} \qquad (12.4\text{-}7)$$

$C_x = \mathrm{const} \Rightarrow$

$C_{in} \cdot \cos(\alpha_{in}) = C_{out} \cdot \cos(\alpha_{out}) \Rightarrow$

$$C_{in} = C_{out} \cdot \frac{\cos(\alpha_{out})}{\cos(\alpha_{in})} \qquad (12.4\text{-}8)$$

Eqn (12.4-7) in eqn (12.4-6) $\Rightarrow$

$$\mathrm{C_j} = \sqrt{\mathrm{C_{out}^2} - \left(C_{out} \cdot \frac{\cos(\alpha_{out})}{\cos(\alpha_{in})} \right)^2 \cdot \sin^2(\alpha_{in})} =$$

$$= \mathrm{C_{out}} \cdot \sqrt{1 - \cos^2(\alpha_{out}) \cdot \tan^2(\alpha_{in})} \qquad (12.4\text{-}9)$$

Eqn (12.4-9) in eqn (12.4-6a) $\Rightarrow$

$$\frac{\mathrm{m_L}}{\mathrm{m_M}} = \frac{k \cdot C_C \cdot \sqrt{\mathrm{C_{out}^2} - \mathrm{C_{j\theta}^2}}}{h \cdot C_{out} \cdot \cos(\alpha_{out})} =$$

$$\frac{k}{h} \cdot C_C \cdot \frac{C_{out}}{C_{out}} \sqrt{\frac{1 - \cos^2(\alpha_{out}) \cdot \tan^2(\alpha_{in})}{\cos^2(\alpha_{out})}} =$$

$$= \frac{k}{h} \cdot C_C \cdot \sqrt{\frac{1}{\cos^2(\alpha_{out})} - \tan^2(\alpha_{in})} \qquad (12.4\text{-}10a)$$

=(5-2a)

Or

Eqn (12.4-9) in eqn (12.4-6b) $\Rightarrow$

$$\frac{\mathrm{m'_L}}{\mathrm{m'_M}} = \frac{k \cdot C_C \cdot \sqrt{\mathrm{C_{out}^2 - C_{j\theta}^2}}}{h \cdot C_{out} \cdot \cos(\alpha_{out})} =$$

$$\frac{k}{h} \cdot C_C \cdot \frac{C_{out}}{C_{out}} \sqrt{\frac{1 - \cos^2(\alpha_{out}) \cdot \tan^2(\alpha_{in})}{\cos^2(\alpha_{out})}} =$$

$$= \frac{k}{h} \cdot C_C \cdot \sqrt{\frac{1}{\cos^2(\alpha_{out})} - \tan^2(\alpha_{in})} \qquad \text{(12.4-10b)}$$

$$= \text{(5-2b)}$$

Under the assumption that the stagnation temperature is the same in the both streams the entropy creation can be estimated according to what Denton stated in [3] with equation 22 (originally from Shapiro [45]). The assumption of constant stagnation temperature is not really true, because the mainstream have compared to the leakage flow a lower temperature due to the work extraction in the passage. But for these propose it is believed to be accurate enough.

$$T \cdot \Delta \mathrm{s} \cdot \frac{\mathrm{m_M}}{\mathrm{m_L}} = V_{x,out}^2 - V_{x,out} \cdot V_{x,L} + V_{\theta,out}^2 - V_{\theta,out} \cdot V_{\theta,L} =$$

$$= V_{x,out}^2 \cdot (1 - \frac{V_{x,L}}{V_{x,out}}) + V_{\theta,out}^2 \cdot (1 - \frac{V_{\theta,L}}{V_{\theta,out}}) \qquad \text{(12.4-11)}$$

The axial velocity of the leakage flow $V_{x,L}$ is normally small due a comparable great ejection area and radial direction of the injection, so it can be neglected, $V_{x,L} \approx 0$.
Eqn (12.4-11) will then be

$$\left.\begin{aligned} & T \cdot \Delta \mathrm{s} \cdot \frac{\mathrm{m_M}}{\mathrm{m_L}} = V_{x,out}^2 + V_{\theta,out}^2 - \frac{V_{\theta,L}}{V_{\theta,out}} \cdot V_{\theta,out}^2 \\ & V_{\theta,out}^2 = V_{out}^2 \cdot \sin(\alpha_{out}) \\ & V_{x,out}^2 + V_{\theta,out}^2 = V_{out}^2 \end{aligned}\right\} \Rightarrow$$

$$\Rightarrow T \cdot \Delta \mathrm{s} \cdot \frac{\mathrm{m_M}}{\mathrm{m_L}} = V_{out}^2 \cdot \left[1 - \frac{V_{\theta,L}}{V_{\theta,out}} \cdot \sin^2(\alpha_{out})\right] \qquad \text{(12.4-12)}$$

Normally is the axial velocity approximately constant across a blade row, $V_{x,in} = V_{x,out} = V_x$ = constant. $\Rightarrow$

$$\tan(\alpha_{in}) = \frac{V_{\theta,L}}{V_x}, \ \tan(\alpha_{out}) = \frac{V_{\theta,out}}{V_x}$$

If both left and right hand side is divided by $\frac{V_{out}^2}{2}$, eqn (12.4-12) will be

$$\frac{T\cdot\Delta s}{0.5\cdot V_{out}^2}=2\cdot\frac{m_L}{m_M}\left[1-\sin^2(\alpha_{out})\cdot\frac{\tan(\alpha_{in})}{\tan(\alpha_{out})}\right] \qquad (12.4\text{-}13)$$

=(5-1)

Where $\frac{m_L}{m_M}$ can be expressed by either eqn (12.4-10a) or eqn (12.4-10b)

If eqn (12.4-10a) is used eqn (12.4-13) represent Denton's equation for shrouded blades.

12.4.1.2 Unshrouded blades

For an unshrouded blade the leakage flow are from the pressure to the suction side of the blade across the blade tip. The velocity at the pressure respective suctionside in the direction of the chord are C_p and C_s, and it is assumed that the leakage jet velocity component along the chord are constant and equal to the pressure sides, $C_{j,chord}=C_{p,chord}=C_p$ and also that the mixing occur immediately as the leakage flow enters the suction side. The treatment for the mixing of the two flows are then treated analogy to that for shrouded blades, eqn (12.4-11) or equation A6.1 from Denton [3] where the use of $\Delta T_0\approx 0$ have been used.

If

$$\Delta s=c_p\cdot(\gamma-1)\cdot M_s^2\cdot\left(1-\frac{C_p}{C_s}\right)\cdot\frac{1}{m_M}\cdot dm_L \qquad (12.4\text{-}14)$$

$$\left.\begin{aligned}c_p&=R+c_v\\ \gamma&=\frac{c_p}{c_v}\end{aligned}\right\}\Rightarrow c_p=R+\frac{c_p}{\gamma}\Rightarrow c_p=\frac{R}{(1-\frac{1}{\gamma})}=\frac{\gamma\cdot R}{\gamma-1} \qquad (12.4\text{-}15)$$

Eqn (12.4-15) in eqn (12.4-14), and $M_s=\frac{C_s}{\sqrt{\gamma\cdot R\cdot T}}\Rightarrow$

$$\Delta s=\frac{\gamma\cdot R}{\gamma-1}\cdot(\gamma-1)\cdot\left(\frac{C_s}{\sqrt{\gamma\cdot R\cdot T}}\right)^2\cdot\left(1-\frac{C_p}{C_s}\right)\cdot\frac{1}{m_M}\cdot dm_L=$$

$$=\frac{C_s^2}{T}\cdot\left(1-\frac{C_p}{C_s}\right)\cdot\frac{1}{m_M}\cdot dm_L \qquad (12.4\text{-}16)$$

If eqn (12.4-16) is integrated along the chord (c).

$$T\cdot\Delta s=\frac{1}{m_M}\cdot\int_0^c C_s^2\cdot\left(1-\frac{C_p}{C_s}\right)\cdot dm_L \qquad (12.4\text{-}17)$$

If the velocity component along the chord at the pressure side are kept constant and equal to the leakage jets component as it enters the suctionside Bernoulli's equation

can be applied with the jets velocity at the suctionside split into a component along the chord and a perpendicular. For incompressible flow the density are constant and the equation are.

$$\left.\begin{aligned} & p_p + \frac{1}{2}\cdot\rho\cdot C_p^2 = p_s + \frac{1}{2}\cdot\rho\cdot C_s^2 \\ & C_s = C_{s,chord} + C_{s,\perp chord} = C_p + C_{s,\perp chord} \end{aligned}\right\} \Rightarrow$$

$$\Rightarrow p_p + \frac{1}{2}\cdot\rho\cdot C_p^2 = p_s + \frac{1}{2}\cdot\rho\cdot C_p + \frac{1}{2}\cdot\rho\cdot C_{s,\perp chord}^2 \Rightarrow$$

$$\Rightarrow p_p - p_s = \Delta p = \frac{1}{2}\cdot\rho\cdot C_{s,\perp chord}^2 \qquad (12.4\text{-}18)$$

The mass flow across the tip is

$$dm = \rho\cdot k\cdot C_C\cdot C_{s,\perp chord}\cdot dr \qquad (12.4\text{-}19)$$

Eqn (12.4-18) in eqn (12.4-19)

$$m = \rho\cdot k\cdot C_C\cdot\sqrt{\frac{\Delta p\cdot 2}{\rho}}\cdot dr = k\cdot C_C\cdot\sqrt{\Delta p\cdot 2\cdot\rho}\cdot dr \qquad (12.4\text{-}20)$$

where, k = clearance, C_C = contraction coefficient ≈ 0.6 - 0.8

(depends on the geometry and flow condition as for example radius of corner, Re, and)

$$p_p + \frac{1}{2}\cdot\rho\cdot C_p^2 = p_s + \frac{1}{2}\cdot\rho\cdot C_s^2 \Rightarrow p_p - p_s = \Delta p = \frac{1}{2}\cdot\rho\cdot(C_s^2 - C_p^2) \qquad (12.4\text{-}21)$$

Main mass flow in the row

$$m_M = \rho\cdot h\cdot s\cdot C_{out}\cdot\cos\ (\alpha_{out}) \qquad (12.4\text{-}22a)$$

Or

$$m'_M = \rho\cdot\pi\cdot\frac{\left(r_{tip}^2 - r_{rot}^2\right)}{z-1}\cdot C_{out}\cdot\cos(\alpha_{out}) \qquad (12.4\text{-}22b)$$

z = number of blades in the row

Eqn (12.4-20), eqn (12.4-21) and eqn (12.4-22a) in eqn (12.4-17)

$$T\cdot\Delta s = \left\{\begin{aligned} & \frac{1}{\rho\cdot h\cdot s\cdot C_{out}\cdot\cos\ (\alpha_{out})}\cdot \\ & \cdot\int_0^c C_s^2\cdot\left(1-\frac{C_p}{C_s}\right)\cdot k\cdot C_C\cdot\sqrt{\frac{1}{2}\cdot\rho\cdot(C_s^2 - C_p^2)\cdot 2\cdot\rho}\cdot dr \end{aligned}\right\} =$$

$$= \frac{C_C\cdot k}{h\cdot s\cdot C_{out}\cdot\cos(\alpha_{out})}\cdot\int_0^c C_s^2\cdot\left(1-\frac{C_p}{C_s}\right)\cdot\sqrt{(C_s^2 - C_p^2)}\cdot dr$$

To get a loss factor it is divided by $\frac{1}{2}\cdot C_{out}^2$

$$\zeta = \frac{T \cdot \Delta s}{\frac{1}{2} \cdot C_{out}^2} = \frac{2 \cdot C_C \cdot k}{h \cdot s \cdot \cos(\alpha_{out})} \cdot \int_0^c \frac{C_s^2}{C_{out}^3} \cdot \left(1 - \frac{C_p}{C_s}\right) \cdot C_s \cdot \sqrt{(1 - \frac{C_p^2}{C_s^2})} \cdot dr =$$

$$= 2 \cdot \frac{k}{h} \cdot C_C \cdot \frac{1}{s \cdot \cos(\alpha_{out})} \cdot \int_0^c \frac{C_s^3}{C_{out}^3} \cdot \left(1 - \frac{C_p}{C_s}\right) \cdot \sqrt{(1 - \frac{C_p^2}{C_s^2})} \cdot dr \qquad \text{(12.4-23a)}$$

= (5-3a)

Analogy for eqn (12.4-20), eqn (12.4-21) and eqn (12.4-22b) in eqn (12.4-17)

$$\zeta' = 2 \cdot C_C \cdot \frac{k \cdot (z-1)}{\pi \cdot \left(r_{tip}^2 - r_{rot}^2\right) \cdot \cos(\alpha_{out})} \cdot \int_0^c \frac{C_s^3}{C_{out}^3} \cdot \left(1 - \frac{C_p}{C_s}\right) \cdot \sqrt{(1 - \frac{C_p^2}{C_s^2})} \cdot dr \qquad \text{(12.4-23b)}$$

=(5-3a)

In eqn (12.4-23a) eqn (12.4-23b) the ratio between velocity at the pressure and suction side are needed and can be estimated as

If use the continuity equation and the assumptions that the mean velocity is equal to the average between suction and pressure side.

$$\frac{C_p + C_v}{2} = C_{out} \cdot \cos(\alpha_{out}) \qquad \text{(12.4-24)}$$

The average force working on the blade can be expressed with momentum equation as

$$F = m \cdot \Delta C_\theta = \rho \cdot C_x \cdot s \cdot (C_{\theta,2} - C_{\theta,1}) \qquad \text{(12.4-25)}$$

and from the circulation

$$F = m \cdot \oint C \cdot ds = \rho \cdot C_x \cdot c \cdot (C_s - C_p) \qquad \text{(12.4-26)}$$

Eqn (12.4-25) should be equal to eqn (12.4-26)

$$\rho \cdot C_x \cdot s \cdot (C_{\theta,2} - C_{\theta,1}) = \rho \cdot C_x \cdot c \cdot (C_s - C_p) \Rightarrow$$

$$\Rightarrow C_s - C_p = \frac{s}{c} \cdot C_x \cdot \left[\tan(\alpha_{out}) - \tan(\alpha_{in})\right] \qquad \text{(12.4-27)}$$

Combining eqn (12.4-24), eqn (12.4-27) and $C_{out} \Rightarrow$

$$\frac{C_s}{C_{out}} = \frac{\cos(\alpha_{out})}{\cos(\alpha')} + \frac{1}{2} \cdot \frac{s}{c} \cdot \left[\tan(\alpha_{out}) - \tan(\alpha_{in})\right] \cdot \cos(\alpha_{out}) \qquad \text{(12.4-28)}$$

= (5-4)

$$\frac{C_p}{C_{out}} = \frac{\cos(\alpha_{out})}{\cos(\alpha')} - \frac{1}{2} \cdot \frac{s}{c} \cdot \left[\tan(\alpha_{out}) - \tan(\alpha_{in})\right] \cdot \cos(\alpha_{out}) \qquad \text{(12.4-29)}$$

= (5-5)

Where α' is the local blade angle and was supposed by Denton to wary linear between the inlet and outlet flow angle. This assumption would be interest to modify to a more normal blade profile, to find out its effect.

12.4.2 Cambridge

12.4.2.1 Shrouded Blades

The driving force is the pressure gradient across the whole blade row, and the skewing as the flow crosses the tip are neglected so the tangential velocity of the leakage flow are kept constant across the clearance, $\Delta C_{j,\theta} = 0$. The leakage flow are approximated as isentropic, so that the change in total pressure to the point of mixing between the main flow and leakage jet are neglected, $p_{0j}=p_{0,out}$.
The static pressure in the jet are approximated as equal to the static pressure at the downstream flow, $p_j=p_{out}$. Assuming a constant axial velocity in the blade row is a good approximation, $\Delta C_x = 0$

Bernoulli's equation through both the clearance and blade row
Clearance

$$\left.\begin{aligned} p_j + \frac{1}{2}\cdot\rho\cdot C_j^2 = p_{in} + \frac{1}{2}\cdot\rho\cdot C_{in}^2 \\ C_{\theta,in} = C_{\theta,j} \end{aligned}\right\} \Rightarrow \frac{1}{2}\cdot\rho\cdot C_{j,x}^2 = p_{in} - p_j + \frac{1}{2}\cdot\rho\cdot C_{in,x}^2$$

$$= p_{in} - p_{out} + \frac{1}{2}\cdot\rho\cdot C_{in,x}^2 \qquad (12.4\text{-}30)$$

Blade row

$$\left.\begin{aligned} p_{in} + \frac{1}{2}\cdot\rho\cdot C_{in}^2 = p_{out} + \frac{1}{2}\cdot\rho\cdot C_{out}^2 \\ C_{x,in} = C_{x,out} \end{aligned}\right\} \Rightarrow p_{in} - p_{out} = \frac{1}{2}\cdot\rho\cdot\left[C_{\theta,out}^2 - C_{\theta,in}^2\right]$$

$$= \frac{1}{2}\cdot\rho\cdot C_x^2\cdot\left[\tan^2(\alpha_{out}) - \tan^2(\alpha_{in})\right] \qquad (12.4\text{-}31)$$

Eqn (12.4-30), eqn (12.4-31) and $p_j = p_{out} \Rightarrow$

$$\Rightarrow \frac{1}{2}\cdot\rho\cdot C_{j,x}^2 = \frac{1}{2}\cdot\rho\cdot C_x^2\cdot\left[\tan^2(\alpha_{out}) - \tan^2(\alpha_{in})\right] + \frac{1}{2}\cdot\rho\cdot C_{in,x}^2 =$$

$$= \frac{1}{2}\cdot\rho\cdot C_{in,x}^2\left[\tan^2(\alpha_{out}) - \tan^2(\alpha_{in}) + 1\right] \Rightarrow$$

$$\Rightarrow C_{j,x}^2 = C_{in,x}^2\left[\tan^2(\alpha_{out}) - \tan^2(\alpha_{in}) + 1\right] \qquad (12.4\text{-}32)$$

The leakage mass flow is

$$\left.\begin{aligned} m_L = Area\cdot\rho\cdot C_{j,x} \\ Area = \pi\cdot((r_t + k)^2 - r_t^2) = 2\cdot\pi\cdot r_t\cdot k \end{aligned}\right\} \Rightarrow$$

$$\Rightarrow m_L = 2\cdot\pi\cdot r_t\cdot k\cdot\rho\cdot C_{in,x}\cdot\sqrt{\tan^2(\alpha_{out}) - \tan^2(\alpha_{in}) + 1} \qquad (12.4\text{-}33)$$

Main mass flow in the blade row is

$$\left.\begin{aligned} m_M = Area\cdot C_C\cdot\rho\cdot C_x \\ Area = \pi\cdot(r_t^2 - r_r^2) \end{aligned}\right\} \Rightarrow$$

$$m_M = \pi\cdot(r_t^2 - r_r^2)\cdot C_C\cdot\rho\cdot C_x \qquad (12.4\text{-}34)$$

Where C_c is a contractions coefficient

Ration between the leakage and main mass flow, eqn (12.4-33) divided by eqn (12.4-34)

$$\frac{\mathrm{m_L}}{\mathrm{m_M}} = \frac{2\cdot\pi\cdot r_t\cdot k\cdot C_C\cdot\rho\cdot C_{in,x}\cdot\sqrt{\tan^2(\alpha_{out})-\tan^2(\alpha_{in})+1}}{\pi\cdot(r_t^{\,2}-r_r^{\,2})\cdot\rho\cdot C_x} =$$

$$= \frac{2\cdot r_t\cdot k\cdot C_C\cdot\sqrt{\tan^2(\alpha_{out})-\tan^2(\alpha_{in})+1}}{(r_t^{\,2}-r_r^{\,2})} \qquad (12.4\text{-}35)$$

When the leakage jet then mixes out after the seals, all it is axial velocity are lost with a negligible increase in total pressure. The lost are then approximately equal to the axial velocity of the leakage jet and can be expressed as

$$\frac{\Delta p_0}{\frac{1}{2}\cdot\rho\cdot C_{out}^2} = \frac{\mathrm{m_L}}{\mathrm{m_M}}\cdot\frac{\frac{1}{2}\cdot\rho\cdot C_{j,x}^2}{\frac{1}{2}\cdot\rho\cdot C_{out}^2} = \frac{2\cdot r_t\cdot k\cdot C_C\cdot\sqrt{\tan^2(\alpha_{out})-\tan^2(\alpha_{in})+1}}{(r_t^{\,2}-r_r^{\,2})}\cdot\frac{C_{in,x}^2\left[\tan^2(\alpha_{out})-\tan^2(\alpha_{in})+1\right]}{C_{out}^2} =$$

$$= \frac{2\cdot r_t\cdot k\cdot C_C}{(r_t^{\,2}-r_r^{\,2})}\cdot\left[\tan^2(\alpha_{out})-\tan^2(\alpha_{in})+1\right]^{3/2}\frac{C_{in,x}^2}{C_{in,x}^2/\cos(\alpha_{out})} =$$

$$= \frac{2\cdot r_t\cdot k\cdot C_C}{(r_t^{\,2}-r_r^{\,2})}\cdot\left[\tan^2(\alpha_{out})-\tan^2(\alpha_{in})+1\right]^{3/2}\cdot\cos(\alpha_{out})\Rightarrow$$

Finally giving the relation

$$\frac{\Delta p_0}{\frac{1}{2}\cdot\rho\cdot C_{out}^2} = \frac{2\cdot r_t\cdot k\cdot C_C}{(r_t^{\,2}-r_r^{\,2})}\cdot\left[\tan^2(\alpha_{out})-\tan^2(\alpha_{in})+1\right]^{3/2}\cdot\cos(\alpha_{out}) \qquad (12.4\text{-}36)$$

This loss is only due to the axial kinetic energy loss. Another loss is the loss increase when the different tangential velocity between the leakage and main flow mixes out. It is calculated as

$$\left.\begin{aligned}&\frac{\Delta p_0}{\frac{1}{2}\cdot\rho\cdot C_{out}^2} = \frac{\mathrm{m_L}}{\mathrm{m_M}}\cdot\frac{\frac{1}{2}\cdot\rho\cdot\Delta C_\theta^2}{\frac{1}{2}\cdot\rho\cdot C_{out}^2}\\ &\Delta C_\theta = C_{\theta,j}-C_{\theta,out} = C_{\theta,in}-C_{\theta,out} = C_x\left[\tan(\alpha_{in})-\tan(\alpha_{out})\right]\end{aligned}\right\}\Rightarrow$$

$$\Rightarrow \frac{\Delta p_0}{\frac{1}{2}\cdot\rho\cdot C_{out}^2} = \frac{2\cdot r_t\cdot k\cdot C_C\cdot\sqrt{\tan^2(\alpha_{out})-\tan^2(\alpha_{in})+1}}{(r_t^{\,2}-r_r^{\,2})}\cdot\frac{C^2{}_x\cdot\left[\tan(\alpha_{in})-\tan(\alpha_{out})\right]^2}{\frac{C^2{}_x}{\cos^2(\alpha_{out})}}$$

$$\Rightarrow \frac{\Delta p_0}{\frac{1}{2}\cdot\rho\cdot C_{out}^2} = \left\{ \begin{array}{l} \dfrac{2\cdot r_t\cdot k\cdot C_C\cdot\sqrt{\tan^2(\alpha_{out})-\tan^2(\alpha_{in})+1}}{(r_t^{\,2}-r_r^{\,2})}\cdot \\ \cdot\left[\tan(\alpha_{in})-\tan(\alpha_{out})\right]^2\cdot\cos^2(\alpha_{out}) \end{array} \right\} \qquad (12.4\text{-}37)$$

Here only the kinetic energy losses are taken into concern and not the enthalpy rise as Denton used in [3], originally from Shapiro. To get the total loss the summation of eqn (12.4-36) and eqn (12.4-37) should be used.

12.4.2.2 Unshrouded Blades

Just as Denton [3] is it assumed that both the static and total pressure in the leakage jet and at the suction surface is equal.

$$\left.\begin{array}{l} p_{0j} = p_{0s} \\ p_j = p_s \end{array}\right\} \Rightarrow C_s = C_j$$

The pressure gradient acting on the leakage jet as it passes the tip is also neglected so that the jet keeps the chord wise velocity from the pressure to the suction side, $C_{j,chord} = C_{p,chord} = C_p$. The angle that the leakage jet enters the suction surface (Figure 12.4-1) is then

$$\cos(\alpha_j) = \frac{C_p}{C_j} = \frac{C_p}{C_s} \qquad (12.4\text{-}38)$$

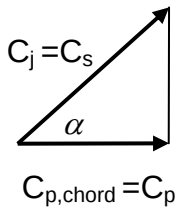

Figure 12.4-1: Angle that the leakage jet enters the suction surface for an unshrouded blade.

With the assumption of equal stagnation temperature, incompressible and that $m_{L<<}m_M$ the entropy generation can be estimated as, (Denton [3] eqn 22).

$$T\cdot\Delta s = \frac{m_L}{m_M}\cdot\left[C_s^2 - C_s\cdot C_j\cdot\cos(\alpha_j)\right] \qquad (12.4\text{-}39)$$

Eqn (12.4-38) in eqn (12.4-39)

$$T\cdot\Delta s = \frac{m_L}{m_M}\cdot\left[C_s^2 - C_s\cdot C_p\right] = \frac{m_L}{m_M}\cdot C_s^2\cdot\left[1-\frac{C_p}{C_s}\right] \qquad (12.4\text{-}40)$$

Make it dimensionless by division with $\frac{1}{2}\cdot C_s^2$ and assume that $\zeta \approx Y \Rightarrow$

$$\zeta = \frac{T\cdot\Delta s}{\frac{1}{2}\cdot C_s^2} = 2\cdot\frac{m_L}{m_M}\cdot\left[1-\frac{C_p}{C_s}\right] \approx \frac{\Delta p_0}{\frac{1}{2}\cdot\rho\cdot C_s^2} = Y \qquad (12.4\text{-}41)$$

An average value of the blade loading is get from the tangential change of momentum, as also seen in eqn (12.4-)

$$\Delta p_{avg} = \frac{m \cdot \Delta C_\theta}{c_x} = \rho \cdot C_x^2 \cdot \frac{s}{c_x} \cdot \left[\tan(\alpha_{out}) - \tan(\alpha_{in})\right] \qquad (12.4\text{-}42)$$

It is now assumed that the velocity at the pressure side is small compare to the suctionside so that the stagnation and static pressure at pressure side are approximately equal. Then the static pressure difference is approximately determined by the jet velocity, and then also the leakage jet velocity is close to the leakage jet component perpendicular to the chord.

$$\left.\begin{aligned} &p_{0p} = p_p + \frac{1}{2} \cdot \rho \cdot C_p^2 = p_s + \frac{1}{2} \cdot \rho \cdot C_s^2 \\ &p_{0p} \approx p_p \end{aligned}\right\} \Rightarrow$$

$$\Rightarrow p_p - p_s = \Delta p \approx \frac{1}{2} \cdot \rho \cdot C_s^2 = \frac{1}{2} \cdot \rho \cdot C_j^2 \qquad (12.4\text{-}43)$$

The leakage jet across the tip is then estimated as

$$\left.\begin{aligned} &\mathrm{m}_\mathrm{L} = \rho \cdot k \cdot c \cdot C_C \cdot C_{j,\perp chord} \\ &C_{j,\perp chord} = \sqrt{C_j^2 - C_{j,\perp chord}^2} = C_j \cdot \sqrt{1 - \frac{C_{j,\perp chord}^2}{C_j^2}} = C_j \cdot \sqrt{1 - \left(\frac{C_p}{C_s}\right)^2} \approx C_j \end{aligned}\right\} \Rightarrow$$

$$\Rightarrow \mathrm{m}_\mathrm{L} = \rho \cdot k \cdot c \cdot C_C \cdot C_j \qquad (12.4\text{-}44)$$

For large velocity ratios as normally seen at the first part at a blade, but will be little uncertain at the last part of the trailing edge, the main mass flow can be estimated as eqn (12.4-45) for a linear cascade and as eqn (12.4-46) for an annular.

$$\mathrm{m}_\mathrm{M} = \rho \cdot s \cdot h \cdot C_x \qquad (12.4\text{-}45)$$

$$\mathrm{m'}_\mathrm{M} = \rho \cdot \pi \cdot \frac{(r_t^2 - r_r^2)}{z - 1} \cdot C_x \qquad (12.4\text{-}46)$$

The ratio between the leakage and main mass flow is.

$$\frac{\mathrm{m}_\mathrm{L}}{\mathrm{m}_\mathrm{M}} = \frac{\rho \cdot k \cdot c \cdot C_C \cdot C_j}{\rho \cdot s \cdot h \cdot C_x} = C_C \cdot \frac{k}{h} \cdot \frac{c}{s} \cdot \frac{C_j}{C_x} \qquad (12.4\text{-}47)$$

Eqn (12.4-42) and eqn (12.4-43)

$$\frac{C_j}{C_x} = \frac{\sqrt{\frac{2 \cdot \Delta p_{avg}}{\rho}}}{\sqrt{\frac{\Delta p_{avg} \cdot c_x}{\rho \cdot s \cdot \left[\tan(\alpha_{out}) - \tan(\alpha_{in})\right]}}} = \sqrt{\frac{2 \cdot s \cdot \left[\tan(\alpha_{out}) - \tan(\alpha_{in})\right]}{c_x}} \qquad (12.4\text{-}48)$$

Eqn (12.4-48) in eqn (12.4-47) and finally in eqn (12.4-41)

$$\frac{\Delta p_0}{\frac{1}{2}\cdot\rho\cdot C_s^2} = 2\cdot C_C\cdot\frac{k}{h}\cdot\frac{c}{s}\cdot\left[1-\frac{C_p}{C_s}\right]\cdot\sqrt{\frac{2\cdot s\cdot\left[\tan(\alpha_{out})-\tan(\alpha_{in})\right]}{c_x}} \qquad (12.4\text{-}49)$$

Eqn (12.4-42) in eqn (12.4-43)

$$\frac{1}{2}\cdot\rho\cdot C_s^2 \approx \Delta p_{avg} = \rho\cdot C_x^2\cdot\frac{s}{c_x}\cdot\left[\tan(\alpha_{out})-\tan(\alpha_{in})\right]\Rightarrow$$

$$\Rightarrow C_s^2 = 2\cdot C_x^2\cdot\frac{s}{c_x}\cdot\left[\tan(\alpha_{out})-\tan(\alpha_{in})\right] \qquad (12.4\text{-}50)$$

Eqn (12.4-50) in eqn (12.4-49) and divide by $C_2^2 = \frac{C_x^2}{\cos(\alpha_{out})}\Rightarrow$

$$\frac{\Delta p_0}{\frac{1}{2}\cdot\rho\cdot C_2^2} = \left\{\begin{array}{l} 2\cdot C_C\cdot\frac{k}{h}\cdot\frac{c}{s}\cdot\left[1-\frac{C_p}{C_s}\right]\cdot\sqrt{\frac{2\cdot s\cdot\left[\tan(\alpha_{out})-\tan(\alpha_{in})\right]}{c_x}}\cdot \\ \cdot 2\cdot C_x^2\cdot\frac{s}{c_x}\cdot\left[\tan(\alpha_{out})-\tan(\alpha_{in})\right]\cdot\frac{1}{C_2^2} \end{array}\right\} =$$

$$= 2\cdot C_C\cdot\frac{k}{h}\cdot\frac{c}{s}\cdot\left[1-\frac{C_p}{C_s}\right]\cdot\left[\frac{2\cdot s\cdot\left[\tan(\alpha_{out})-\tan(\alpha_{in})\right]}{c_x}\right]^{3/2}\cdot\frac{C_x^2}{C_2^2}\Rightarrow$$

The equation for unshrouded blades is seen in eqn (12.4-51) where the velocity ratio is estimated just as eqn (12.4-28) and eqn (12.4-29)

$$\frac{\Delta p_0}{\frac{1}{2}\cdot\rho\cdot C_2^2} = \left\{\begin{array}{l} 2\cdot C_C\cdot\frac{k}{h}\cdot\frac{c}{s}\cdot\left[1-\frac{C_p}{C_s}\right]\cdot \\ \cdot\left[\frac{2\cdot s\cdot\left[\tan(\alpha_{out})-\tan(\alpha_{in})\right]}{c_x}\right]^{3/2}\cdot\cos^2(\alpha_{out}) \end{array}\right\} \qquad (12.4\text{-}51)$$

Note that in the Cambridge course the expression is divided by the $\left[\tan(\alpha_{out})-\tan(\alpha_{in})\right]^{3/2}$ term instead of as here multiplied. This is a believed error in the course, but because Cambridge use the same expression both in the course from (17-21 June 1996) and 2004 it is not totally obvious.

12.5 Appendix Chapter 6

12.5.1 Trends for Tip Leakage Loss Models

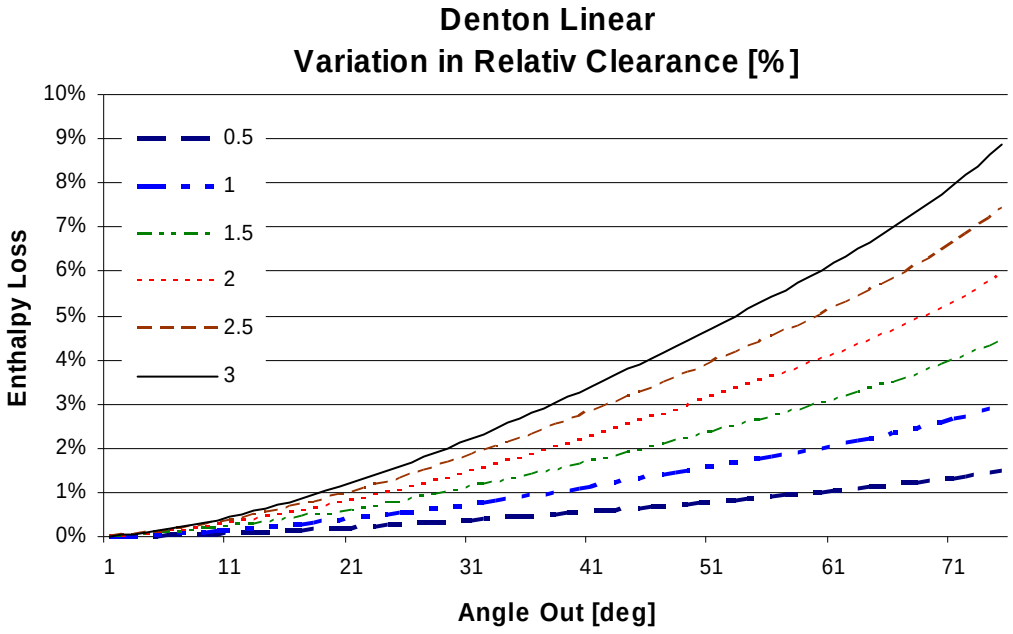

Figure 12.5-1: Variation of the Enthalpy loss with outlet flow angle for Denton Linear.

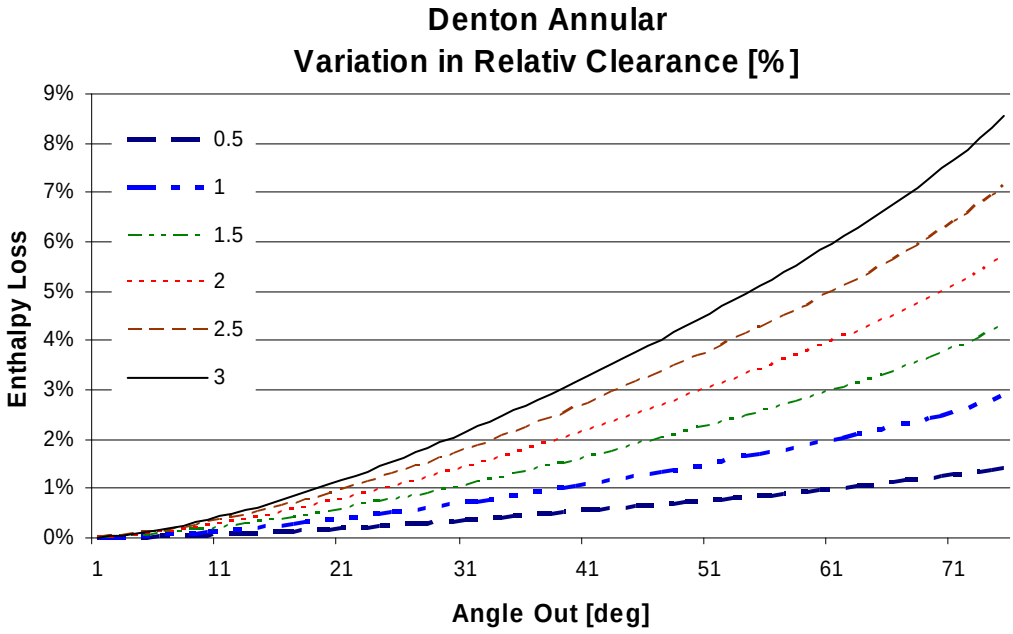

Figure 12.5-2: Variation of the Enthalpy loss with outlet flow angle for Denton Annular.

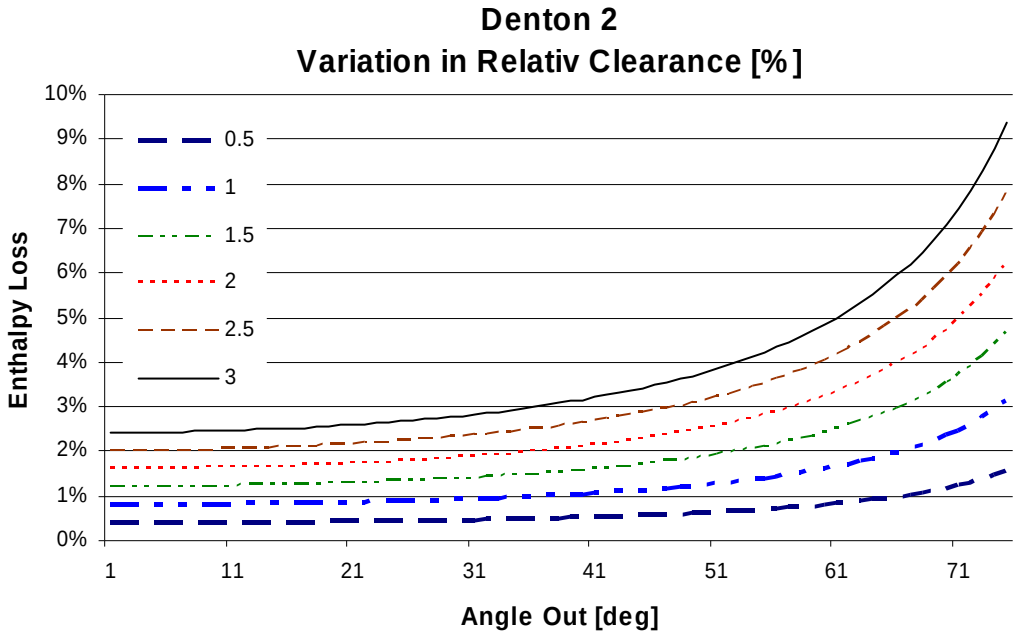

Figure 12.5-3: Variation of the Enthalpy loss with outlet flow angle for Denton 2.

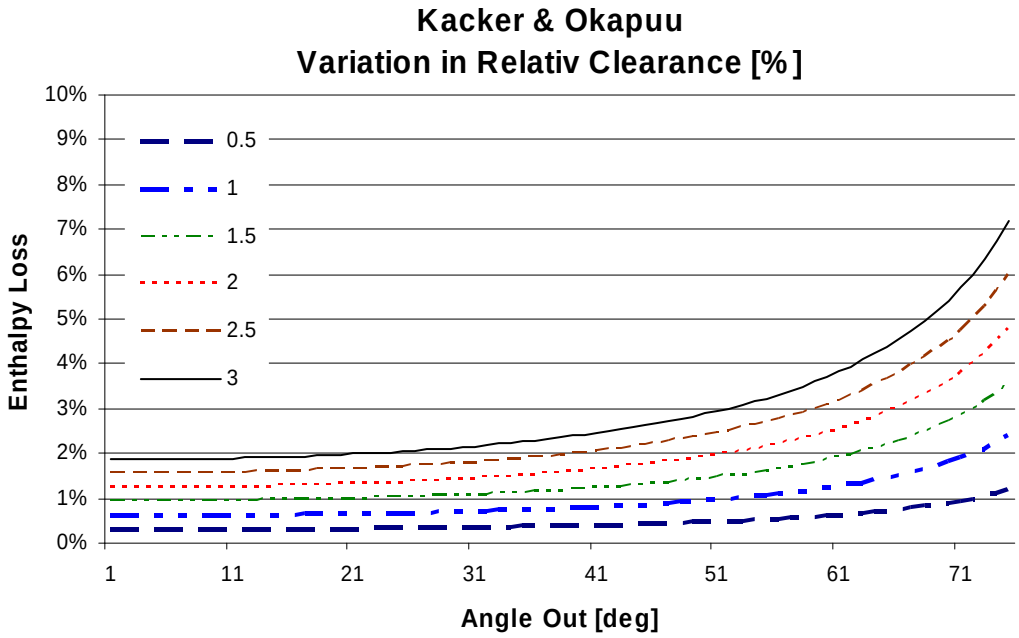

Figure 12.5-4: Variation of the Enthalpy loss with outlet flow angle for Kacker & Okapuu.

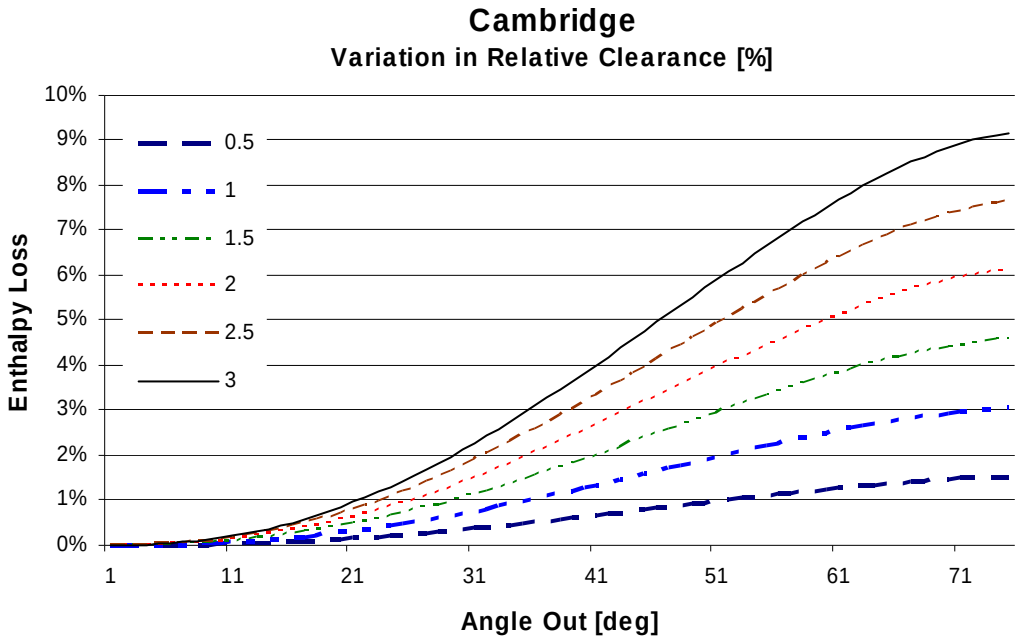

Figure 12.5-5: Variation of the Enthalpy loss with outlet flow angle for Cambridge.

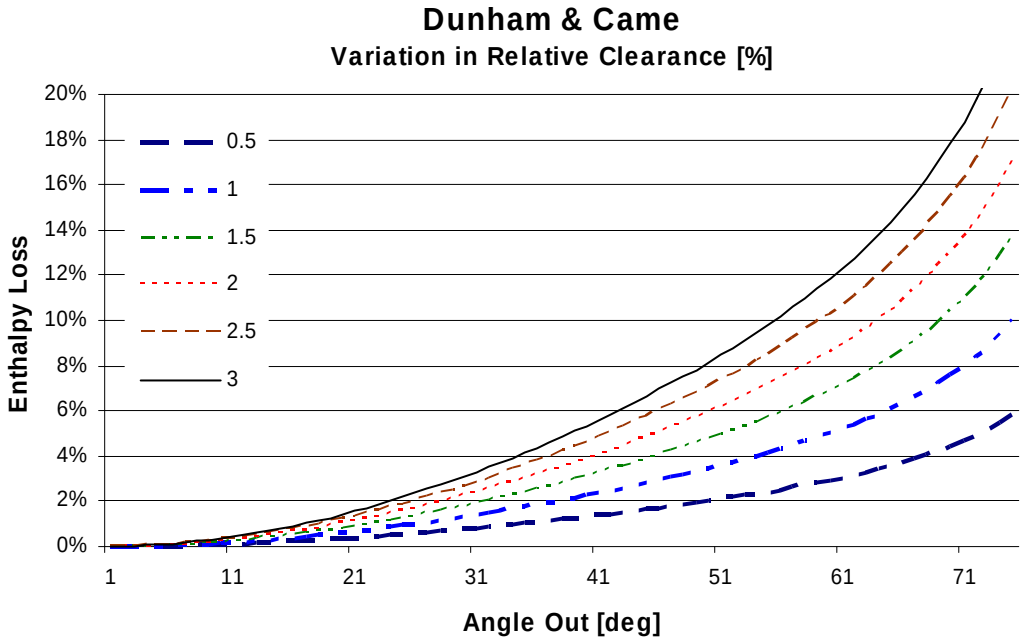

Figure 12.5-6: Variation of the Enthalpy loss with outlet flow angle for Dunham & Came. Note the loss level at the y-axis.

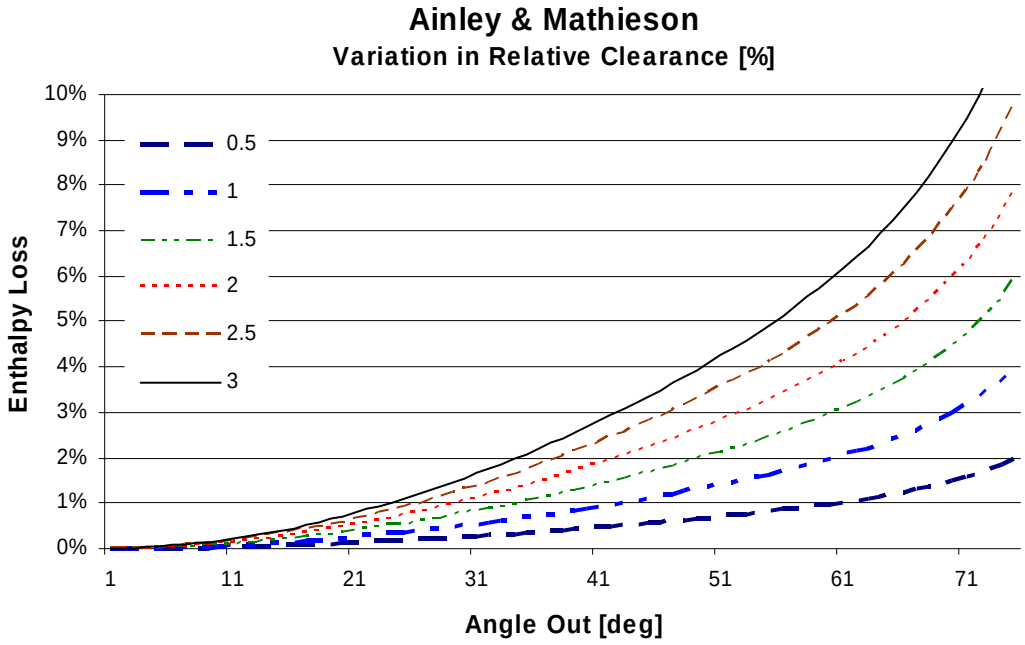

Figure 12.5-7: Variation of the Enthalpy loss with outlet flow angle for Ainley & Mathieson.

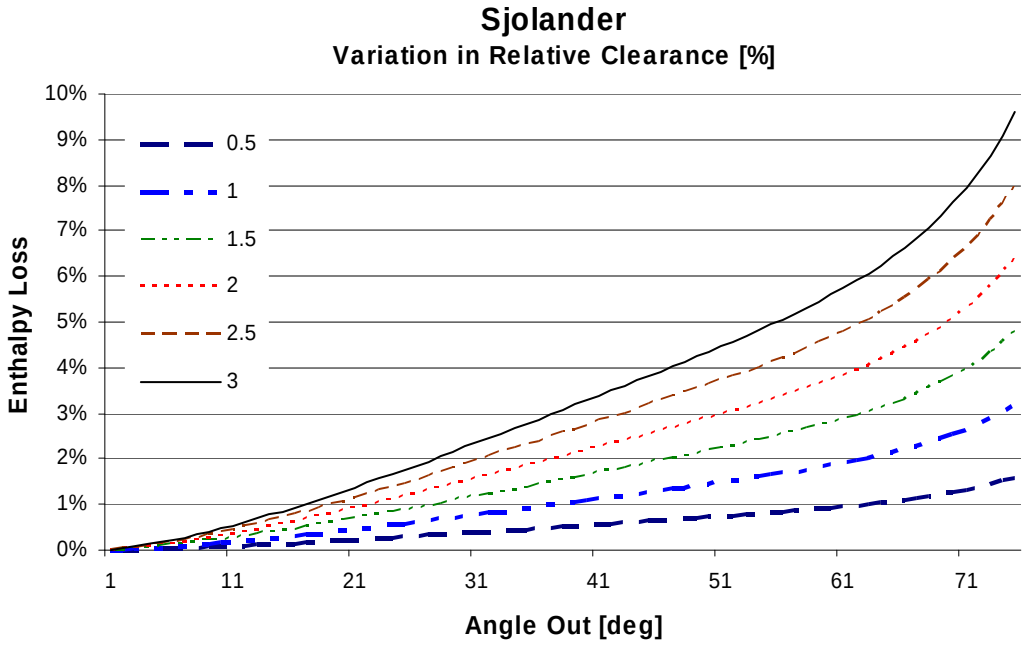

Figure 12.5-8: Variation of the Enthalpy loss with outlet flow angle for Sjolander.

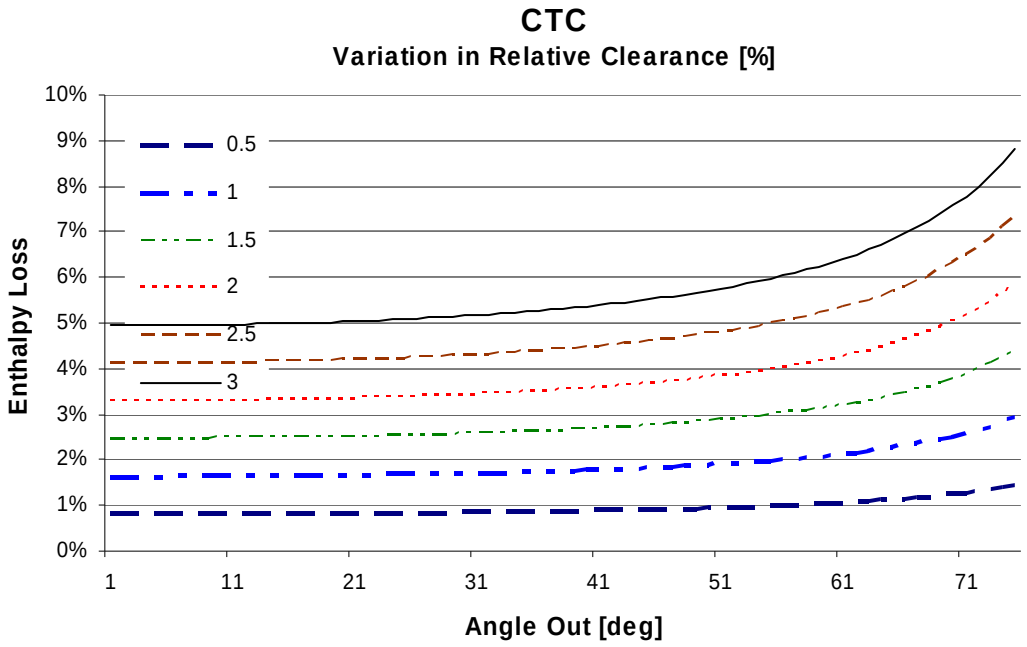

Figure 12.5-9: Variation of the Enthalpy loss with outlet flow angle for CTC.

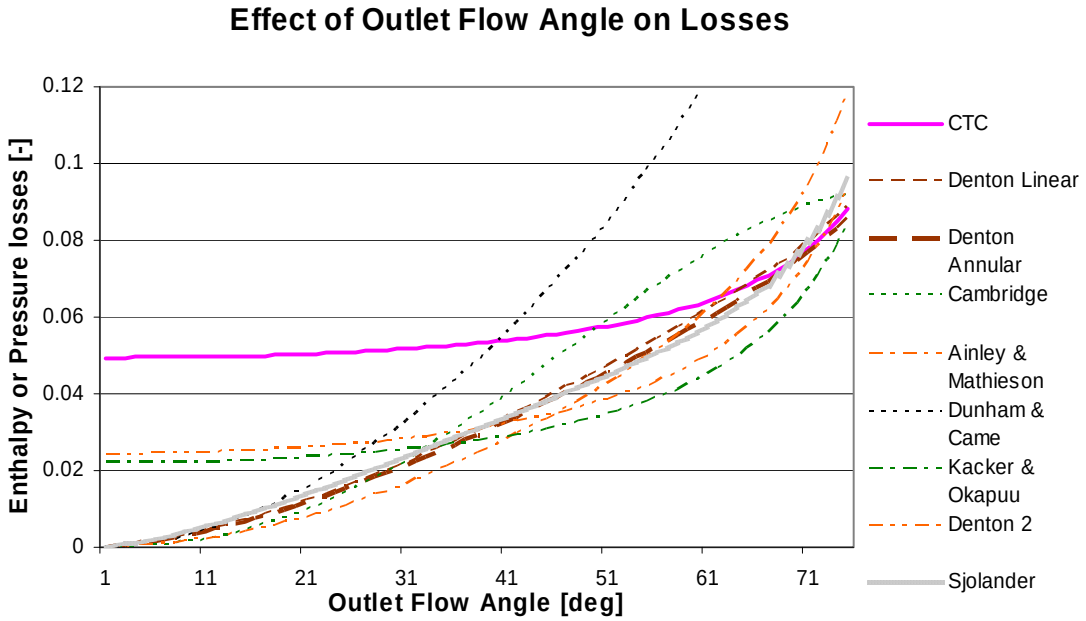

Figure 12.5-10: Variation of the Enthalpy loss with outlet flow angle for different tip leakage models.

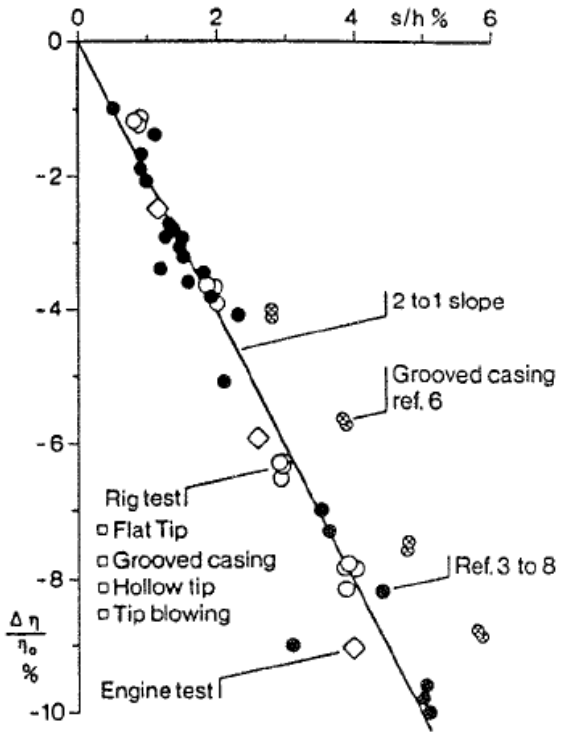

Figure 12.5-11: Effect of tip clearance on the efficiency. Figure 5 [36] (Originally from Hourmouziadis & Albrecht 1987)

12.6 Appendix Chapter 7

12.6.1 Derivation of how to Convert between Laval and Mach number

Eqn (7.1) in chapter 7 give the relation between the Laval (λ) and Mach number (M). The reason for use Laval number instead of Mach number is that the Mach number definition has two big disadvantages. For the first it is not proportional to the velocity alone and for the second it tends towards infinity as the expansion is carried out towards low pressure and a corresponding high fluid velocity (page 81 [45]). The reason that M approaches infinity is that for when expand against low pressure the temperature (T) will decrease and therefore also the local speed of sound (a). None of these disadvantages are seen for the dimensionless Laval number defined as the locally fluid velocity divided by the critical speed of sound at a reference point (M*). With this definition will a specific Laval value always correspond to the same velocity.

Below are the derivation and some simple thermodynamic relation for an ideal gas and isentropic relation (ds = 0) given

$$M = \frac{C}{a} \tag{12.6-1}$$

Speed of sound in the fluid, based on static properties

$$a = \sqrt{\gamma \cdot R \cdot T} \tag{12.6-2}$$

$$p \cdot \nu = R \cdot T \tag{12.6-3}$$

$$\frac{T_0}{T} = 1 + \frac{\gamma - 1}{2} \cdot M^2 \tag{12.6-4}$$

$$\frac{p_0}{p} = \left[1 + \frac{\gamma - 1}{2} \cdot M^2 \right]^{\frac{\gamma}{\gamma - 1}} \tag{12.6-5}$$

$$\frac{\rho_0}{\rho} = \left[1 + \frac{\gamma - 1}{2} \cdot M^2 \right]^{\frac{1}{\gamma - 1}} \tag{12.6-6}$$

For the critical states where M is one equation 12.6-6 can be formulated as.

$$\frac{T_0}{T^*} = 1 + \frac{\gamma - 1}{2} \cdot 1^2 = \frac{2}{2} + \frac{\gamma - 1}{2} = \frac{\gamma + 1}{2} \Rightarrow$$

$$\Rightarrow \frac{\gamma + 1}{2} = \frac{T_0}{T^*} \tag{12.6-7}$$

Analog for the pressure and density give

$$\frac{p_0}{p^*} = \left[\frac{\gamma+1}{2}\right]^{\frac{\gamma}{\gamma-1}} \tag{12.6-8}$$

$$\frac{\rho_0}{\rho^*} = \left[\frac{\gamma+1}{2}\right]^{\frac{1}{\gamma-1}} \tag{12.6-9}$$

Applying the conservation of mass in a row the relation is

$$\rho \cdot C \cdot A = \rho^* \cdot C^* \cdot A^* \Rightarrow$$

$$\frac{A}{A^*} = \frac{\rho^* \cdot C^*}{\rho \cdot C} \tag{12.6-10}$$

The use of the equations for the critical speed (C*) at a Mach number of unity

$$C^* = \sqrt{\gamma \cdot R \cdot T^*} \tag{12.6-11}$$

$$C = M \cdot \sqrt{\gamma \cdot R \cdot T} \tag{12.6-12}$$

Give

$$\frac{A}{A^*} = \frac{\rho^*}{\rho} \cdot \frac{\sqrt{\gamma \cdot R \cdot T^*}}{\sqrt{\gamma \cdot R \cdot T}} \cdot \frac{1}{M} = \frac{\rho^*}{\rho_0} \cdot \frac{\rho_0}{\rho} \cdot \frac{\sqrt{T^*/T_0}}{\sqrt{T/T_0}} \cdot \frac{1}{M} \tag{12.6-13}$$

Combining eqn (12.6-13) with eqn (12.6-4), eqn (12.6-6), eqn (12.6-7) and eqn (12.6-9)

$$\frac{A}{A^*} = \left[\frac{2}{\gamma+1}\right]^{\frac{1}{\gamma-1}} \cdot \left[1+\frac{\gamma-1}{2}\cdot M^2\right]^{\frac{1}{\gamma-1}} \cdot \sqrt{\frac{\frac{2}{\gamma+1}}{\frac{1}{1+\frac{\gamma-1}{2}\cdot M^2}}} \cdot \frac{1}{M} =$$

$$= \left[\left(\frac{2}{\gamma+1}\right)\cdot\left(1+\frac{\gamma-1}{2}\cdot M^2\right)\right]^{\frac{1}{\gamma-1}} \cdot \sqrt{\frac{2}{\gamma+1}\cdot\left(1+\frac{\gamma-1}{2}\cdot M^2\right)} \cdot \frac{1}{M} =$$

$$= \left[\left(\frac{2}{\gamma+1}\right)\cdot\left(1+\frac{\gamma-1}{2}\cdot M^2\right)\right]^{\frac{1}{\gamma-1}+\frac{1}{2}} \cdot \frac{1}{M} \tag{12.6-14}$$

where

$$\frac{1}{\gamma-1}+\frac{1}{2} = \frac{2+\gamma-1}{2\cdot(\gamma-1)} = \frac{\gamma+1}{2\cdot(\gamma-1)} \tag{12.6-15}$$

and

$$\left(\frac{2}{\gamma+1}\right)\cdot\left(1+\frac{\gamma-1}{2}\cdot M^2\right)=\frac{2}{\gamma+1}+\frac{2}{\gamma+1}\cdot\frac{\gamma-1}{2}\cdot M^2=\frac{1+\frac{\gamma-1}{2}\cdot M^2}{1+\frac{\gamma-1}{2}} \qquad (12.6\text{-}16)$$

Eqn (12.6-15) and (12.6-16) in (12.6-14) give

$$\frac{A}{A^*}=\left[\frac{1+\frac{\gamma-1}{2}\cdot M^2}{1+\frac{\gamma-1}{2}}\right]^{\frac{\gamma+1}{2\cdot(\gamma-1)}}\cdot\frac{1}{M} \qquad (12.6\text{-}17)$$

Laval number (λ) is defined as local velocity over the critical a*

$$\lambda=\frac{\mathrm{C}}{a^*}=\frac{\mathrm{C}}{\sqrt{\gamma\cdot R\cdot T^*}}=\frac{M\cdot\sqrt{\gamma\cdot R\cdot T}}{\sqrt{\gamma\cdot R\cdot T^*}}=M\cdot\sqrt{\frac{T}{T^*}}=M\cdot\sqrt{\frac{T/T_0}{T^*/T_0}}=$$

$$=M\cdot\sqrt{\frac{\frac{1}{1+\frac{\gamma-1}{2}\cdot M^2}}{\frac{2}{\gamma+1}}}=M\cdot\sqrt{\left(\frac{1}{1+\frac{\gamma-1}{2}\cdot M^2}\right)\cdot\frac{\gamma+1}{2}}=$$

$$=\sqrt{\left(\frac{M^2(\gamma+1)}{2+(\gamma-1)\cdot M^2}\right)}=\lambda \qquad (12.6\text{-}18)$$

And from this equation the Mach number can be expressed in terms of Laval number as

$$\lambda^2=\frac{M^2(\gamma+1)}{2+(\gamma-1)\cdot M^2}\Rightarrow 2\cdot\lambda^2=M^2\left[(\gamma+1)-(\gamma-1)\cdot\lambda^2\right]\Rightarrow$$

$$\Rightarrow M=\sqrt{\frac{2\cdot\lambda^2}{(\gamma+1)-(\gamma-1)\cdot\lambda^2}} \qquad (12.6\text{-}19)$$

and is equal to eqn (7.1) in chapter 7. =eqn (7.1)

If γ is 1.4 as for air at standard temperature and pressure (STP) some general rule for the relation between M and λ is

Form eqn (12.6-18) can it be shown that the Laval number never exceeds a value of about 2.45 for air. To do this start with eqn (12.6-18) and rewrite it as

$$\lambda=\sqrt{\left(\frac{M^2(\gamma+1)}{2+(\gamma-1)\cdot M^2}\right)}=\sqrt{\left(\frac{(\gamma+1)}{2/M^2+(\gamma-1)}\right)}$$

Then as the Mach number approaches infinity the Laval number approaches $\sqrt{\frac{\gamma+1}{\gamma-1}}$

$$\left.\begin{array}{l}\lambda = \sqrt{\left(\dfrac{(\gamma+1)}{2/M^2+(\gamma-1)}\right)} \\ M \to \infty\end{array}\right\} \Rightarrow \lambda = \sqrt{\frac{(\gamma+1)}{(\gamma-1)}} \approx 2.45\,.$$

Some general trends are between Mach and Laval number are seen in Table 12-1

Table 12-1: Relation between Mach and Laval number

Relations between Mach and Laval Number	
When	Then
M<0	λ <0
M<1	λ <1
M=1	λ =1 (only at ref. point)
M>1	λ >1
M$\to\infty$	$\lambda \to 2.45$

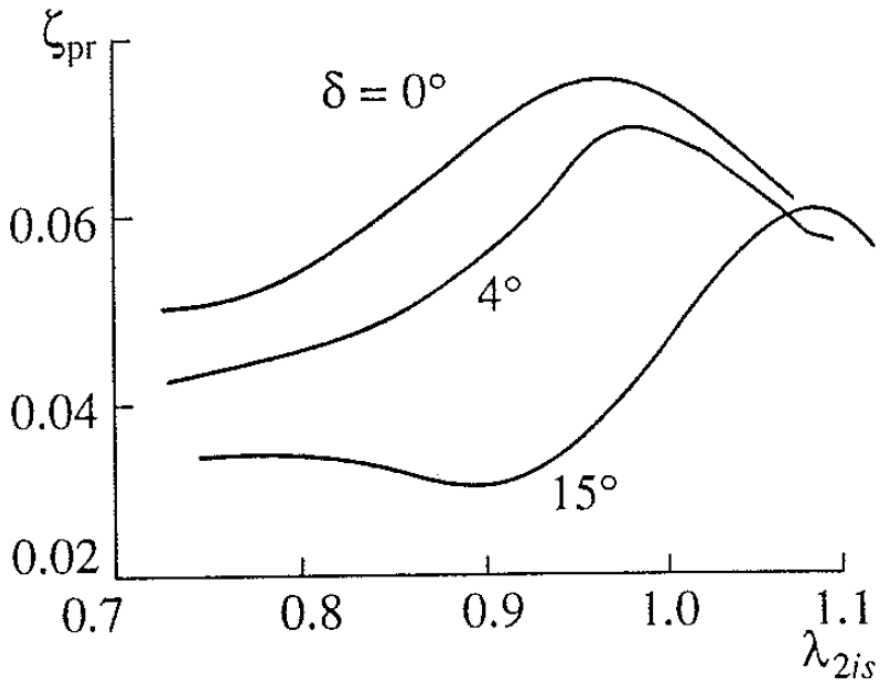

Figure 12.6-1: Show the unclear effect of Laval number and deviation on the profile loss suggested by Venedictov and Rudenko in [40]. The loss trend is quite uncertain and does not conformably to AM and CC prediction.